NASA CONTRACTOR REPORT

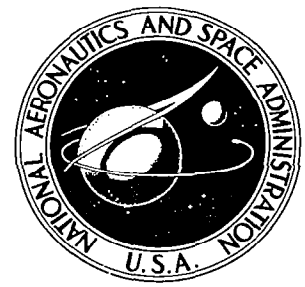

NASA CR-977

STUDY AND APPLICATIONS OF RETRODIRECTIVE AND SELF-ADAPTIVE ELECTROMAGNETIC-WAVE PHASE CONTROLS TO A MARS PROBE

by C. A. Hacking, R. B. Battelle, C. H. Dawson, R. C. Kunzelman, J. A. Martin, and L. A. Robinson

Prepared by
STANFORD RESEARCH INSTITUTE
Menlo Park, Calif.
for Ames Research Center

NATIONAL AERONAUTICS AND SPACE ADMINISTRATION • WASHINGTON, D. C. • MARCH 1968

NASA CR-977

STUDY AND APPLICATIONS OF RETRODIRECTIVE AND SELF-ADAPTIVE ELECTROMAGNETIC-WAVE PHASE CONTROLS TO A MARS PROBE

By C. A. Hacking, R. B. Battelle, C. H. Dawson, R. C. Kunzelman, J. A. Martin, and L. A. Robinson

Issued by Originator as SRI Project 5574

Prepared under Contract No. NAS 2-2933 by
STANFORD RESEARCH INSTITUTE
Menlo Park, Calif.

for Ames Research Center

NATIONAL AERONAUTICS AND SPACE ADMINISTRATION

For sale by the Clearinghouse for Federal Scientific and Technical Information
Springfield, Virginia 22151 – CFSTI price $3.00

ABSTRACT

A theoretical study has been made of several aspects of communication by means of adaptive antenna techniques, from the earth to an interplanetary vehicle (bus), and between the bus and a smaller vehicle (capsule) launched from the bus to land on a planet. The study has been restricted to some of the antenna problems associated with such a communication system, particularly where the vehicle is spin-stabilized. The environment to be expected near a planet, particularly Mars, and its effects on the operation of an adaptive system is discussed in some detail. Consideration is given to the various phenomena associated with atmospheric entry, including plasma, atmospheric inhomogeneities, voltage breakdown, and so forth.

Four separate antenna configurations that might be suitable for use on a spinning vehicle were investigated theoretically. Particular attention was paid to the retrodirective mode of operation. One of these, a novel configuration called a Cylindrical-Geodesic-Lens Biconical-Horn Phased-Array Antenna was given particular attention because it appeared to offer the most potential for meeting the system requirements. Several computer programs were written to analyze various aspects of these antennas, only one of which relied on switching of antenna elements as the vehicle rotated, in order to realize maximum effective radiated power. Radiation patterns and the variation in peak gain were computed. A study was made of the important problem of spectral splitting of a signal received or transmitted by a rotating antenna. It is shown that the effect of spectral splitting can probably be made negligible by careful design of the antenna and adaptive circuitry. No attempt was made to arrive at an optimum antenna configuration.

System problems are discussed, some proposed operational techniques are described, and a summary of work done by other investigators is given.

CONTENTS

CONTENTS

CONTENTS

ILLUSTRATIONS

ILLUSTRATIONS

ILLUSTRATIONS

TABLES

I INTRODUCTION

This report represents work performed during the first 16 months of a study to investigate some of the many possible uses of adaptive antenna circuits for communication to and between vehicles on an interplanetary mission. It is assumed that the main vehicle, the bus, flies by or orbits the target planet and when in the vicinity releases a smaller vehicle, the capsule, to enter the planet's environment for a hard or soft landing. Communication between the earth and the bus is specified as being within the S-band of frequencies presently used by the Deep Space Instrumentation Facility (DSIF), but between the bus and capsule the best frequency of operation was a subject of study. In addition to communication, use of the adaptive antenna circuitry was briefly considered for other purposes as well, such as providing navigational and environmental information.

Since there appear to be no unique definitions of adaptive antenna types it is necessary to make our own definitions of some of the commonly used terms in order to avoid confusion. It is hoped that these very general definitions will not vary appreciably from those eventually adopted by the IEEE. These definitions are as follows:

Adaptive antenna—A generic term including all antennas having a receiving and/or transmitting beam that is controlled by the direction of one or more incoming signals. Such an antenna may be active or passive. (One simple form of an adaptive antenna is the well known corner reflector.)

Retrodirective antenna—An antenna that radiates its major lobe back in the direction from which a pilot signal is received.

Self-steering antenna—A special type of adaptive antenna array that adjusts phases of element signals to allow in-phase addition, thereby extracting maximum power from the incident signal, even if it is in the radiating near field of the aperture (in which case, it is called self-focussing). A self-steering antenna may be used for receiving only, in which case it is referred to as an adaptive receiving antenna, or it may transmit as well.

Since most of the study on this program has been directed specifically to retrodirective arrays, a more detailed description of this type of antenna follows.

A retrodirective antenna is an array of elementary antennas which, when it receives a pilot signal from a command station, automatically returns it to the source without the need for first orienting its physical direction. In general, the returned signal is amplified and modulated. This automatic beam-scanning technique is a phase-diversity technique where the phase of the signal received in each subantenna in the retrodirective array is processed and the signal transmitted has a corresponding conjugate phase. As a result of this phase compensation, the signal adds coherently at the command station and the gain increases roughly as the number of elements used.

It has been assumed that each of the specific antenna configurations studied will be attached to a spin-stabilized space vehicle, which presents antenna problems obviously not associated with a fully stabilized vehicle. One of these problems is making effective use of array elements that are nominally shadowed by the space vehicle as it rotates. During the first quarter the analysis was started of a particular cylindrical antenna configuration conceived to overcome this problem, in which all the receiver/transmitter elements are used for any azimuthal direction of the antenna beam. This is done by focusing the energy to and from the elemental radiators by means of a cylindrical geodesic lens. For this antenna the gain as computed appeared to be generally less than 1 dB below the postulated theoretical maximum value and required no switching of elements as the vehicle rotated. These initial computations were greatly simplified by assuming that the retransmitted signal had exactly the same frequency as the incoming pilot signal. The study was later expanded and made more general by including a small frequency translation before retransmitting.

The First Quarterly Report[1]* also included a study of the conditions to be expected in the vicinity of Mars, particularly as they would relate to communications with a capsule entering the Martian environment. This study has been greatly expanded to include more general conditions relating to the effects of environment on antenna operation, and now forms the second section of this report. It is self-contained and essentially independent of the rest of the report although it does deal with specific antenna element configurations.

* References are listed at the end of the report

In the Second Quarterly Report[2] three new antenna configurations were introduced and analyzed to some degree while some consideration was also given to direction-finding problems without relating them to any particular configuration. Each configuration was treated as a retrodirective antenna, rather than as the more general self-adaptive antenna. A start was also made on the analysis of various communications systems that might be used on the proposed mission, as well as on the consideration of adaptive circuitry.

In the Third Quarterly Report,[3] primary consideration was given to the problem of spectral splitting due to the rotation of an antenna array. Each of the specific antenna configurations that has so far been studied assumes that it is mounted on a vehicle that is stabilized only by spinning about an axis approximately perpendicular to the line of transmission. The problem of signal distortion—*i.e.*, spectral splitting due to such spin—is therefore very important. It is closely related to the variation of antenna gain as a function of azimuthal orientation of the antenna with respect to the line of transmission. This gain modulation, or amplitude modulation, constitutes one component of the spectral splitting so that in the present report the two subjects have been expanded and treated together. The other primary component is phase modulation.

Several aspects of each of four distinct circular antenna configurations have been treated in this report, but in the time available it was not possible to analyze the large number of combinations and permutations of conditions relating to all the antennas. Some indication of the characteristics of one configuration can sometimes be postulated by reference to the analysis made on another, but in general each specific antenna must be analyzed to obtain the characteristics with any accuracy.

One important simplifying assumption made throughout this study is that mutual coupling between any elements of a given antenna is negligible. In some cases the assumption is justified in practice. In others it will result in differences between theory and practice unless steps are taken to reduce the effects of mutual coupling.

In almost every case the antenna has been treated only as a retrodirective radiator—that is, a device for radiating a relatively high-gain beam in exactly the opposite direction (the retrodirective) from an incoming pilot (or received) signal. It is a very simple matter to send data down such a re-radiated beam by modulating the signal source, or

local oscillator, that is co-phasally connected to each of the transmitting elements of the array. In practice, the transmitted and received signals must generally have different frequencies to prevent interference in the receiver. However, for simplicity, much of the work in this report assumes the frequencies to be the same. Making this assumption does not necessarily negate the results of the studies since even a very small frequency separation could produce sufficient decoupling between input and output without substantially changing the results of the analysis. Since in each case the antenna dimensions are given in terms of wavelength, the "equal frequency" analysis can be used in its exact form if one antenna is used for receiving the pilot beam and another for transmitting in the retrodirection. The antennas would have to be exactly similar and scaled to the respective operating wavelengths, with the corresponding elements connected together through appropriate phase-conjugating circuitry.

It may sometimes be desirable to use the same antenna operating with appreciably different receiving and transmitting frequencies. Then there arises the problem of obtaining good focusing, in order to maximize the gain, at the transmitting frequency. Under certain circumstances this problem can be solved by making the transmitting frequency a rational fraction of the pilot frequency; a range of alternative discrete frequency separations between receiver and transmitter can be obtained in this manner without making the separation large. An example of such a system is given in this report, but it is not related directly to the specific problems associated with spin of the antenna, and is not necessarily applicable to all of the configurations treated in this report. Adaptation to any particular circular-array configuration will have to be a subject of further study. However, the technique is particularly important because, apart from correctly phasing each radiator, it permits the use of frequency-multiplication circuits, leading the way toward all-solid-state circuitry and then to integrated circuitry, with its inherent cost advantage, built-in redundancy, and improved reliability.

The program is not sufficiently advanced to result in any preferred overall system model, so that particular frequency bands have not generally been associated with any of the studies presented in this report. However, because of the problem of communication blackout on entering the atmosphere of any planet, there are definite advantages to

operating the bus-capsule link at frequencies above the anticipated critical plasma frequencies—that is, at millimeter wavelengths. An added advantage of such a link is that the range, range rate, and relative angular location of the capsule, with respect to the bus, can be obtained at any instant during the capsule landing trajectory with much greater accuracy than if, say, VHF frequencies are used.

As is usually the case in analyzing antennas, and particularly in determining radiation characteristics, the assumption has been made that a radiation pattern, measured on a relative scale, is independent of the distance of the observation point from the antenna, provided that it is well into the *far field* region of the antenna. This condition is easily met in the case of a planetary probe, but the great distances involved could give rise to an additional problem if the antenna consists of a phased array. For instance, at a range of 150 million kilometers, should one of the elemental transmitters of an otherwise correctly phased array happen to differ or appear to differ in frequency from the rest of the elements by only 0.001 Hz, or an odd multiple of this value, the contribution of that element would appear in exact opposition (or antiphase) to the amplitudes of all the rest of the elements at the observation point. This problem does not normally arise with earth-bound systems, and the likelihood of such a frequency error occurring at one or more of the elements of an interplanetary communication antenna is very much dependent on the particular circuitry used with the space-vehicle array. Since the consideration of specific circuitry was only touched upon in this program this interesting aspect was not studied, but it is mentioned here to draw attention to a potentially serious problem.

It became apparent during the study that the feasibility, or otherwise, of using spinning antennas of the types described was somewhat dependent on the type of modulation to be used in the transmission link. However, no attempt was made to consider modulation problems in any detail, and signals were generally assumed to be CW except when modulated by the motion of the antenna.

II ENVIRONMENT STUDY

A. Introduction

Effects of environment on adaptive antenna operation for space missions are considered for a planet-orbiting or fly-by bus and for an entry capsule. Primary emphasis is given to retrodirective antenna operation.

The study involves characterizing the electromagnetic environment through which adaptive antennas may operate. The Mars environment is referred to in the study to reflect the unknowns that exist in characterizing a planetary environment. Antenna operation in environments similar to the vicinity of the earth and the earth's atmosphere is assumed. Departures from an earth model are also considered.

B. Modification of Retrodirective Signal Characteristics

Turbulence in the refractive structure of a planetary atmosphere or an entry plasma can limit antenna operation. Three primary effects are involved: signal phase fluctuations, antenna gain reduction, and signal angle-of-arrival variations. Adaptive antennas are useful in controlling these effects. The adaptive antenna adjusts the phase of signals received or transmitted by array subapertures so that the subaperture signals will be in phase and will add coherently. The subaperture size is chosen such that gain reduction and angle-of-arrival variations are negligible.

Basic to retrodirective array operation is that coherent, in-phase signals are returned from array subapertures in the direction of the pilot signal. The signals are coherent provided phase fluctuations are time-coherent along pilot and return propagation paths.

Summation of the discrete retrodirective signals at the pilot station can be less than ideal because of system design, environment imperfections, or antenna orientation. A list of factors that may cause phase errors in the discrete subaperture signals is given in Table I.

The fractional reduction in signal power received from a retrodirective array, received in an adaptive receiving array, or received in a

Table I

FACTORS THAT MAY MODIFY THE RETRODIRECTIVE SIGNAL CHARACTERISTICS

(1) Systems Design

- (a) A shift in carrier frequency during the retrodirective phasing processes
- (b) Unequal phase shifts induced by subaperture circuitry
- (c) Non-linear effects such as amplifier gain and coupling between subaperture circuitry and antennas.

(2) Environment Imperfections

- (a) Refractive variations of correlation scales less than the size of subapertures (partially eliminated by aperture smoothing)
- (b) Refractive variations of correlation scales that are less than the extent of the array and that are time-incoherent along the pilot signal and return signal paths
- (c) Non-reciprocal plasma (important only if a strong magnetic field exists)
- (d) Planetary reflections that may be different along pilot-signal and return-signal paths because of propagation time, Doppler effects, and planetary roughness.

(3) Antenna Orientations

- (a) Differences in polarization between receiving and transmitting at array subapertures and the pilot terminal
- (b) Separate antennas for receiving and transmitting in the array.

conventional antenna as a result of small statistical phase errors is approximated as:

$$\text{Signal power reduction, } \frac{P}{P_0} \approx \{1 - [\delta\varphi(t)]^2\} \quad ; \quad \delta\varphi(t) << 2\pi \qquad (1)$$

where $\delta\varphi(t)$ is the maximum phase error over the antenna aperture. A 1-dB loss in signal power corresponds to a phase error of 0.45 radians or 26 degrees.

The signal-reduction effect represented in Eq. (1) corresponds to signal phase fluctuations or jitter that are uncorrelated over the antenna aperture. The degree of decorrelation depends upon the turbulent refractive medium and upon antenna size; a large antenna is illuminated by a greater degree of uncorrelated phase jitter than a small antenna and thus suffer more signal reduction.

Amplitude imperfections can also cause retrodirective antenna signal loss or variation. An example would be unequal and varying subaperture

propagation losses such as could exist for a planetary entry capsule. Amplitude imperfections can alsc be caused by time-varying retrodirective array orientation, the amplitude effect being induced by array configuration and subaperture antenna gain and polarization.

In general, amplitude and phase imperfections are not necessarily separable and discrete in effect. Modification of Doppler frequency, phase, and amplitude in the signal received at the pilot station are complex.

Factors that modify the signal received at the pilot station will also modify the retrodirective array pattern in directions other than along the pilot-signal path. Planetary reflections and antenna orientation will change the pattern shape of a retrodirective antenna, which might give incorrect directional information, as is also the case with a wide-open DF system in a multi-signal environment.

C. Orbiting or Fly-By Bus

1. Background

The propagation environment for a planetary bus includes the planetary atmosphere, interplanetary space, and the earth's atmosphere. Both the planetary atmosphere and the earth's atmosphere have a molecular refractive medium, referred to as a troposphere, in the lower atmosphere and an electron plasma medium, referred to as an ionosphere, in the upper atmosphere.

Studies[4-6] indicate that random fluctuations in refractivity of the propagation media are a limitation to the reception of deep-space signals on the earth. Radio astronomy and satellite measurements indicate the earth's atmosphere to be the primary cause of the random fluctuations. Thus, particular attention has been given to the study of refractive effects in the earth's atmosphere relative to deep-space communications (in addition to earth and near-earth space communications).

The aperture size for earth-based communication at which refractive fluctuations cause antenna degradation exceeds 30 meters at 1 GHz.

Retrodirective array operation does not eliminate gross refractive bending of the propagation paths of the pilot signal and retrodirective return signals.

2. Earth Atmosphere

The propagation environment of the earth's atmosphere which affects conventional as well as adaptive antennas is substantially documented in the literature and will not be extensively reviewed here. A summary of phase and angle-of-arrival fluctuations for propagation through the earth's atmosphere is presented in Table II. The data typically represent a clear and dry troposphere and a normal ionosphere.

Angle-of-arrival fluctuations limit the allowable beamwidth of an antenna looking through the earth's atmosphere. Above 1 GHz, angle-of-arrival fluctuations are generally caused by tropospheric refractive variations. The antenna size for which the rms beam tilt is equal to the 1-dB antenna beamwidth for a one-percent probability of occurrence is typically 125 λ to 330 λ (40 meters to 100 meters at 1 GHz).

The earth's atmosphere is located far away from a planetary bus—for example 10^{11} to 3.5×10^{11} meters from Mars, a minimal planetary distance. The associated time-varying refractive medium in the earth's atmosphere will change during the earth-planet-earth signal transit time. The correlation times of significant fluctuations in the earth's refractive media are typically less than 100 to 200 seconds (from Table II) and thus are less than the signal transit time between the earth and a planet—for example, Mars, 330 to 1200 sec. As a result, phase jitter induced by the earth's transmission environment will not be equal for the pilot signal path and the retrodirective return-signal path. This does not, however, affect coherent signal formation since spatial correlation scales of phase jitter will exceed the size of the retrodirective array, and rays from subapertures will essentially lie along the same propagation path.

The gross refractive characteristics of the earth's transmission environment may also not be equal on the pilot and return paths due to the large time delay and earth antenna-pointing-angle differences. The earth terminal antenna will be pointed in different parts of the earth's atmosphere for transmission and for reception (for example, a difference in earth elevation angle of 5 degrees), and the pilot and return paths may not be equal in length.

It is thus concluded that retrodirective cancellation of phase delays along pilot and return paths will not be complete for deep-space-to-earth applications. Conceivably, the phase-delay characteristics of the

Table II

SUMMARY OF PHASE AND ANGLE-OF-ARRIVAL FLUCTUATIONS
DUE TO REFRACTIVE FLUCTUATIONS IN THE EARTH'S ATMOSPHERE

(a) TYPICAL CHARACTERISTICS OF ATMOSPHERE

	TROPOSPHERE (Clear and Dry)	IONOSPHERE (Normal)
Spatial Correlation of Refractive Irregularity (Blob Size), l_0	60 meters	5 Kilometers
Propagation Path Length, L	6 Kilometers	65 Kilometers (scale height of F-region)
Deviation in Surface Refractivity, $\overline{(\Delta N)^2}$	0.25	--
Fractional Deviation in Electron Density, $(\Delta N_E/N_E)^2$	--	3×10^{-4}
Peak Electron Density --	--	1.24×10^6 el/cm^3
Fluctuation Correlation Time, T_c	1 to 100 seconds	1 to 200 seconds

(b) ORDER-OF-MAGNITUDE PREDICTION OF PHASE JITTER DUE TO THE TROPOSPHERE AND IONOSPHERE

θ_0 = Earth elevation angle

FREQUENCY (GHz)	RMS PHASE JITTER, σ_α, IN DEGREES			
	Troposphere (Clear)		Ionosphere (Normal)	
	$\theta_0 = 90^\circ$	$\theta_0 = 4^\circ$	$\theta_0 = 90^\circ$	$\theta_0 = 4^\circ$
1.0	0.43	1.7	47	94
2.2	0.97	3.7	21	42
4.6	2.0	7.8	10	20
10.0	4.3	17.0	4.7	9.4

(c) ORDER-OF-MAGNITUDE PREDICTION OF ANGLE OF ARRIVAL FLUCTUATIONS DUE TO THE TROPOSPHERE AND IONOSPHERE

θ_0 = Earth elevation angle

Antenna diameter $D < l_0$

FREQUENCY (GHz)	RMS ANGLE-OF-ARRIVAL FLUCTUATION, σ_β, IN DEGREES			
	Troposphere (Clear and Dry)		Ionosphere (Normal)	
	$\theta_0 = 90^\circ$	$\theta_0 = 4^\circ$	$\theta_0 = 90^\circ$	$\sigma_0 = 4^\circ$
1.0	8×10^{-4}	3×10^{-3}	9×10^{-4}	1.8×10^{-3}
2.2	(Independent	(Independent	1.9×10^{-4}	3.8×10^{-4}
4.6	of	of	4.2×10^{-5}	8.5×10^{-5}
10	frequency)	frequency)	9×10^{-6}	1.8×10^{-5}

retrodirective sum signal could be eliminated for near space and for capsule-to-bus applications unless the carrier frequency is shifted at the subapertures.

3. Interplanetary Space

Typical plasma characteristics of the interplanetary space are summarized in Table III.[7-9] The solar interplanetary plasma is a weak plasma relative to the earth's ionosphere. The gyromagnetic frequency

Table III

TYPICAL PLASMA CHARACTERISTICS OF INTERPLANETARY SPACE

Solar Interplanetary Magnetic Field

Strength - At 1 A.U., average 2 or 3 gammas 0 to 100 gammas
Between 1 A.U. and 1.75 A.U., average <3 gammas (lack of definite data exists at these solar distances).

Strength depends upon solar activity. Fluctuations of one or two orders of magnitude occur, depending upon solar activity.

Solar-Wind Electron Streams

SOLAR CONDITION	MINIMUM		MAXIMUM	
	Gas Flow	Electron Density	Gas Flow	Electron Density
Quiet sun	600 km/sec	5 elec/cm^3	25,500 km/sec	0.12 elec/cm^3
Disturbed sun	1500 km/sec	100 elec/cm^3	63,000 km/sec	2.3 elec/cm^3
During Pioneer VI Flight	--	5 elec/cm^3	--	9 elec/cm^3

Minimum Scale of Electromagnetic Irregularities

Gyro radius of electrons $\gtrsim 10$ meters
Gyro radius of ions $\gtrsim 1$ km

Mean Free Path of Electrons and Ions

$\gtrsim 10^5$ km, typically 3×10^7 km

SOURCES: Refs. 7-9.

in the earth's atmosphere is 1.42 MHz, which is large compared to the gyromagnetic frequency in interplanetary space, typically 0 to 300 Hz. The maximum plasma frequency in the earth's ionosphere is typically 2 to 20 Mhz, which is also large compared to the plasma frequency in interplanetary space, typically 0 to 90 kHz.

The scale of electromagnetic irregularities in interplanetary space is sufficiently large (> 10 meters) that phase jitter will be correlated

across adaptive arrays on space vehicles. Interplanetary space environment will not limit antenna operation at frequencies of interest.

4. Mars Atmosphere

Defining the propagation environments of near planets such as Mars is in the crude stage. Results of the recent 1965 Mariner radio occultation experiment have been published and are summarized in Table IV.[10,11] The radio occultation experiment was concerned with the measurement of refractive effects in the bus-to-earth signal at occultation. Refractive effects in the amplitude, phase, and Doppler characteristics of the received signal were used to deduce surface pressure and scale height in the lower atmosphere of Mars and to deduce ionization and scale height in the Martian ionosphere.

Table IV

SUMMARY OF MARINER IV OCCULTATION EXPERIMENT AT MARS

ATMOSPHERE	
Surface refractivity	$3.6 \pm 0.2N$ units
Scale height	8 to 10 km
Surface number density	
100% CO_2	$1.9 \pm 0.1 \times 10^{17}$ mol/cm^3
Up to 20% A or N_2, or a mixture	$2.1 \pm 0.2 \times 10^{17}$ mol/cm^3
50% A	$2.5 \pm 0.15 \times 10^{17}$ mol/cm^3
Surface mass density	
100% CO_2	$1.43 \pm 0.1 \times 10^{-5}$ g/cm^3
Up to 20% A or N_2, or a mixture	$1.5 \pm 0.15 \times 10^{-5}$ g/cm^3
50% A	$1.75 \pm 0.10 \times 10^{-5}$ g/cm^3
Temperature	
100% CO_2	$180 \pm 20^\circ$K
Up to 20% A or N_2, or a mixture	$175 \pm 25^\circ$K
50% A	$170 \pm 20^\circ$K
Surface pressure	
100% CO_2	4.1 to 5.7 mb
Up to 20% A or N_2, or a mixture	4.1 to 6.2 mb
50% A	5.0 to 7.0 mb
IONOSPHERE	
Maximum electron density ($\chi = 70^\circ$)	$9 \pm 1.0 \times 10^4$ el/cm^3
Altitude of maximum	120 to 125 km
Electron scale height above maximum	20 to 25 km
Temperature	$< 200^\circ$K at 120 to 200 km

SOURCE: Ref. 10.

Results of the Mars radio-occultation experiment do not provide exact surface pressure as no absolute altitude scale is available.

Magnetometer and trapped-radiation measurements of the Mariner fly-by have indicated that no magnetic field exists near Mars in excess of the ambient magnetic field of interplanetary space. Thus, the transmission environment in the Martian ionosphere should be reciprocal. The effects of Faraday rotation, of anisotropy due to field-aligned ionization, and of other phenomena induced by the magnetic field and magnetic disturbances observed in earth's ionosphere will not occur in the Martian ionosphere (or in interplanetary space).

5. Hypothetical Planetary Atmosphere

Planetary atmospheres similar to the earth's atmosphere will not complicate or degrade adaptive antenna performance on a planetary bus to any greater degree than the same antenna on a bus orbiting the earth. In particular, scale size of refractive variations in the earth's atmosphere exceed 30 meters and are considerably larger than practical antenna apertures for airborne and space applications. It is apparent that adaptive antenna operation on a planetary bus is not limited by electromagnetic constraints in the environment. Adaptive antenna performance should be readily predictable and propagation characteristics would be the same as for any conventional antenna.

To affect the operation of an adaptive antenna, the principal scale size of refractive irregularities in a hypothetical planetary atmosphere would have to be less than the size of the antenna aperture—for example, 3 meters. (The diameter of the Centaur shroud is 3 meters.) No such atmosphere has been postulated or experimentally measured.

In addition to scale size, the propagation path length and the extent of the refractive medium would have to be sufficiently long to cause large phase fluctuations. For example, the required path length for a 30-degree phase jitter due to a molecular atmosphere with a scale of refractive fluctuation of 3 meters and a deviation in surface refractivity of 0.25 would be 580 million meters at 1 GHz and 5.8 million meters at 10 GHz.*

---

* Phase fluctuation of a signal propagating through a molecular atmosphere varies approximately as

$$\sqrt{(\text{path length}) \times (\text{scale of refractive fluctuation}) \times (\text{frequency})}$$

Data in Table II is used to scale path length in the hypothetical atmosphere. The 30-degree phase jitter would correspond to roughly a 1-dB signal loss.

These ridiculously large distances (assuming an exponential atmospheric profile and a mean free path less than 3 meters) would require planetary surface pressure and density exceeding ten orders of magnitude above earth conditions.

While irregular structure in an ionosphere may exist in all sizes, minimum bounds exist for those blob sizes important to electromagnetic wave propagation. The minimum bounds can be predicted by considering the charged electrons and ions in the ionosphere. In the absence of a magnetic field, or along a magnetic field, the mean free path represents the minimum scale of electromagnetic irregularities.

Typical electron mean-free-path l_e in the earth's ionosphere is:

E-Region—	80-km altitude,	$l_e \approx$ 10 meters
	140-km altitude,	$l_e \approx$ 100 meters
F-Region—	200- to 700-km altitude,	$l_e \approx$ 0.5 to 2 km
	1000-km altitude,	$l_e \approx$ 10 km .

The scale of ionic irregularities is a factor of $4\sqrt{2}$ less than l_e. Transverse to the magnetic field the minimum scale of irregularities approaches the minimum logitudinal scale. In the *F*-region, the minimum transverse scales are defined by the gyroradius of electrons, $\approx 10^{-2}$ meters, and of ions, $\approx$ 5 meters.

The evidence of significant magnetic fields of internal origin is compelling for only two planets—the earth and Jupiter. Thus, the minimum scale of refractive fluctuations in Mars and Venus ionospheres should be 10 meters, the gyroradius of electrons in interplanetary space and of the mean free path of electrons in the *E*-region of the earth's ionosphere.

It is concluded that a planetary ionosphere is not likely to exist in which principal refractive-irregularity scale sizes are sufficiently large to cause adaptive antenna degradation.

6. Multipacting Breakdown[12,13]

At high-vacuum conditions, such as those that exist in the earth's ionosphere, the electron mean free path is generally large compared to the dimensions of the RF equipment. Under such conditions multipactor discharge can occur, and is the result of secondary electrons produced by electrons being accelerated by the RF field.

For multipacting voltage breakdown, the voltage between the terminals is important (not the electric field strength as is the case for gas-breakdown discharge). For typical structures, multipacting breakdown occurs for voltages between 50 to 300V. A high-voltage cutoff exists in multipacting breakdown when the electron transit time becomes shorter than a half-period of the RF wave. Assuming a biconical antenna structure with an input impedance of 50 Ω, the power required for multipacting breakdown will lie in the region of 50 to 1800W.

Laboratory measurements indicate that the multipacting discharge itself does not produce signal loss difficulties; however, outgassing and possible surface phenomena associated with the electron energy dissipated at the surface can produce an arc. Arc discharges that have been observed greatly modify the electrical characteristics of the structure and can also do considerable mechanical damage as well. It is important to keep surfaces of antennas and transmission lines clean, as arc discharges are more likely to occur from contaminated surfaces. Surface contamination, such as a carbonaceous film, a fine layer of dust particles, or an oxide film, is a source of secondary emission, and as a result the arcing potential can be lowered.

D. Entry Capsule

1. Background

During atmospheric braking entry a plasma sheath is formed around the vehicle. A wake or trail is also formed in the rearward void of the vehicle. Ionization in the sheath around the vehicle arises from three sources: thermal ionization caused by the compressive shock wave, thermal ionization generated by viscous effects in the boundary layer, and chemical ionization produced as ablative heat-shield material is introduced into the boundary layer. If propulsive slowing down of the entry capsule is employed, ionization is also created by rocket exhausts.

Constraints of entry environment are to a large degree similar for adaptive antennas and for conventional antennas. Effects of entry plasmas on antenna systems are not easily predictable. Idealized propagation concepts, such as plane-wave propagation, can be completely inadequate to describe propagation in entry plasma. The ionization effects of ablative products cannot be predicted. Laboratory and flight experiments are required to evaluate effects of entry environment. Constraints of entry

environment are described in the following discussion, and examples of antenna degradation are presented. Particular constraints affecting adaptive antennas are described.

2. Entry Environment

a. Atmosphere Models

Planetary atmospheres can be classified as to whether aerodynamic or propulsive braking is required for slowing down a capsule exploring the atmosphere. The negligible atmospheres of Mercury and the moon require propulsive braking. The thin atmosphere of Mars may also require propulsive braking or a combination of propulsive and aerodynamic braking. The atmospheres of the earth and Venus are sufficiently dense that aerodynamic braking can be used.

The state of the art in defining the atmosphere of Mars is presented in the following discussion to illustrate the limitations that exist in planetary exploration and in predicting antenna operation in entry plasma.

Defining the gas composition of the Martian atmosphere from Earth-based astronomy is limited by atmospheric attenuation of the radiating bands of possible species. Only carbon dioxide (CO_2) and water vapor (H_2O) have been positively identified. Nitrogen (N_2) and argon (A) have been proposed as other constituents of the atmosphere.

The gas compositions and surface pressure of various models of the Martian atmosphere are given in Table V.

The dense atmospheres, 41 to 133 mb, based on optical measurements are believed to be upper bounds. The atmospheres, 10 to 40 mb, are based on spectroscopic observation of the CO_2 content in the Mars atmosphere. (Unfortunately, these models are based on analysis of a single photographic plate, thus reducing the reliability of the results.) The Mariner IV occultation experiment, and data evaluated, point to surface pressures as low as 4 mb. However, an absolute altitude scale was not measurable during the occultation.

The atmospheric structure as a function of altitude above Mars is either postulated on theoretical considerations or is simulated from the earth's structure.[17,18] This uncertainty in altitude structure, in addition to uncertainties in surface conditions, compound the uncertainty

Table V

VOLUMETRIC COMPOSITION OF MARTIAN ATMOSPHERE

	KAPLAN[14]			SPIEGEL[15]		deVAUCOULEURS[16]	MARINER IV OCCULTATION EXPERIMENT[10,11]		
	10 mb* (percent)	25 mb* (percent)	40 mb* (percent)	41 mb* (percent)	133 mb* (percent)	85 mb* (percent)	4.9 ± 0.8 mb* (percent)	5.1 ± 1.1 mb* (percent)	6.0 ± 1.0 mb* (percent)
CO_2	60	16 16	8 7	0.7	7.2	0.3	100	80 100	50
N_2	20	76 8	45 88	98.7	86.8	98.5	--	20 --	--
A	20	8 76	47 5	0.6	6.0	1.2	--	20 --	50

* Surface pressure.

in man's knowledge of the Martian atmosphere. For example, the decrease of gas density from the surface to an altitude of 120 km may be two orders of magnitude for one model and six orders of magnitude for another model.[19]

b. Nose-Cone Types

1) Basic Configurations

The design of capsules for early planetary entry explorations appears to be based upon high drag, small exposed surface area, and sufficient payload volume. The ideal shape for maximum drag per unit surface area is a flat plate, while a sphere is preferred for maximum volume per unit surface area. A compromise of these shapes is the blunted vehicle such as the Apollo or a shallow blunted cone. The resulting ratio of surface area to drag is typically 0.6 to 0.8.[20]

A spherical entry capsule has been proposed to measure the atmosphere-density as a function of entry time, using the equation of motion.[21-23] The spherical shape is preferred because of symmetrical aerodynamics, as the aerodynamic coefficients of a sphere are insensitive to angle of attack. The diameter of a ballistic entry sphere for Mars applications has been estimated to be 2 to 8 feet based upon an 11-mb surface pressure and vertical entry at 25,000 ft/s.[20]

The importance of blunt entry bodies rather than slender pointed cones of less drag is that deceleration will occur as soon and as high as possible in a planetary atmosphere. However, blunt bodies undergo periods when radio communication is prevented by plasma attenuation.[24] This condition is commonly called radio blackout.

2) β Effects

The weight-to-drag ratio β of an entry capsule and the structure of the atmosphere determine the altitude of peak aerodynamic heating and the total entry flight time. These factors in addition to vehicle shape determine the period during which radio communication is possible.

The retrodirective antenna may be advantageous over a conventional antenna by reducing communication system weight and thus reducing β. In the following discussion, reduction in β is shown to increase entry time and possibly time available for radio communication.

A systems tradeoff study based upon the weight of a retrodirective antenna and a conventional antenna is discussed in Sec. II-G.

The effect of β on velocity slowdown and entry time are illustrated in Figs. 1 and 2. Exponential and isothermal atmospheres are assumed with pressure and density profiles proportional to $e^{-h/25}$, where h is altitude in kilofeet. A flat earth is assumed, an assumption correct only for vertical entry.

In Fig. 1, velocity slowdown for vertical entry is plotted as a function of pressure and β. Slowdown required to eliminate plasma effects on radio communication is shown as being between 0.3 and 0.5 V/V_E (velocities $\lesssim$ 10,000 ft/s). This velocity interval is representative if only ionization due to aerodynamic heating is significant. The pressure scale is converted on the left into an altitude profile for the earth's atmosphere and for Mars atmospheres corresponding to a 40-mb surface pressure and to a 4-mb surface pressure.

A typical minimum payload for an entry capsule is β = 5 lb/ft^2, corresponding to a power supply and a communication system. A β of 5 lb/ft^2 in Mars atmosphere corresponds to β' = 1.9 lb/ft^2 for vertical entry and 0.65 lb/ft^2 for 20° entry angle.

Plasma effects, β = 5 lb/ft^2, for vertical entry are estimated in Fig. 1 to exist to altitudes of $\approx$63 kilofeet for the 40-mb Mars atmosphere and $\approx$13 kilofeet for the 4-mb Mars atmosphere. For a 20° entry the altitudes are increased to $\approx$100 kilofeet (40 mb) and $\approx$40 kilofeet (4 mb). These estimates of altitudes where plasma effects are assumed negligible can be considered representative for ballistic entry only if ablation does not modify the entry plasma. Under realistic conditions, chemical ionization caused by ablation products may predominate over thermal ionization caused by aerodynamic heating. The effects of ablation should be considered in future work, as ionization caused by ablation could reduce the aerodynamic advantages of decreased β and decreased communication system weight.

Figure 2 illustrates the constraints of minimum payload and communication time on β for Mars 4-mb and 40-mb atmospheres and for vertical entry. A minimum required communication time of 30 seconds is assumed. The 4-mb Mars atmosphere is seen to be too thin to permit sufficient slow-down for adequate radio communication. Using oblique entry

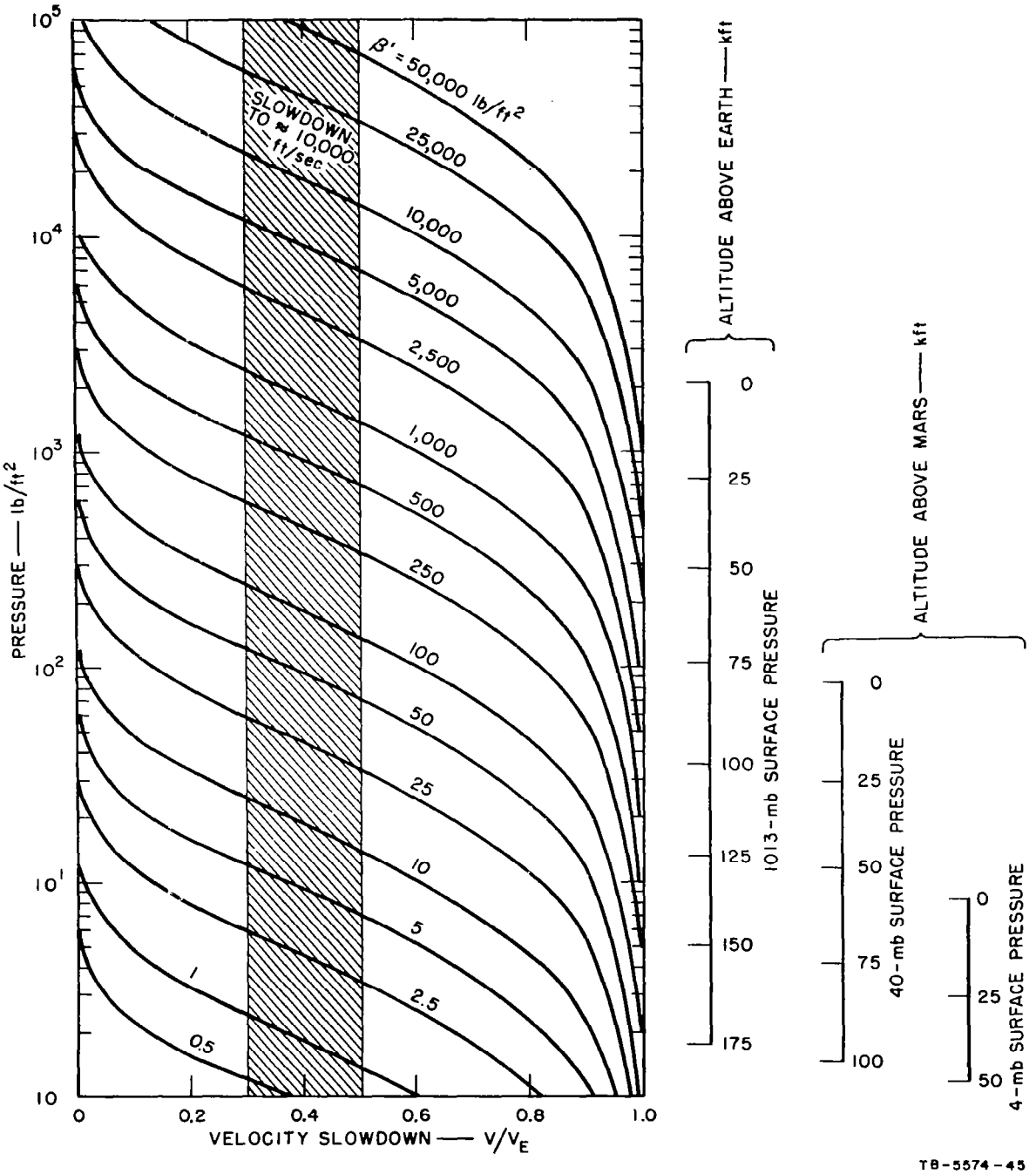

FIG. 1 ILLUSTRATION OF β-EFFECTS ON VELOCITY SLOWDOWN FOR BALLISTIC ENTRY INTO ISOTHERMAL ATMOSPHERES. Flat-earth assumption (exact for vertical entry; approximate for oblique entry).[25-27] $\beta' = (g_p)/(g_e)\,\beta \sin \psi_E$; $\psi_e > 10°$
where: g_p = Planetary gravitational constant, g_e = Earth gravitational constant, ψ_E = Entry angle

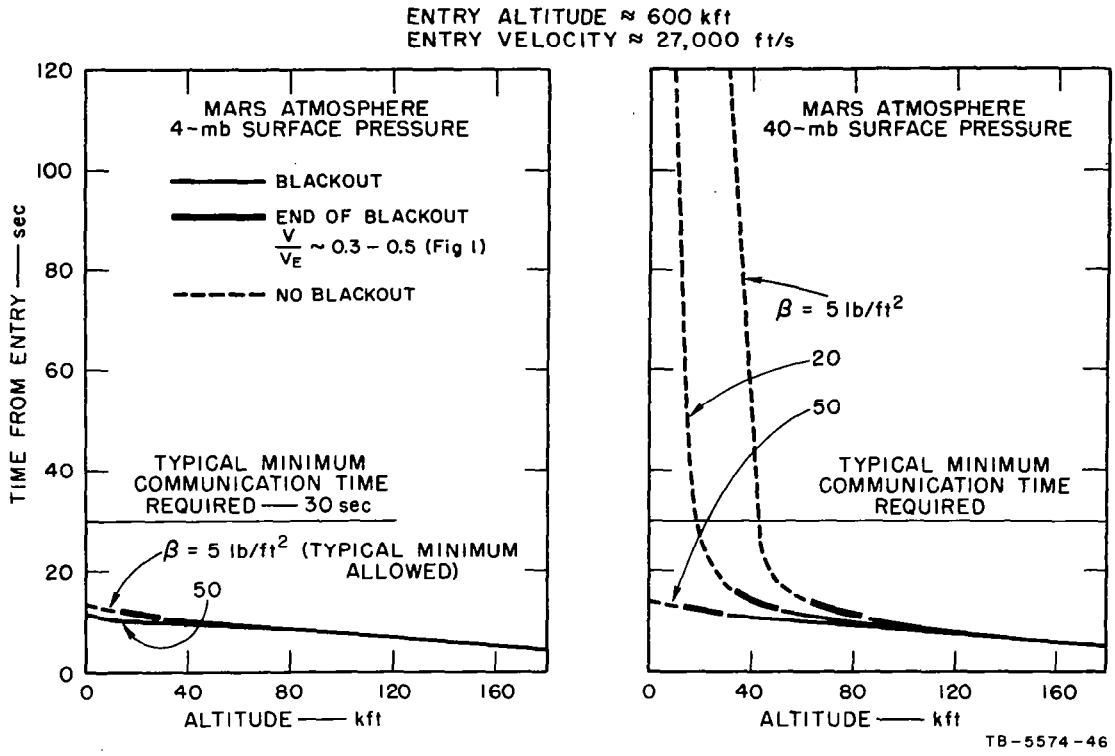

FIG. 2 ILLUSTRATION OF β-EFFECTS ON ENTRY AND COMMUNICATION TIME FOR VERTICAL BALLISTIC ENTRY INTO TWO ISOTHERMAL ATMOSPHERES

could increase radio communication time for the minimum type payload to greater than 30 seconds. However, for practical payloads > 5 lb/ft^2, the radio communication time could be less than 30 seconds.

In atmospheres such as that of Mars, where radio communication time is marginal due to uncertainties and payload requirements, parachute or propulsive braking may be required to slow the entry capsule down and to eliminate blackout. Propulsive braking, however, creates ionization through rocket exhausts, and propagation through the rocket exhaust environment is a consideration.

3) Material Effects

The effects of heat-shield ablation are difficult to assess except in flight tests. In most instances of contaminant seeding, the chemical reactions and reaction rates are not well known. Consequently, it is difficult to determine to what extent the reactions

occurring for a general material contaminant are contributing to electron production. Heat shields ablating contaminants with low ionization potentials, such as sodium (Na) and potassium (K), can significantly alter entry-capsule plasma characteristics.

Ablation can also limit the accuracy of spectroscopic measurements during entry.[28]

c. Plasma Reduction Techniques

Methods to reduce the effects of ballistic entry plasma on radio communication include vehicle shaping, antenna location, injection of chemicals, liquids, or gases, and choice of radio frequency. The use of a magnetic field to obtain propagating modes does not appear feasible because of the high collision frequencies.[29] Electric field as well as magnetic field techniques present weight constraints.

The slender cone is a vehicle shaping technique to reduce plasma effects.[24] However, the blunt body is preferred over the slender cone for planetary entry because of weight, drag, and volume considerations.

The effect of plasma can also be changed by selective location of the antenna. For example, a cone-cylinder-flare vehicle has three aerodynamic flow regimes. Plasma effects for antennas on the cone, the cylinder, and the flare (and the back of the flare) differ and vary with altitude. Thus antennas in all flow regions and retrodirectively or adaptively controlled could increase radio communication capability over that of a single antenna.

Laboratory experiments have been conducted with antennas in plasma modified by injection of liquids and gases to cool the boundary layer or increase the gas density adjacent to the antenna and by injection of chemicals to recombine or attach the electrons.[30-34] Unfortunately flight-test data are lacking for material injection except for water injection during RAM B-2 flight and Gemini GT-3 flight.[35,36]

Another method to eliminate plasma effects in communications, and possibly the best method for planetary exploration, is to choose a frequency higher than the plasma frequencies that exist during entry. Peak electron densities in entry plasmas of 10^{13} to 10^{16} el/cm^3 correspond to plasma frequencies between 30 Gc and 900 Gc. Thus adaptive antennas operating at millimeter wavelengths are attractive for radio communication in entry plasma.

3. Antenna Considerations[37,38]

a. Near-Field Effects

The modifications of antenna patterns and impedance during entry are important considerations for an entry antenna system. These parameters, not easily calculated, have been studied in the laboratory. Differences between theory and experiment can be considerable. During entry plasmas in the antenna near fields alter the antenna impedance and far-field radiation characteristics by (1) dissipating energy normally stored in near fields and (2) redistributing near fields and surface currents, in addition to the usual wave attenuation. Decreases in signal caused by the near-field effects are noticeable at frequencies slightly less than critical. Usually near-field effects are negligible at frequencies less than 0.5 critical.

Dissipation losses and reduced antenna efficiency are more severe for electrically small, high-Q dipole and loop antennas than for resonant antennas. Dissipation losses in the near field can be minimized by insulating antennas, especially the feeds, with dielectric heat shield materials.

The effect of a lossy plasma on the radiation pattern of an X-band slot antenna is illustrated in Fig. 3(a). The antenna-plasma configuration is shown in Fig. 3(b), and the electron density profile above the slot is shown in Fig. 3(c). The angle Φ_c corresponds to the critical angle for refraction based upon plane-wave theory in infinite plasma. At larger angles rays should be trapped in the plasma layer and the antenna pattern should abruptly drop to zero. The poor correlation between Φ_c based upon plane-wave theory in infinite plasma and the measured data shown in Fig. 3(a) is attributed to the finite plasma and antenna configuration.

The top curve in Fig. 3(a) corresponds to no plasma. The pattern is seen to be sensitive to peak electron density $N_{e\,max}$ in the boundary-layer profile. (Electron density N_{ec} corresponds to critical plasma frequency.) Pattern loss increases to 23 dB for $N_{e\,max}/N_{ec} = 0.85$ and to 10 dB for $N_{e\,max}/N_{ec} = 0.6$. The pattern amplitude increases for propagation along the ground plane $\Phi_c = 90°$ to within 5 to 10 dB of the amplitude at normal incidence $\Phi = 0$.

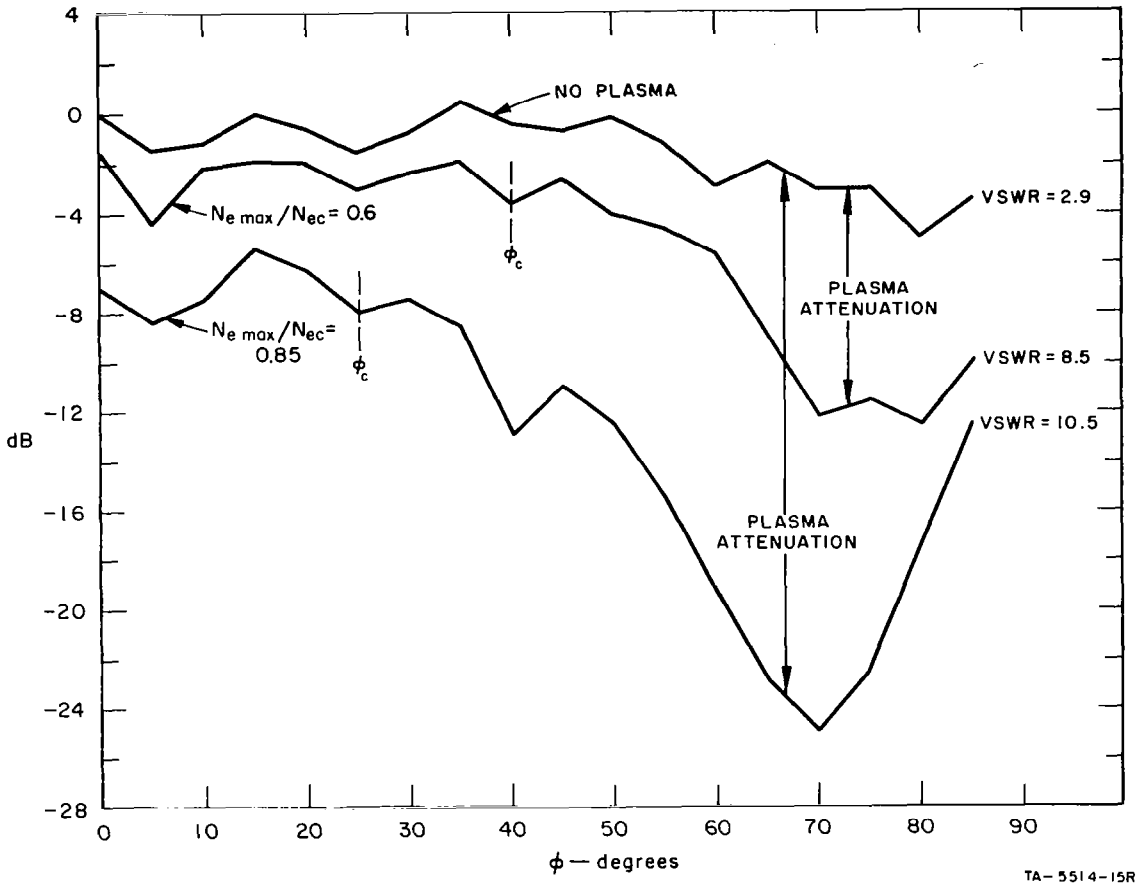

FIG. 3(a) PATTERNS OF TEFLON-FILLED SLOT COMPARED WITH FREE SPACE

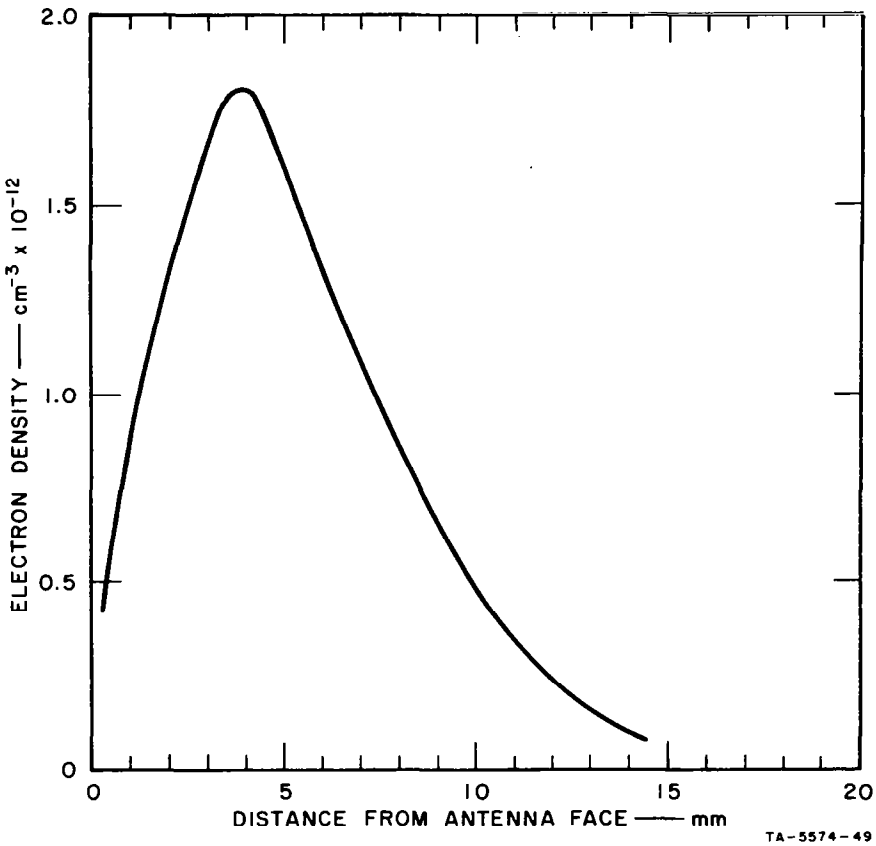

FIG. 3(b) ELECTRON-DENSITY PROFILE INFERRED FROM ION-CURRENT MEASUREMENTS

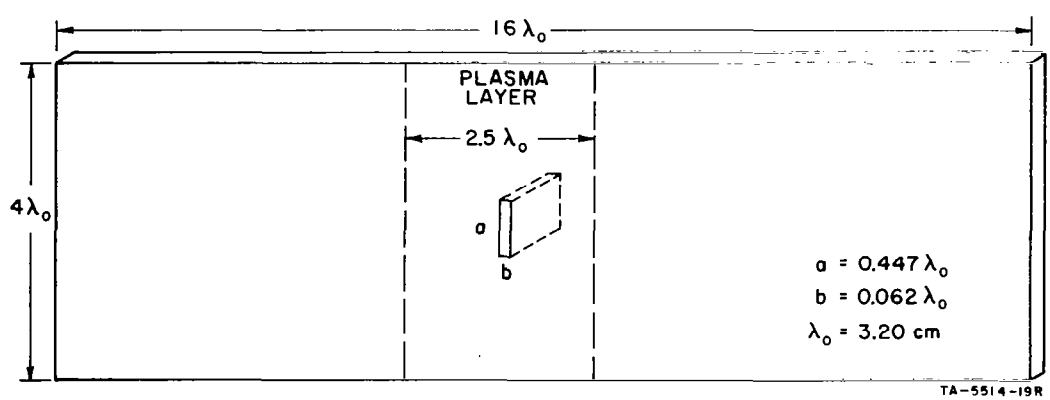

FIG. 3(c) TEFLON-FILLED SLOT WITH GROUND PLANE

Low-gain adaptive-array subapertures are preferred during entry over high-gain subapertures. High-gain antennas are more strongly influenced by plasma environment than are low-gain antennas. Thus the adaptive antenna, an array of low-gain subapertures with controlled phase, could be superior to a conventional antenna of equivalent aperture.

Antenna VSWR is also shown in Fig. 3(a); however, VSWR losses are not included in the field pattern. The power loss is 6.3 dB for the no-plasma condition, VSWR = 2.9. Additional VSWR losses occur in the presence of plasma, 4 dB for VSWR = 8.5 and 5 dB for VSWR = 10.5.

Measurements of plasma reflection coefficients are available for open-waveguide and slot antennas. Representative measurements for an open waveguide at X-band are given in Fig. 4. Large reflection coefficients that will exist during entry may place a load isolation requirement on retrodirective circuitry, as well as create a system oscillation problem.

Figure 5 shows theoretical predictions and measured values of admittance of an open-waveguide antenna at X-band. Theoretical predictions correspond to a uniform and semi-infinite plasma. The susceptance is seen to become inductive around the critical frequency $\omega_p \approx \omega$, and the conductance goes to a minimum there.

b. Antenna-Plasma Coupling

The most important limitation on a retrodirective antenna operating continuously is the isolation between the received signal and the transmitted signal. Leakage energy due to coupling between circuitry and antennas could cause the retrodirective system to oscillate under certain conditions.

In entry plasma, the principal source of coupling between transmitting and receiving circuitry may be the plasma sheath or dielectric heat shield reflecting transmitted signal back into the antenna system. Ducting in the plasma sheath can also occur. As a result, the decoupling between antennas can differ from free-space conditions. The decoupling will vary as a function of altitude during the entry penetration.

Measurements of decoupling between antennas in entry environments are lacking. Because of the complicated nature of the problem, initial consideration of antenna coupling in a plasma environment should

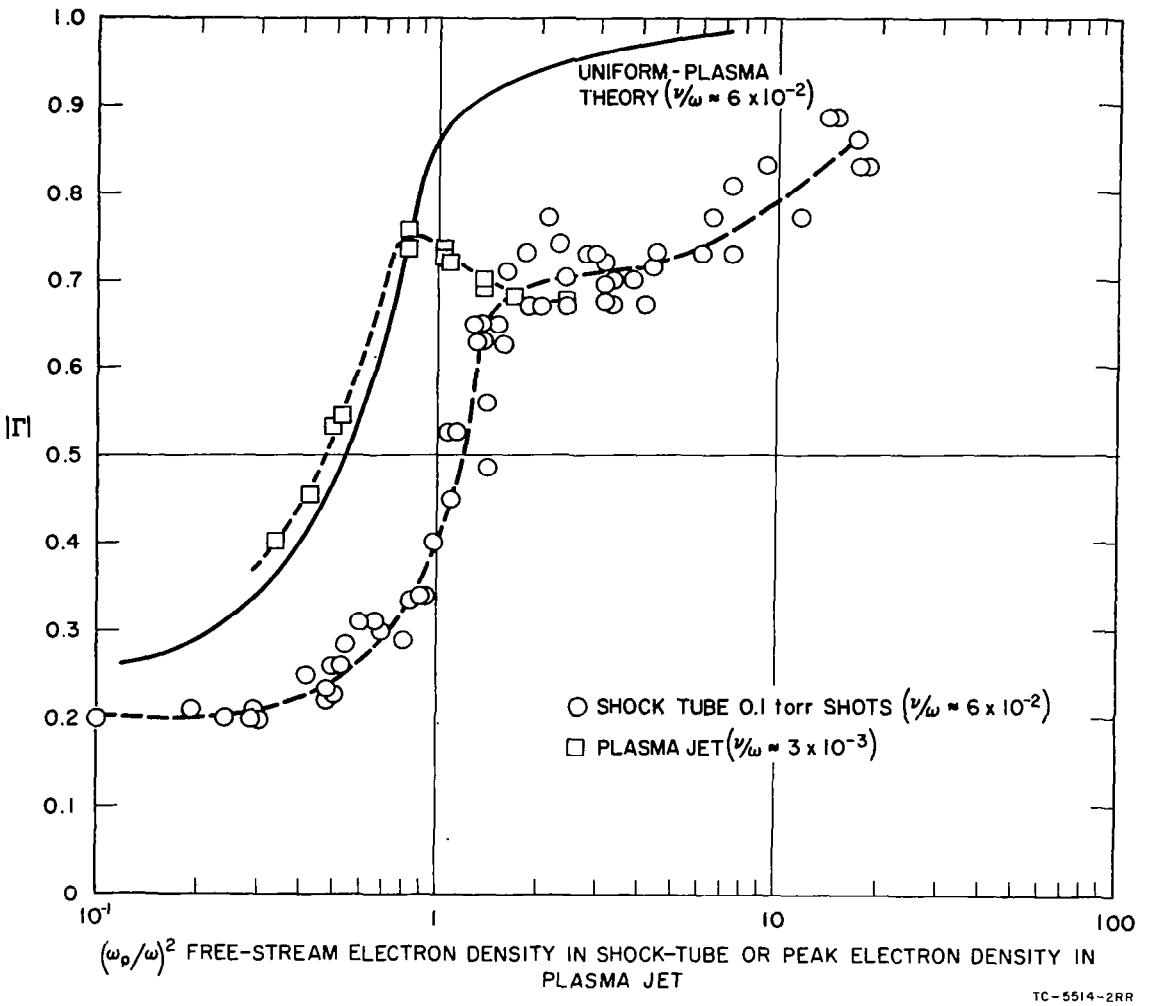

FIG. 4 REFLECTION-COEFFICIENT MEASUREMENTS OF OPEN WAVEGUIDE COMPARED WITH THEORY

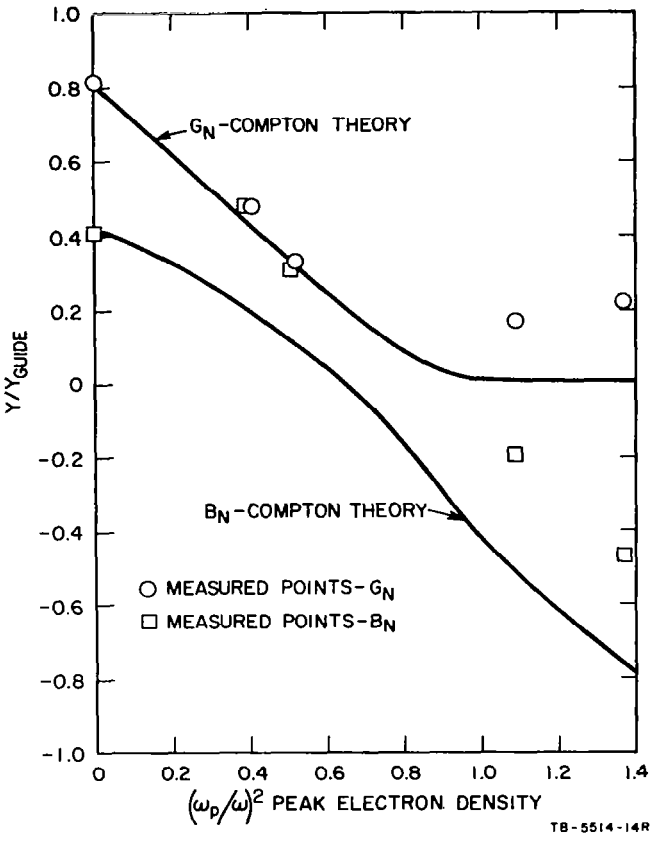

FIG. 5 MEASURED NORMALIZED ADMITTANCE OF OPEN WAVEGUIDE TERMINATED WITH GROUND PLANE IN PLASMA JET, COMPARED WITH THEORY FOR UNIFORM PLASMA

be measurements of some selected antenna configurations to obtain a feel for the magnitude of the effect.

4. Adaptive Antenna Operation

All antenna types on an entry capsule are limited by signal loss due to plasma attenuation and near-field effects. Depending on the frequency, amplitude and phase, fluctuations can exist due to turbulence in the wake plasma. Both near-field plasma (directly over the antenna) and plasma throughout the wake are important as the capsule will be communicating essentially rearward toward the bus. Particularly important to adaptive antenna operation are the spatial and frequency correlation, magnitude, and frequency spectrum of the amplitude and phase fluctuations.

Adaptive receiving circuitry in entry capsules must be designed to handle rapid fluctuations in amplitude and phase. Fluctuation rates as large as hundreds and thousands of Hz can be expected. These rates are typically several orders of magnitude faster than fluctuations associated with tropospheric and ionospheric propagation. The rates can be comparable to Doppler shifts in frequency due to relative transmitter-receiver motion.

The characteristic scales of refractive fluctuations due to turbulence in the plasma near an adaptive antenna may be smaller than, or comparable to, the size of the subapertures in the array, and the associated phase jitter summed over the subaperture may be partially coherent or random. As a result, adaptive phase adjustment may be degraded.

The correlation of phase fluctuations at different carrier frequencies is also important when retrodirective array operation requires a shift in carrier frequency. Phase correlation in a homogeneous plasma at different carrier frequencies $f1$ and $f2$ is discussed elsewhere,[39,40] and is illustrated in Fig. 6. Phase correlation for this simple model is seen to be poor for far-zone scattering.

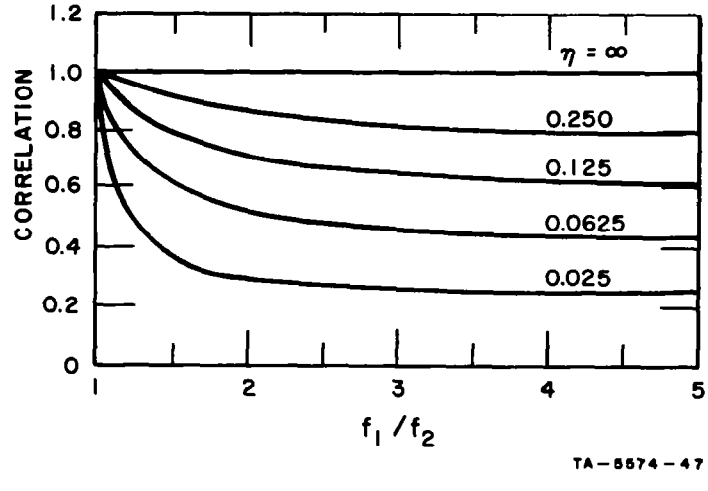

FIG. 6 CORRELATION OF SIGNAL PHASE FLUCTUATION IN A HOMOGENEOUS PLASMA AT DIFFERENT CARRIER FREQUENCIES. Note: η is a measure of whether one is in the near or far zone of blob scattering; $\eta \to 0$ in the far zone; $\eta \to \infty$ in the near zone. (Single scattering is assumed.) $f_1 = f_2 + \Delta f$ where Δf is a shift in carrier frequency.

Evaluation of the effect of wake turbulence on adaptive antenna operation would require flight-test measurements in the earth's atmosphere in order to obtain any realistic data.

5. Antenna Breakdown[41-46]

An extreme case of pattern alteration, attenuation, and nonlinearity is the voltage breakdown of gas over the antenna surface. The breakdown of antennas at low pressure has been studied in the past by various investigators. Gas breakdown is dependent upon the gas density, the electric field magnitude, and the distribution as well as the plasma configuration in the vicinity of the antenna. Representative data to illustrate these effects are presented here.

Voltage breakdown at subsonic speeds or for static conditions can be measured in the laboratory under ambient conditions. For geometrically similar antennas, frequency scaling is applicable. Aside from the usual electromagnetic similitude principle, it is required that the product of pressure and wavelength be constant.

Applicability of antenna scaling is illustrated in Fig. 7, where the tip breakdown for monopole antenna is generalized for eight monopole diameters. Minimum breakdown in a 4-mb (3 mmHg) Mars atmosphere could occur at the surface for $f \gtrsim 1$ GHz.

A study of antenna breakdown in gas compositions such as the atmospheres of Venus and Mars was conducted in 1963.[47] In simulated atmospheres defined by the Jet Propulsion Laboratory, the breakdown-power level of several typical linear and circularly polarized antennas was measured and observed to be similar to that experienced in air. Figure 8 shows representative data for a $\Omega = 7.8$ monopole. In an environment of pure Argon gas, the breakdown of an $\Omega = 5$ monopole was observed to be twice the breakdown level in air and in the gas mixtures listed in Fig. 8.

For supersonic speeds, the gas density near the antenna surface is modified from ambient conditions at high pressures and low altitudes. The degree of modification depends upon the location of the antenna relative to the flow field. Breakdown of a quadraloop antenna in a vehicle traveling at supersonic speeds is illustrated in Fig. 9, where flight test and laboratory data are compared.[48] Good agreement in initiate breakdown level is seen except at high pressures where gas density at the antenna differs

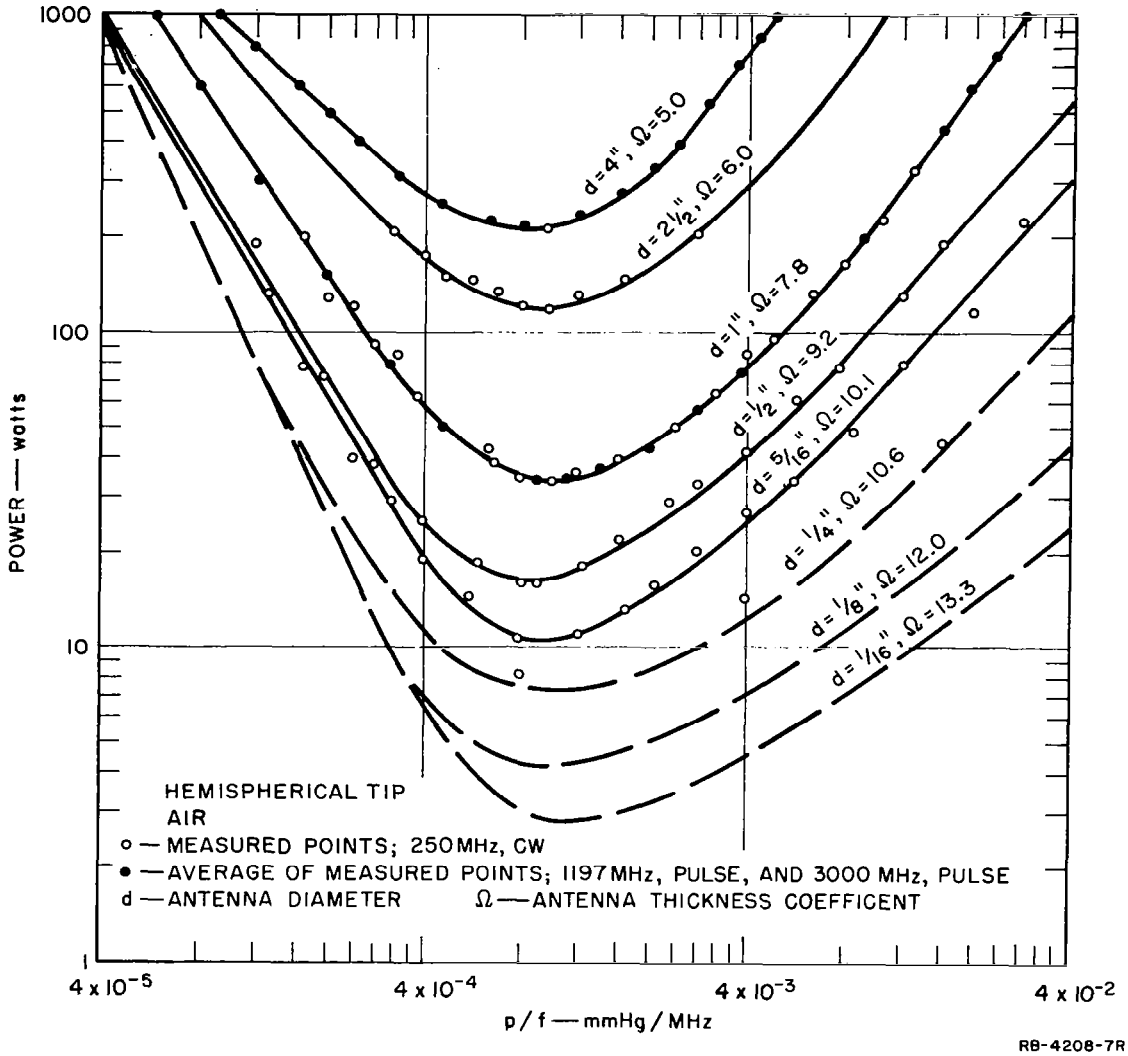

FIG. 7 POWER REQUIRED TO INITIATE BREAKDOWN IN AIR, OF 0.26λ MONOPOLES AS A FUNCTION OF PRESSURE AND FREQUENCY

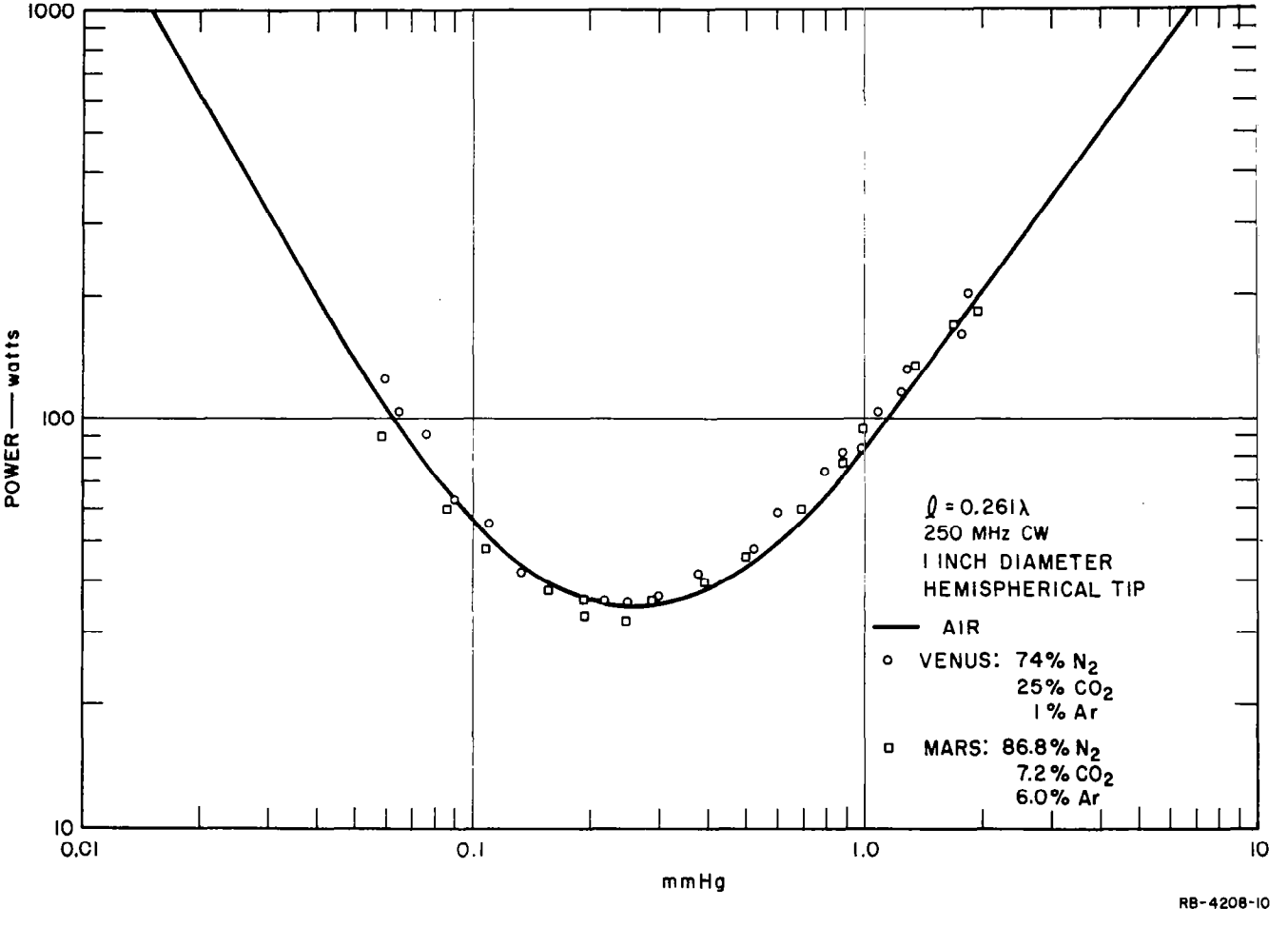

FIG. 8 MEASURED VALUES OF POWER TO INITIATE CW BREAKDOWN OF AN Ω = 7.8 MONOPOLE IN SIMULATED ATMOSPHERES OF MARS AND VENUS

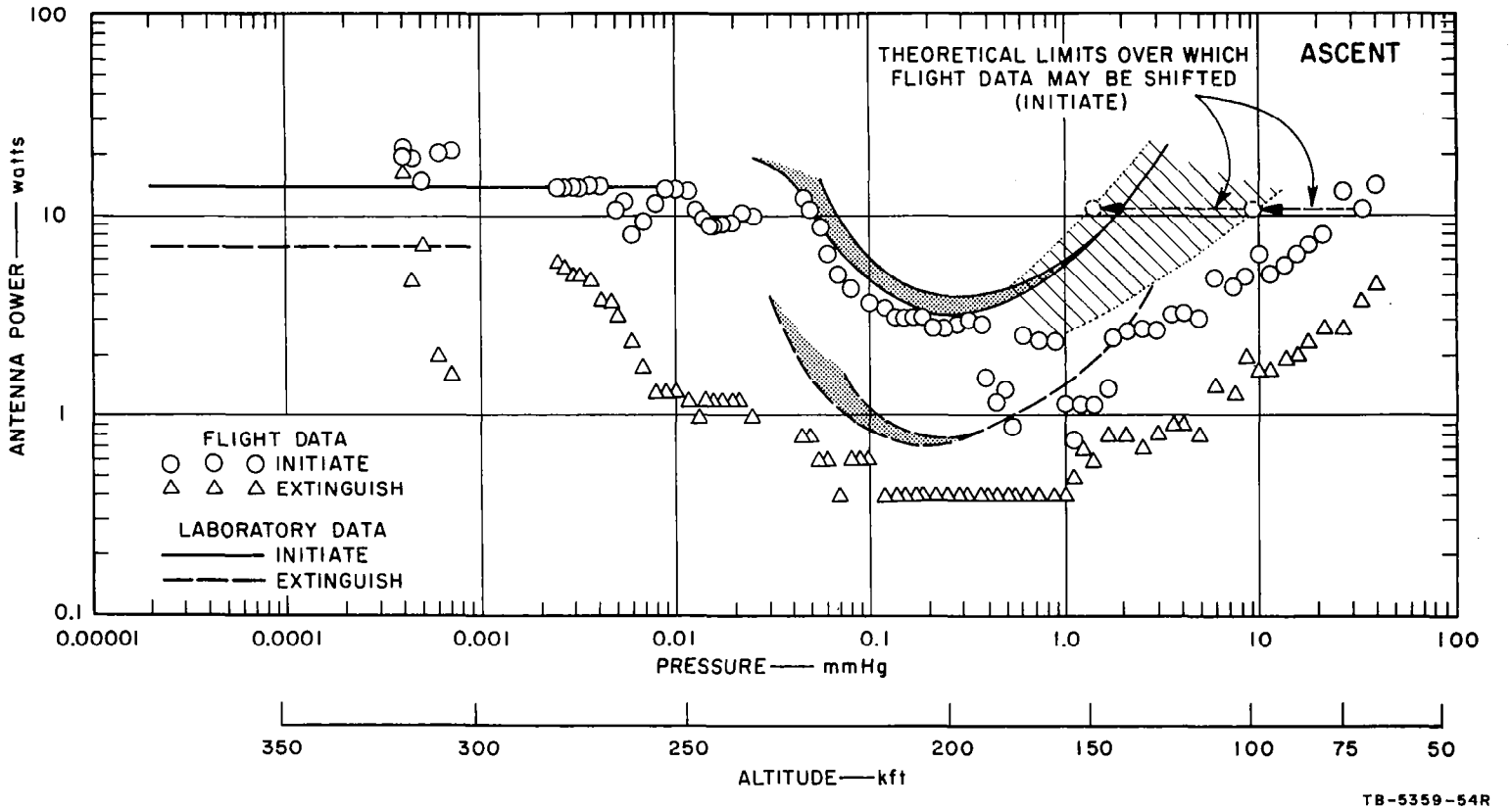

FIG. 9 VHF ANTENNA BREAKDOWN DURING ASCENT — NIKE-CAJUN ROCKET AFCRL AD 6.841

from the ambient density. Breakdown at pressures below 3×10^{-2} mmHg is of the multipactor type. Flight data, however, indicated that the multipactor discharge was modified to a gas breakdown made possible by outgassing.

In a non-ionized gas or one of a very low degree of ionization, as typified in Figs. 7, 8, and 9, the free-diffusion coefficient determines the breakdown field strength. At high altitudes, the important parameter determining the minimum field strength of antenna breakdown is the diffusion coefficient for electrons; this coefficient is radically altered if the air is already ionized, in which case the diffusion becomes ambipolar. Plasmas surrounding ballistic entry vehicles can have electron densities sufficient to make the diffusion ambipolar over most of the region of interest.

Figure 10 presents the power required for breakdown as a function of collision frequency ν. The top curve indicates the breakdown power level

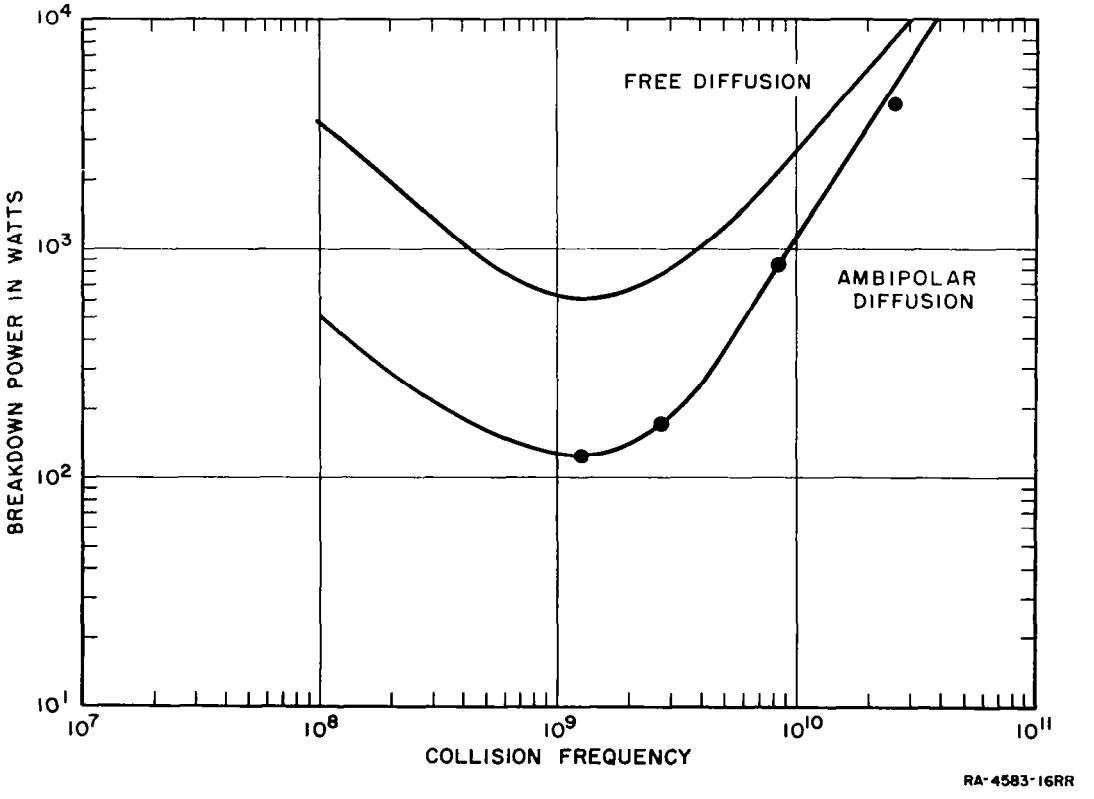

FIG. 10 BREAKDOWN CHARACTERISTICS OF 2-INCH L-BAND SLOT ANTENNA

for free diffusion D_f, and the lower curve for ambipolar diffusion D_a. In the breakdown process, the diffusion loss mechanism dominates below the minimum breakdown power point and the breakdown power is lowered by 6 to 10 dB.

In Fig. 11, the power radiated normal to an L-band slot antenna is given for various ratios of ω_p/ω. The collision frequency corresponds to the minimum breakdown power. When the plasma is such that $\omega_p << \omega$

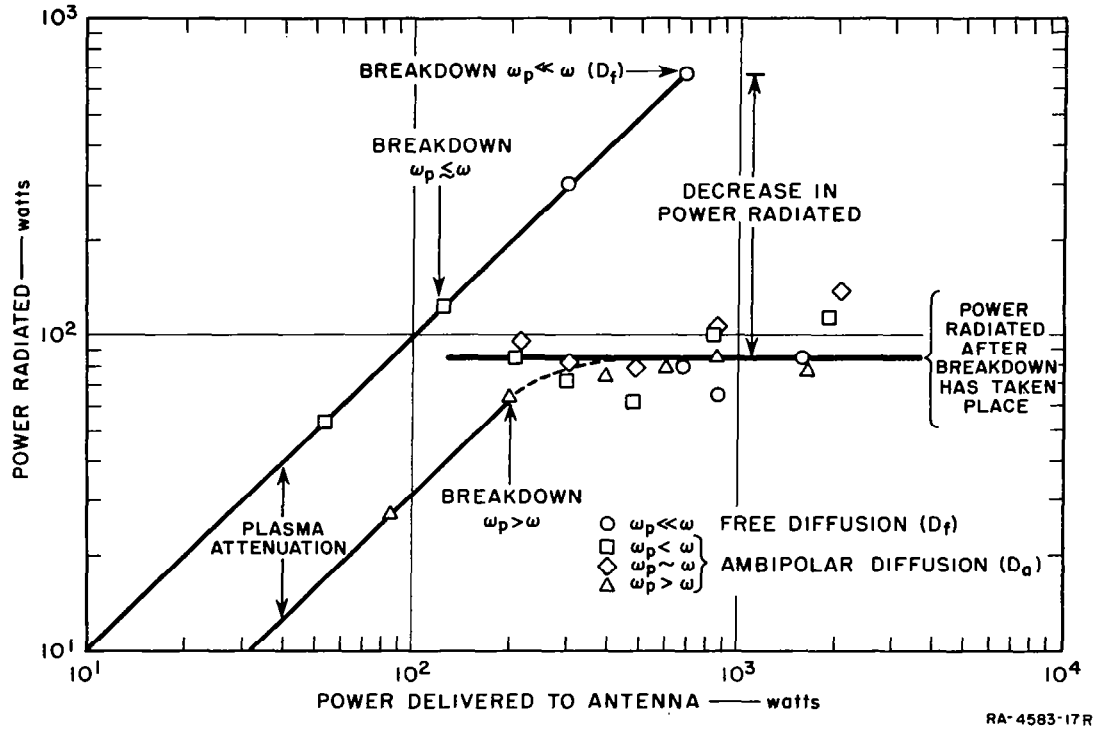

FIG. 11 POWER RADIATED NORMAL TO AN L-BAND SLOT ANTENNA AT $\nu = 1.3 \times 10^9$ FOR VARIOUS RATIOS OF ω_p/ω

and the electron loss is by free diffusion, the change in the plasma is abrupt and the power radiated typically decreases by an order of magnitude. When $\omega_p \leq \omega$ and the diffusion is ambipolar, the decrease in the radiated power is only a few decibels, since the initial breakdown level has now decreased. In the case where $\omega_p > \omega$, the transition to the nonlinear plasma condition is gradual, with no abrupt change in signal level. As the power is increased beyond the breakdown level, the

additional power is absorbed in the plasma, which grows in extent as power delivered increases.

Typically slot antennas can be designed to handle 100 watts or more output power at microwave frequencies without experiencing voltage breakdown under conditions of free diffusion. However, in a practical entry environment where ambipolar diffusion conditions exist, the power-handling capability may be only a few watts.

There are two ways to increase the power-handling capability of antennas in the plasma medium. One is to alter the antenna field configuration, and another is to modify the environment over the antenna. In order to increase the power that can be radiated from a given aperture, the amplitude of electric field per unit power in the aperture must be reduced. This could be accomplished, for example, by increasing the size of the antenna aperture. However, increasing the aperture to reduce the field introduces problems. As the aperture gets larger, it becomes more difficult to control the phase and amplitude of the field to ensure the proper pattern. Thus, the antenna pattern becomes more susceptible to the plasma environment existing over the surface. The retrodirective antenna alleviates this problem by distributing power over a number of subapertures rather than a single aperture, and by controlling phase.

E. Planetary Reflections

1. Description

Major parameters determining surface reflection characteristics are surface roughness, angle at which the transmitted signal is incident, signal polarization, radio-wave frequency, and the complex dielectric constant of the reflecting surface. The effect of reflections on a particular antenna system is dependent upon surface reflection characteristics and upon the geometry and relative motion of the transmitter, the reflecting surface, and the receiver, and upon the transmitting and receiving antenna patterns.

A specularly reflected field, associated with smooth surfaces, is directional and obeys the laws of classical optics. The reflected field is coherent with the incident signal.

Diffuse reflection associated with very rough surfaces and multiple scattering has little directivity and usually is smaller in amplitude than specular reflection. The diffuse reflected field is incoherent with the incident signal. Surface roughness can be described from the measured reflected field.

Smooth surfaces are normally theoretically hypothesized as a continuous surface with a root-mean-square surface roughness less than a wavelength. The Rayleigh criterion for a smooth surface suggests that the rms vertical scale of surface irregularities is less than $\lambda/8$ at normal signal incidence and λ at a signal incidence angle $\approx 7°$. At grazing incidence the concept of roughness ceases to exist. Conversely, rough surfaces (diffuse reflection) have rms surface roughness dimensions in many wavelengths.

The reflected field due to multiple scattering from a rough surface is approximately independent of polarization. A smooth surface also modifies the polarization of the incident field, as the reflection characteristics for the orthogonal polarizations usually differ.

Of primary importance to coherent scattering is the surface area or horizontal surface length over which reflection is averaged—*e.g.*, the area and diameter of the first Fresnel zone. At planetary distances and at normal incidence the diameter of the first Fresnel zone is $\sqrt{2\lambda a}$, where a is the radius of the planet. When the receiver or the transmitter, or both, are located near the planetary surface the diameter is $\sqrt{2\lambda r}$ where r is the minimum range to the reflecting surface.

The Fresnel zone diameters for earth-to-planet distances (typically 10^7 ft) and for a bus orbiting 10^5 to 10^6 ft above a planet are comparable to an order of magnitude. Thus, planetary scattering measured from the earth should be indicative of scattering characteristics at a planetary bus.

The Fresnel zone diameter for an entry capsule decreases as the capsule approaches the planetary surface—*e.g.*, at 1 GHz a diameter of 140 ft at an altitude of 10^4 ft and 45 ft at an altitude of 10^3 ft. Conceivably, specular reflection could occur when capsules are near planetary surfaces such as sometimes is the case for aircraft communication near the earth, communication from a mountain ridge to a valley, or communication over water or iced landscape.

2. Experimental Data

Pulse measurements of backscattering from the moon at 3000 MHz indicate that the moon is a rough surface and a diffuse scatterer at that frequency.[48] The pulse shape and fluctuation can be explained by diffuse reflection rather than by specular reflection from several smooth areas on the moon's surface. Measurements at 400 MHz, however, indicate that the radar echo from the moon is a combination of specular reflection from a quasi-smooth surface and diffuse reflection from a rough surface, with the former predominating.[49-51] The power reflectivity of the moon for CW and long-pulse transmission (pulse length $\lesssim 200$ μs) lies between 0.1 and 0.01.[52,53] The reflectivity is reduced for short pulses, which see a smaller cross-section than larger pulses. The power reflectivity corresponding to a pulse of 5 μs duration or shorter is typically 5×10^{-4}.

Venus is a better reflector than the moon, with a power reflectivity of 0.10 to 0.15 (CW and long-pulse transmission).[53] Radar measurements indicate that the roughness of Venus is comparable to the roughness of the moon.

Thus, planetary surfaces should have rms surface roughness dimensions in many wavelengths at frequencies considered for retrodirective arrays on space vehicles (frequencies $\gtrsim 1$ GHz). The power reflection coefficient of rough planetary surfaces should typically be less than 0.1.[53] Signals reflected from the surfaces will be diffuse and will statistically fluctuate in time due to the rotation of the planet and the movement of the space vehicle. The statistics of fading could in general be described by the Rayleigh distribution.

The fluctuations in the reflected signal from the planet will be correlated at all retrodirective array subapertures. As a result of this signal correlation, the retrodirective antenna, if it were to handle only signals reflected from the planet, would still produce a coherently summed signal at the distant (Earth) receiving station (assumed to be located at the pilot transmitting station). There would, however, be a superimposed phase and amplitude modulation, which would be a function of the surface roughness and the relative rotation of the planet and retrodirective link. When the direct link between the Earth station and the vehicle is also considered, the planetary reflected signal will not be correlated with the direct signal.

3. Received Signal Power

The signals received at retrodirective array subapertures interrogated by both direct and planetary reflected signals will be uncorrelated and will add in power. The received power at subapertures interrogated by only a planetary reflected signal will be a maximum of 10 percent of the power received by those apertures directly interrogated, assuming a 10-percent power reflectivity at the planetary surface.

Thus the signal power received at the terminal receiving antenna, assuming that all subapertures under consideration are interrogated by both direct and planetary reflected signals, might fluctuate as much as 0.5 dB above the nominal level if no planet existed. If half of the subapertures are interrogated by direct signals and half by planetary reflected signals (*i.e.*, when the vehicle is near the line joining the planet and the terminal station), if the vehicle is near the planet, and if equal power output is directed at all activated subapertures, the power received could be 55 percent of the power received if no planet existed. Roughly 3 dB gain in power could be obtained by activating in the transmission mode only subapertures interrogated directly.

Activating only selected subapertures in the transmission mode would require a signal-to-noise sensing device that activates the transmitting circuit only above a minimum threshold. The minimum threshold could, for instance, be 10 or 20 percent of the maximum subaperture signal-to-noise ratio.

Diffuse planetary reflections can modify the "free-space" retrodirective antenna pattern. The power pattern can thus vary by 10 percent of the maximum level.

In the event an entry capsule is close to a planetary surface and specular reflection occurs, the power-reflection coefficient should typically be less than 0.25 (except, for example, over good reflectors such as smooth ice caps). The corresponding variation in signal power at retrodirective subapertures could be as large as +6 dB to -3.5 dB relative to the signal power received directly. The variation is similar to that for a conventional antenna. Unless constant signal levels are radiated from the retrodirective subapertures, the signal power received at the pilot station could vary as much as +12 dB to -7 dB. Fortunately, in the frequency range being considered, diffuse scattering is to be expected.

4. Spectral Broadening

Signals reflected from rough planetary surfaces will be spread in Doppler frequency. The characteristics of the Doppler spread are dependent upon surface roughness characteristics and upon relative motions of the transmitter, the receiver, and the planet.

Doppler spread, if planetary rotation determines the relative motion of the planetary reflecting surfaces and the elementary scatterers, can be in order of tens of Hz for the moon, Venus, and Mercury, thousands of Hz for Mars, Pluto, and Neptune, and hundreds of thousands of Hz for Jupiter and Uranus.[53] If the relative surface and scatterer motion is determined by spacecraft velocities (transmitter and/or receiver), the Doppler spread could be thousands of Hz.

Doppler spread may determine the minimum input receiver bandwidth and thus the maximum received signal-to-noise ratio.

F. Noise Considerations

The effects of noise in a retrodirective array should be considered in the sum signal received at the pilot station. If the subaperture circuitry has linear gain, the signals retransmitted to the pilot station may be considered as the coherent addition of signal components and the incoherent addition of noise components.

The signal-to-noise ratio, S/N, received at the pilot station from n retrodirective subapertures is represented as

$$\frac{S}{N} = \frac{n^2 K \alpha S_n}{N_{pr}} \left[\frac{1}{1 + n\gamma_n K \alpha \dfrac{T_{nr}}{T_{pr}}} \right] \tag{2}$$

where

K = Retrodirective subaperture power gain

α = Signal propagation loss between the retrodirective subapertures and the pilot receiving station (including the effects of retrodirective-subaperture-antenna transmitting gain and the pilot receiving-antenna gain)

S_n = Pilot signal level received at the retrodirective subapertures

N_{pr} = "Background" and receiver noise in the pilot receiving antenna (does not include noise radiated from retrodirective subapertures)

T_{nr} = Equivalent received noise temperature in the retrodirective subapertures due to background and receiver noise

T_{pr} = Equivalent received noise temperature in the pilot receiving antenna corresponding to N_{pr}

γ_n = Noise-compression factor in the retrodirective subaperture circuitry.

Equivalent receiving and transmitting conditions are assumed to exist at all n retrodirective subapertures.

The signal-to-noise loss at the pilot receiving station due to incoherent noise radiated by retrodirective antenna subapertures can be represented as

$$S/N \text{ (loss)} = 10 \log \left[1 + \frac{\gamma_n (S/N)_p}{n(S/N)_s} \right] \quad \text{in dB} \tag{3}$$

where $(S/N)_s$ is the received signal-to-noise ratio at the retrodirective subapertures, and $(S/N)_p$ is the received signal-to-noise ratio at the pilot station in absence of noise radiated by retrodirective subapertures. The loss in S/N is plotted in Fig. 12 as a function of n and a factor $K = \gamma_n (S/N)_p / (S/N)_s$. Considerable loss is seen unless $\gamma_n (S/N)_p < n(S/N)_s$ (or $n\gamma_n K_d T_{nr} < T_{pr}$).

It can be concluded that care should be taken in the system planning of a retrodirective communication link to prevent noise degradation such as illustrated in Eq. (3) and in Fig. 12.

G. System Tradeoffs

A retrodirective antenna is attractive in regard to increased effective radiated power capability and to reduced antenna system weight. Tradeoffs with conventional antennas can be made from a systems viewpoint.

The power radiated by a single antenna can be expressed as

$$P_r = P_i G \tag{4}$$

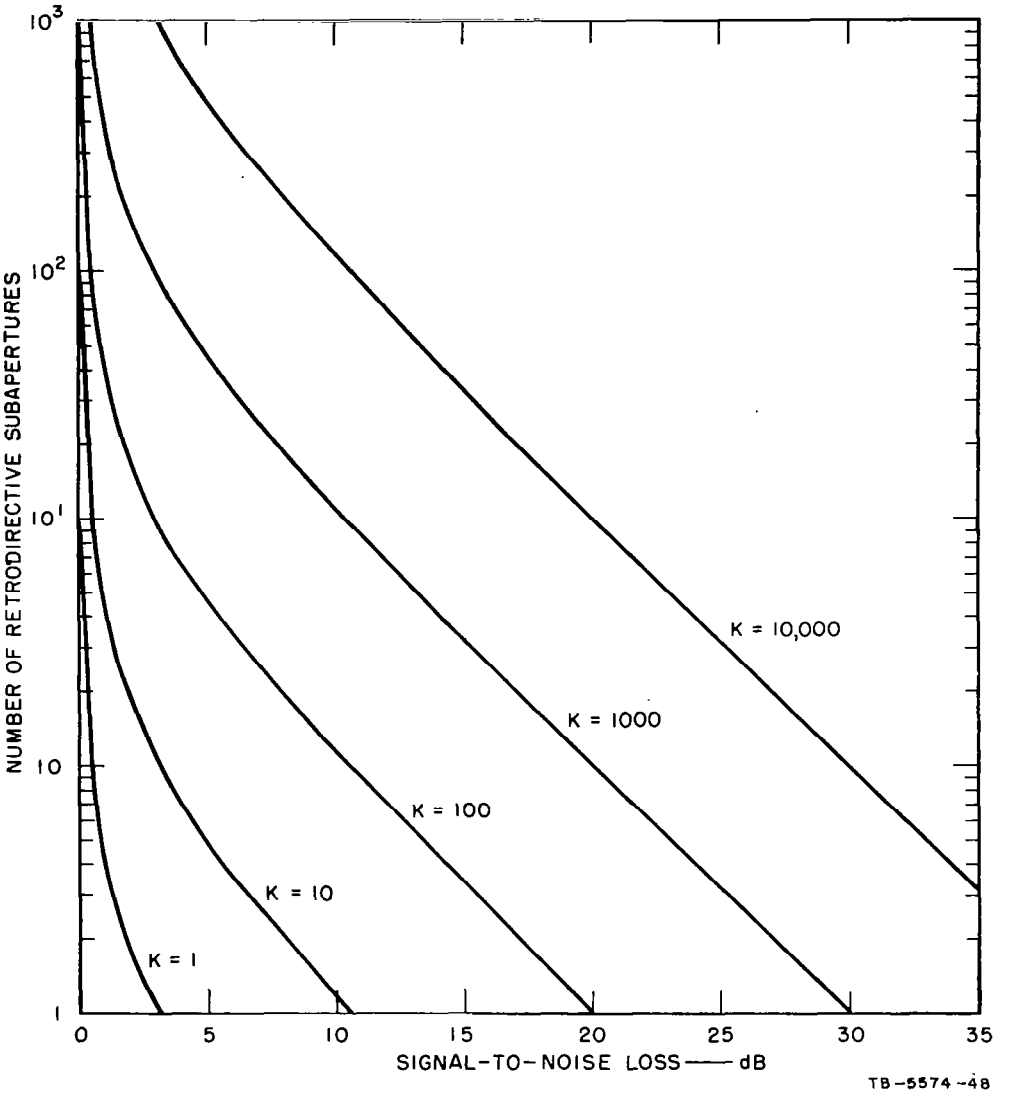

FIG. 12 SIGNAL-TO-NOISE LOSS DUE TO NOISE RADIATED BY RETRODIRECTIVE SUBAPERTURES

$K = \gamma_n \; [n(S/N)_p] / [(S/N)_s]$

where: γ_n = Factor by which noise level is reduced at retrodirective subapertures, $\gamma \geq 1$; $(S/N)_s$ = Received signal-to-noise ratio at retrodirective subapertures; $(S/N)_p$ = Received signal-to-noise ratio at pilot station in absence of noise radiated by retrodirective subapertures. Signal loss is referred to $(S/N)_p$.

where P_i is the antenna input power and G is the antenna gain. If n similar antennas of gain G are operated as a retrodirective antenna and the total output power is divided equally to all n elements, the power radiated by the retrodirective antenna for coherent signal addition can be expressed as

$$P_r' = \frac{P_i}{n} \times n^2 G = nP_i G \tag{5}$$

A gain in radiated power by a factor n is seen. Similarly, a retrodirective antenna with subapertures of gain G can radiate an equivalent amount of power as a single antenna of gain G with only $1/n$ the input power required for the single antenna.

In most cases the increase in weight in an antenna system caused by the addition of antenna elements and for the retrodirective self-phasing is more than compensated for by the saving in weight by decreasing the power subsystem requirements. However, the optimum number of elements for minimum weight can be exceeded, and additional radiated power obtained at the price of additional weight.

The weight of a retrodirective antenna, assuming a constant radiated power, may be expressed by

$$W_T = \frac{P}{n} \times W_1 + nW_2 + W_3 \tag{6}$$

where P is the power required if a single, conventional, low-gain antenna element is used, W_1 is the weight of the power subsystem per watt, n is the number of elements in the retrodirective antenna, W_2 is the weight of electronics needed per element to achieve self-phasing, and W_3 is the weight required for self-phasing and is independent of the number of elements. For convenience, W_1 is assumed constant, but it might be a nonlinear function in practice. Differentiating this expression and equating to zero to find the number of elements for minimum weight of a retrodirective array gives

$$n_{opt} = (PW_1/W_2)^{1/2} \tag{7}$$

For example, if the power P is 100W, W_1 = 1 pound/watt, and W_2 = 4 pounds, the optimum number of elements for minimum weight is 5.

The optimum number of elements increases if the weight of attitude control systems is included in Eq. (6). Vehicle stabilization may be required if only a single antenna is used. Considering an attitude-control system of weight W_4 required for a single antenna and a decrease in weight W_4 as other antennas are added and operated retrodirectively, the optimum number of antenna elements for minimum weight is

$$n_{opt} = \left(\frac{PW_1 + W_4}{W_2}\right)^{1/2} \tag{8}$$

Assuming $W_4 > PW_1$, the optimum number of elements exceeds five for the assumed values of P, W_1, and W_2 in the preceding paragraph.

A systems study such as described in the preceding paragraphs be extended to include tradeoffs relative to wavelengths and signal-to-noise ratio. For the entry case, the constraint of the ballistic coefficient and the signal loss due to near-field effects and plasma attenuation could be included if sufficient data were available.

H. Environment Measurements

1. Comparison of System Types

The adaptation of retrodirective antennas to space missions may require the use of the antenna for scientific measurements and antenna functions other than a radio relay. A comparison of frequency and phase characteristics of a retrodirective antenna and of radar and transponder systems indicates no essential difference in the frequency characteristics of the systems, provided the retrodirective signal frequency is shifted at array subapertures.

Without a frequency shift, the Doppler frequency characteristic in the retrodirective signal may cancel. Such a condition could exist with conjugate networks that operate from a self-stabilized local oscillator having a frequency of twice the received (and therefore the transmitted) frequency. One method of retaining the Doppler information without shifting signal frequency is to stabilize the local oscillator by means of the incoming signal, which is already shifted by the one-way Doppler frequency.

Phase characteristics of the retrodirective, radar, and transponder systems are also similar except that the return-path phase characteristics

and the pilot-path phase characteristics of the retrodirective signal are opposite in sign. This is important in that time-coherent refractive effects near the retrodirective antenna may cancel for retrodirective types in which the carrier frequency is not shifted.

If the frequency is shifted in a retrodirective array, the phase characteristic φ for short and equal paths is

$$\varphi = 2\pi\Delta f/c \int n\,dl$$

where Δf is the shift in signal frequency f, c is the velocity of light, n is the refractive index in the propagation medium along the element of path dl. This phase characteristic, except for frequency magnitude, is comparable to the transponder system where

$$\varphi = 2\pi f/c(2 + \Delta f/f) \int n\,dl$$

and to a monostatic radar where

$$\varphi = 4\pi f/c \int n\,dl \quad .$$

The retrodirective phase characteristic is similar to the phase-difference characteristic in a two CW-frequency radar-range measurement.[54] The maximum unambiguous range is $f/\Delta f$. For a 1-percent increase in carrier frequency, the maximum unambiguous range is 10 wavelengths or 10 cycles of phase.

Fluctuating refractive effects are known to limit accuracy of the antenna systems. In particular, Doppler fluctuations caused by refractive fluctuations in an entry wake or in a rocket exhaust may be incoherent with frequencies comparable to or greater than the vehicle Doppler shift. Ideally, the retrodirective antenna has an advantage over other antenna types by cancelling time-coherent phase fluctuations near the antenna. This advantage is not obtained with signals that are not correlated across the aperture.

2. Environment Measurements

Environment measurements using radio signal characteristics involve principally measuring Doppler frequency and phase. From these measurements, the refractive properties and associated parameters of planetary atmospheres can be predicted. Signal amplitude is useful in determining

radio absorption in the environment. The measurement of planetary surface characteristics requires radar antenna types (retrodirective antennas are not applicable). Signal amplitude phenomena defined as refraction gain, rate of change in refraction gain, and Fresnel stretch are useful in occultation type experiments.[55]

The relations of Doppler frequency and phase characteristics to the refractive index of a planetary atmosphere in a retrodirective antenna signal are as follows:

Doppler

$$f_d = \frac{\Delta f}{c} \int_{path} n\dot{d}/dtdl \tag{9a}$$

Phase

$$\varphi = 2\pi\Delta f/c \int_{path} ndl \tag{9b}$$

A shift in carrier frequency Δf is assumed, and pilot and return paths are assumed to be equal.

The refractive index n in the lower atmosphere of a planet (troposphere) is related to the surface refractivity N_s by

$$n = 1 + N_s \times 10^{-6} \tag{10}$$

Measurements of Doppler shift or phase yields surface refractivity and the decay of refractivity with increasing altitude (scale height).

A measure of scale height, in addition to a knowledge of surface temperature and surface gravity,* permits the mean molecular weight at the surface to be predicted. Mean molecular weight m provides a relation between the density n_v of different gas constituents:

$$\sum_{v=1}^{m} (m_v - m)n_v = 0 \tag{11}$$

* Temperature is fairly well known from measurements of radiation at centimeter and infrared wavelengths. Surface gravity can be found with good precision from orbital perturbations during fly-by missions.

where v refers to the vth constituent, and m is the number of constituents. Surface refractivity is related to surface density by

$$\sum_{v=1}^{m} \alpha_v n_v = n_s \tag{12}$$

where $\alpha_v n_v$ is the refractivity for expected planetary gases. Surface pressure is obtained from mean molecular mass, temperature, and density.

In a molecular medium, the group and phase velocity are synonymous, since, in the frequency range of interest, the index of refraction is independent of frequency. For an ionosphere, however, the refractive index is a function of frequency and is represented as

$$n^2 = 1 - (f_0/f)^2 \tag{13}$$

or

$$n \cong 1 - \frac{1}{2}(f_0/f)^2 \tag{14}$$

where f_0 is the plasma frequency. At the frequencies under consideration, the ionosphere is equivalent to a plasma in which magnetic field and electron collisions do not exist or are negligible. The plasma frequency in the ionosphere is related to the electron density and is an alternative way of expressing it. Numerically, the critical frequency f_0 is related to electron density N_e as

$$f_0 = 9 \times 10^{-3} N_e^{1/2} \quad \text{MHz} \tag{15}$$

for N_e in elec/cm^3.

For bus-earth occultation-type experiments at DSIF frequency, current tracking-data noise accuracy is reported to be 0.3 Hz in Doppler and less than 2 cycles in phase.[56] A change in Doppler frequency of 10 Hz at the surface and 2 Hz in the ionosphere are typical for the Mars atmosphere. Typically the phase path is 300 cycles (maximum) in the ionospheres and 100 to 200 cycles in the lower atmospheres. The range and range rate of a planetary bus is determined using orbit-determining techniques applied to two-way Doppler tracking data (*e.g.*, range rate accuracy to 0.005 ft/s). Frequency is stabilized to 1 part in 10^{10} for long-term

effects (0.2 Hz at 2 GHz) and one part in 10^{11} for short-term effects (0.02 Hz at 2 GHz), which is most important. Phase fluctuations in the earth's atmosphere appear as phase and Doppler bias on data. However, changes in bias during periods of interest (such as 1 min for the lower atmosphere) are small compared to tracking data accuracy. Equipment errors should also be negligible.

It is apparent that if a retrodirective antenna is to be used for bus-earth measurements of refractive effects in planetary atmospheres, phase anomalies must be predicted to 2 cycles in magnitude and 0.3 c/s in fluctuating frequency. If these accuracies cannot be obtained, a conventional high-gain antenna would be preferred over the retrodirective antenna. Possible causes of phase anomalies in the retrodirective signal are non-linear effects, power gain and mutual coupling at retrodirective subapertures, and planetary reflections.

The feasibility of measuring refractive properties in planetary atmospheres using a capsule-bus retrodirective signal is determined by a number of factors. First, refractive characteristics of entry plasma must be negligible in comparison to the ambient atmosphere. The degree to which plasma effects are negligible for an entry capsule is difficult to assess and would require an extensive analysis of the entry signal data. Second, the accuracy to which refractive effects can be measured is determined by the accuracy to which spatial and time-varying coordinates can be determined. Measurement or prediction of these coordinates must be made independently of the retrodirective system or other system used for the refractive measurements. Third, the choice of frequency and the relative capsule-bus motion determine the magnitude of refractive effects.

Change in phase due to refractive effects in the lower atmosphere of a planet is directly proportional to frequency. A change of 100 cycles (typical for lower planetary atmosphere) at 1 GHz corresponds to a change of 1000 cycles at 10 GHz. In an ionosphere, the change in phase is inversely proportional to frequency. A maximum phase change of 300 cycles (typical for a planetary ionosphere) at 1 GHz corresponds to change of 30 cycles at 10 GHz. Measurements of phase change in a planetary ionosphere do not appear to be feasible at millimeter wavelengths where the change in phase is comparable to or less than measurement accuracies.

Refractive measurements with subsonic range rate between capsule and bus do not appear to be feasible. Assuming a refractivity of 300

(typical at the earth's surface), the change in Doppler is 100 Hz at 3.3 GHz for a relative bus-capsule range-rate of 10,000 ft/s (velocity where plasma effects cease). At subsonic velocities $\lesssim$1000 ft/s the Doppler shift is less than 10 Hz.

Ionospheric measurements are not feasible at range rates comparable to capsule entry velocities and at microwave and millimeter frequencies. In an ionosphere with a maximum plasma frequency of 10 MHz, the maximum change in Doppler is 0.2 Hz at 3.3 GHz for a range rate of 10,000 ft/s.

I. Conclusions

Environmental constraints on retrodirective antenna operation are more serious for the entry capsule than for the orbiting or fly-by bus. Signal characteristics (amplitude, phase, and frequency) for the earth-bus link are readily calculated within reasonable limits.

Signal characteristics for adaptive antennas and for conventional antennas on an entry capsule are not easily predicted, owing to uncertainties in the atmospheric structure and composition and in the plasma surrounding the capsule. A particular problem of entry pertaining to the retrodirective antenna and requiring experimental investigations is antenna-plasma coupling. Important to all types of adaptive antennas are the spatial and frequency correlation, magnitude, and frequency spectrum of the refractive fluctuations in the entry wake and rocket exhaust. Evaluation of adaptive antenna operation on an entry capsule will require flight-test measurements in the earth's atmosphere. Initial measurement of antenna-plasma coupling could be performed in the laboratory to obtain a feel for the magnitude of the effect.

Antennas operating at millimeter wavelengths are an attractive means of reducing or eliminating effects during entry. Millimeter-wave frequencies are comparable to critical plasma frequencies that are estimated to exist in the plasma sheath surrounding entry capsules. A study should be conducted to define the capabilities and problems of millimeter communication on space vehicles and to document the state of the art for millimeter antennas and communication equipment in the time frame of planetary exploration. A major problem associated with millimeter communication is signal acquisition with narrow-beam antennas.

The retrodirective antenna system may be superior to other antenna types in radiating more signal power per unit weight of the combined antenna, power-supply, and attitude-control systems. A system weight saving using a retrodirective antenna on an entry capsule could increase the entry time available for successful communication beyond the time available using a conventional antenna. A study is recommended that would consider tradeoffs between retrodirective antennas and other antenna types. This study could complement the millimeter-antenna-system study suggested above.

Voltage breakdown of antennas on entry capsules may occur at the surface of planets with thin atmospheres such as Mars. Antenna voltage breakdown, in addition to plasma signal attenuation and antenna near-field effects, will determine the maximum signal margin of a planetary capsule-bus communication link. Multipacting breakdown in antennas on a planetary bus should not directly affect transmitted signal levels. However, mechanical damage to the antenna caused by the multipacting mechanism may occur and as a result the antenna function could be degraded or destroyed.

Planetary reflection should be diffuse at retrodirective array frequencies greater than 1000 MHz. Variations in received power should not exceed 0.5 dB except when an array subaperture receives only a planetary signal, or in the unlikely event there is specular reflection from the planet. The power received at subapertures from planetary reflection will be no more than 10 percent of the power received from the direct signal (assuming a power reflectivity of 0.1). The planetary reflected signal and the direct signal will, in general, be uncorrelated. A Doppler spread as large as hundreds of thousands of Hz can be expected in the planetary reflected signal.

The usefulness of a retrodirective array may be negated unless attention is given to noise effects in system design. A degradation in signal-to-noise ratio at the pilot receiving station can be caused by noise radiated by retrodirective subapertures. The amount of degradation is a function of the number of retrodirective subapertures, the retrodirective circuit gain, the one-way propagation-path loss, the noise compression available at the subapertures, and system noise levels.

A shift in carrier frequency at retrodirective antenna subapertures may be required if the retrodirective antenna is to be used for scientific

measurements and antenna functions other than a radio relay. The shift in carrier frequency may also be required to allow sufficient decoupling between transmitting and receiving antenna modes. With a shift in carrier frequency, the frequency and phase characteristics of the retrodirective signal are similar to the signal characteristics of a radio beacon, a radar, or a transponder. The retrodirective phase characteristic is similar to the phase characteristic in a two-CW-frequency radar-range measurement. Doppler information can be retained without a shift in carrier frequency by properly designed retrodirective circuitry. The retrodirective antenna has the advantage over conventional antennas of cancelling time-coherent phase fluctuations along pilot and return signal paths.

Limitations on a retrodirective antenna system in measuring Doppler and phase effects in a planetary atmosphere are not too severe for bus-to-earth occultation-type measurements. For the retrodirective antenna to be as effective as a high-gain dish, the phase anomalies in the retrodirective sum signal must be less than 2 cycles in magnitude and 0.3 Hz in fluctuating frequencies.

Measuring planetary refractive characteristics using a capsule-bus signal is limited principally by entry plasma effects that are difficult to predict. Other limitations include the accuracy to which spatial and time-varying coordinates can be determined, the choice of radio frequency, and the relative capsule-bus motion.

III ANTENNA CONCEPTS

A. Introduction

There has been considerable interest in adaptive antennas during the last few years. One complete issue of the Institute of Electrical and Electronic Engineers Transactions on Antennas and Propagation[57] was devoted to particular aspects of the subject. However, most attention has been paid to planar array types. This report deals with four cylindrical phased-array antenna configurations that have been studied with a view to obtaining a high-gain adaptive antenna, to apply to the problem of communicating with a spin-stabilized space vehicle. It has been assumed that the antenna should have its maximum gain in some direction that will always lie in the azimuthal plane. The analysis methods could readily be adapted to apply to pointing in any other plane making a constant (and large) angle with the spin axis (*i.e.*, conical plane) but the important point is that only one-dimensional phasing, or scanning, techniques have been considered.

Primary consideration has been given to use of each antenna as a retrodirective device. In its simplest form, the phase configuration at each element of a retrodirective antenna is obtained by mixing each incoming (pilot) signal with a common local oscillator having approximately twice the pilot frequency, and extracting the lower sideband, amplifying it, and re-radiating it. This will be referred to as a *simple* retrodirective system. It has also been assumed throughout that individual amplifier/transmitters will be used for each transmitting element where applicable, and that these would be of the all-solid-state type. Since the total RF power output from individual solid-state amplifiers at the higher frequencies is likely to be limited for the foreseeable future, the retrodirective-array configuration provides a relatively simple method of summing the output—in the correct phase—of any number of elements. However it is also necessary to use each amplifier as effectively as possible in order to maximize the effective radiated power (ERP) in the direction of primary interest—generally the retrodirection.

Of the configuration studied, at least the first two types, which use geodesic lens techniques, can be considered novel, and the first of

these received major attention because of its apparent practical advantages. Non-adaptive antennas similar to the Type-3 have been extensively analyzed by several other workers,[58-65] and Davies[66] has considered a retrodirective cylindrical Van Atta array, but these have generally had only a few radiating elements. The basic configuration has, however, apparently been developed further than any other configuration, and one version[62,67], using programmed phase control of the radiators, should be placed on a spin stabilized earth-orbiting experimental satellite in the near future. A similar version,[68] in which the axial gain is obtained by means of a biconical horn flare rather than by using stacked dipoles, is also being developed for use on a spin-stabilized, synchronous, commercial communications satellite. Because of its relative simplicity the Type-3 configuration is considered first in this report.

The fourth antenna configuration received least attention in this program, although it has some important advantages over the other three. However, it has one serious disadvantage that none of the others have. Provision must be made to switch off each of the elemental transmitters for most of each revolution of the antenna, in order to realize the maximum ERP. This problem of designing some sensing and logic circuitry that will act satisfactorily in a low signal or multipath environment is not easily solved. Also, more total power capability must be carried on the antenna than is normally used.

The study of this antenna has therefore only been of a rather general nature and no specific models (in which number of elements and other dimensions are specified) were investigated.

A very significant difference, between a spinning space antenna and one which is three-axis stablized is that the spinning, in general, modulates any signals received by or transmitted from the antenna. Since the primary purpose of the antenna is communication of information, the degree to which the spurious modulation degrades the quality of data transmission is of great importance. A fair amount of attention has therefore been given to this problem, referred to as "spectral splitting."

B. Spectral Splitting

The fact is well known that a signal having a constant single frequency transmitted from a fixed point is not received at the same frequency at a second point that is in motion. This is the Doppler effect which,

for a constant relative velocity, results in a constant frequency offset. However, the problem of Doppler shift associated with a receiver on a spinning vehicle is generally not so well appreciated although it has been studied, for instance, by Bolljahn.[69]

If an omni-azimuthal antenna is located with its axis of symmetry coincident with the spin axis of the vehicle, then the signals received by it will only be subject to the "gross" Doppler effect associated with the relative motion of the vehicle as a whole. However, a signal received on any other elemental antenna will be subjected to a combined "gross" and "differential" Doppler, the latter being related to the velocity of the element relative to the spin axis, and its instantaneous orientation relative to the direction of the communication link.

In a retrodirective system it is possible, theoretically, to eliminate virtually all the effects of Doppler shift. For instance, if all the signals received at each of the elements of a retrodirective array mounted on a vehicle are mixed with a signal having twice the frequency of the transmitted signal f_0 (*i.e.*, $f_{LO} = 2f_0$) then, the signal frequency received at the transmitting point will be $f_r = f_0[1 - (v^2/c^2)]$ plus higher-order terms, where v is the relative velocity of the vehicle in the direction of signal transmission, and c is the velocity of light.

Since v/c is of the order 10^{-4} or less for a typical mission, it can be seen that f_r is almost independent of v. Although the second-order Doppler term could perhaps be detected, it could not lead to an accurate determination of the value of v, which is essential for accurate navigation. Hence, apart from a need to separate the up and down frequencies, such a simple retrodirective system would not be satisfactory. What is desired is to retain the gross Doppler shift while eliminating the differential shift due to vehicle spin.

There are two separate manifestations of the effect of differential Doppler shift due to vehicle spin. One of them is primarily related to receiving and the other to transmitting from the vehicle. These are considered below in turn.

In the case of an adaptive receiving array antenna it is necessary for the circuitry associated with each element to adjust its phase so that when the signals from each are eventually summed, the RF (or IF) signals will all be in phase. Phase-locked loops with very narrowband filters

are often used to assist in this process when received signal strength is very low. Since, as is shown below, the spectral content of the signal received by each individual element of a spinning array is very large, a phase-locked loop may not be able to operate unless its filter bandwidth is increased, thus increasing the noise and lowering the signal-to-noise ratio associated with each element.

In the case of a purely retrodirective array, it is not always necessary that the signal-to-noise ratio be greater than unity for any of the individual elements, and in any case, it is found that the spectral content of the signal transmitted in the retrodirection can be remarkably free of spectral splitting.

The problem is discussed in the following text as it relates to each of the cylindrical configurations for which it was studied.

C. Specific Antenna Configurations

1. General

Four configurations, or types, are discussed below. Because it is simplest in concept, the first configuration to be discussed is the Type-3 antenna, so named because it was the third configuration to be studied during the program. The main limitation associated with the analysis of this antenna is that mutual coupling has in general been assumed negligible, an unlikely situation in practice. Although mutual coupling has also been neglected in the three other configurations the problem is not so serious because by good engineering design the coupling can be made very small in these three.

For practical reasons the symbols used in the analyses are only consistent for each configuration. For instance, the number of elemental transmitters is not necessarily the same as the number of line-source radiators in the Type-2 antenna, so that a symbol used for one configuration is not necessarily used in the same way for any of the others. Some confusion might therefore arise, but care has been taken to see that it is minimal.

The peak gain or directivity of any antenna—*i.e.*, the ratio of the maximum signal intensity radiated from an antenna compared with the signal level if the same power were radiated uniformly in all directions, is of primary concern. However, in the case of a space-borne retrodirective

array, for instance, the effective radiated power (ERP) that can be obtained from an antenna and its amplifying circuitry, when only a limited amount of total input power is available, is of more importance.

When all the available power is distributed among the various elements of an array the ERP should generally increase approximately proportionally as the number of elements. However, if each element that is added to the array delivers as much power as the average of those to which it is added, the ERP should increase approximately with the square of the number of elements. This consideration is important when dealing with power-limited devices, such as solid-state amplifiers designed to the limits of the current state of the art.

In the discussions that follow the terms *gain* and ERP will be used more or less interchangeably. Since only one dimension of beam steering is assumed, the value of gain will be relative to an omni-azimuthal element having the same axial beamwidth as the complete antenna, rather than to an isotropic element as is usually the case. While this simplifies the analysis generally it makes the accurate computation of gain difficult. The total radiated power should be determined by integrating the complete radiation pattern over all space. Since the axial beamwidth of an azimuthal plane array of elements is not always the same as the axial beamwidth of each of the elements considered separately, and since only azimuthal plane patterns were considered, some error in computation of gain is to be anticipated.

When an adaptive array is operating as a retrodirective antenna, it is not obvious what the relative transmitter powers for each element should be to make best use of the antenna. For instance, each elemental transmitter could be driven at its maximum output power irrespective of the relative level of pilot signal received at the element. Such a mode of operation, variously referred to as the *hard limited, saturated amplifier,* or *equal power* case, is very important since it represents one of the easiest methods to implement and also makes maximum use of the on-board amplifiers. Many of the computations assume such a mode of operation, and it is designated Mode-1. Another possible simple model of amplifier electronics is to assume that each of the elemental amplifiers produces an output power proportional to its input power. This is referred to as the *linear amplifier* or *weighted power* case. Although somewhat more difficult to implement in practice, linear amplification is a simple concept in principle and has also been used in many of the computations, where it is designated Mode-2 or Mode-3 operation, depending on the method of treating the total radiated

power. Apart from its simplicity of concept and introduction into computations, it is easy to demonstrate that the highest gain to be obtained from a simple array of correctly phased elemental radiators is when each is fed a fraction of the total available power in direct proportion to the relative gain of the particular element.

Specific examples of this principle have been demonstrated theoretically by Villeneuve[70]—for instance, for elements having fairly complex radiation patterns.

There are, of course, an infinite number of formulae for weighting the output power of each element—that is to say, it could be related to the input pilot power or any measurable quantity. However, only the three modes of operation were employed in the calculations.

One of the primary objectives of the computations was to determine the gain—or more exactly, the relative ERP—in the retrodirection.

The actual gain value computed in the following sections represents the ratio between the signal in the retrodirection (which is usually but not necessarily the maximum of the re-radiation pattern), and the signal strength that would exist (in every azimuthal direction) if all the available power were fed into an omni-azimuthal antenna having the same beamwidth, in the axial plane, as the array. In the case of Mode-1 operation there is no problem relating this mathematical model to a simple practical situation where each amplifier merely operates at maximum (and constant) output, but for the linear-amplifier case there are several alternatives, particularly for a spinning antenna. For instance, the absolute gain of each amplifier can be kept constant at all times. This would mean that the total radiated power would fall off as the square of the range from the pilot transmitter, unless the pilot signal power were increased with range to maintain a constant average pilot signal level at the space vehicle. Another possibility is to keep the gain of each amplifier the same at any instant in time, but at a value such that the total radiated power remained constant at all times. This was the model used for Mode-2 operation but no attempt was made to establish the practicality of providing circuitry to do this. The input power distribution to each of the transmitter/amplifiers, as well as the common value of elemental amplifier gain, would generally have to change continuously with antenna rotation to keep the total radiation power constant, because of the variation of elemental antenna gain. Another alternative would be to keep the common

value of elemental amplifier gain constant with antenna rotation but changing slowly with range, thus keeping only the *average* output power constant. Under these conditions, designated Mode-3 operation, there would in general be a cyclical variation of total radiated power with at least as many cycles per antenna revolution as there are elemental radiators. The above arguments relating to calculation of gain do not affect the calculations that follow for the Type-3 antenna because mutual coupling has been ignored.

It has been assumed throughout that all components and transmission lines are matched and remain so as the antenna rotates and other conditions change.

2. Circular Array of Omnidirectional Elements (Type-3 Antenna)

a. Assumptions

One configuration for a cylindrical adaptive antenna that has already been found suitable for use with a spin-stabilized vehicle consists of omni-azimuthal line-source elements mounted at one end of a cylindrical vehicle, as shown in Fig. 13.

A communication antenna having a similar configuration, but with far fewer (16) elemental radiators has been developed for use on the Earth-orbiting synchronous Application Technology Satellite (ATS),[67] due to be launched shortly. In the first portion of this section, each antenna is treated only as a simple degenerate retrodirective antenna in which it is assumed that each element radiates with equal amplitude and is phased so that contributions from all elements add in phase in the retrodirection—*i.e.*, the direction from which the pilot signal arrived. In other words, the retrodirective antenna has equal receive and transmit frequencies and uses saturated amplifiers. (Mode-1 operation is indistinguishable from Mode-2 or Mode-3 in this case, when mutual coupling is neglected.)

The cases involving unequal receive and transmit frequencies or linear amplifiers have not been treated. The total problem of spectral splitting in a complete retrodirective antenna of this type has not been specifically studied either, but an investigation of the amplitude-modulation component has been made and so has a study of the spectral content associated with just a single element. (As is shown later, there

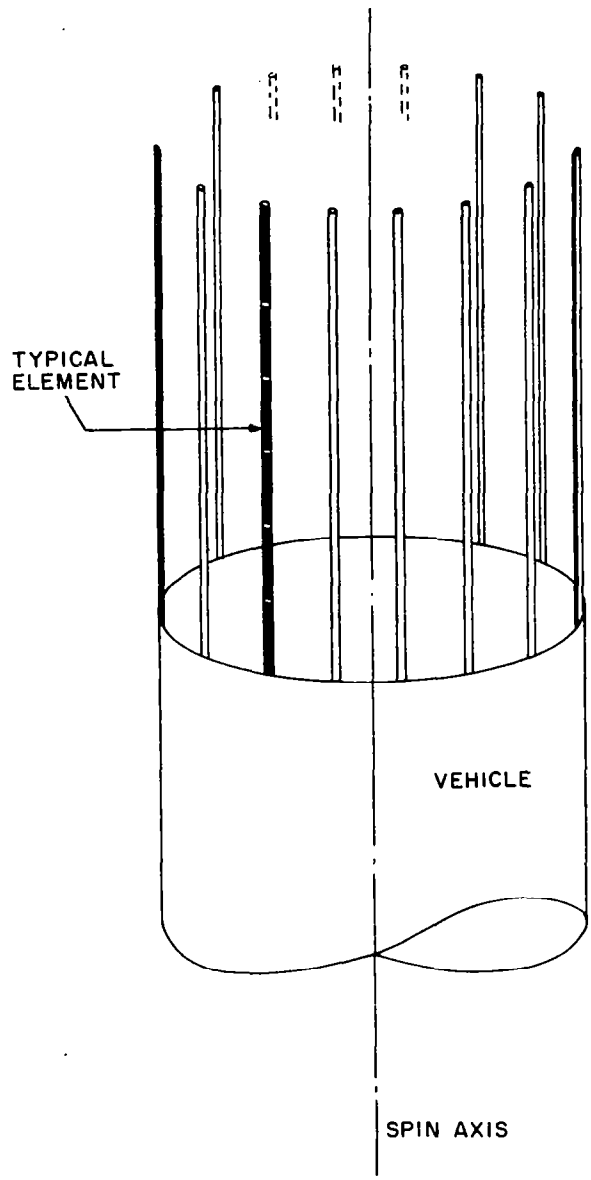

FIG. 13 OMNIAZIMUTH-ELEMENT CIRCULAR ARRAY ON THE END OF A CYLINDER

is no phase-modulation component when the receive and transmit frequencies of simple lower-sideband phase-conjugating system are the same.)

The beamwidth of each element in a plane through the vehicle spin axis (*i.e.*, in the axial plane) would be relatively narrow, as determined by the length of the element in wavelengths. Again, orientation of the beam in this plane would be provided by spin stabilization of the vehicle. Each element would have a very broad beam in the plane perpendicular to the spin axis, but the array as a whole would have a narrow beam in this plane. Orientation of the array beam would be provided by retrodirective circuitry connected to each line-source element.

For purposes of the present analysis, it is assumed that each element has an omnidirectional pattern in the plane perpendicular to the spin axis, and that mutual coupling and shadowing of one element by another will have negligible effect on the array pattern. In actual practice, the element diameter would probably be large enough, compared to the wavelength and the interelement spacing, that shadowing would not be completely negligible. Hence the element pattern for an element in the array would not be exactly omniazimuthal, due to mutual coupling, even if the element pattern was omniazimuthal for a single element in free space. An additional effect of mutual coupling would be to make the input impedance of each element a function of its location in the array. Therefore, the assumption of equal current flowing on each element, which is used in calculating the radiation patterns, is not equivalent to having equal power radiated from each element.

Analyses of circular arrays of omnidirectional radiators are available in the literature, but the numerical results that have been presented are for smaller numbers of elements and for smaller array diameters than are of interest for the present application. In this section of the report, properties of circular arrays will be reviewed, and some calculated patterns will be presented for arrays of 30, 60, and 90 elements on a 20-wavelength diameter. Also, the dependence of gain on array orientation in the azimuth plane will be discussed.

b. Pattern Shape

The amplitude and phase of the current in each element determine whether a circular array of elements radiates a broad or a pencil beam, and the direction of the beam. Of primary interest in the present

application is a pencil beam radiated in the plane perpendicular to the spin axis of a space probe. It will be convenient here to refer to this plane as the *azimuth plane*. The proper current distribution to form a pencil beam from a circular array has been considered in detail by several authors,[58-61] and thus need not be derived in detail here. Rather, a few of the fundamental equations will be given, and some calculated patterns shown. The primary reason for considering the pattern shape and sidelobe behavior is to understand why the gain of the array changes with array orientation and to establish how many elements are required to keep the gain reasonably constant. The form of the equations presented will closely follow Knudsen.[58]

Referring to Fig. 14, it is readily seen that in order to launch a plane wave the proper current phase lag in the kth element in an array of N identical omniazimuth elements equally spaced around a circle of radius R is given by

$$\Omega_k = 2\pi R \cos\left(\frac{2\pi k}{N} - \theta_i\right), \quad k = 1, 2, \ldots, N.* \tag{16}$$

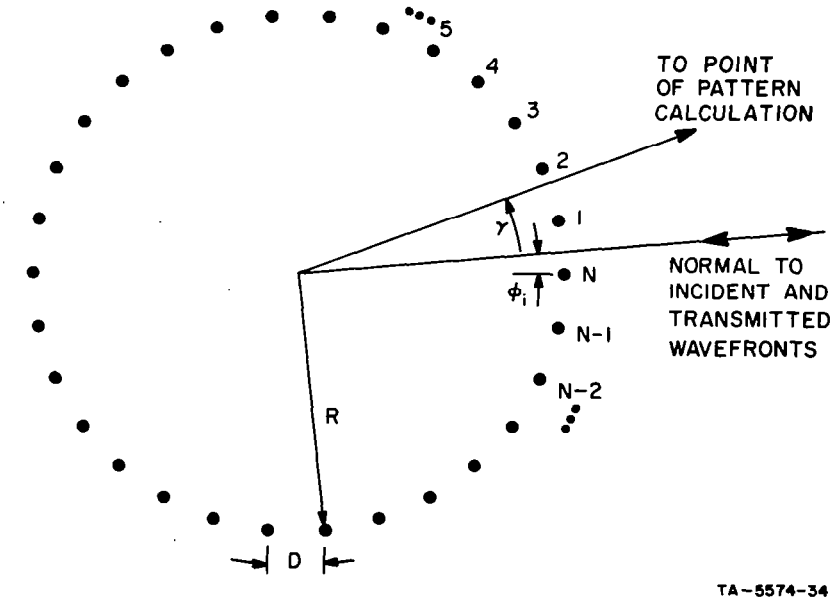

FIG. 14 DEFINITION OF RING-ARRAY PARAMETERS

* The symbols used for the discussion of a particular antenna type will in general be applicable only to that type.

Here R is measured in units of wavelength, and the phase is in radians. The phase reference is the center of the circle. The angle ϕ_i defines the orientation of the array with respect to the incident ray along which the transmitted beam is to be pointed (the retrodirection). Equation (16) also gives, of course, the relative phase *lead* of the current induced in each element by a plane-wave incident pilot signal, assuming mutual coupling between elements to be insignificant. Changing phase *lead* for an incident signal to phase *lag* of a transmitted signal is another way of stating that a phase-conjugate network is required on each element of a retrodirective array.

The far-field amplitude pattern is obtained by summing the contribution of the individual elements in the array. For unity current amplitude in each element, the resultant amplitude pattern is proportional to[58]

$$E = \sum_{k=1}^{N} \exp\left\{ j 2\pi R \left[\cos\left(\frac{2\pi k}{N} - \phi_i - \gamma \right) - \cos\left(\frac{2\pi k}{N} - \phi_i \right) \right] \right\} . \quad (17)$$

For the special case of an even number of elements, $\exp(jx)$ can be replaced by $\cos(x)$.[62] To reduce the time for a digital computer to calculate the patterns, Eq. (17) was rewritten using a trigonometric identity to obtain Eq. (18):

$$E = \sum_{k=1}^{N} \exp\left[j 4\pi R \sin\frac{\gamma}{2} \sin\left(\frac{2\pi k}{N} - \phi_i - \frac{\gamma}{2} \right) \right] . \quad (18)$$

The computer evaluates trigonometric functions using a many-termed power series, which is relatively time consuming compared to operations of multiplication and addition. Thus even more computer time was saved by using the following recursion relations:

$$\frac{2\pi k}{N} - \phi_i - \frac{\gamma}{2} = \left[\frac{2\pi(k-1)}{N} - \phi_i - \frac{\gamma}{2} \right] + \frac{2\pi}{N} \quad (19)$$

thus

$$\sin\left(\frac{2\pi k}{N} - \phi_i - \frac{\gamma}{2}\right) = \sin\left[\frac{2\pi(k-1)}{N} - \phi_i - \frac{\gamma}{2}\right]\cos\frac{2\pi}{N} + \cos\left[\frac{2\pi(k-1)}{N} - \phi_i - \frac{\gamma}{2}\right]\sin\frac{2\pi}{N} \tag{20}$$

$$\cos\left(\frac{2\pi k}{N} - \phi_i - \frac{\gamma}{2}\right) = \cos\left[\frac{2\pi(k-1)}{N} - \phi_i - \frac{\gamma}{2}\right]\cos\frac{2\pi}{N} - \sin\left[\frac{2\pi(k-1)}{N} - \phi_i - \frac{\gamma}{2}\right]\sin\frac{2\pi}{N} \tag{21}$$

for $k = 1, 2, \ldots, N$.

That is, to find

$$\sin\left(\frac{2\pi k}{N} - \phi_i - \frac{\gamma}{2}\right)$$

for all values of k, it was necessary to use the power series for the trigonometric functions to evaluate only

$$\sin\left(-\phi_i - \frac{\gamma}{2}\right) \quad , \quad \cos\left(-\phi_i - \frac{\gamma}{2}\right)$$

$$\sin\frac{2\pi}{N} \quad , \quad \text{and} \quad \cos\frac{2\pi}{N} \quad .$$

Some characteristics of the radiation patterns of circular arrays having different numbers of elements on the same diameter circle are illustrated in Figs. 15 through 17.* For each of these figures the array diameter is 20 wavelengths, and the number of elements is 30, 60, and 90 for the respective figure. It is seen that the main beam and the

* These patterns were machine plotted, connecting the computed points that are spaced every degree by straight lines. The finite point spacing does not show the true depth of the nulls, or the peaks of some lobes.

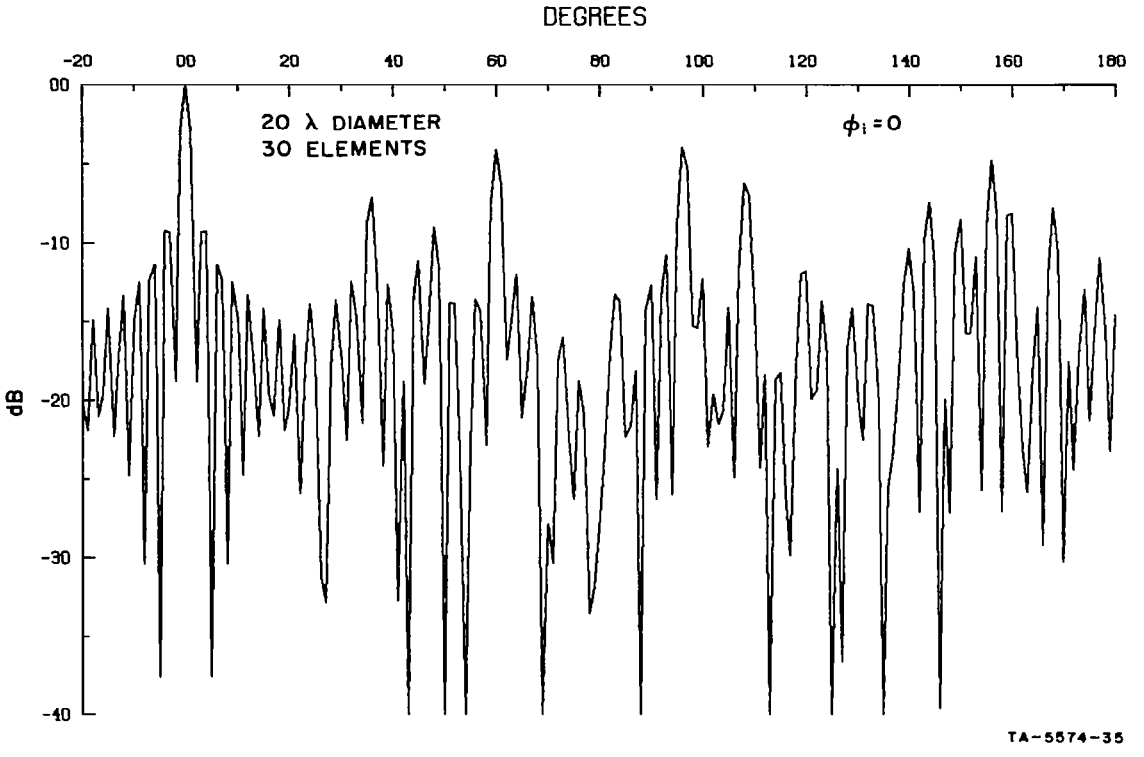

FIG. 15 COMPUTED PATTERN OF A 20λ-DIAMETER, 30-ELEMENT CIRCULAR ARRAY

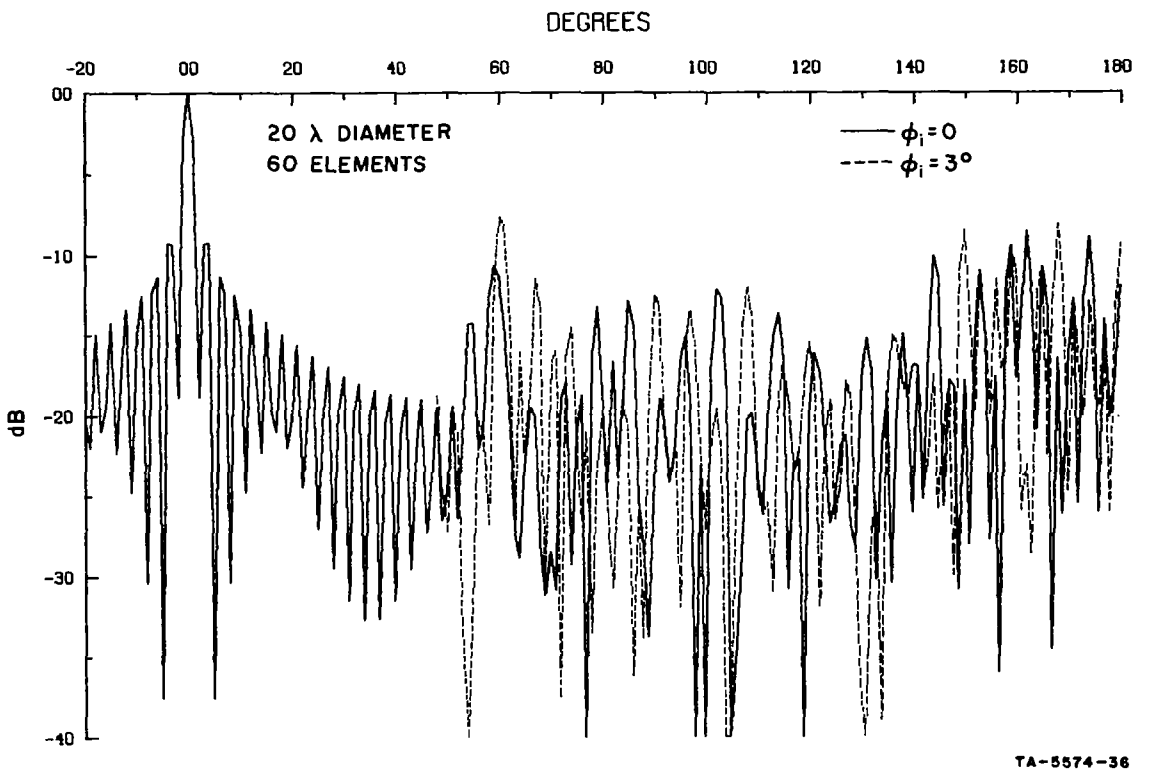

FIG. 16 COMPUTED PATTERN OF A 20λ-DIAMETER, 60-ELEMENT CIRCULAR ARRAY

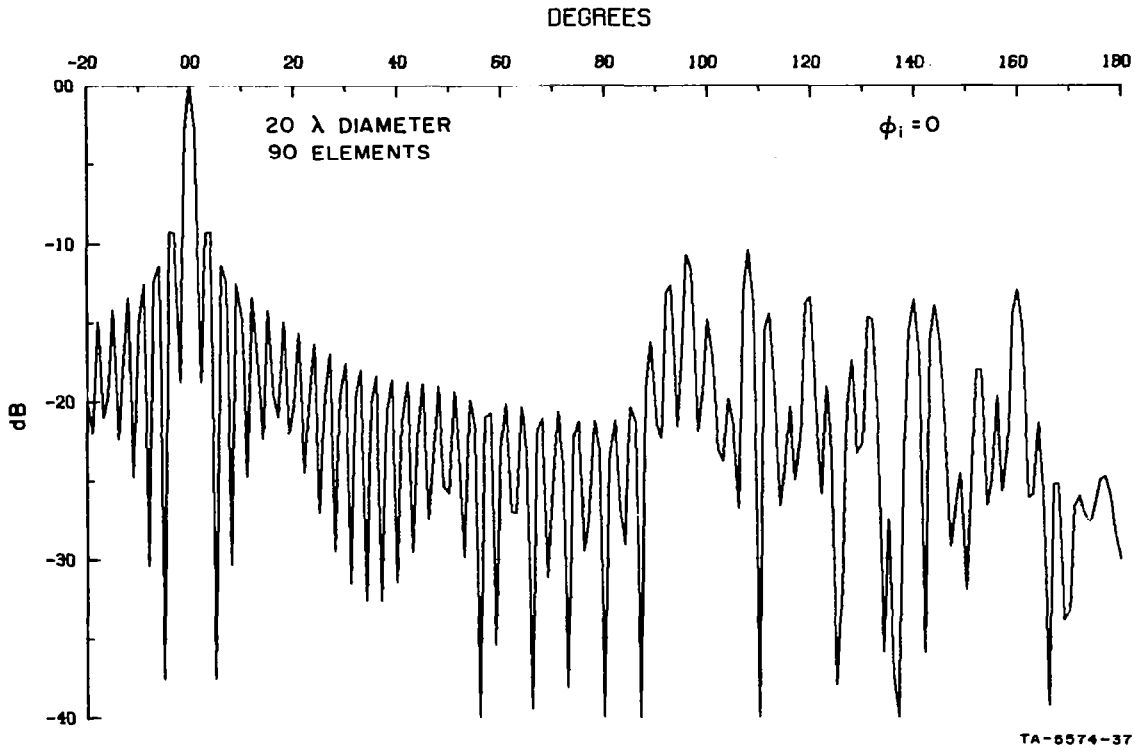

FIG. 17 COMPUTED PATTERN OF A 20λ-DIAMETER, 90-ELEMENT CIRCULAR ARRAY

first several sidelobes are identical in the three figures. Also note that the sidelobes fall off in a well-behaved manner out to a certain angle, beyond which the lobe height increases significantly and the lobe shape becomes less systematic. The more elements there are in the array, the further out in angle are the sidelobes well behaved.

These characteristics of the patterns from circular arrays can be explained by rewriting Eq. (17) as a series of Bessel functions:[58]

$$E = J_0\left(4\pi R \sin\frac{\gamma}{2}\right) + 2\sum_{p=1}^{\infty} J_{pN}\left(4\pi R \sin\frac{\gamma}{2}\right)\cos\left[pN\left(\frac{\gamma}{2} + \phi_i\right)\right] \qquad (22)$$

for N even, and

$$E = J_0\left(4\pi R \sin\frac{\gamma}{2}\right) + 2\sum_{p=1}^{\infty} J_{2pN}\left(4\pi R \sin\frac{\gamma}{2}\right)\cos\left[2pN\left(\frac{\gamma}{2} + \phi_i\right)\right]$$

$$+ j2\sum_{p=0}^{\infty} J_{(2p+1)N}\left(4\pi R \sin\frac{\gamma}{2}\right)\sin\left[(2p+1)N\left(\frac{\gamma}{2} + \phi_i\right)\right] \qquad (23)$$

for N odd. Here $J_k(x)$ is the Bessel function of the first kind and of order k. The leading term, which involves the J_0 function, is the amplitude pattern resulting if the circular array consisted of an infinite number of identical omniazimuth elements. The summations can be considered as correction terms to account for the fact that the number of array elements is finite. The main lobe and the first several sidelobes in the patterns of Figs. 11 through 13 are given by the J_0 term of Eq. (22). Where the sidelobes no longer decrease monotonically is where the first term in the correction series becomes important.

The first correction term that becomes significant in both Eqs. (22) and (23) is a $J_N(x)$ function, where the order N is the same as the number of elements in the array. For an array 20 wavelengths in diameter, practical numbers of elements might lie in the range 50 to 100, thus the correction series involve Bessel function of high order. It is characteristic of Bessel functions of the first kind and of high order that they have small value for arguments small compared to the order. As the argument approaches the order, the function increases rapidly to a positive peak, and then becomes oscillatory, eventually approaching a decaying sinusoidal waveform. For discussion of these

functions see, for example, Jahnke and Emde,[71] and Watson.[72] The location of the first positive peak of the function $J_N(x)$ is given approximately by[73]

$$x \approx N + 0.808 N^{1/3} \tag{24}$$

That is, the location of the highest of the first spurious sidelobes of the array pattern would be given approximately by

$$\sin \frac{\gamma}{2} \approx \frac{N + 0.808 N^{1/3}}{4\pi R} \tag{25}$$

The exact location of the highest spurious sidelobe will also depend on the factor $\cos N(0.5\gamma + \phi_i)$ in Eq. (22), or $\sin N(0.5\gamma + \phi_i)$ in Eq. (23), and on the sidelobes of the J_0 leading term.

Equation (25) gives the location of the first spurious sidelobes in terms of the number of elements and the array radius. Based on experience with the more familiar linear arrays, a more fundamental relationship for spurious sidelobes might be expressed in terms of the element-to-element spacing. (In the case of linear arrays, the spurious sidelobes are referred to as diffraction or grating-lobes.) If we define D as the element-to-element spacing measured around the circumference of the array,* and measured in units of wavelength, then

$$D = \frac{2\pi R}{N} \tag{26}$$

Defining γ_{sl} as the angle at which the highest spurious sidelobe due to the first correction term in Eqs. (22) and (23) can occur, we have

$$\sin \frac{\gamma_{sl}}{2} \approx \frac{1}{2D} + \frac{0.404}{(2\pi R)^{2/3} D^{1/3}} \tag{27}$$

* The circumferential spacing D defined here is nearly the same as the spacing measured along the cord connecting adjacent elements when the number of elements is large. The two ways of measuring spacing are equal to the same accuracy as the approximation $\sin(\pi/N) \approx \pi/N$, where N is the number of elements in the array.

Equation (27) has been plotted in Fig. 18 for several values of array diameter. It is seen that the angle at which the first spurious sidelobes can occur is rather insensitive to the array diameter.

The sidelobes far beyond the first spurious lobes require additional terms in the correction series of Eqs. (22) and (23). For the array diameters and numbers of elements that would be practical for retrodirective arrays on space probes, however, only a few terms of the correction series need be evaluated. As an example, for a 20-wavelength-diameter array with as few as thirty elements, only the J_{30}, J_{60}, J_{90}, and J_{120} functions would have significant amplitude. (For sixty elements on the same diameter, only the J_{60} and J_{120} correction terms would have to be taken into account.) Taking $4\pi R = 40\pi = 125.7$, the first positive peaks in the correction series in Eqs. (22) and (23) occur at 30.0 degrees for the J_{30} term, at 60.3 degrees for J_{60}, at 96.2 degrees for J_{90}, and at 161.2 degrees for J_{120}.

c. Signal-Amplitude-Modulation Due to Change in Array Orientation

Having discussed in some detail the shape of the array radiation pattern, let us now consider the effect that the pattern shape has on the gain (directivity) at the peak of the main beam. Referring back to Eqs. (22) and (23), we see that the shape of the main beam and the first several sidelobes is determined by a J_0 function that is independent of the array-orientation angle ϕ_i defined in Fig. 14. The correction series, which influence the far-out sidelobes, are functions of the array-orientation angle ϕ_i. Thus, as a spin-stabilized space probe with a circular retrodirective array rotates, the sidelobes of the array will change as a function of time. An example was shown by the solid and dashed patterns of Fig. 16. As the amount of power radiated into the sidelobes changes with time, the gain at the peak of the main beam will change also. This will result in amplitude modulation of the transmitted signal at a frequency related to the rotation rate of the space probe and the number of array elements. This represents spectral splitting and is discussed further below.

The computer program of Eq. (18) has been used to calculate the directivity of some arrays as a function of array orientation. The directivity at the beam peak was determined from the values of the amplitude pattern, $E(\gamma)$, by numerically integrating

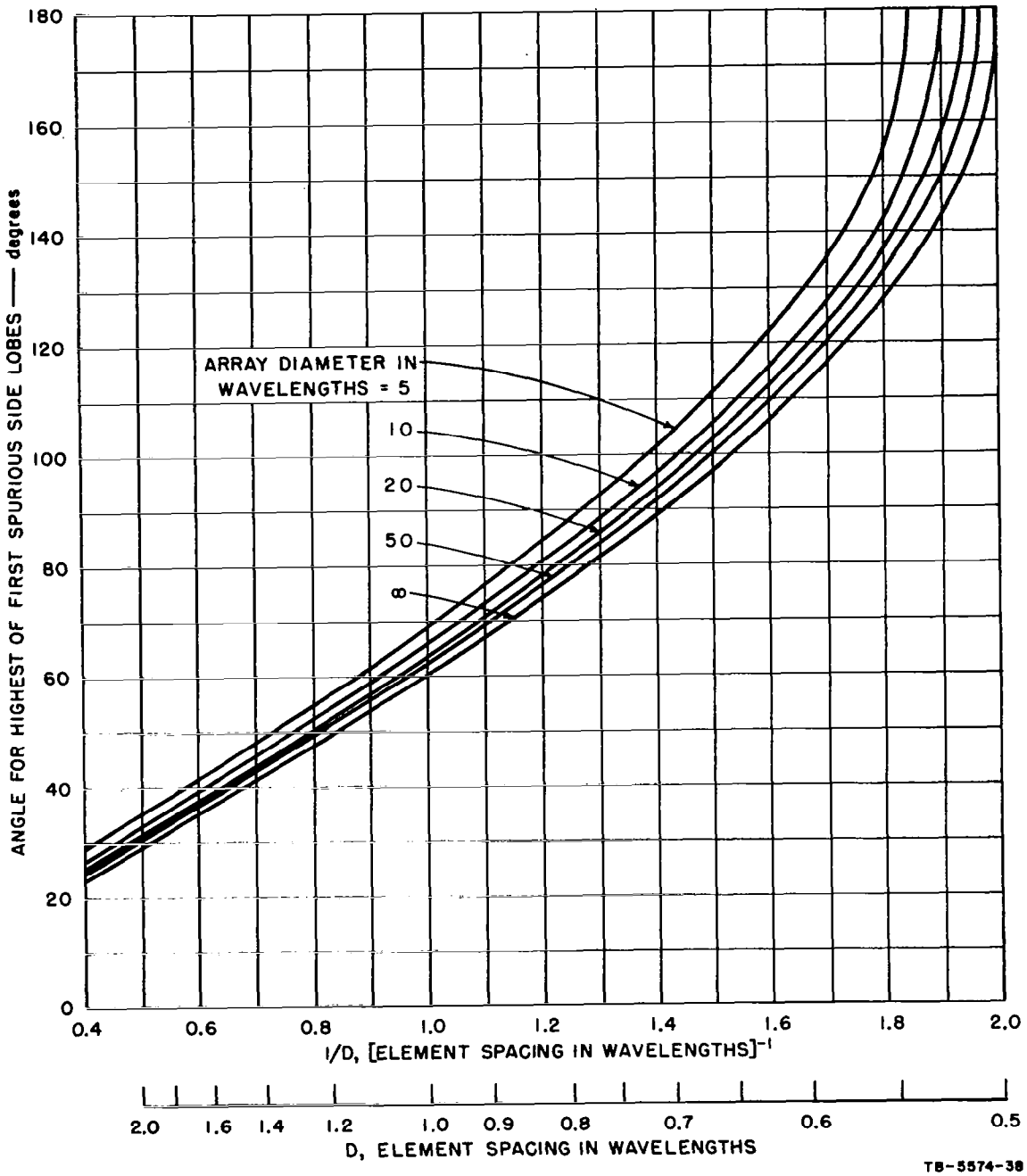

FIG. 18 SPURIOUS-LOBE LOCATION AS A FUNCTION OF ELEMENT SPACING

$$G = \frac{2\pi E_{max}^2}{\int_0^{2\pi} E^2(\gamma)\,d\gamma} \quad . \tag{28}$$

An increment of one degree was used for the angle, and Simpson's rule was used to perform the numerical integration.* The factor 2π rather than 4π occurs here since the integration is performed only over the azimuth plane rather than over all space. It is assumed here that the line sources are sufficiently long that the pattern amplitude out of the azimuth plane is negligible. To find the total directivity of an actual array, the pattern in all directions would have to be taken into account.†

The calculated variation in array directivity as a function of changing orientation with respect to the retrodirection is shown in Fig. 19. Curves for several values of the number of elements in the array are included in the figure. The angle scale is normalized so that the retrodirection passes through an antenna element at each end of the scale (see Fig. 14). For the combinations of array diameter and numbers of elements studied, the calculated directivity variation is of the order of one decibel or less.

For an even number of elements, the directivity variation is seen from Fig. 19(a) to go through one complete cycle as the array orientation changes $1/N$ revolution. That is, there is one cycle as the retrodirection changes from through one antenna element to through the next. Thus, for an even number N, of elements on a vehicle spinning at a rate f_r revolutions per second, the directivity modulation would be at a frequency

$$f_m = Nf_r \quad \text{hertz} \tag{29}$$

---

* The error introduced by the one-degree increment in the calculated pattern is negligible. An indication of the sampling error is given by the fact that decreasing the sampling interval for a few 20-wavelength-diameter arrays changed the calculated directivity by no more than 0.13 dB in going from 2- to 1-degree increments, and no more than 0.01 dB in going from 1.0- to 0.5-degree increments.

† In order to obtain a limit on the error due to neglect of power out of the azimuth plane, some simple calculations were made for 2- and 4-element linear arrays. First, Eq. (28) was used to compute the directivity of an array of long line elements (referred to the gain of a single element). Then the conventional directivity was computed by integration over all space for the extremely different case of an array of isotropic elements. Comparing the two directivity figures for arrays with the same element spacing, differences up to 1.6 dB were found. With the length of elements that might actually be used, Eq. (28) would give better than 1.6-dB accuracy.

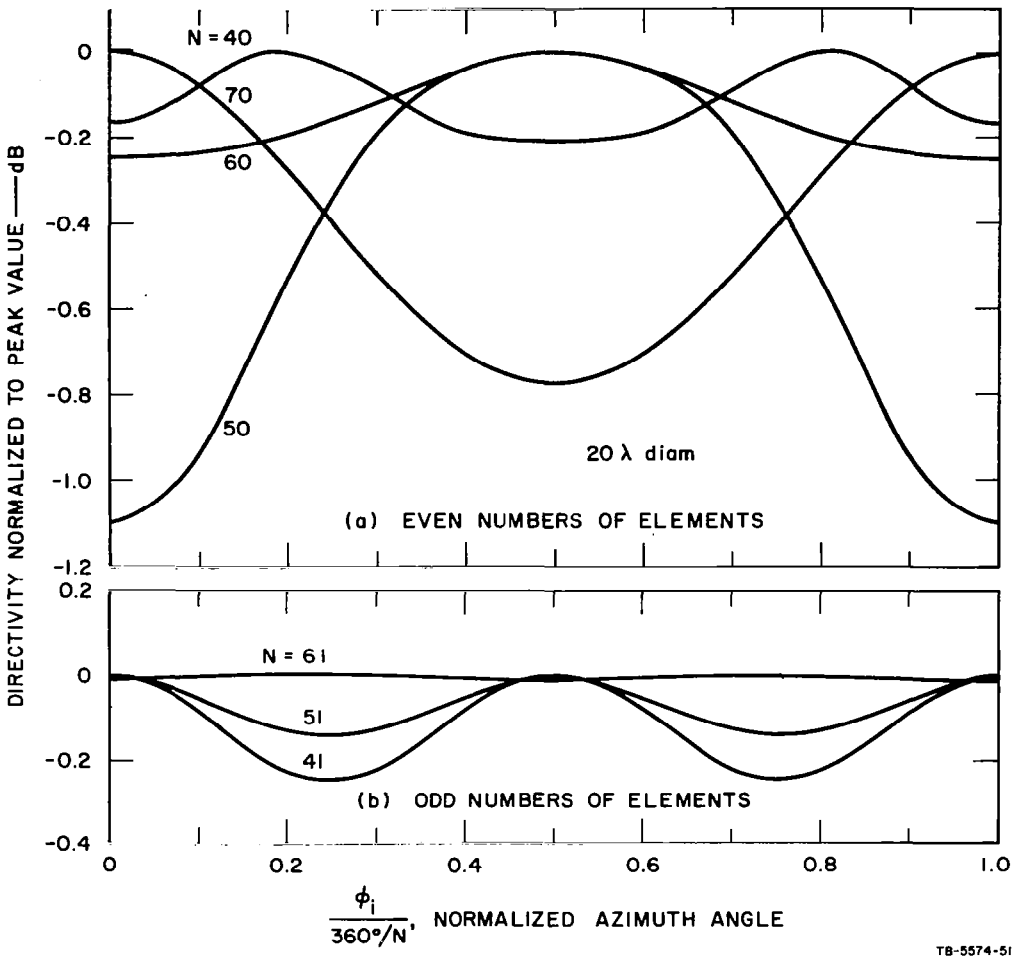

FIG. 19 DIRECTIVITY NORMALIZED TO PEAK VALUE — dB

and its harmonics. For an odd number of elements, Fig. 19(b) and Eq. (23) show that there are two cycles of directivity variation as the array orientation changes $1/N$ revolution. Thus, for an odd number of elements, the directivity modulation would be at

$$f_m = 2Nf_r \quad \text{hertz} \tag{30}$$

and its harmonics.

The maxima and minima of the directivity in general fall in the symmetry planes of the array. It is found, as shown in Fig. 19, that for some numbers of elements a maximum of directivity falls in a given

symmetry plane, but for other numbers of elements a minimum will fall in the same plane. This is further illustrated in Fig. 20 where directivity is plotted as a function of the number of elements. Circular points are used for the directivity in symmetry planes passing through an antenna element, and crosses are used for symmetry planes that are equally spaced

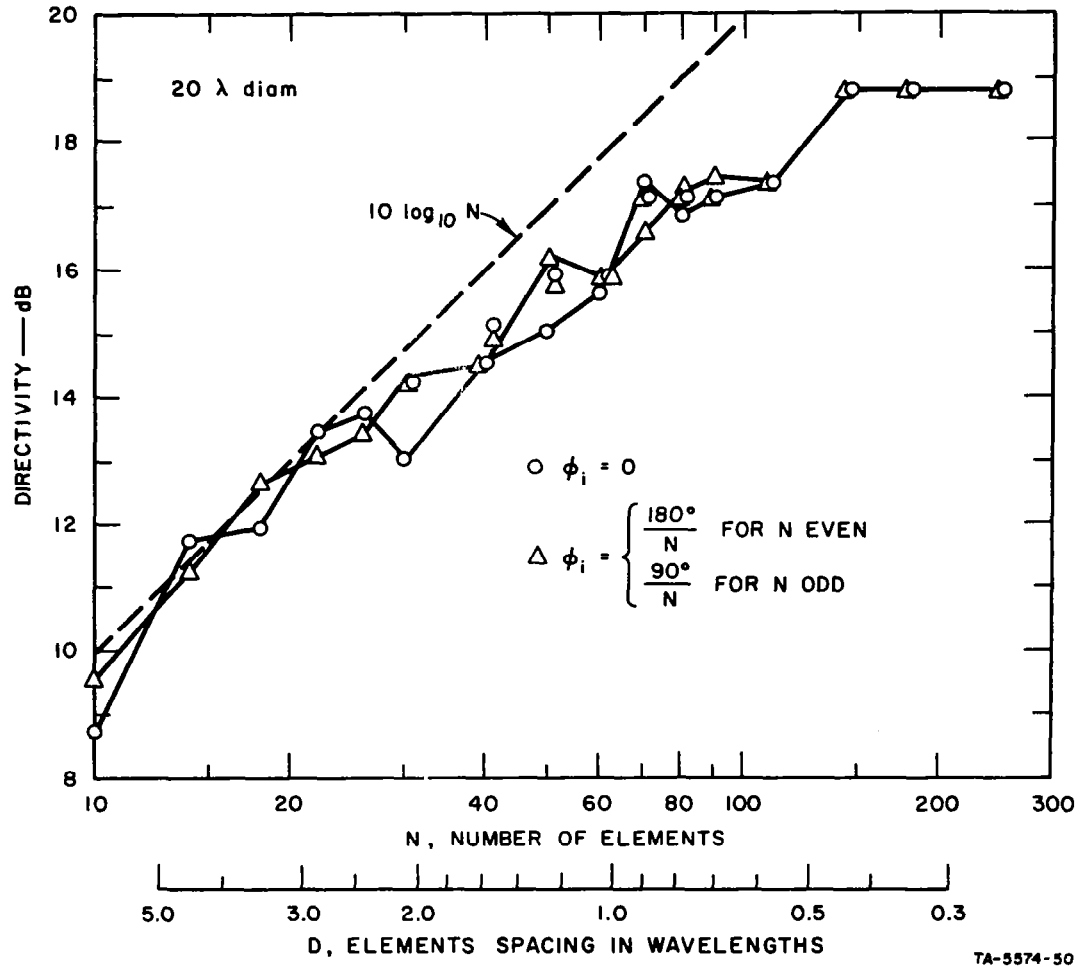

FIG. 20 DIRECTIVITY AS A FUNCTION OF THE NUMBER OF LINE SOURCES

from the antenna elements. Solid lines connect the points for even numbers of elements. Points for odd elements are left unconnected. Except where these lines cross, the spread between the two lines is thought to be the same as the peak-to-peak directivity variation *vs.* array orientation. This is true, at least, for the cases plotted in Fig. 19. Note in Fig. 20 that the spread between the two solid curves does not monotonically

decrease as the number of elements increases, but rather is a cyclical function. At the points where the two solid curves in Fig. 20 cross, the directivity variation with orientation is small, but not zero. Also, the maxima and minima do not necessarily occur in the symmetry planes, as illustrated by the 40-element curve in Fig. 19. It is probable that the cyclic variation shown in Fig. 20 for N even also occurs for N odd, but insufficient points are available to demonstrate this assumption.

In Fig. 20, the number of elements was used as the abscissa, but a more basic parameter would be the inter-element spacing. Thus an auxiliary scale of spacing is included below the figure. For element spacing less than about one-half wavelength, the two solid curves merge, and there would be essentially no directivity (amplitude) modulation due to changing sidelobes as the array was rotated (still assuming that the effects of mutual coupling are negligible). Other work,[67] dealing with smaller arrays, showed that in a practical axially polarized array, mutual coupling can cause 0.4-to-1.2-dB directivity modulation even though the calculated value was less than 0.01 dB.

Figure 20 also illustrates that for small numbers of elements the array directivity is approximately proportional to the number of elements, N, although on the average it is slightly less than $10 \log_{10} N$ dB.* (Recall that for zero ohmic losses, directivity is the same as the more commonly used term, gain.) As the element spacing becomes less than a couple of wavelengths, the directivity definitely becomes less than $10 \log_{10} N$, and finally becomes constant for element spacing less than about one-half wavelength. For closely spaced elements, none of the correction terms in Eqs. (22) and (23) have significant amplitude, so the pattern shape is completely specified by the leading J_0 term (also see Fig. 18). Since the pattern shape is independent of N when the elements are closely spaced, the directivity, which is determined by pattern integration, must also be independent of N.

d. Odd and Even Values of *N*

The fact that the 51- and 61-element arrays gave less gain modulation than did the 50- and 60-element arrays is now discussed. This

* The slight difference between the directivity and $10 \log_{10} N$ might be related to the difference mentioned earlier in discussing Eq. (28).

was anticipated based on the fact that previous investigations dealing with smaller circular arrays had found that an odd number of elements was better than an even number.[58,63,64] For a large number of elements, such as 60 or 61, the pattern does not appear by visual inspection to be a significantly better approximation to a J_0 function for an odd number of elements than for an even number, in contrast to the results for small numbers of elements.[58] What is important here, however, is not obtaining a specific pattern shape, but having the amount of power radiated into the sidelobes relatively independent of the array orientation.

Note that, for both Eqs. (22) and (23), the first correction term involves the same function (except one has a cosine factor and the other a sine factor). The significant difference between Eqs. (22) and (23) is that for N even, the correction terms add either in or out of phase with the leading J_0 term, but for N odd the first correction term adds in quadrature to the leading J_0 term. At any given angle γ, the correction term will sometimes be positive and sometimes negative, depending on the array orientation ϕ_i. Since the correction term is of the same order of magnitude as the sidelobes of the J_0 function, adding or subtracting the two terms in phase can produce a much larger change in magnitude of the resultant than does adding the two terms in quadrature. Stated in symbols,

$$\left|\frac{a + b}{a - b}\right| > \left|\frac{a + jb}{a - jb}\right| \tag{31}$$

where a represents the J_0 term at a given angle γ, and b represents the first correction term at the same angle.

Although more than the first correction terms can be significant in Eqs. (22) and (23), the presence of the imaginary terms in Eq. (23) is a significant fact that should not be overlooked. The presence of the imaginary terms makes the power radiated into the sidelobes generally less dependent on array orientation for an odd number of elements than for an even number. Exceptions to this general rule have, however, been found. One exception is illustrated in Fig. 19 for the case of 40- and 41-element arrays. It was already pointed out in the discussion of Fig. 20 that the 40-element array was a special case. The other exception was found during some calculations where the diameter was changed slightly to 20.25 wavelengths. Then a 60-element array was

found to have 0.14 dB less directivity at $\phi_i = 0$ than at 3.0 degrees, whereas a 61-element array had 0.44 dB less directivity at $\phi_i = 0$ than at 1.48 degrees. The directivity is not known except for those cases where the combination of array diameter and number of elements can be chosen to minimize the directivity variation for an even number of elements. It appears, from the standpoint of reducing gain modulation due to array rotation, that it would be advantageous to use an odd number of elements. This possible advantage of an odd number of elements probably only applies for arrays such as in Fig. 13 (Type-3 antenna) where all the elements (theoretically) contribute approximately equal amplitude in the retrodirection. Such is not likely to be the case for a practical Type-3 antenna, at least when the elements are linearly polarized.

e. Spectral Splitting

Apart from the probability of amplitude modulation, as just considered, when an antenna is spinning about an axis not in the plane of the received or transmitted signal, the spinning results in periodic frequency modulation of the signal. This combined effect has been defined *spectral* splitting.

Consider now the limited case of a single theoretically omnidirectional element in a circular array of the Type-3 antenna shown in Fig. 13. The antenna is assumed to be either only receiving or only transmitting a CW signal. The result is a spectrum having lines at the CW frequency and at lower and higher frequencies separated from the CW frequencies by multiples of the spin frequency. The spectrum is derived in Appendix A and the values associated with a particular antenna configuration are tabulated there. It is found to peak in the neighborhood of $2\pi R f_s$ where

R = Distance of the element from the spin axis (radius) in wavelengths

f_s = Spin frequency.

A plot of the relative power in each of the upper sidebands is shown in Fig. 21. The complete power spectrum is symmetrical about the carrier frequency f_0 (sideband number = 0).

It can be seen that the *maximum* power occurs in the sixtieth sideband, but it is insignificant for all sideband numbers greater than 70. Since only one elemental radiator has been considered, these numbers

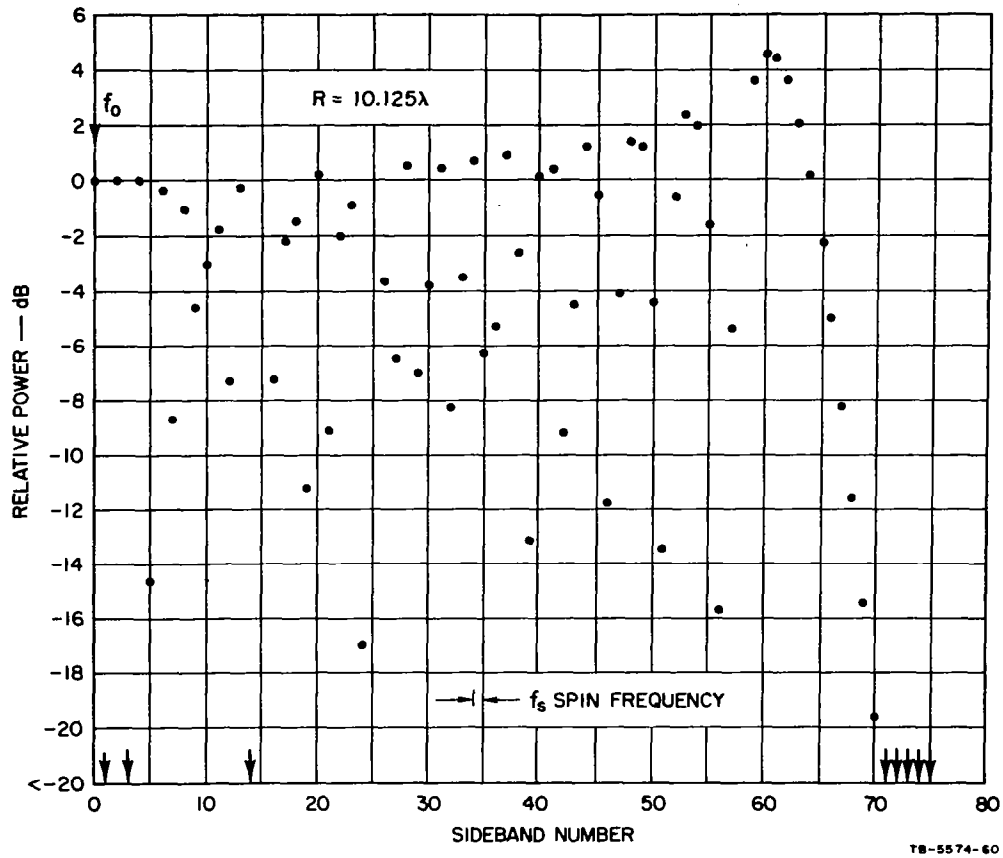

FIG. 21 RELATIVE ENERGY CONTENT OF EACH SIDEBAND FOR A SINGLE ELEMENTAL RADIATOR MOVING ON THE CIRCUMFERENCE OF A CIRCLE

cannot be associated with the number of elements; they are in fact related to the path length of the element for one spin revolution ($2\pi R$).

It will be noted that this length is 63.61 wavelengths for the model represented in Fig. 21. The figure was especially chosen to demonstrate that the low-order odd sidebands can be made very small.

As is shown later in this report, when the Type-1 antenna is considered as a retrodirective device and when an antenna similar to Type-3 is considered as an adaptive receiving antenna, this high harmonic content associated with a single element is not as serious as it might appear from Fig. 21.

f. Polarization

The above study of the Type-3 configuration has not been related to any specific polarization. The polarization would have to be specified before the effects of mutual coupling could be taken into consideration. As already mentioned, an antenna of the same general configuration but using fewer elements and programmed phase shifters, rather than phase-conjugating networks, has been developed.[67] This antenna employed 16 elements equally spaced on the circumference of a two-wavelength circle (inter-element spacing approx. 0.39λ). This close spacing, together with the fact that the elements were axially polarized, would indicate that mutual coupling between elements would be high. This indeed was the case, as indicated by a typical elemental azimuthal pattern shown in Fig. 22 (reproduced from Ref. 70). It was measured in the presence of the fifteen other elements which were each terminated in the nominal characteristic impedance of the antenna element. Far from being omnidirectional, the pattern contains several lobes and varies in amplitude by more than 10 dB.

Similar patterns are to be expected if axial polarization, or azimuthal polarization (although perhaps to a lesser extent), were used for the antenna configurations discussed in this section, so that much of the theoretical pattern and modulation data that has been derived could be subject to serious modification. It is also reasonable to suppose that the phase center of an element with a pattern such as that as shown in Fig. 22 does not remain fixed at the center of the element. For the degenerate case where the receive and transmit frequencies of a simple retrodirective antenna are the same, the conjugating networks will automatically adjust the phase to be correct for reradiation in the retrodirection, although the amplitudes contributed by each element will, of course, be different. The movement of phase center would, however, change the radiation pattern slightly and could modify the theoretical power spectrum appreciably, particularly if the receive and transmit frequencies were different.

It is possible that if some other polarization were used, such as 45-degree linear, or circular, it might be possible to obtain radiation patterns better approximating to the ideal omni-azimuthal shape. The practical design of such elements would be quite a problem and may not even be practical. In any case the theoretical data obtained for the Type-3 configuration will at best be only partially applicable to any practical antenna. Use of such exotic polarization, particularly circular,

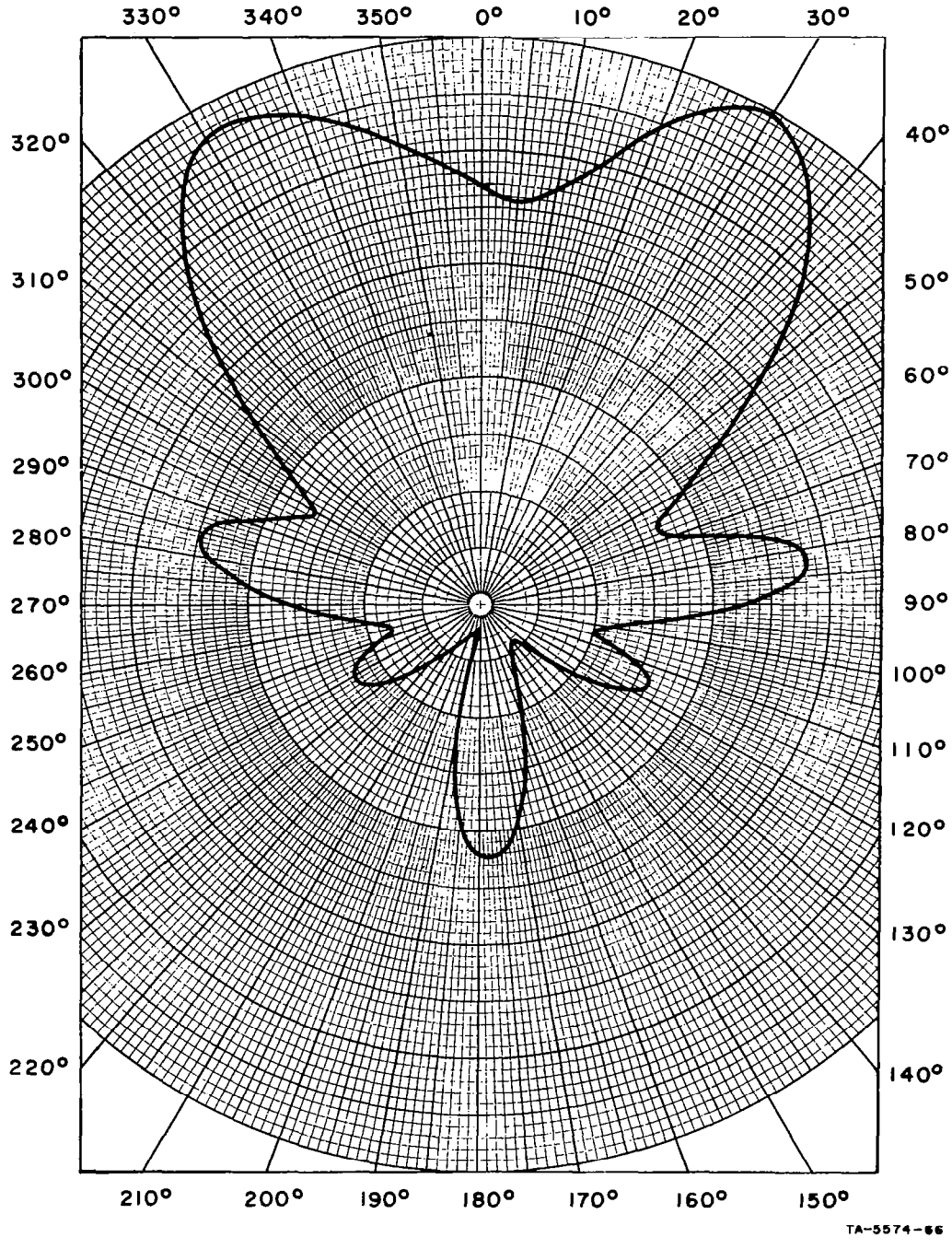

FIG. 22 MEASURED AZIMUTHAL POWER PATTERN OF SINGLE ELEMENT IN 16-ELEMENT CIRCULAR ARRAY. All other elements terminated in 50Ω.

could reduce the seriousness of the mutual coupling and its varying with antenna rotation on matching between the elemental transmitter and elemental radiator.

3. The Cylindrical-Geodesic-Lens Biconical-Horn Antenna (Type-1 Antenna)

a. General

Figure 23 shows a simplified view of this novel configuration consisting of a combination of an array and two-dimensional lens system. A similar lens system has been used previously by the author[74,75] in association with a classified beam-forming technique. Figure 23 also shows the primary dimensions of the antenna as well as the N principal rays from the N radiating structures, which, it is assumed, make up the

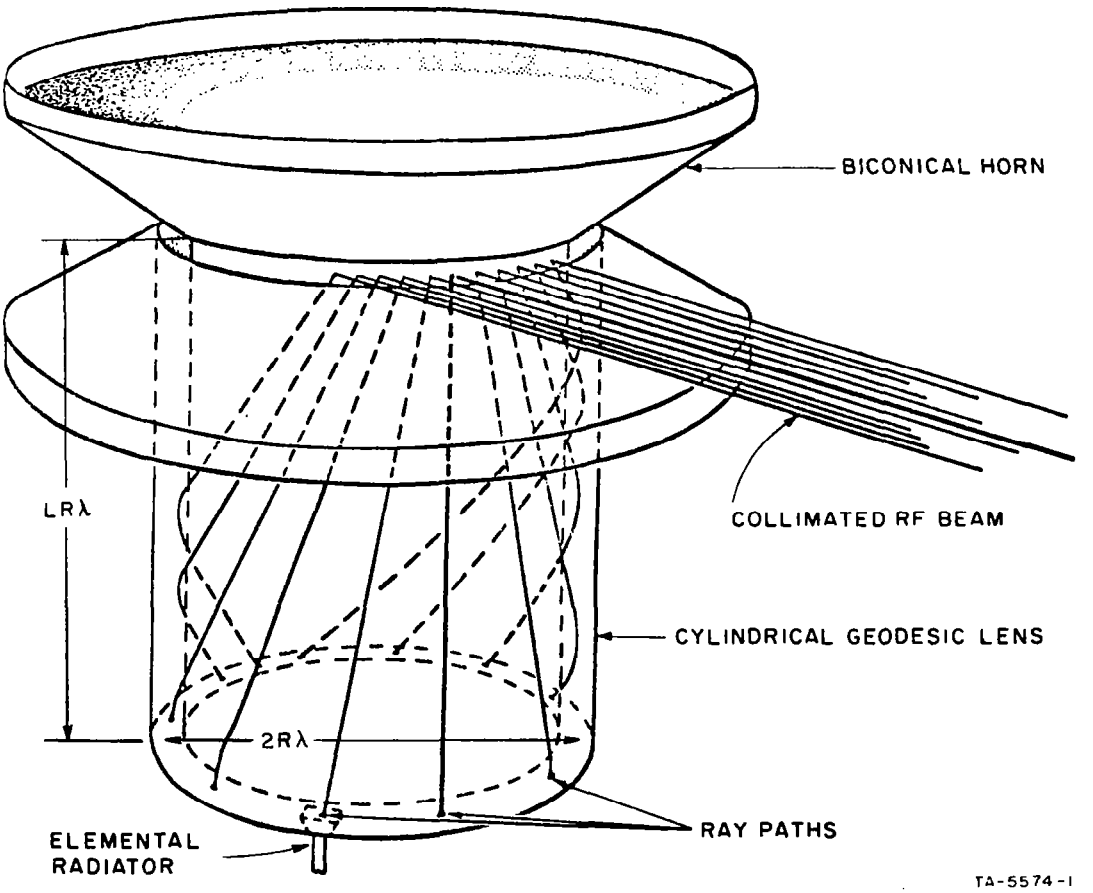

FIG. 23 CYLINDRICAL-GEODESIC-LENS BICONICAL-HORN ADAPTIVE ANTENNA (Type 1 antenna)

collimated RF beam. Each of these rays represents the shortest distance between the particular elemental radiator and the "distant observation point." Of course, this figure is an oversimplification, since radiation occurs in many directions from each of the elemental antennas and is eventually radiated by the biconical horn in all azimuthal directions, but this radiation does not, in general, add in phase except in the direction of the main beam. In the present study it is assumed that the values of L and R and the radiation pattern of each elemental radiator within the geodesic lens [denoted by $G(\alpha)$] are such that only two or three rays from each elemental radiator contribute significantly to the final antenna radiation pattern for any particular azimuthal direction. One of these rays travels around the cylindrical lens in one direction, while the other travels in the opposite direction. The third ray, when considered, travels around the lens in the same direction, but for a much greater distance, than the first. The inaccuracies introduced by this assumption or simplification are shown to be insubstantial, particularly when compared with the other assumptions and simplifications (such as the use of ray optics) employed in this study.

More than one computer program was used in investigating the various aspects of this antenna and it was found possible to check the accuracy of some assumptions. For instance, it was considered desirable to have greater accuracy when computing spectral content than when determining radiation patterns.

b. Basic Theory of the Analysis Procedure

In addition to the assumptions mentioned above, two other important assumptions have been made for this analysis: (1) that the mutual couplings between the elemental radiators at the bottom of the geodesic lens are negligible, and (2) that the discontinuity between the biconical horn and the coaxial cylinders presents a negligible mismatch to all the significant rays considered in the analysis. Neither of these assumptions is considered to be a serious limitation of the analysis since both conditions can be reasonably well met by good engineering design.

The procedure adopted in this analysis was as follows: The radiation pattern, described in both amplitude and phase by $B(\gamma)e^{j\Omega(\gamma)}$*,

* The symbols used for the discussion of a particular antenna type will in general be applicable only to that type.

was first computed for the biconical antenna with the assumption that just a single elemental radiator at the bottom of the geodesic lens was excited. The ray geometry associated with such an element, and a particular azimuthal direction γ, is shown in Fig. 24. A portion of the modulus of such a typical amplitude function or pattern, based only on the two most

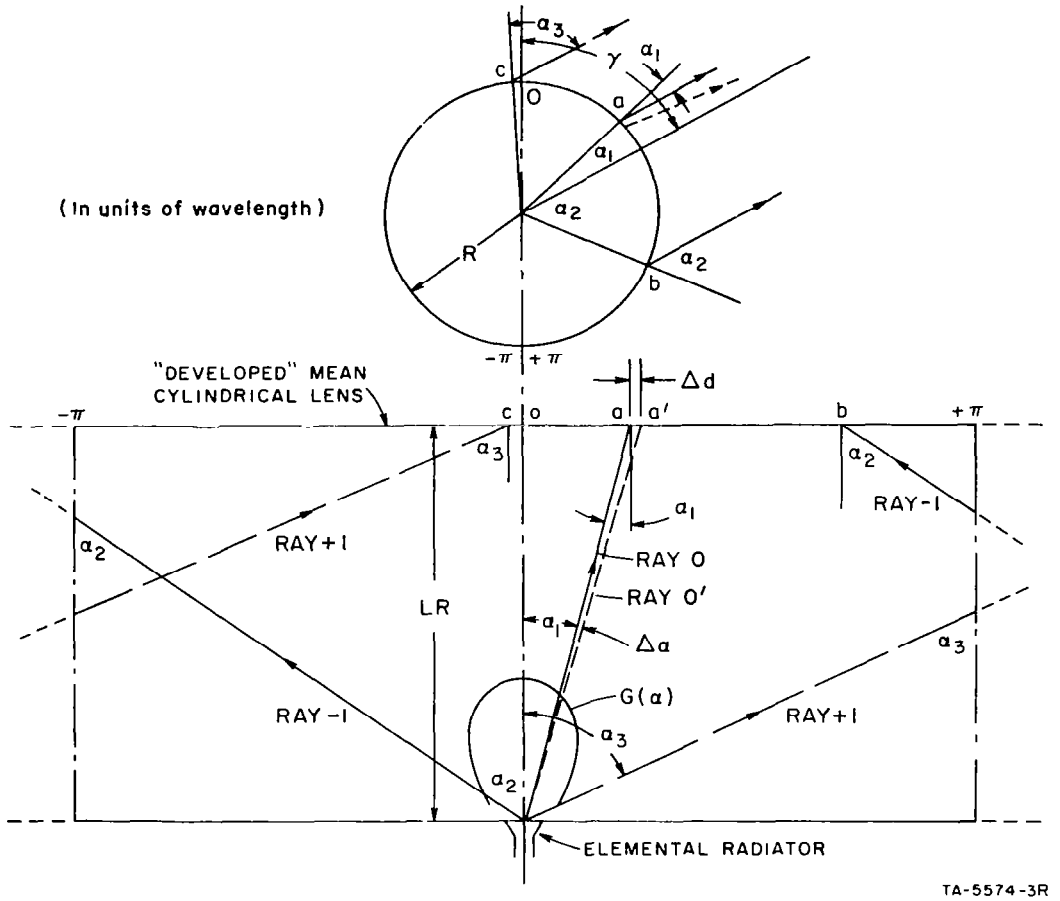

FIG. 24 RAY GEOMETRY ASSOCIATED WITH A SINGLE RADIATOR AND SINGLE AZIMUTH ANGLE

significant rays, is reproduced in Fig. 25 for azimuthal angles γ from 0 to 180 degrees. The elemental radiator is situated at $\gamma = 0$, and the pattern is, of course, symmetrical; its derivation is considered in more detail below. It will be noted that this pattern is much more nearly omnidirectional than the radiation pattern of the element itself within the cylindrical geodesic lens, which is also plotted in Fig. 25 as a function of α, using the same angle scale. Indeed, the lens may be said

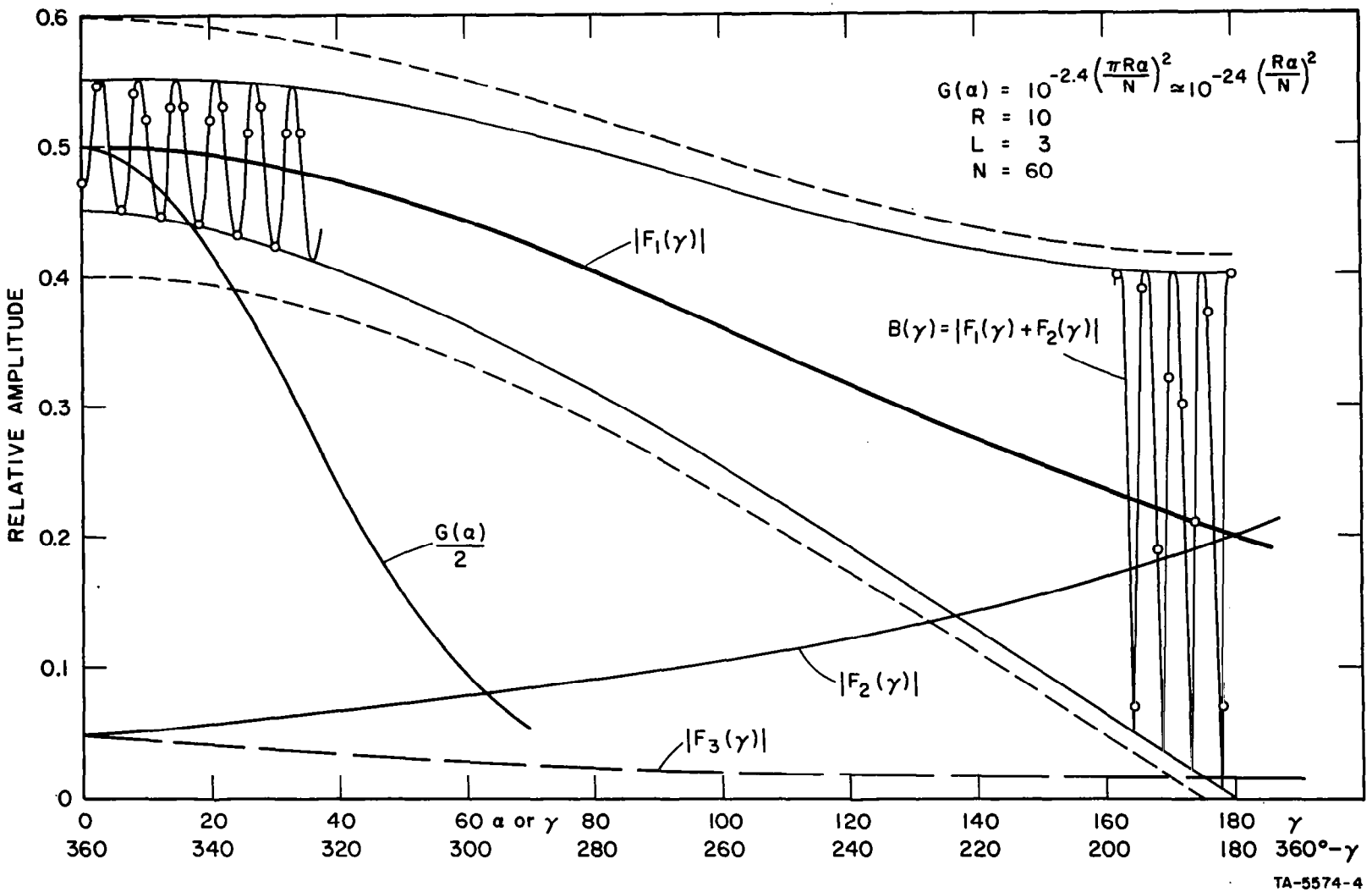

FIG. 25 RADIATION COMPONENTS FROM A SINGLE ELEMENTAL RADIATOR

to transform the original relatively narrow beam into an approximately omnidirectional pattern, albeit with some severe interference ripples. This pattern will be referred to as the "single-element pseudo-omni" pattern.

Figure 25 indicates that when the angle γ is nearly 180° there are extremely deep nulls in the pattern $B(\gamma)$ (approaching -40 dB). Such nulls could seriously affect the operation of some circuitry associated with one or another adaptive technique, but the null depth can be kept from falling too low by appropriate engineering design and taking into account the 3rd and 4th most significant rays.

By reciprocity, this pattern can be treated as either the transmitting or receiving pattern associated with one element. For the computations of radiation patterns, the further assumption is made that the transmitting antenna is essentially identical (measured in wavelengths) to the receiving antenna. If different antennas and simple lower-sideband phase conjugation are used, exact focussing will be obtained only when one antenna is an exact scale model of the other, the scale factor being the ratio of the respective wavelengths. This latter arrangement allows for any separation between the two frequencies.

In the receiving mode, the ordinate of the pattern represents the signal received by the particular element as a function of the azimuthal angle γ of the whole structure when the structure is illuminated by unit radiation from that particular azimuthal direction. The technique now being considered to make the antenna structure retrodirective is to provide electronic circuitry, a conjugating network, to operate on the incoming signal at each element in such a way that the element then reradiates a signal that has a relative phase angle of sign opposite to that of the incoming signal. In addition, the electronic circuitry will amplify, and thus determine the amplitude of, the reradiated signal.

The reradiated amplitude could theoretically be made to have any desired relationship to the incoming amplitude, but only three reradiated amplitude functions have been considered in the computer programs. These "modes of operation," or simply "modes," have already been discussed in Sec. III-C-1. In Mode 1 all elements radiate with equal amplitude, while in Mode 2 and Mode 3 they reradiate with an amplitude directly proportional to the relative amplitude received at that element. In practice, this can be implemented as follows: In Mode 1, the final

elemental amplifiers are each driven into saturation and thus deliver maximum RF power regardless of the incoming signal strength. In Mode 2 and Mode 3, linear amplifiers are used to amplify the incoming signals in such a way that no output amplifier is ever saturated.

In order to compute the reradiated antenna pattern, the principle of superposition is used to add (vectorially) the amplitudes of the patterns from each of the N elemental radiators. The relative phase of each of these elemental radiators is automatically adjusted by the conjugate network to put the contribution from each element in phase when observed from the direction of the incoming (pilot) signal. The pattern radiated from the biconical horn when a single element is illuminated is derived as described below.

With reference to Figs. 23 and 24, the following parameters are defined:

$R\lambda$ is the mean radius of the cylindrical geodesic lens and also the throat diameter of the biconical horn.

$LR\lambda$ is the length of the cylindrical lens.

$G(\alpha)$ is the radiation pattern of each elemental radiator within the geodesic lens.

α is the angle measured from the axis of each elemental radiator within the cylindrical geodesic lens and is therefore the angle that a particular ray makes with the direction of the main lobe of the elemental antenna. It is also the angle of incidence and reflection at the right-angle junction between the cylindrical and radial (biconical) lines.

γ is the azimuthal angle.

From Fig. 24, it is seen that

$$\tan \alpha = \frac{R(2\pi i + \gamma - \alpha)}{LR} \qquad \text{where} \qquad \pm i = 0, 1, 2 \ldots$$

which leads to the following very useful, but transcendental, parametric equations:

$$\alpha_1 + L \tan \alpha_1 = \gamma \qquad \text{for} \qquad \text{Ray } 0$$

$$\alpha_2 + L \tan \alpha_2 = 2\pi - \gamma \qquad \text{for} \qquad \text{Ray } -1$$

$$\alpha_3 + L \tan \alpha_3 = 2\pi + \gamma \qquad \text{for} \qquad \text{Ray } +1 \text{ etc.}$$

It can also be seen from the geometry that the higher-order rays contribute progressively lesser amounts of energy in the direction γ, because the gain function $G(\alpha)$ of the elemental antenna decreases and the space taper within the lens increases with α.

In order to determine the space taper for the biconical structure, consider the power radiated from an elemental radiator between the angles α and $\alpha + \Delta\alpha$.* The power density of the radiation into this angle $\Delta\alpha$ can be defined as

$$G(\alpha)^2 \text{ watts/unit angle} \qquad \text{as } \Delta\alpha \text{ is small}$$

The total power radiated into $\Delta\alpha$ is then $G(\alpha)^2\Delta\alpha$. Since we assume there is a perfect match at the transition, this same power is radiated from the biconical antenna, after reflection from the junction between the cylindrical and biconical lines, into an angle $\Delta\epsilon$ (defined in Fig. 26), resulting in a power density

$$G(\alpha)^2 \frac{\Delta\alpha}{\Delta\epsilon}$$

Now, at some distant observation point, the virtual point p (see Fig. 26) is indistinguishable from the center of the antenna (point q), except for a phase term, so that $\Delta\epsilon$ is equivalent to a small azimuthal angle $\Delta\gamma$ of equal value. Hence,

$$|F(\gamma)| = G(\alpha)\Delta\alpha/\Delta\epsilon)^{1/2}$$

where $F(\gamma)$ is the complex amplitude function of the biconical horn (excluding the effects of multipath interference).

---

* It will be assumed that the space taper in the azimuthal direction for radiation from the biconical horn is independent of the space taper in the axial (elevation) plane. This is a common and usually satisfactory simplification in the computation of antenna patterns. The effect of axial space taper will therefore be neglected at present, since it applies equally to the radiation patterns to be computed and to the patterns of the hypothetical omni-azimuthal antenna, which, as has been mentioned above, is being used as the reference antenna.

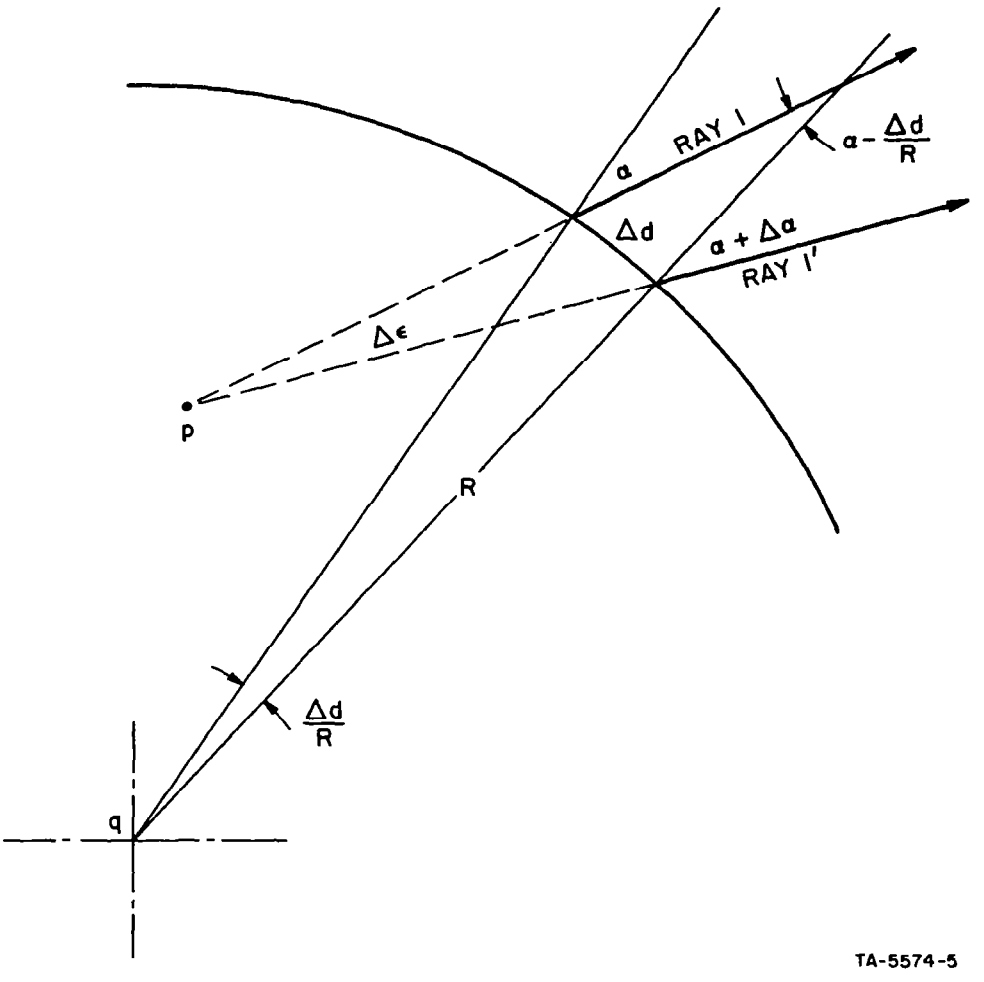

FIG. 26 ENLARGEMENT OF PORTION OF FIG. 24 SHOWING THE APPARENT SOURCE OF RADIATION

Referring to Fig. 24,

$$\Delta d = LR[\tan(\alpha + \Delta\alpha) - \tan\alpha]$$

$$\frac{\Delta d}{R} = L\,\frac{\tan\alpha + \tan\Delta\alpha - \tan\alpha + \tan\Delta\alpha\tan^2\alpha}{1 - \tan\Delta\alpha\tan\alpha}$$

$$= L\Delta\alpha\,\frac{1 + \tan^2\alpha}{1 - \Delta\alpha\tan\alpha} \quad \text{since} \quad \tan\Delta\alpha = \Delta\alpha \ \text{ if } \ \Delta\alpha \text{ is small} \ .$$

Referring to Fig. 26,

$$\Delta\epsilon = (\alpha + \Delta\alpha) - \left(\alpha - \frac{\Delta d}{R}\right)$$

$$= \Delta\alpha\left(1 + L\,\frac{\sec^2\alpha}{1 - \Delta\alpha\,\tan\alpha}\right)$$

and

$$\lim_{\Delta\alpha \to 0} \Delta\epsilon = \Delta\alpha(1 + L\sec^2\alpha) \quad \text{except where} \quad \alpha \to \pm\frac{\pi}{2} \quad .$$

Hence,

$$|F(\gamma)| = G(\alpha)(1 + L\sec^2\alpha)^{-1/2} \quad .$$

To determine the relative phase of the radiation, again associated with a single elemental radiator and observed at points at a large but constant distance D from the center of the biconical structure, consider the length of each ray, or geodesic, as a function of γ, or more conveniently as a function of α:

The length within the lens is $LR\lambda\sec\alpha$.

The length outside the lens is $D - R\lambda\cos\alpha$.

The relative length is then $R\lambda\left(\frac{L}{\cos\alpha} - \cos\alpha\right)$.

The relative phase difference is $2\pi R\left(\frac{L}{\cos\alpha} - \cos\alpha\right)$.

Hence,

$$F(\gamma) = \frac{G(\alpha)}{(1 + L\sec^2\alpha)^{1/2}} \exp\left[j2\pi R\left(\frac{L}{\cos\alpha} - \cos\alpha\right)\right] \quad .$$

As can be seen from Fig. 24, there is more than one ray, or geodesic (*i.e.*, line of minimum electrical length), joining the elemental radiator with any distant observation point, depending on which way the ray turns around the cylinder and how many turns it makes within the cylindrical portion of the antenna. These several rays will interfere with each other to produce ripples in both amplitude and phase as a function of azimuthal angle γ. The amplitudes of the first-, second-, and third-order rays are plotted in Fig. 25 for some typical antenna parameters.

It can be seen that the third-order ray is everywhere less than 10 percent (>20 dB down) of the first-order or principal ray; therefore, for the purposes of computation of antenna patterns it was neglected. One justification for this simplification is that the very principle of operation of the retrodirective antenna array employing conjugate networks tends to compensate automatically for such perturbations as the effects of mutual coupling and, in this case, higher-order rays.

Because the length of the first-order ray increases with γ, while the second-order ray decreases, the addition of $F_1(\gamma)$ and $F_2(\gamma)$ produces an interference pattern whose amplitude varies between

$$|F_1(\gamma)| + |F_2(\gamma)| \quad \text{and} \quad |F_1(\gamma)| - |F_2(\gamma)|$$

These limits are shown in Fig. 25, as well as an estimation of portions of the pseudo-omni pattern function:

$$B(\gamma) = |F_1(\gamma) + F_2(\gamma)|$$

based on points computed every two degrees which are indicated in Fig. 25. If $F_3(\gamma)$ had also been taken into account, $B(\gamma)$ would have varied between the two dashed limits shown in Fig. 25. The somewhat more complex curve of a typical $B(\gamma)$ function, obtained by considering the three most significant rays, computing many more points, and plotting the results automatically on the computer, is shown in Fig. 27.

The elemental antenna amplitude function $G(\alpha)$ used in these computations was chosen to give the antenna a 3-dB beamwidth of 1 radian per wavelength/aperture, and a commonly used parabolic logarithmic beam shape—*i.e.*, the beamwidth relationship over the angles of interest is given by

$$\frac{dB_1}{dB_2} = \left(\frac{\alpha_1}{\alpha_2}\right)^2$$

It has been further assumed that the bottom of the cylindrical lens is completely filled with contiguous elemental antennas. Thus, the

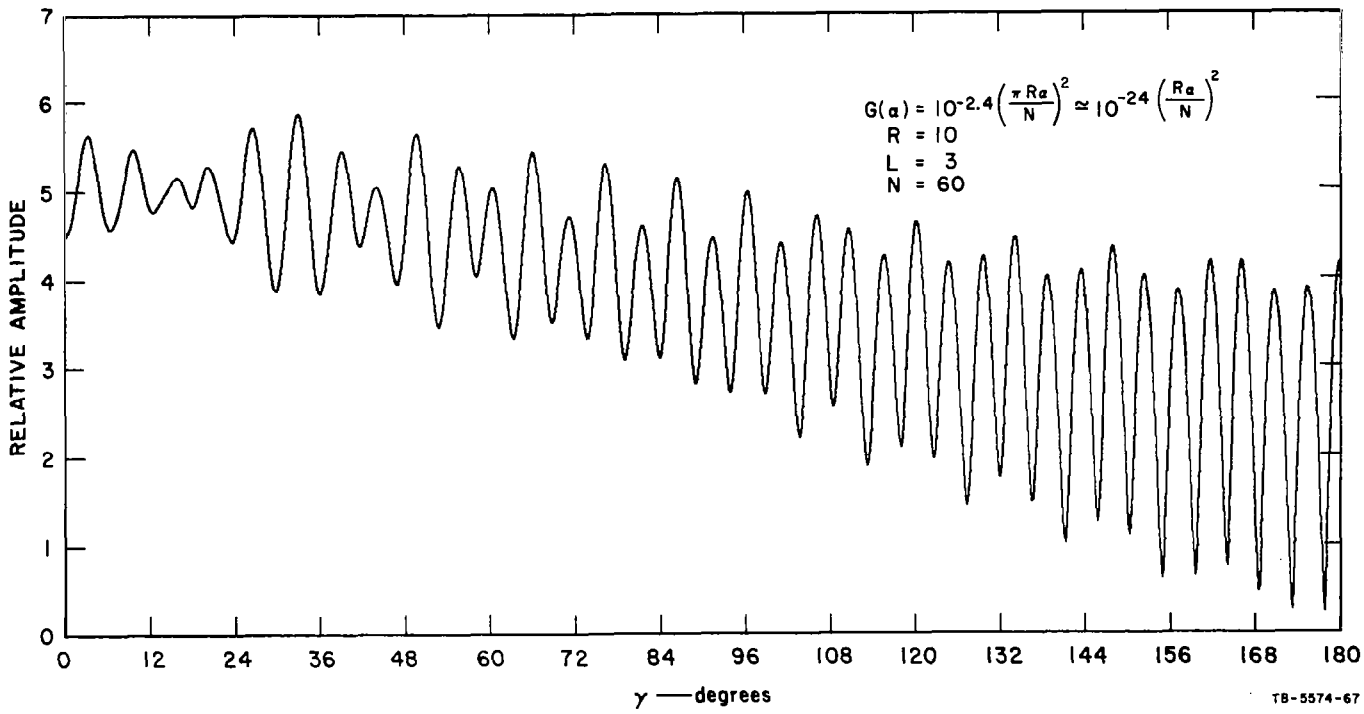

FIG. 27 COMPUTED "PSEUDO-OMNI" PATTERN FOR A SINGLE ELEMENT USING THREE MOST SIGNIFICANT RAYS

size of each aperture is $2\pi R/N$ wavelengths. This leads to an elemental amplitude function given by

$$G(\alpha) = 10^{-2.4}\left(\frac{\pi R\alpha}{N}\right)^2 \simeq 10^{-24(R\alpha/N)^2}$$

which has been used for all the computations to date.

c. Computation of the Reradiation Pattern

Once the radiation pattern of the biconical horn due to a single elemental antenna, given by

$$B(\gamma)e^{j\Omega(\gamma)} \quad ,$$

has been determined, it is assumed that when the whole structure is used as a retrodirective antenna, the nth radiator will retransmit a pattern given by

$$D_n B(\gamma + \Delta_n)e^{j[\Omega(\gamma+\Delta_n)-\Omega(\Delta_n)]}$$

which gives each of the pseudo-omni patterns a net electrical phase angle equal to zero in direction $\gamma = 0$.

Using the principle of superposition, these N complex patterns are summed to obtain the final retrodirected transmitter pattern. The azimuthal position of the nth elemental radiator is defined by Δ_n, and D_n is an amplitude weighting function. As has already been mentioned, for Mode-1 operation, $D_n = 1$, and for Mode 2, $D_n = B(\Delta_n)$.

The conjugate networks assure that in the retrodirection, all the elements add in phase regardless of the complexity of the radiation pattern characteristics in that direction. There is, however, no assurance that any particular element will contribute to the gain in the desired direction, since the elemental pattern may have a null in that direction. The antenna parameters can be chosen so that the deepest nulls, usually occurring for values of γ near ±180 degrees, can be prevented from falling to too low a value.

d. Computation of Azimuthal Gain

In order to determine the gain of any given antenna, the peak power of the radiation pattern is compared with the average power radiated in all azimuthal directions. This average power can be computed in several ways, and at least two methods were employed for each of the six computed patterns represented in Table VI. These methods are as follows:

Method 1. Compute the average scalar power value of the pseudo-omni single-element pattern and then add the contribution from each of the N elements, without regard to phase relationship. The average value can only be approximated, since the pseudo-omni pattern, like the final radiation pattern, is only computed every $360/m$ degrees, which in practice is relatively large compared to the ripples in the pattern.

Table VI

SUMMARY OF DATA FOR SIMPLE RETRODIRECTIVE TYPE-1 ANTENNA WITH EQUAL RECEIVE AND TRANSMIT FREQUENCIES

FIG. NO.	PARAMETER										
	R	L	N	ψ	Mode	Gain 1	Gain 2	Gain 3	Gain 4	P	Beamwidth
28	10	3	60	0	1	17.13	17.10	17.35	16.99	17.78	4.2°
29	10	3	60	0	2,3	17.42	17.41	--	17.19	17.78	4.4°
30	10	3	90	0	1	19.09	19.15	--	18.70	19.55	3.4°
31	10	3	90	0	2,3	19.53	19.47	--	--	19.55	3.2°
32	10	3	30	0	1	13.01	12.99	--	12.91	14.77	5.5°
33	10	3	30	2	1	13.01	12.99	--	12.91	14.77	5.5°
34	5	3	30	2	1	14.27	14.24	14.49	14.11	14.77	8.0°
35	5	3	30	2	2,3	14.65	14.65	--	--	14.77	8.3°
--	10	3	60	*	1	17.41* ± 0.3	--	--	--	17.78	--
--	10	3	61	*	1	17.48* ± 0.4	--	--	--	17.86	--
--	10	3	61	*	2	17.84* ± 0.4	--	--	--	17.86	--
--	10	3	61	*	3	17.89* ± 0.9	--	--	--	17.86	--
--	10	3	60	†	1	17.40† ± 0.3	--	--	--	17.78	--
--	10	3	60	†	2	17.77† ± 0.3	--	--	--	17.78	--
--	10	3	60	†	3	17.77† ± 0.6	--	--	--	17.78	--
--	10	2	60	0	1	17.84	--	--	--	17.78	--
--	10	2	60	0	2,3	17.78	--	--	--	17.78	--
--	10	5	60	0	1	17.89	--	--	--	17.78	--
--	10	5	60	0	2,3	18.17	--	--	--	17.78	--
--	10	5	60	2	2,3	17.57	--	--	--	17.78	--

* Averaged over a complete cycle with computed points every 1 degree.

† Using 3-ray computation rather than just 2-ray, and averaged over complete cycle with points computed every 0.25 degree.

This is obvious in the plot of $B(\gamma)$ in Fig. 21, where $m = 180$. Expressed in dB, this average value is given by

$$K_1 = 10 \log \frac{1}{m} \sum_{j=1}^{m} B_j^2 \sum_{n=1}^{N} D_n^2 \quad .$$

Method 2. Provided the complete azimuthal radiation pattern $S(\gamma)$ has been computed, compute the average scalar power value of $S(\gamma)$. For reasons similar to those given above, this method is only approximate and should give similar accuracy. Again, expressed in dB this average value is given by

$$K_2 = 10 \log \frac{1}{m} \sum_{j=1}^{m} S_j \quad .$$

Method 3. Instead of assuming that each element reradiates the conjugate phase, it is assumed that each radiates with equal phase. (This mode of operation may well be used in practice to establish contact between two adaptive antennas as discussed in Sec. V-C). The final radiation pattern is then computed in the same way, and should result in an approximately omnidirectional pattern. This pattern will have at least N ripples in it, but its average value is readily estimated and is designated by K_3.

Method 4. Compute the average power value of the radiation pattern within the cylindrical lens and sum the contribution from each element without regard to phase relationship. Expressed in dB, this average value is given by

$$K_4 = \frac{C}{2\pi} \int_{-\pi}^{\pi} G(\alpha)^2 d\alpha \sum_{1}^{N} D_n^2$$

where C is a normalization factor relating power density within the cylindrical lens to power density radiated from the biconical horn.

e. Results of Some Computations

Table VI shows the results of some sample computations, for equal receive and transmit frequencies, that are associated with the computed antenna patterns shown in Figs. 28 through 35, together with

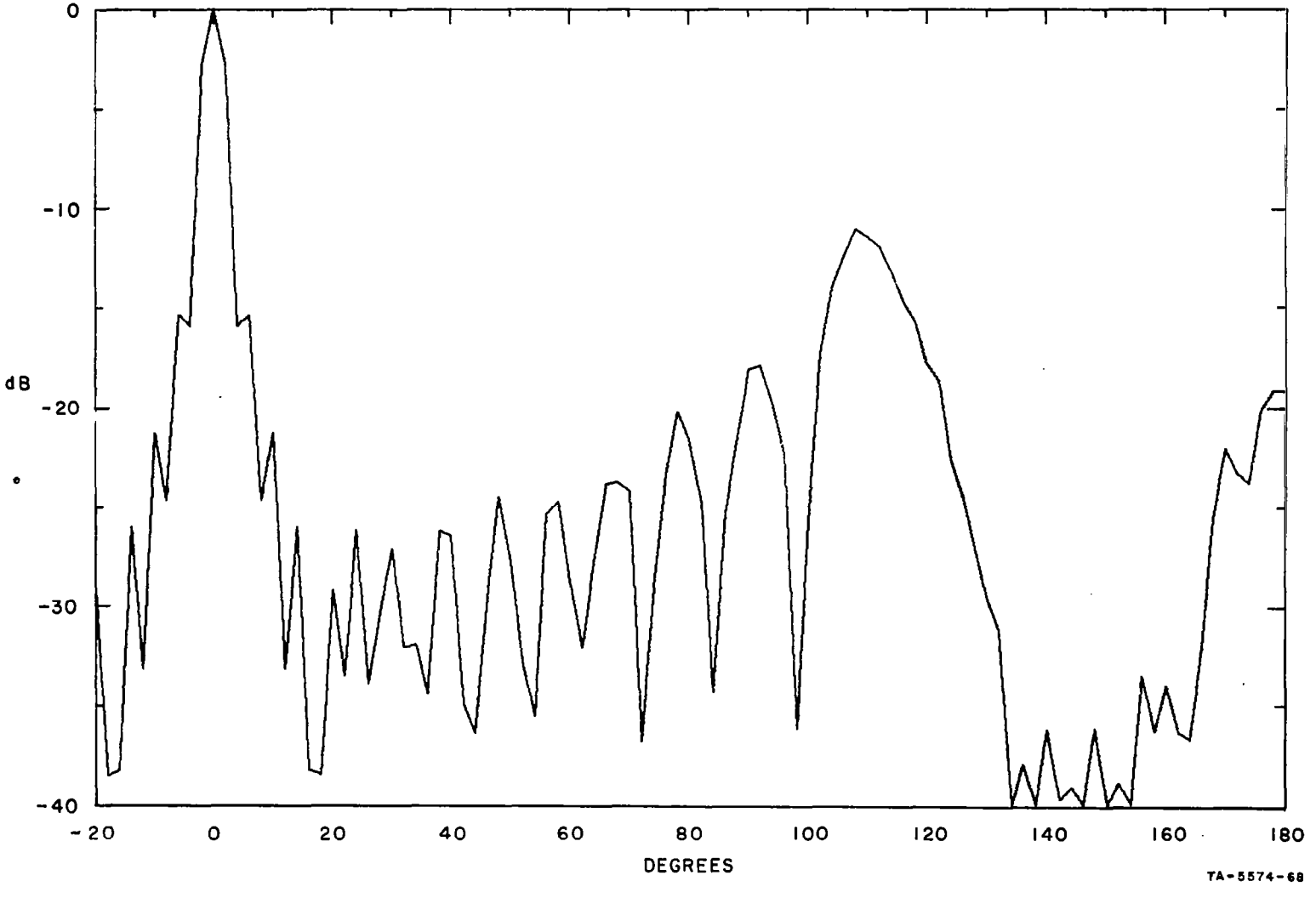

FIG. 28 PATTERN FOR 20λ-DIAMETER ANTENNA OF 60 EQUAL-POWER ELEMENTS

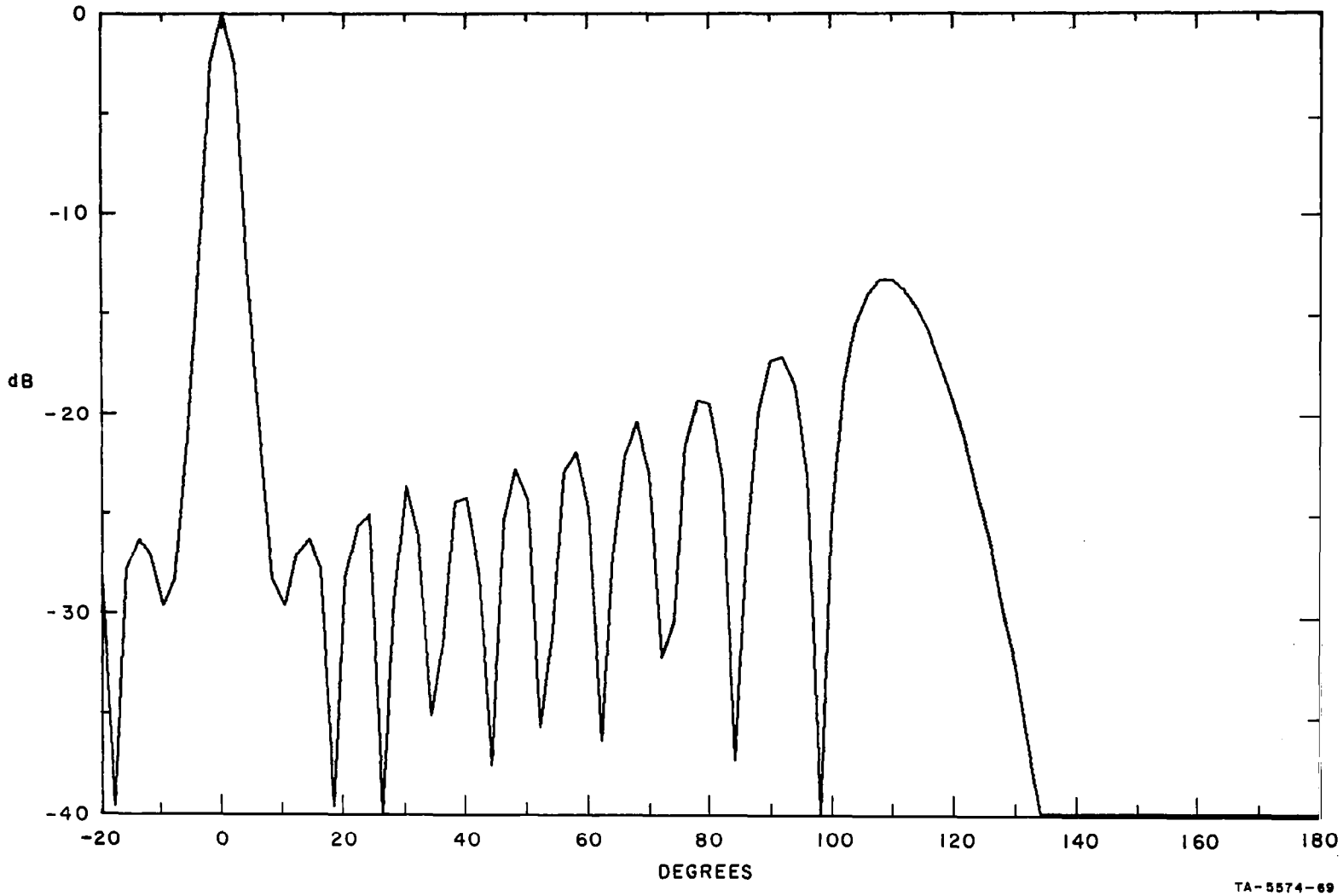

FIG. 29 PATTERN FOR 20λ-DIAMETER ANTENNA OF 60 WEIGHTED ELEMENTS

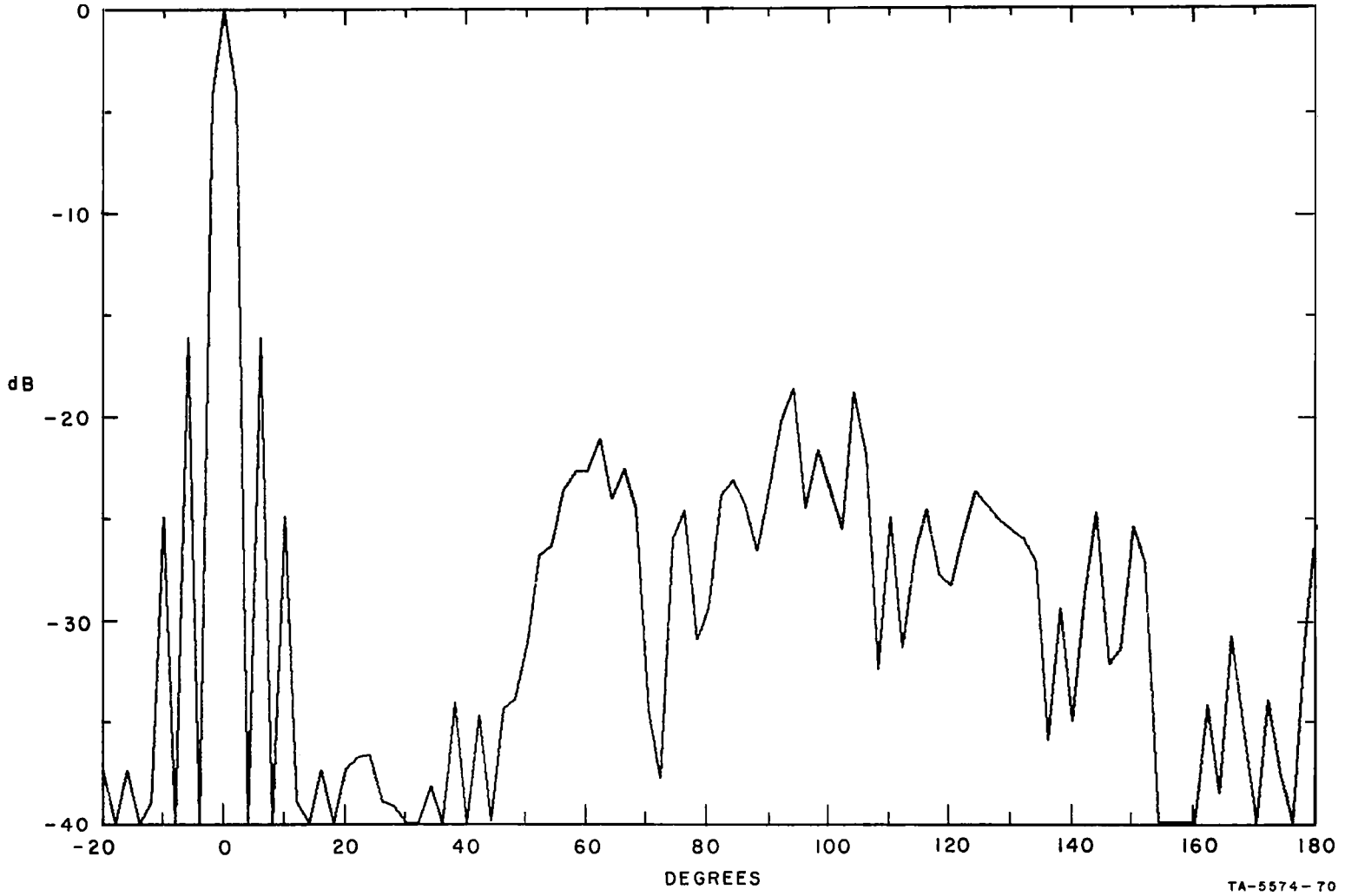

FIG. 30 PATTERN FOR 20λ-DIAMETER ANTENNA OF 90 EQUAL-POWER ELEMENTS

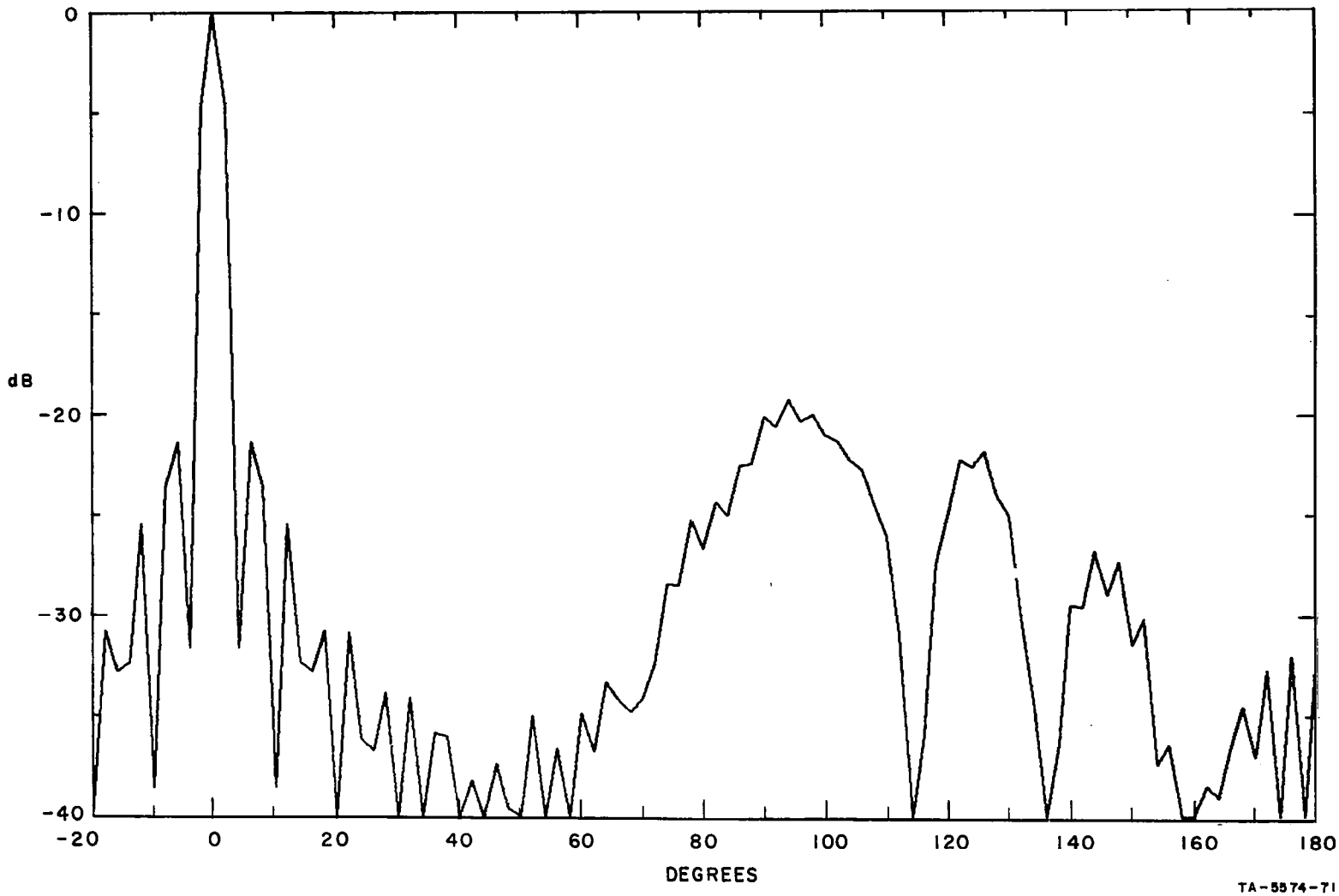

FIG. 31 PATTERN FOR 20λ-DIAMETER ANTENNA OF 90 WEIGHTED ELEMENTS

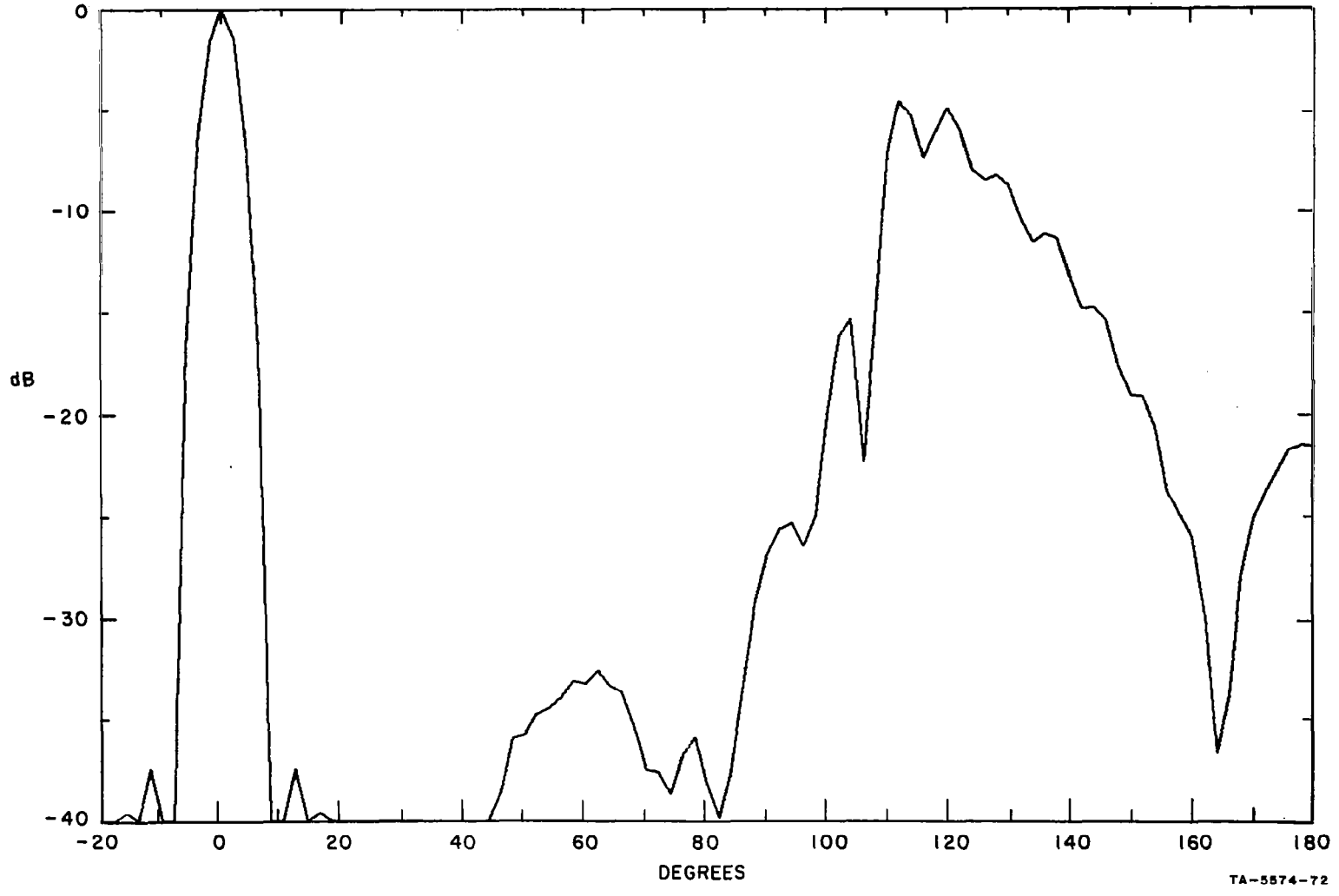

FIG. 32 PATTERN FOR 20λ-DIAMETER ANTENNA OF 30 EQUAL-POWER ELEMENTS

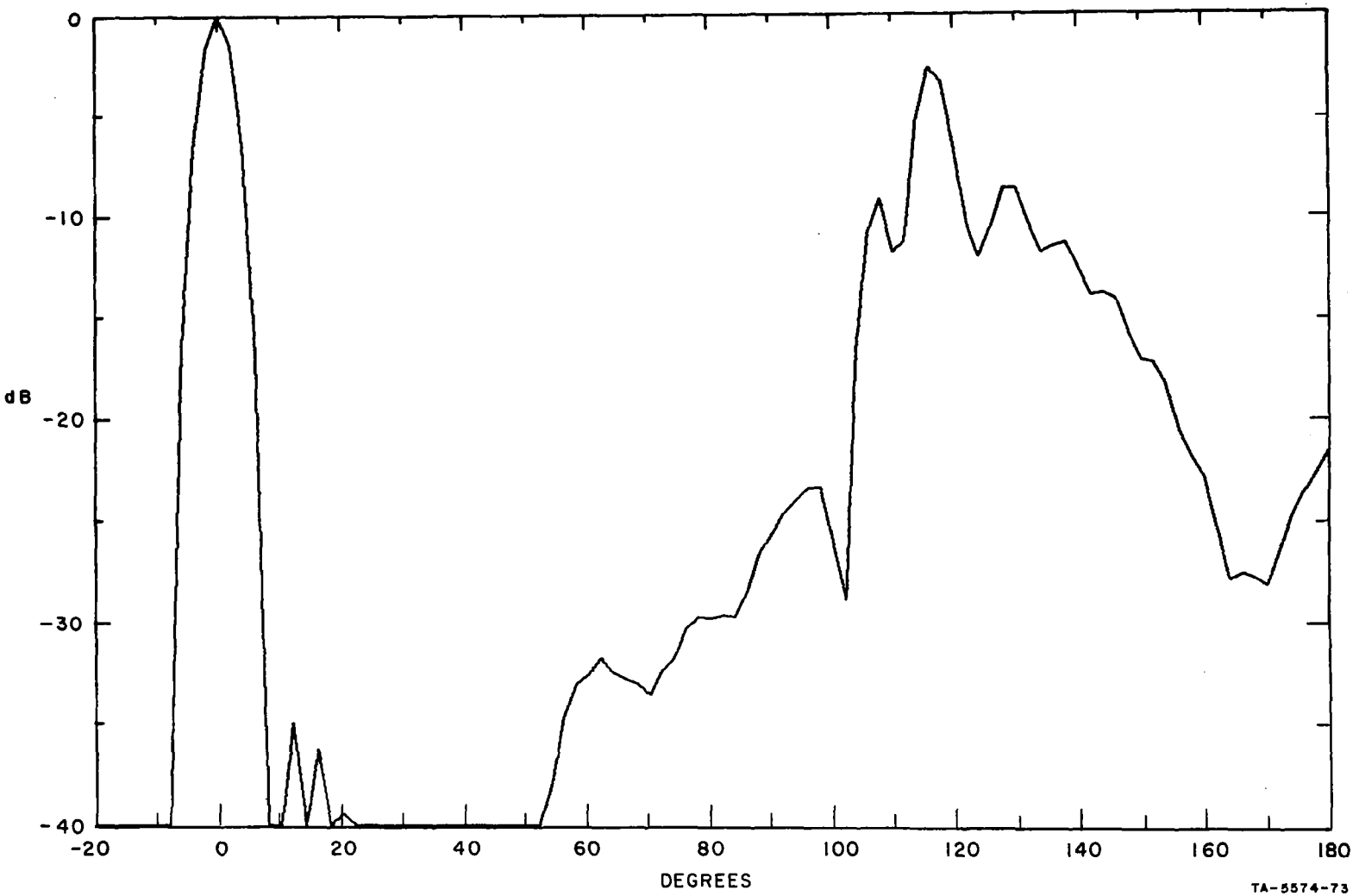

FIG. 33 PATTERN FOR 20λ-DIAMETER ANTENNA OF 30 EQUAL-POWER ELEMENTS (Asymmetrical)

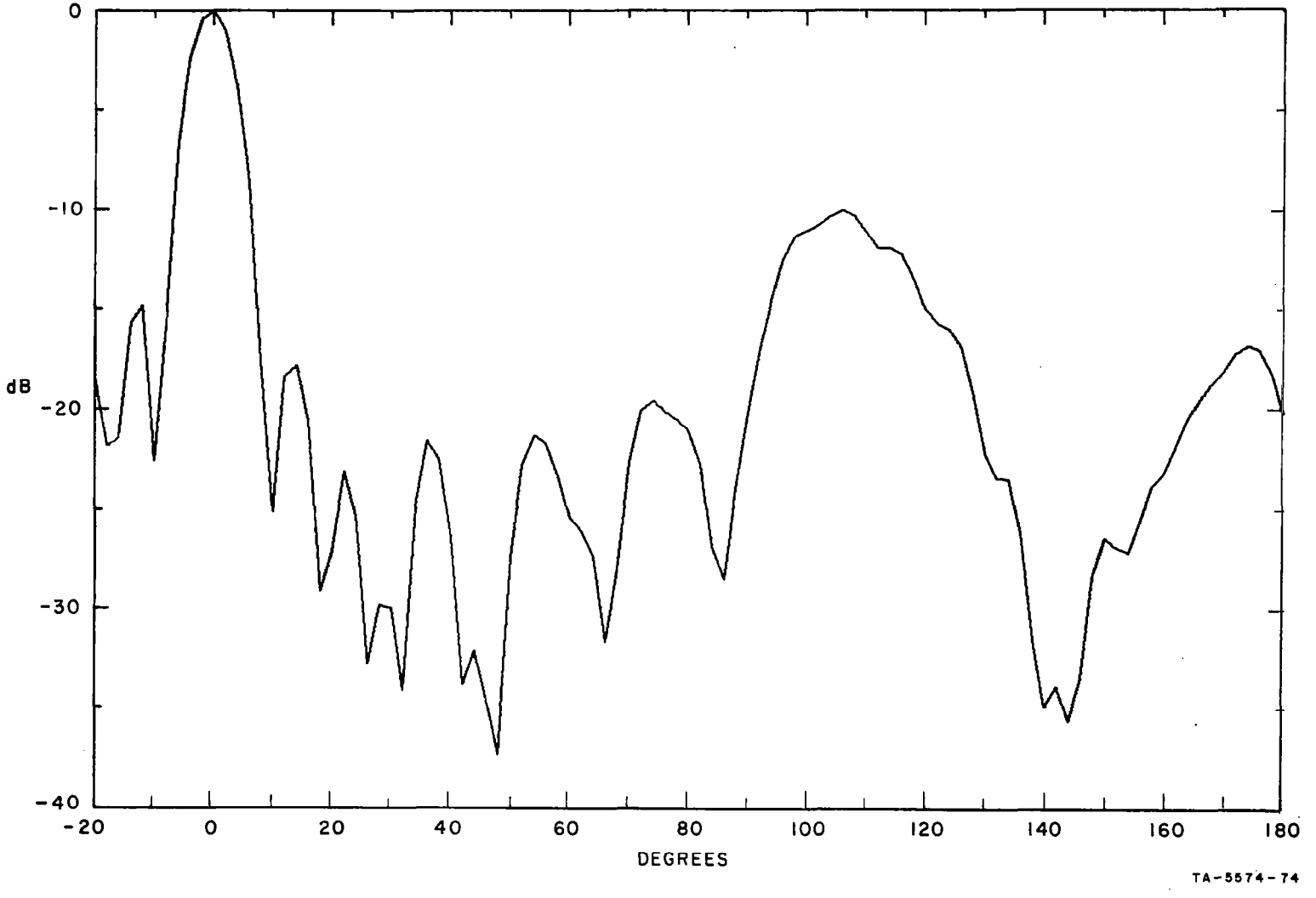

FIG. 34 PATTERN FOR 10λ-DIAMETER ANTENNA OF 30 EQUAL-POWER ELEMENTS

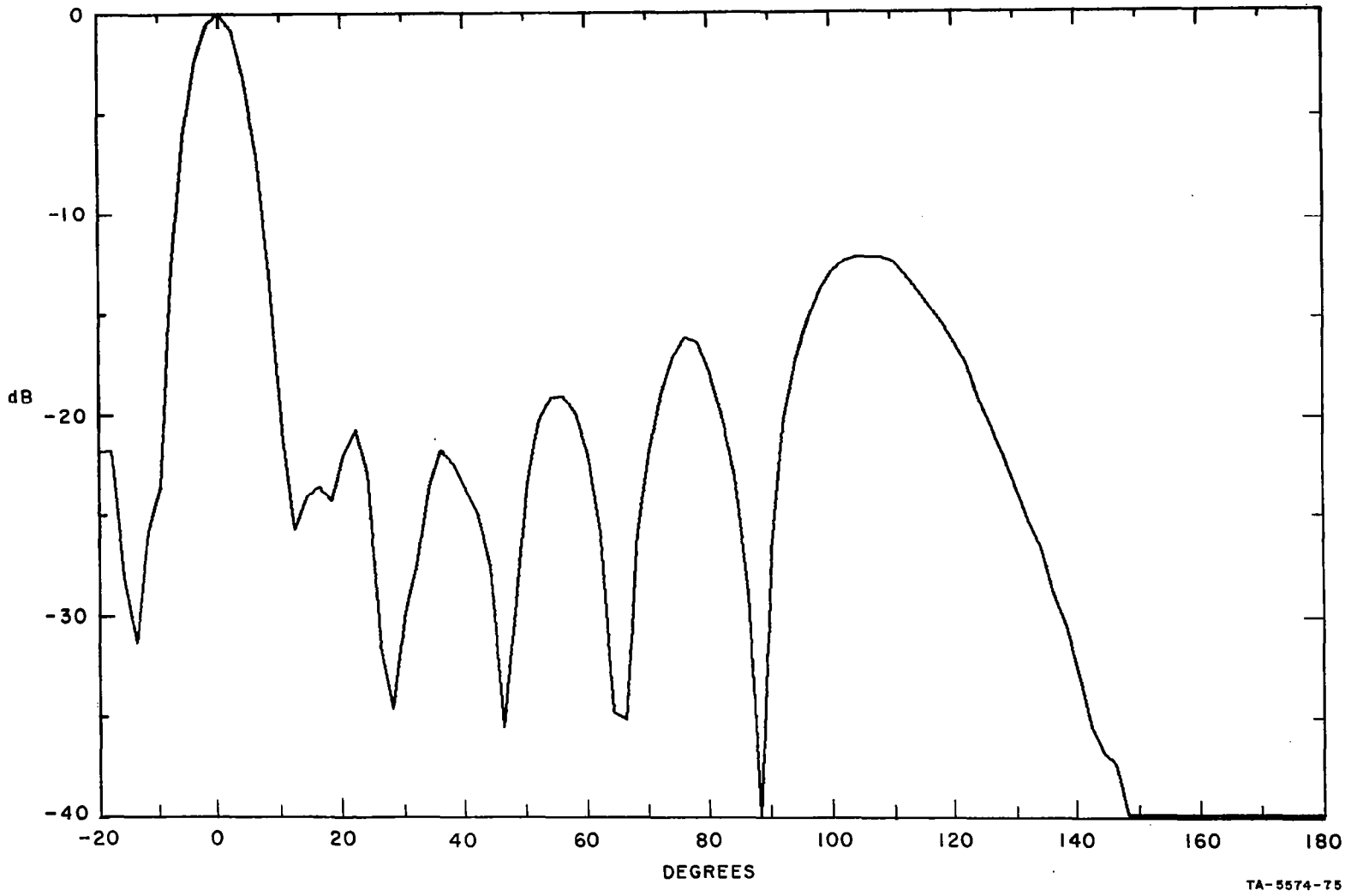

FIG. 35 PATTERN FOR 10λ-DIAMETER ANTENNA OF 30 WEIGHTED ELEMENTS

other data for which complete radiation patterns were not computed. Also tabulated are some of the input parameters. It should be noted that points on each pattern were only computed every 2 degrees and the plotting machine is not capable of predicting the peak value of the sidelobes of the radiation patterns. Either Mode 2 or Mode 3 can be assigned to the patterns using "weighted elements"—*i.e.*, linear amplifiers—since the data was computed in each case for a single azimuthal angle. Consequently, no averaging over a cycle was involved.

It has been shown by Cutler *et al.*,[76] that the maximum overall average antenna gain G', of N elements each with a peak gain of g', and with the elemental main lobes directed more or less uniformly in all directions, is given by $G' = N/g'$. The same arguments can be used to show that the maximum gain for an antenna that radiates only in the azimuthal direction is also given by $G'' = N/g''$, if g'' is now the azimuthal gain of each element. The overall azimuthal gain G'' obviously has a maximum of N when g'' is unity—that is, when the elemental antennas have omniazimuthal patterns. It is assumed that these elements are randomly located in free space, with their radiation planes all parallel, and that they are sufficiently separated from each other that all mutual coupling effects are negligible. This gain is realizable in any azimuthal direction provided the elements are appropriately phased and power is equally divided among them. Hence, the maximum theoretical gain to be expected from any of the antennas for which patterns were computed, averaged over all values of retrodirection and expressed in dB, is

$$P = 10 \log N \quad .$$

This value is also tabulated for comparison in Table VI. The 3-dB beamwidth, estimated from the pattern plots, is also included in Table VI. The various gain values are obtained from the computed values of K_i and the amplitude of the gain function in the retrodirection, V, computed in dB. The gain is then given by

$$\text{Gain } (i) = V - K_i \quad .$$

It must be remembered, however, that this value of gain refers only to a particular value of retrodirection (with respect to element location). As is seen in the later data, this gain value does vary with retrodirection angle ψ.

The following significant points are apparent from the computed curves and values of gain in the retrodirection.

(1) The sidelobe levels are relatively high and when linear (weighted) amplifiers are used and the inter-element spacing around the circumference of the lens is of the order of one wavelength, the sidelobe structure has a remarkably monotonic characteristic until the level falls to less than -40 dB in the back region of the antenna.

(2) The far-out sidelobe levels are considerably lower for the $N = 90$ case—*i.e.*, when the inter-element spacing is 0.70λ, having a maximum value approximately equal to the omni-azimuthal level.

(3) The postulated maximum theoretical gain, P, is generally larger than any of the computed values of gain which, when the value is computed by more than one method, are very similar.

(4) Values of $L = 2$ or 5 appear to give higher values of gain than for $L = 3$, but computations for all values of ψ will have to be made before it can be determined what the relative *average values* of computed gain are. Only the case of $L = 3$ was explored in any detail.

(5) The computed gain values for linear amplifiers are generally slightly higher than for Mode-1 operation as has been anticipated.

(6) The average value of gain for Mode-3 operation must be the same as for Mode 2 when the rest of the parameters are the same (although the computed average values might not be quite the same if insufficient data points are computed). However, it is seen that the variation in gain, and consequently in amplitude modulation of a spinning antenna, is greater for the Mode-3 operation. This is considered to be pure coincidence since it is anticipated that the gain variation for any predetermined mode can be made very small if the parameters, including operating frequency, are correctly chosen for operation in the particular mode.

(7) There is an apparent gain increase of 1.2 dB when the antenna diameter is halved but N is kept constant at 30. As can be seen from the curves, the larger antenna has the narrower beamwidth but its lower gain is accounted for by the large sidelobes.

(8) If only every alternate element of the 60-element antenna were used to radiate the available RF power, with the unused elements terminated, it is postulated that there would be a loss of gain of only about 3 dB. Such an antenna would appear to have about 1-dB more gain than the computed case for a similarly sized antenna with 30 elements, where the elemental radiators fill the bottom of the cylindrical lens. This indicates that the highest final gain is obtained with elemental radiators having low gain within the cylindrical lens. Whatever $G(\gamma)$ function is employed, using only 30 elements in a 10λ radius lens will produce large sidelobes and a narrow beam.

(9) Comparing Figs. 32 and 33, there is no apparent change in gain when the peak of the beam is changed by 2 degrees, even though the pattern shapes change. This is not a general rule and is purely coincidental in this case, as can be seen from the subsequent data where the value of retrodirective gain sometimes varies appreciably about its average value.

(10) The beamwidth of each antenna is much less than the value $360/N$ degrees, which represents the maximum beamwidth obtainable if all the power associated with the maximum postulated gain, N, is concentrated in the main beam. This indicates that there is a lot of power in the sidelobes. As can be expected, because it has the lowest sidelobes, the largest value of beamwidth times $N/360$ is obtained when $N = 90$. The value is 0.85. In a purely retrodirective antenna in free space, only the maximum ERP in the retrodirection is of consequence, but if the antenna is also to give directional information or operate in more than one direction, sidelobes, main-beam squint, and other pattern characteristics could be of some consequence. In the case of a capsule approaching the planet, sidelobe power reflecting off the planet could cause serious interference with the main transmitted beam, if the reflection is anywhere nearly specular.

(11) There is apparently no significant difference in the results obtained with 60 and 61 elements. There was no apparent reason to anticipate that results obtained with odd and even numbers of elements would be different, but some computations were made for the same reasons mentioned in Secs. III-C-2-d for the Type-3 antenna.

f. Additional Antenna Radiation Patterns

An additional set of radiation patterns was computed to observe the effect of the sidelobe structure for different azimuthal angles. The elementary transmitters are assumed to be correctly phased to produce reinforcement in the particular direction denoted by ψ. The method by which this phasing is achieved is immaterial—it could be by retrodirective techniques, or by programmed phasing, etc.—the patterns are general for the parameters assumed. The patterns are shown in Figs. 36 through 40. It is again assumed that only the first two significant rays contribute to the pattern. In practice, the phasing of each element would have to be modified slightly if programmed phasing is used (phasing is automatically correct for a simple degenerate retrodirective antenna), to take account of the small contributions from the infinite number of rays that theoretically exist. However, the patterns are not expected to differ significantly from the patterns shown.

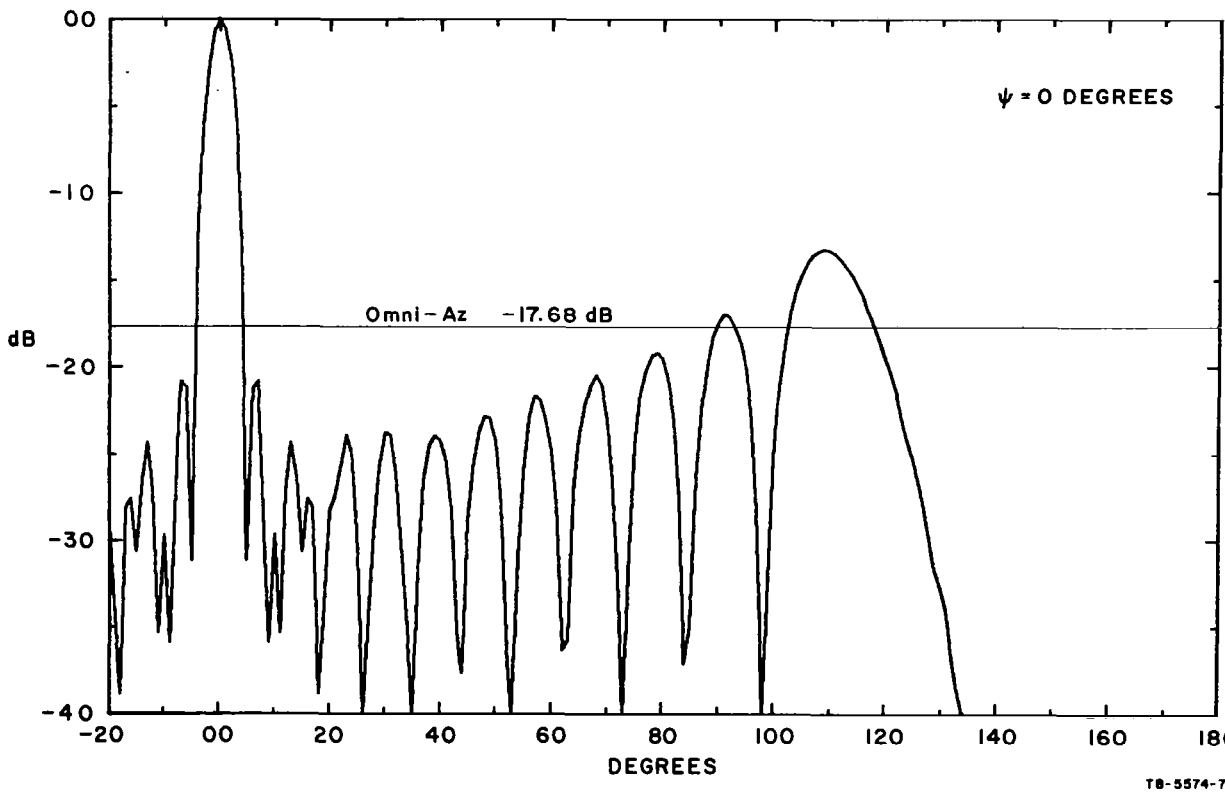

FIG. 36 RADIATION PATTERNS FOR TYPE-1 ANTENNA (2-Ray Theory) FOR VARIOUS ORIENTATIONS — R = 10, L = 3, N = 60, ψ = 0

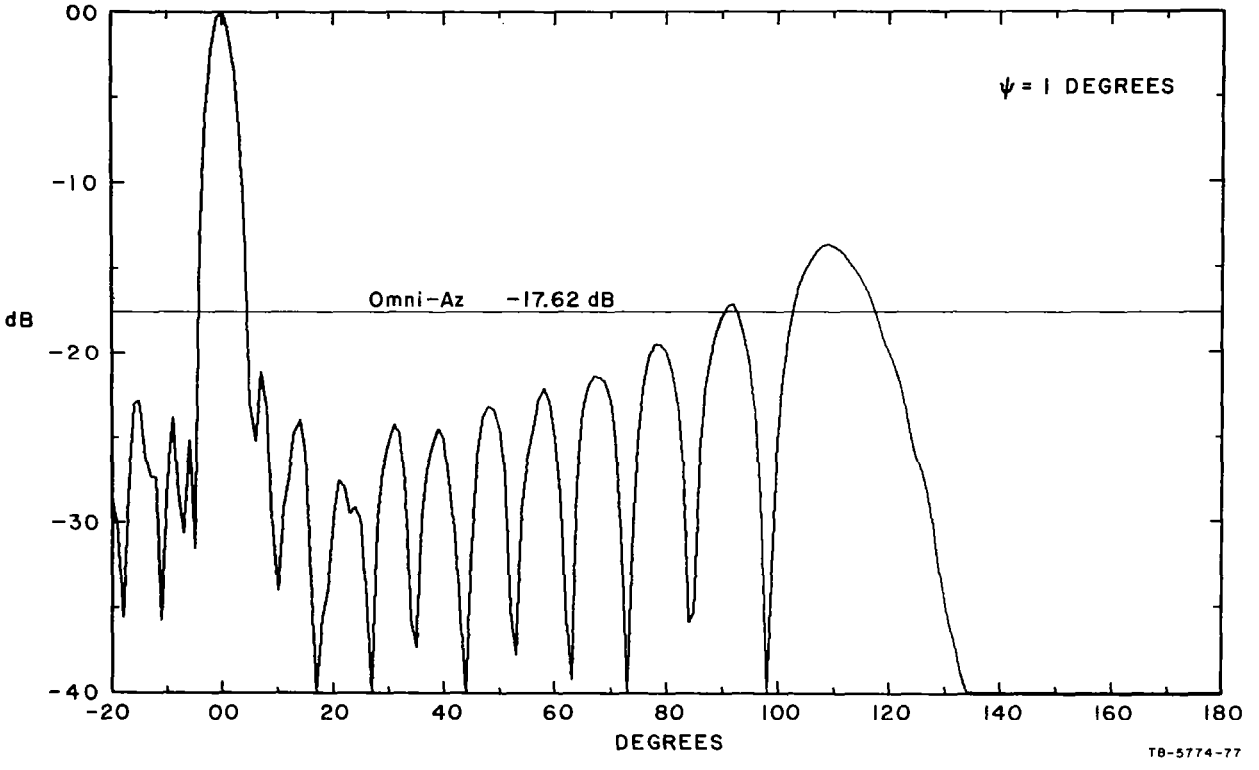

FIG. 37 RADIATION PATTERNS FOR TYPE-1 ANTENNA (2-Ray Theory) FOR VARIOUS ORIENTATIONS — R = 10, L = 3, N = 60, ψ = 1

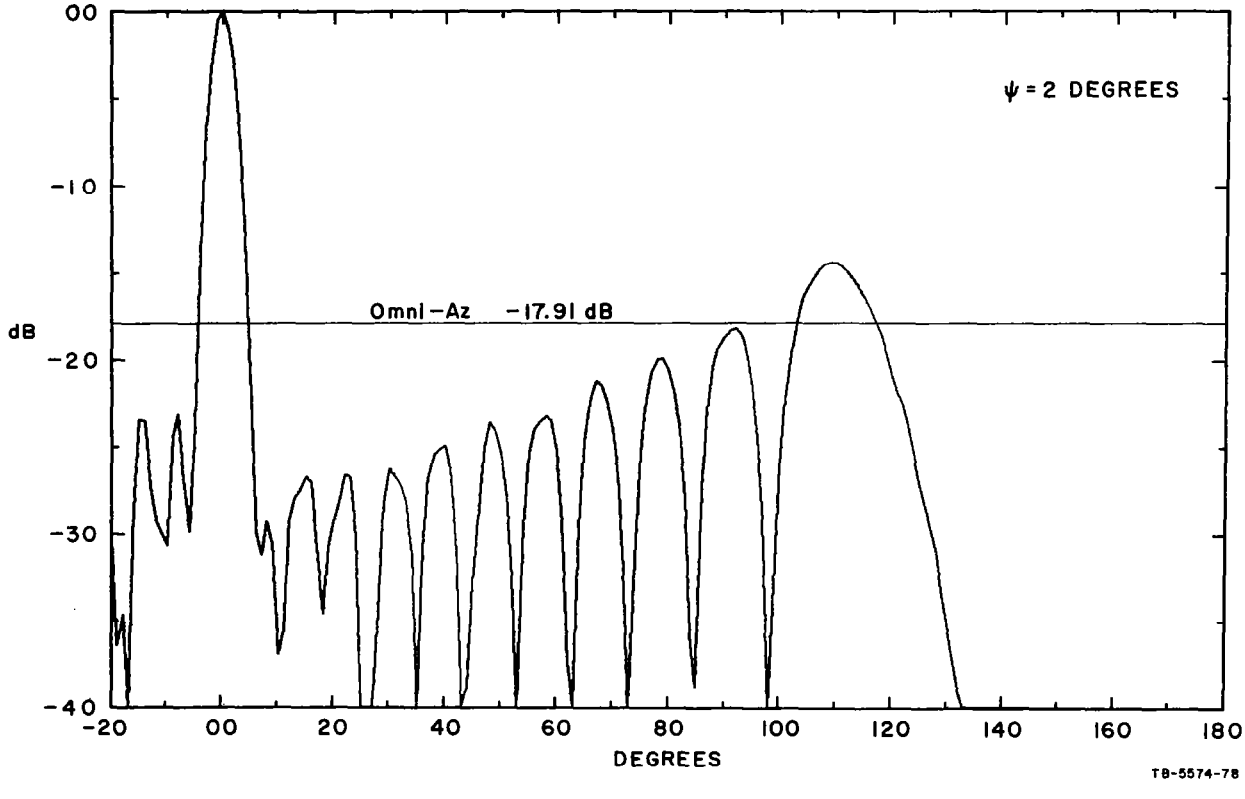

FIG. 38 RADIATION PATTERNS FOR TYPE-1 ANTENNA (2-Ray Theory) FOR VARIOUS ORIENTATIONS — R = 10, L = 3, N = 60, ψ = 2

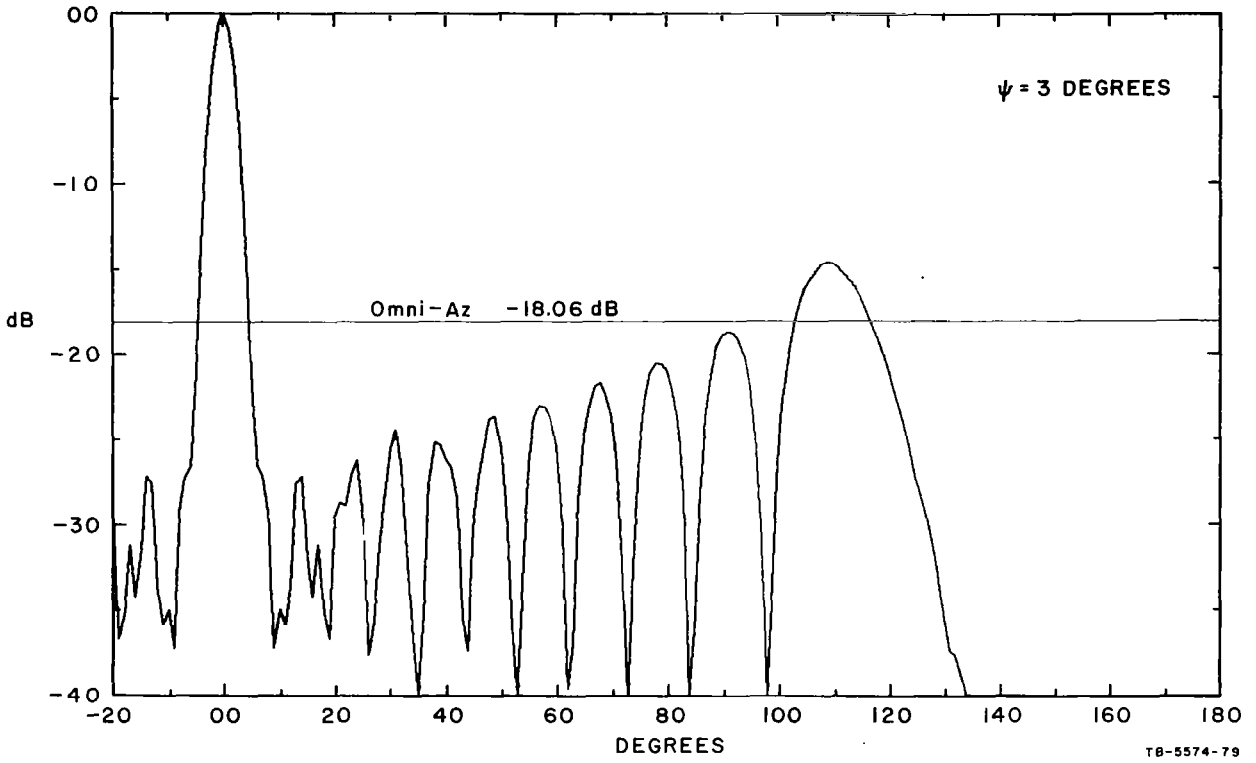

FIG. 39 RADIATION PATTERNS FOR TYPE-1 ANTENNA (2-Ray Theory) FOR VARIOUS ORIENTATIONS — R = 10, L = 3, N = 60, ψ = 3

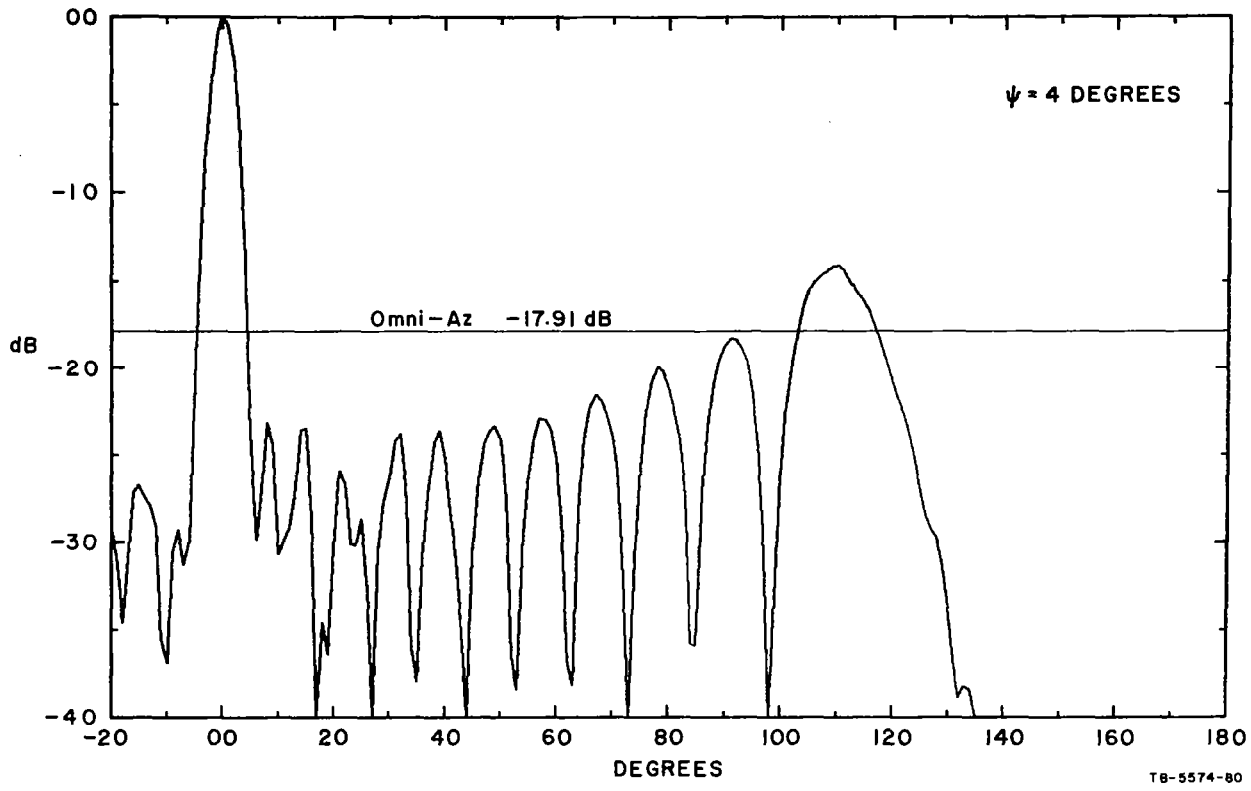

FIG. 40 RADIATION PATTERNS FOR TYPE-1 ANTENNA (2-Ray Theory) FOR VARIOUS ORIENTATIONS — R = 10, L = 3, N = 60, ψ = 4

Other data relating to the patterns is as follows:

Linear amplifiers assumed (Mode 2 or Mode 3)

$R = 10\lambda$

$L = 3$

$N = 60$

$\psi = 0, 1, 2, 3, 4$.

It should be noted that the antenna parameters relating to Fig. 36 are identical to those for Fig. 29. However, because points were computed every 1 degree in Fig. 36 rather than every 2 degrees, more detail of the sidelobe structure is apparent, particularly for the near-in sidelobes which are considerably more complex than indicated in Fig. 29, and presumably also more complex than those indicated in Figs. 28 to 35.

It is readily seen that the patterns shown in Figs. 36 and 39, representing values of ψ equal to 0 and 3 degrees, are symmetrical about the retrodirection. This is to be expected since each of these directions is one of the 120 axes of symmetry existing for this antenna configuration. Only for these values of ψ does the main beam point exactly in the retrodirection; otherwise it oscillated about the retrodirection by ±0.25 degrees as the antenna rotates.

Patterns shown in Fig. 38 and 40 are mirror images of each other, as would be expected.

In all cases the maximum sidelobes occur at about ±104 degrees from the retrodirection and each has a level of -14.0 ± 0.7 dB when referred to the peak of the particular pattern. When referred to the omni-azimuthal level, the value is +3.9 ± 0.5 dB. Each of the other far-out sidelobe levels remains equally constant with ψ and displays the monotonic characteristic previously mentioned.

g. Variation if ERP as the Retransmitted Frequency is Changed

The three most significant rays were used to determine the variation in ERP of a Type-1 antenna operating in each of the retrodirective modes 1, 2, and 3. Both the pilot and retransmitted signals are assumed to be unmodulated but differing in frequency by as much as 10 percent of their average value. The phase-conjugating circuitry attached to each elemental receiver/amplifier/transmitter is assumed to be a simple lower-sideband mixer in which the pilot frequency varies between 0.500 and 0.475 of the constant value of the local-oscillator frequency. Computations were made for values of ψ every 0.25 degree. The analysis appears in Appendix D.

The computations below are not directly related to spectral splitting since the gain is computed for steady-state azimuthal positions of the antenna. However, if the gain varies for different positions, there will obviously be some spectral splitting, due to amplitude modulation at least, as the antenna rotates. The computations show that in the special case of the receive and transmit frequencies being exactly equal, the spectral splitting is due entirely to this amplitude modulation.

Equation (D-11) was evaluated assuming that all elemental radiators were active, for a variety of receive and transmit frequencies f_t

and f_r. In all cases the lens mean radius R corresponds to 10 average wavelengths and the lens length to 3 radii. Since 60 elements were assumed, a range of only 0 to 3 degrees, representing half a period, needs to be considered. Some of the results are shown in Figs. 41 through 43. (Other data are shown in Table VII, presented later.) The quantity plotted is the ratio of the actual power in the retrodirective beam to the power that would have been transmitted by a single omnidirectional elements of equal gain in the axial plane. As has already been discussed, the maximum anticipated gain, averaged over all azimuthal directions, is given by

$$10 \log_{10} N = 17.78 \text{ dB} \quad \text{for} \quad N = 60 \quad .$$

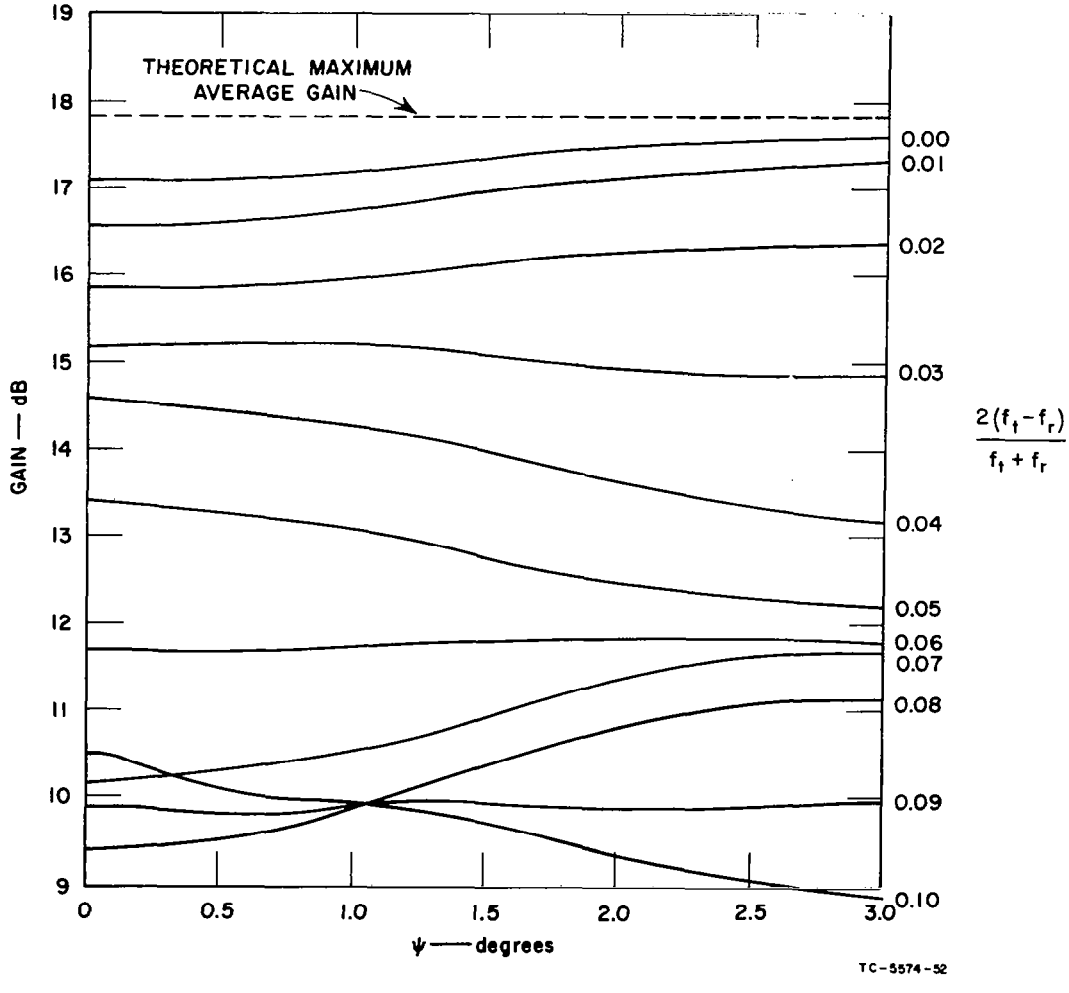

FIG. 41 RETRODIRECTIVE GAIN AS A FUNCTION OF AZIMUTHAL POSITION (Mode-1 Operation)

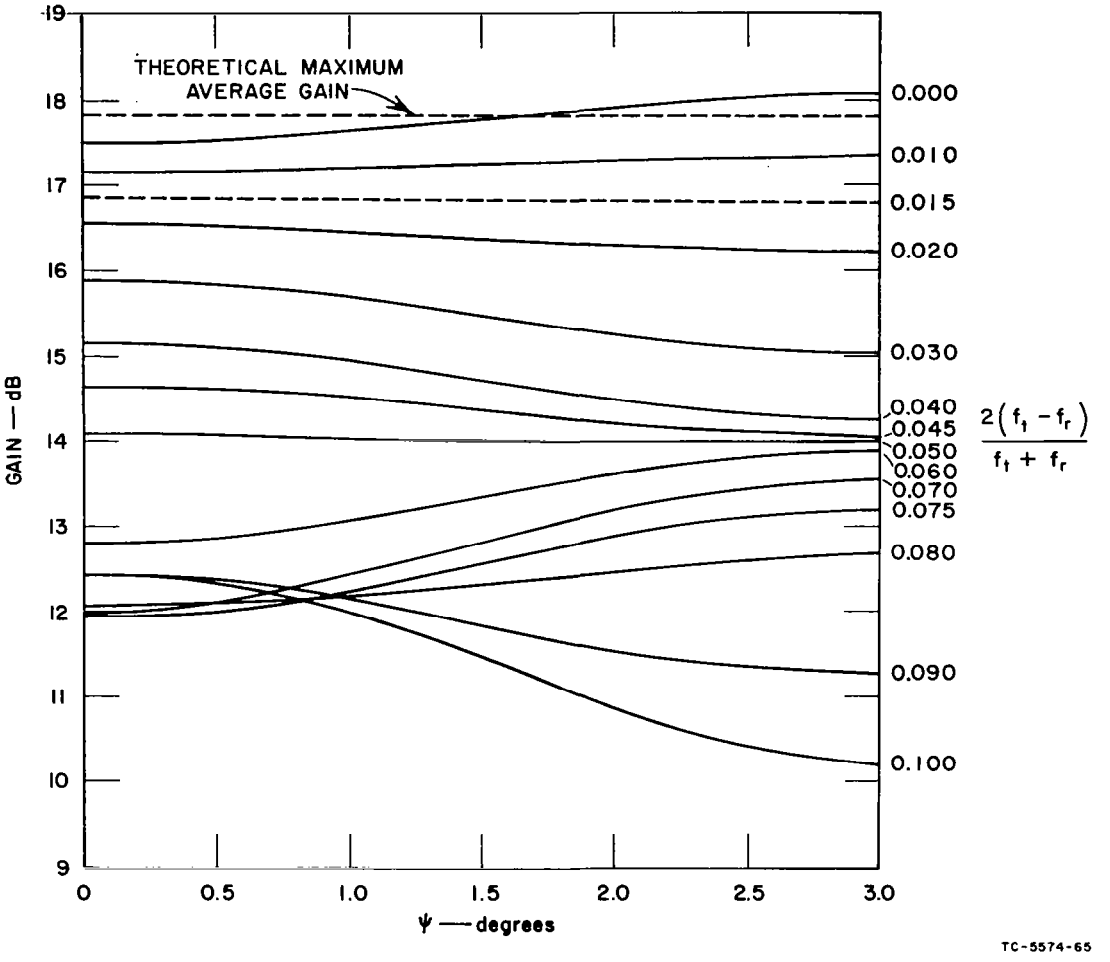

FIG. 42 RETRODIRECTIVE GAIN AS A FUNCTION OF AZIMUTHAL POSITION
(Mode-2 Operation)

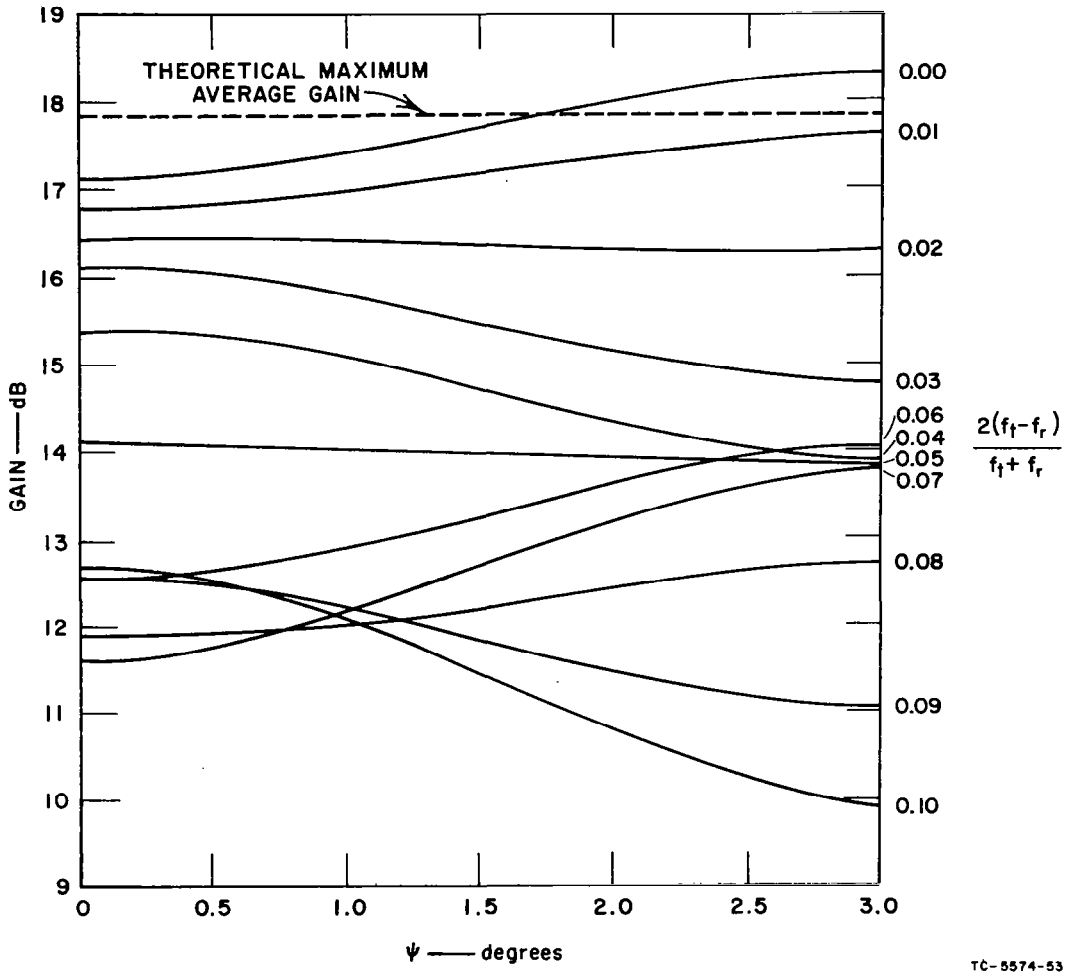

FIG. 43 RETRODIRECTIVE GAIN AS A FUNCTION OF AZIMUTHAL POSITION (Mode-3 Operation)

As can be seen in Figs. 42 and 43, the maximum gain, when averaged over a complete period, is very nearly realized (within 0.02 dB) when $f_t = f_r$. The gain in the direction exactly between two elements (ψ = 3 degrees) has the maximum value and is a fraction of a dB higher than the gain in the direction through an element. This will lead to amplitude modulation as the antenna rotates, but if R and/or L were varied from their present values it would be reasonable to postulate that a set of values could be found in which the gain variation with rotation was very small. Under these conditions (and again with $f_t = f_r$ and all elements identical except for phase) there would theoretically be no spectral splitting. It can also be seen from Fig. 9 that when $f_t \simeq 1.015 f_r$ there

is virtually no variation in gain. However, this does not mean that there will be no spectral splitting, as can be seen in Sec. III-C-3-j, below. The reason for this is that while there is no amplitude modulation, there is phase modulation, something that is not present when $f_t = f_r$.

It can again be seen that less gain, or ERP, is realized for Mode-1 operation than when linear amplifiers are used, although the variations in gain are comparable. Figure 41 also shows that when the frequency difference is two percent, the variation in gain has virtually disappeared. For all azimuthal positions the computed gain is less than the maximum postulated gain.

h. Spectral Splitting in Type-1 Antenna—Consideration of a Single Element

First a single element operating only in either the receive or transmit mode was studied, as explained in Appendix B. The method used allowed the spectrum of the individual rays to be determined. The ray geometry is basically the same as that used in previous computations[1] and is shown in Fig. 24.

Various computations were made for an antenna model having a cylindrical lens radius, R, of 10λ, and axial length-to-radius ratio, L, of 3.0 and a particular elemental gain function $G(\alpha)$.

Only the three most significant rays associated with a particular antenna element and a particular azimuthal direction were considered; they are referred to as Rays 0, +1, and -1. (In the original study of this Type-1 antenna,[1] only two such rays were considered; they were referred to as Ray 1 and Ray 2.)

The computation techniques used allow the separation of several combinations of rays, and they are presented in the data in the following groupings:

Ray 0

Rays -1 and +1

Rays -1, 0, and +1 .

Higher-order rays, which must travel at least one helical revolution within the cylindrical geodesic lens contribute negligible power for the

particular values of the parameters used in these calculations. In this particular antenna configuration the cylindrical lens has a radius of 10 wavelengths and the elemental radiator has an aperture of one-sixtieth the circumference of the lens [which determines what the value of $G(\alpha)$ will be].

Figure 44 is a curve of cumulative power (on a linear arbitrary scale) *vs.* sideband number for these three combinations.

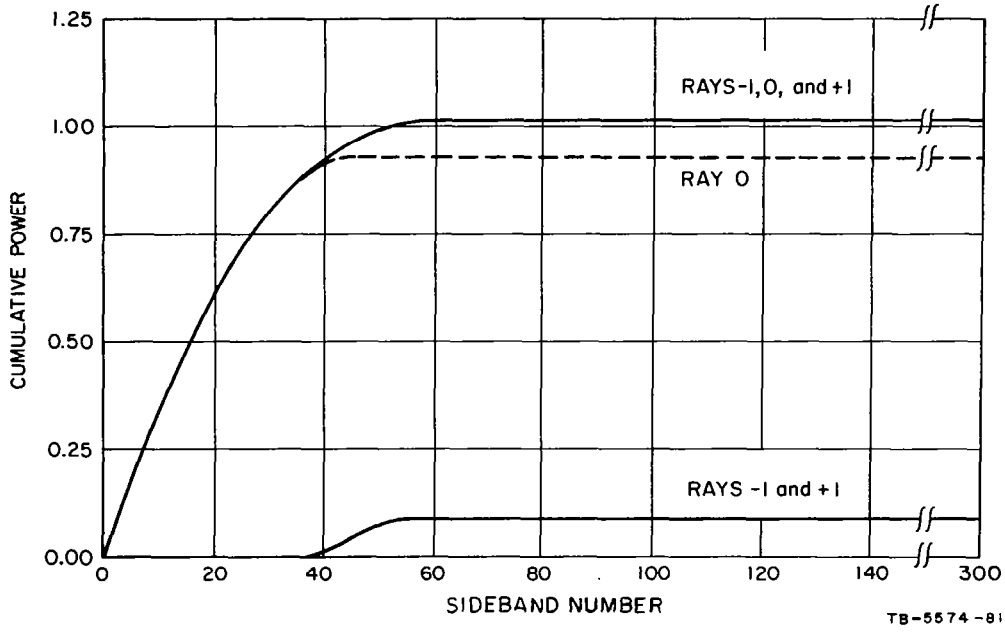

FIG. 44 CUMULATIVE POWER FOR A SINGLE ELEMENT vs. SIDEBAND NUMBER

Note that practically all the power of Ray 0 falls in Sidebands 0 to 40 while that of Rays -1 and +1 falls in Sidebands 40 to 60. This relates to the time rate of change of phase which is proportional to sin α. Since the ranges of α are discontinuous (or disjoint) for Ray 0 and Rays -1 and +1, it is not surprising that their spectra are disjoint (*i.e.*, complement each other, as seen from Figs. 45 and 46).

Figures 45, 46, and 47 present the spectra for Ray 0, Rays -1 and +1, and Rays -1, 0, and +1 respectively. The spectra for larger sideband numbers were also calculated but have not been plotted since they are essentially random and since Fig. 44 shows their minimal

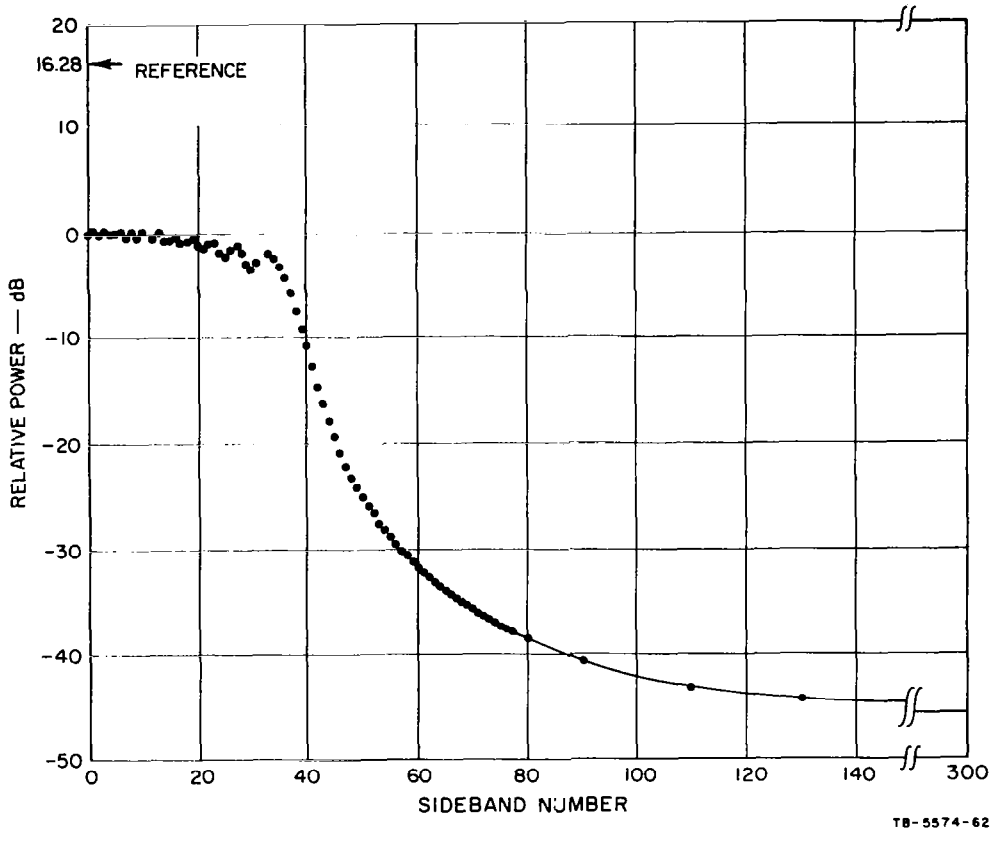

FIG. 45 RAY 0 — RELATIVE POWER IN dB FOR EACH SPECTRAL LINE

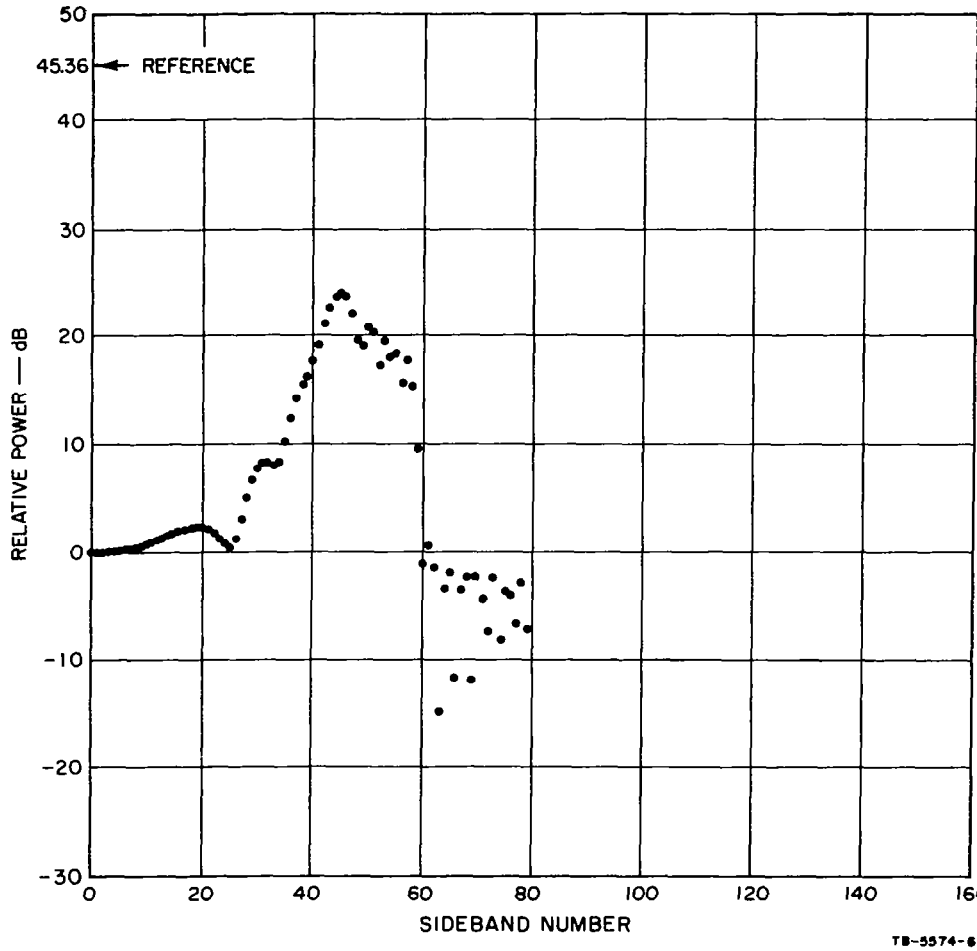

FIG. 46 RAYS −1, +1 — RELATIVE POWER IN dB FOR EACH SPECTRAL LINE

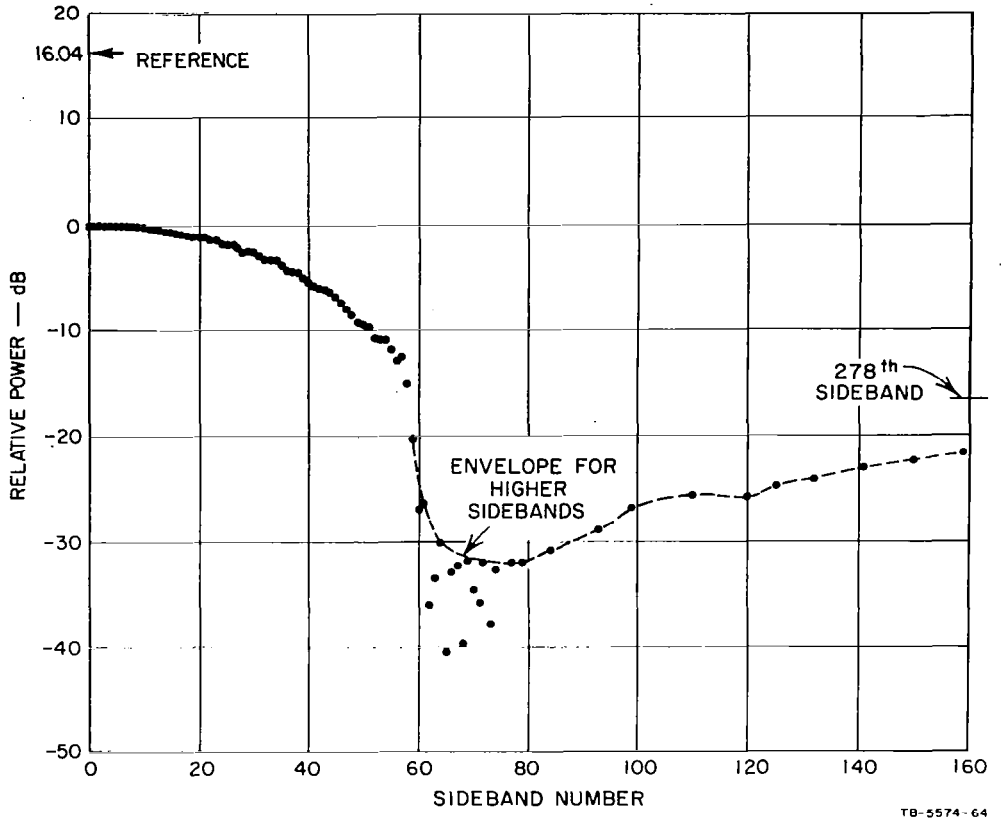

FIG. 47 RAYS -1, 0, +1 — RELATIVE POWER IN dB FOR EACH SPECTRAL LINE

contribution to the total power. The level labelled "reference" in Figs. 45 through 47 corresponds to the maximum cumulative power shown in Fig. 44.

Again the spectrum for Ray 0 is disjoint with that for Rays -1 and +1, and the latter pair alone gives rise to the irregular behavior above Sideband 60.

Since the integrations called for in Eqs. (B-26) and (B-27) of Appendix B are actually computed as sums over a finite set of points, our confidence in the results goes down as the sideband number goes up because the number of samples per cycle of the harmonic goes down. The accuracy obtained is, however, more than adequate for the present study.

It can therefore be concluded that there is spectral splitting in this type of antenna, with appreciable power out to about the 60th sideband, which might be a serious drawback for certain types of array. However, the resulting spectrum does peak at the carrier frequency, in contrast to the configuration considered earlier (see Fig. 2) where the spectrum peaked at about the 60th sideband. This can be attributed to the fact that in this Type-1 antenna, when the element is moving with highest radial velocity—that is, at the limbs of the complete cylindrical antenna—it has relatively low gain in the direction of interest. However, in the Type-3 antenna, the elemental gain is theoretically constant at all values of radial velocity.

If all the elemental radiators of the antenna are active phase-conjugated re-radiators and are identical, to an observer at a fixed point the antenna must look the same after a rotation of $2\pi/N$ radians, where N is the number of elemental radiators. Thus when the antenna is considered as a whole, the spectrum can contain only sidebands whose numbers are multiples of N. Of course, if the elements are not identical or if one or more is otherwise faulty, the intermediate sidebands will not disappear. The spectral contribution from each faulty element will, however, be small compared to the energy in those spectral lines whose numbers are multiples of N. The contribution to the intermediate sidebands of completely inactive elements corresponds to the case where only the inactive elements are operating, except for a reversal of phase.

These considerations can also be applied to the case of an adaptive receiving antenna of the same configuration.

i. Considerations of Total Spectral Power for a Single Element

In Appendix C, the power associated with the infinite number of rays that can exist in a typical Type-1 antenna, having primary dimensions of $R = 10$ (units of wavelength) and $L = 3$, has been calculated. It is shown that the total power, as obtained by summing the spectral content over the first 200 sidebands, associated with Ray 0, is 90% of a theoretical total, and that associated with Rays -1 and +1 an additional 9%. Consequently, consideration of only these three rays is quite justified except when extremely detailed knowledge of the spectral content or other characteristics is needed.

When only the first two significant rays are considered, as has previously been done for computing reradiation patterns, it can be postulated that only about 2 to 3 percent of the total power was not accounted for. In general this small amount of power would only produce minor modifications to the sidelobe structure, since it would never tend to form a plane wavefront.

j. Spectral Power Content in The Retrodirective-Array Case

In this portion of the study the antenna as a whole was considered when operating in the retrodirective (receive, transmit) mode with generally different receive (pilot) and transmit frequencies. Only an unmodulated pilot and retransmitted signal were treated, and these differed by up to 10% of the carrier frequency. The mathematical analysis for obtaining the spectrum of the transmitted signal is given in Appendix D.

Ideal mixers were assumed and computations were made, for Mode-1 and Mode-3 operation, of the actual relative power in each of the spectral lines associated with the same antenna operating at the same range of frequencies as for Sec. III-C-3-8.

A computer program was developed to calculate this power spectrum for the retrodirected wave from the same cylindrical, geodesic-lens, biconical-horn antenna with 60 elemental radiators, a length equal to 3 radii, and a radius equal to 10 wavelengths at the average carrier frequency. The received frequency lay below the average carrier frequency and the transmitted frequency above it by equal amounts. Three rays were considered for both reception and transmission. Since the elements were considered to be identical, only spectral lines corresponding to the cogging frequency were present (the cogging frequency is equal to the number of elemental radiators times the spin rate of the antenna).

Both linear and saturated (hard-limited) amplifiers were considered. The results for the first and second sidebands of the cogging frequency are presented in Table VII. All higher harmonics lie well below those tabulated for the linear-amplifier case. With saturated amplifiers, the powers of all higher harmonics lie below the first harmonic but some are slightly larger than the second harmonic.

Table VII

GAIN AND SIDEBAND POWER FOR A 60-ELEMENT, CYLINDRICAL-GEODESIC-LENS BICONICAL-HORN (TYPE-1) ANTENNA IN THE RETRODIRECTIVE MODE

$\frac{2(f_t - f_r)}{f_t + f_r}$	LINEAR AMPLIFIER CASE†				SATURATED AMPLIFIER CASE			
	Average Antenna Gain (dB down)*	Sideband Power (dB down)			Average Antenna Gain (dB down)*	Sideband Power (dB down)		
		60th Sidebands, Relative to		120th Sidebands Relative to Carrier		60th Sidebands, Relative to		120th Sidebands Relative to Carrier
		Carrier	Omni-Azimuth			Carrier	Omni-Azimuth	
0.000	0.0177	26.57	8.80	74.77	0.3825	33.97	16.57	127.90
0.005	0.16	26.42	8.80	71.94	0.49	29.76	12.47	57.04
0.010	0.53	26.04	8.79	68.35	0.74	27.22	10.18	52.58
0.015	0.96	25.60	8.78	66.14	1.10	26.55	9.87	55.01
0.020	1.40	25.14	8.76	65.22	1.55	27.65	11.42	59.12
0.025	1.86	24.65	8.73	65.46	2.06	30.77	15.05	54.20
0.030	2.31	24.16	8.69	66.97	2.59	33.54	18.35	49.87
0.035	2.72	23.70	8.64	69.60	3.18	28.87	14.27	48.73
0.040	3.00	23.25	8.46	70.72	3.76	24.72	10.70	52.26
0.045	3.42	22.80	8.44	67.87	4.32	22.91	9.45	62.92
0.050	3.73	22.38	8.33	65.00	4.83	23.07	10.12	52.67
0.055	4.05	21.98	8.25	63.39	5.36	25.24	12.82	58.06
0.060	4.44	21.61	8.27	62.99	5.86	29.70	17.88	53.62
0.065	4.73	21.27	8.22	63.79	6.30	28.51	17.03	57.15
0.070	5.00	20.93	8.16	65.73	6.70	23.15	12.07	56.57
0.075	5.24	20.58	8.04	67.80	7.06	20.15	9.43	50.17
0.080	5.40	20.23	7.85	66.86	7.37	19.20	8.79	45.57
0.085	5.66	19.89	7.77	64.07	7.58	20.07	9.83	41.65
0.090	5.90	19.57	7.69	62.07	7.68	23.35	13.25	40.37
0.095	6.21	19.28	7.71	61.26	7.74	28.87	18.83	46.95
0.100	6.45	--	--	--	7.88	24.13	14.23	47.26

* Relative to the theoretical maximum average antenna gain of 17.78 dB.

† Mode-3 operation.

These harmonics are due to both amplitude and phase modulation. The component attributable to phase modulation increases with the difference between the received and transmitted frequencies, while that portion attributable to amplitude modulation oscillates.

In all cases the upper and lower sidebands were found to be equal, apparently corresponding to the even property of the retrodirected wave with respect to the instant when the retrodirection passed through an elemental radiator. The powers listed in Table VII represent the total power in both the lower and upper sidebands.

In all cases considered, the spectrum spreading due to antenna rotation leaves nearly all the power in the carrier and should have only a minor effect on the operation of the system compared to the expected effects of random noise.

Also shown in Table VII are the corresponding values of computed antenna gain in the retrodirection, averaged over all azimuthal angles and compared with the theoretical maximum average gain given by $10 \log_{10} 60 = 17.78$ (see also Figs. 41-43). When linear amplifiers are used it is noticed that the gain decreases monotonically with increasing separation of f_t and f_r, as does the relative power of the 60th sideband when linear amplifiers are used. This gain data has been used to compute approximate values for the 60th-sideband power relative to what might be called the omni-azimuthal level—that is, the level that would result if the antenna consisted of just a single omni-directional element located on the spin axis and having the same gain in the plane of the axis as the complete 60-element antenna. These values are also listed in Table VII and are found to be remarkably constant, decreasing by only one dB while the retrodirective gain decreased by over six dB.

When saturated elemental amplifiers are assumed, it can be seen that the computed gain in the retrodirection relative to the carrier power is lower than that for linear amplifiers. This was to be expected since previous work[1,77] has shown that when the power fed to an element of an antenna array is in proportion to the gain of that element in the desired direction, the gain resulting from all the elements of the array in that direction will be higher than when equal power is fed to the elements. It is also noticed, however, that the sideband power for this model is, in general, considerably less than for the case of linear amplifiers. When the total sideband powers for the first cogging frequency are normalized against the omni-azimuthal power, it can be seen that the values are by no means constant and again are lower than when linear amplifiers are considered; for some values of frequency separations the power is as much as 10 dB lower.

The fact that the sideband power values are not as "well behaved" when saturated amplifiers are used, is compatable with earlier observations made on computed re-radiation patterns in which it was found that antennas using linear amplifiers had patterns with more regular sidelobe structure than when saturated amplifiers were used (see Sec. III-C-3-e).

4. Discrete-Line-Source Radiator Configuration (Type-2 Antenna)

a. General

This second cylindrical-geodesic-lens antenna type is shown in simplistic form in Fig. 48. As will be apparent from the theory of the analysis procedure, the computation necessary to obtain a single point of a retrodirective pattern is quite extensive and increases approximately as the square of the linear dimension of the antenna. Some effort was expended in trying to reduce the cost of computing each point by streamlining the computation procedure; however, it soon became obvious that the cost of computing complete retrodirective antenna patterns for each set of antenna parameters would be prohibitive. Since the shape of the main beam is an important characteristic of any antenna, a portion of the antenna pattern in the vicinity of the main beam was computed in a few cases. In other cases only the gain in the retrodirection was computed. Some effects of the variation in signal frequency, the effect of using a different frequency for receiving and transmitting from the same antenna, and the effects of rotation of the retrodirective antenna (vehicle spin) were investigated. Investigations of the extremely important effects of vehicle spin on signal spectrum will not, however, be analysed in this present work.

b. Theory of Analysis Procedure

The basic cylindrical geodesic-lens multiple-line-source antenna is shown in Fig. 48. It consists of M elemental radiators each connected directly to a receiver/amplifier/transmitter, at what will be referred to as the bottom of the cylindrical geodesic lens. At the top of this lens are N waveguides, each feeding an identical line source radiator which has considerable gain in the axial or vertical direction but only 4 or 5 dB in the azimuthal direction. The peak of this radiation from each line source is assumed to be radially outward. There are, of course, also N of these line source radiators.

Each of the M elemental radiators is coupled to each of the N line source radiators by several different coupling paths within the cylindrical geodesic lens. This is shown in Fig. 49 where the cylindrical lens is "rolled out" or developed into a flat plane so that the coupling can then be represented by straight lines between each of the two points considered to be coupled. There are an infinite number of coupling paths between any point at the bottom of the cylindrical lens and any point at

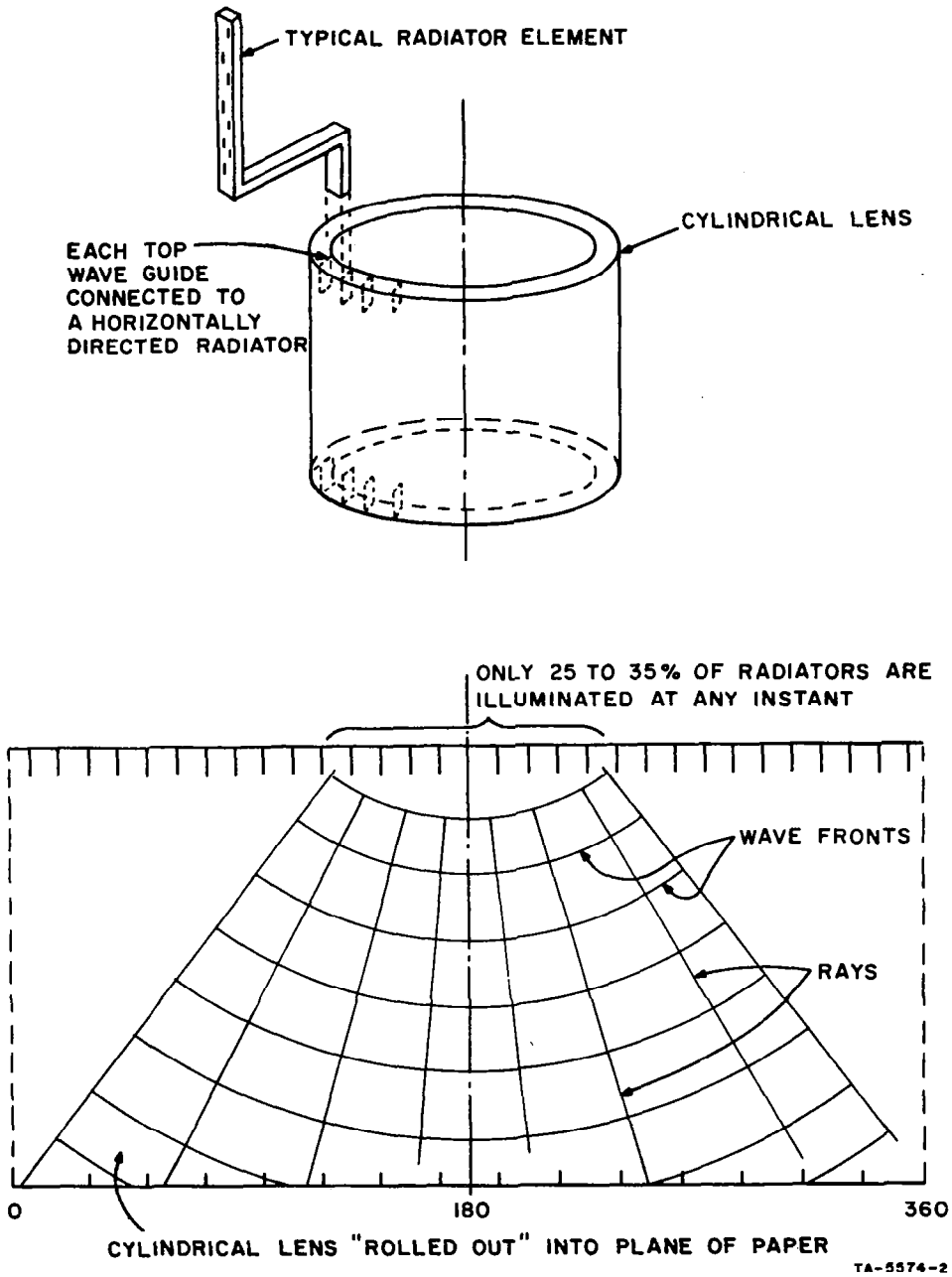

FIG. 48 SIMPLIFIED RAY GEOMETRY FOR A CYLINDRICAL-GEODESIC-LENS MULTIPLE-LINE-SOURCE ANTENNA (Type-2 Antenna)

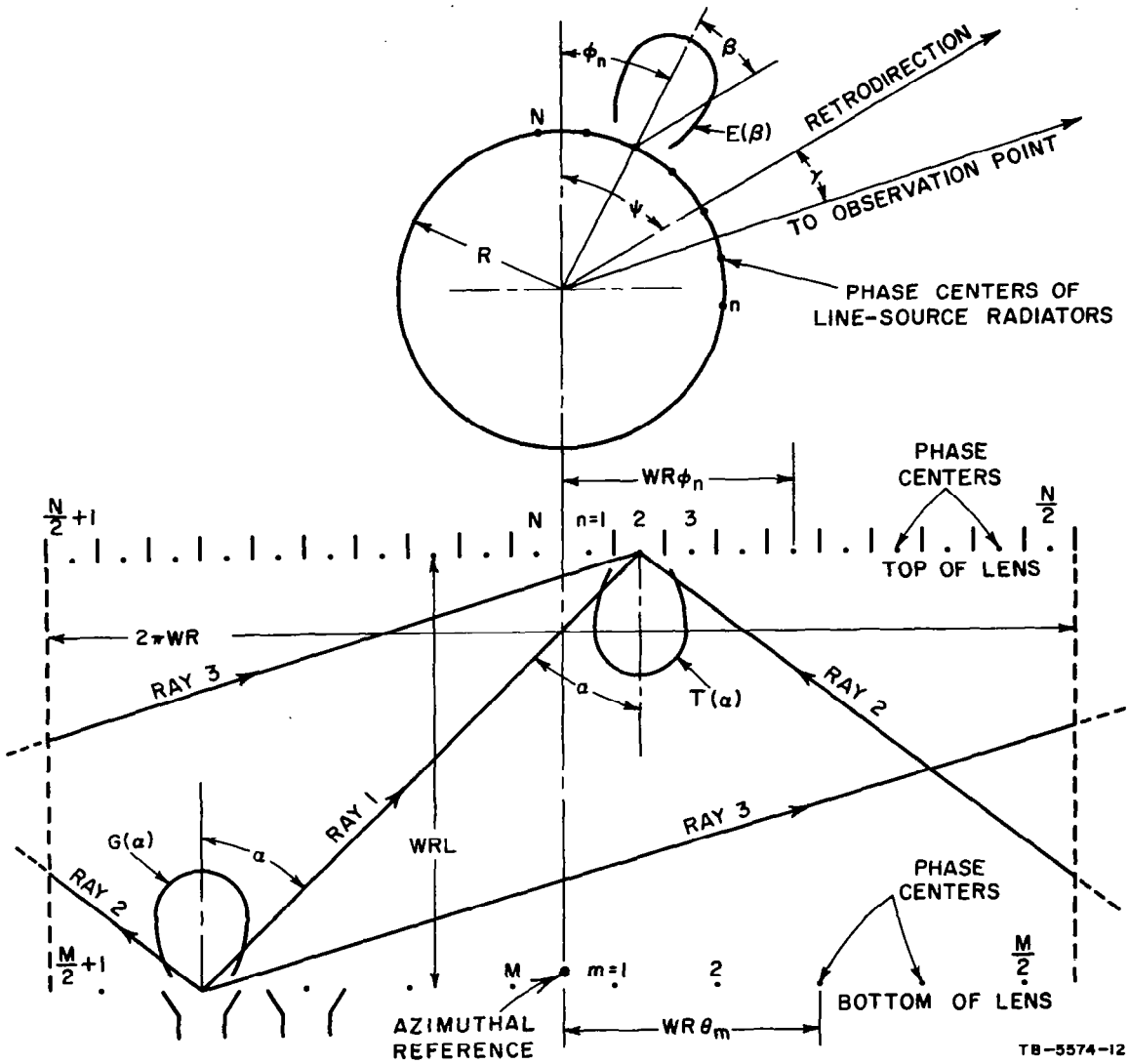

FIG. 49 GEOMETRY FOR A SINGLE GEODESIC-LENS RADIATOR AND A SINGLE LINE-SOURCE RADIATOR (Type-2 Antenna)

the top, but only three such rays will be assumed to exist in this analysis, as shown in Fig. 49. The contributions from higher-order ray numbers is in fact very small and will be assumed negligible. It can now be seen that in order to compute a single point in the far-field radiation pattern of such a retrodirective antenna, it is necessary to sum the electric vectors from $N/2$ line source radiators. Each radiator is in turn coupled to M transmitters by three different paths. Another way of putting this is to say that each of the M amplifier/transmitters feeds each of the $N/2$ effective radiators by three different paths; thus, there are in effect $3N/2$ rays contributing to each point in the radiation pattern from each elemental amplifier/transmitter. This compares with 2 or 3 rays for the biconical-horn antenna configuration previously discussed. Since the contribution from each ray must be added vectorially in the far field, the magnitude of computation becomes apparent.

c. Coupling Within the Geodesic Lens

As is demonstrated in Fig. 49, the coupling between any one of the M amplifier/transmitters and any one of the N waveguides at the top of the lens is the vector sum of three rays, the electric intensity of each being a function of the elemental radiation patterns of the two apertures at the ends of the lens, and the space attenuation between the two phase centers. It is, of course, quite conceivable that at some frequency the resultant vector could be zero, indicating no coupling between these two apertures.* Since the lens is a two-dimensional device, the space attenuation of power within the lens is assumed to be simply proportional to the inverse of ray length $WRL\lambda/\cos\alpha$, giving $\sqrt{\cos\alpha}$ as the amplitude space attenuation factor.

Other parameters of the antenna are defined below:

α_{mni} is the angle between the peak of the mth elemental radiator within the geodesic lens and the nth waveguide at the top of the lens, via the ith ray. In a right-cylindrical lens (see Fig. 49), the same angle applies between the ray and the peak of the elemental pattern of waveguide at the top of the lens. $(-\pi < \alpha < \pi)$.

$\beta_{n\gamma}$ is the angle between the radial at the nth line-source radiator (the azimuthal direction of the peak of its beam) and the far-field observation point for which the pattern is being computed.

* It is assumed that there is no mutual coupling between the separate radiators at the same end of the lens.

ϕ_n is the angle from a fixed azimuthal reference on the vehicle to the phase center of the nth line source radiator. It is also the angle to the nth waveguide within the cylindrical lens.

θ_m is the angle from the same fixed reference to the mth elemental radiator at the bottom of the lens.

ψ is the azimuthal angle between the fixed reference and the retrodirection.

γ is the azimuth angle between the retrodirection and the far field observation point.

N is the total number of line-source radiators (and also the number of waveguides at the top of the lens). They are assumed to be equally spaced.

M is the total number of elemental radiators at the bottom of the lens, (also assumed equally spaced).

R is the effective radius of the line source radiators measured in wavelengths of the pilot signal.

R' is this effective radius measured in wavelengths of the retransmitted signal.

WR is the mean effective radius of the cylindrical geodesic lens.

WRL is the effective length of the cylindrical lens.

$E(\beta)$ is the amplitude function representing the azimuthal radiation pattern of each of the line source radiators. It is assumed to be zero except when $(-\pi/2) \leq \beta \leq (\pi/2)$.

$T(\alpha)$ is the equivalent function associated with the waveguide ends coupling into the top of the geodesic lens.

$G(\alpha)$ is the equivalent function associated with the elemental radiators at the bottom of the lens, each of which is coupled to an individual receiver/amplifier/transmitter.

The azimuthal angle associated with the most direct path between the mth elemental radiator and the nth waveguide can be defined as the first ray and is given by

$$\Delta_{mn1} = 2\pi_p + \theta_m - \phi_n$$

where $p = 0$, or ± 1 such that $-\pi < \Delta_{mn1} \leq \pi$. The second most direct ray is given by

$$|\Delta_{mn2}| = 2\pi - |\Delta_{mn1}|$$

and will satisfy

$$-2\pi < \Delta_{mn2} \leq -\pi \qquad \text{for } \Delta_{mn1} \text{ positive}$$

and

$$\pi \leq \Delta_{mn2} \leq 2\pi \qquad \text{for } \Delta_{mn1} \text{ negative} \quad .$$

(The sign of Δ_{mni} is of no significance if the elemental radiator patterns are symmetrical and the relativistic effects of the vehicle spin can be neglected.)

Similarly,

$$|\Delta_{mn3}| = 2\pi + |\Delta_{mn1}| \quad .$$

By simple geometry (see Fig. 49),

$$\alpha_{mni} = \arctan \frac{\Delta_{mni}}{L} \quad .$$

The net amplitude coupled between the mth amplifier/transmitter and the nth line source waveguide, via the ith path is then given by

$$|A_{mni}| = G(\alpha_{mni})T(\alpha_{mni})\sqrt{\cos \alpha_{mni}} \quad .$$

The electrical length of this ray is given by

$$\epsilon_{mni} = 2\pi RWL \sec \alpha_{mni} \text{ radians} \quad .$$

The net coupling between the mth elemental radiator and the nth waveguide is then the vector sum:

$$\sum_{i=1}^{3} |A_{mni}| e^{j\epsilon_{mni}} \quad .$$

which holds equally for the pilot beam and the retransmitted signal, provided R' replaces R.

The reradiated powers can now be computed using the same general procedure that was described for the cylindrical-geodesic-lens biconical-horn antenna (Type-1) in Sec. III-C-3-c.

Again, the ray length outside the antenna from the distant observation point (located a distance S away and having a relative azimuthal direction γ) to the nth line source radiator is

$$S - R\lambda \cos \beta_{n\gamma} = R\lambda\left(\frac{S}{R\lambda} - \cos \beta_{n\gamma}\right) .$$

The total relative phase difference from each of the M elemental radiators to the distant observation point is

$$\eta_{mni} = 2\pi R(WL \sec \alpha_{mni} - \cos \beta_{n\gamma})^{*} .$$

Since each line-source radiator has its own azimuthal antenna amplitude function $E(\beta_{n\gamma})$ there will be an additional modification to the amplitude of each vector.

If now a pilot signal is received from direction ψ (*i.e.*, $\gamma = 0$) the signal received at each of the M elemental radiators will be the vector sum:

$$B_m = |B_m| e^{j\Omega_m} = \sum_{n=1}^{N} \sum_{i=1}^{3} E(\beta_{n0}) |A_{mni}| e^{j\eta_{mni}} .$$

d. Computation of Reradiation Pattern

It is again assumed that the conjugate circuitry associated with each elemental radiator reverses the sign of Ω_m on reradiation and that the reradiated power is some function of the received signal amplitude $|B_m|$. (In the particular results presented below, the reradiated amplitudes are mostly assumed to be equal—*i.e.*, Mode-1, but Mode-2 operation is also used.)

By using the reverse procedure, the relative signal amplitude apparent at some distant point at an azimuthal angle γ from the pilot signal, which is due to transmission from the mth transmitter via the nth line source radiator and the ith path within the geodesic lens, will be given by

$$D_{mni\gamma} = E(\beta_{n\gamma}) |A_{nni}| e^{j\mu_{mni\gamma}}$$

where

$$\mu_{mni\gamma} = 2\pi R'(WL \sec \alpha_{mni} - \cos \beta_{n\gamma} - \Omega_m) .$$

*It will be assumed for the present that the frequencies appearing at each of the elements is identical; hence, $S/(R\lambda)$ is identical for all values of n and can be ignored. Due to vehicle spin, and hence relative Doppler shift, this will not necessarily be true for very large values of S.

The relative field amplitude in any azimuthal direction γ is then given by the vector sum

$$D_\gamma = \sum_{m=1}^{M} \sum_{n=1}^{N} \sum_{i=1}^{3} D_{mni\gamma} \quad .$$

This value is more appropriately designated in dB by

$$F_\gamma = 20 \log_{10} |D_\gamma| \quad .$$

This value has been computed for several points at or around the retrodirection and some of these results are presented below.

e. Determination of Antenna Azimuthal Gain

As was done in Sec. III-C-3-d above for the biconical-horn antenna, the peak power of the reradiation pattern is compared with the average power radiated in all directions. It was not possible to use Method 2 here, since it requires integration of the complete reradiation patterns. For the present case, patterns were computed only over a small arc, and sometimes for just a single point, rather than for all azimuthal directions. The gain values previously obtained by Methods 1 and 2 were in all cases within 0.06 dB of each other, and in each case about 0.2 dB higher than the value obtained by Method 4. This latter method involved the computation of the total energy radiated by the elemental radiators within the geodesic lens, and then made the assumption that this was all radiated into space without reflection loss from the discontinuities within the antenna. The average value of the resultant radiation intensity is designated by Q (in dB). Such a condition is easier to realize in the case of the biconical-radiator antenna than in this discrete-line-source antenna where the energy must be coupled, without loss, from a TEM line into adjacent waveguides. The computed value of gain resulting from this technique should be reasonably accurate, if perhaps a little optimistic.

It has also been assumed that each radiating element is optimally matched to its appropriate transmitter at all times. This is equivalent to neglecting mutual coupling which, in practice, might cause the input impedance values of elements to vary with vehicle rotation.

f. Results of Computation Using Mode-1 Operation

1) General

Some results of a series of computations are shown in the following figures.

Figure 50 is the computed pattern used as the reference for this series of computations, and has the following initial values of coefficients:

$R = 10.000$ $\quad E(\beta) = 10^{-24(R\beta/N)^2}$

$R'/R = 1.000$ $\quad T(\alpha) = 10^{-24(WR\alpha/N)^2}$

$W = 1.00$ $\quad G(\alpha) = 10^{-24(WR\alpha/cM)^2}$

$L = 3.00$ $\quad \psi = 2$ degrees

$M = 40$ $\quad c = 2$

$N = 80$

The fact that the retrodirection is 2 degrees from the zero reference of the antenna (which is an axis of symmetry) accounts for the computed pattern being asymmetrical. It should be noted that although points have been plotted every one degree, this is not close enough to make a reliable interpretation of the correct pattern shape, including null depths, *etc.* Consequently, the computed points have been joined by straight lines.

It should also be noted that each point represents the vectoral summation of $3 \times M \times N/2 = 4800$ field intensities, each of which involves the product of at least four computed quantities.

The 3-dB beamwidth as well as the gain in dB, computed by subtracting the value of Q from the computed signal intensity in the retrodirection, is shown on Fig. 50 (as well as on subsequent patterns). Using the same argument as used for Type-1 (Sec. III-C-3-e), the maximum possible theoretical gain of this antenna averaged over all azimuthal pointing directions is postulated as

$$P = 10 \log_{10} M = 16 \text{ dB} \quad .$$

The computed value of gain, 14.66 dB, thus appears quite reasonable.

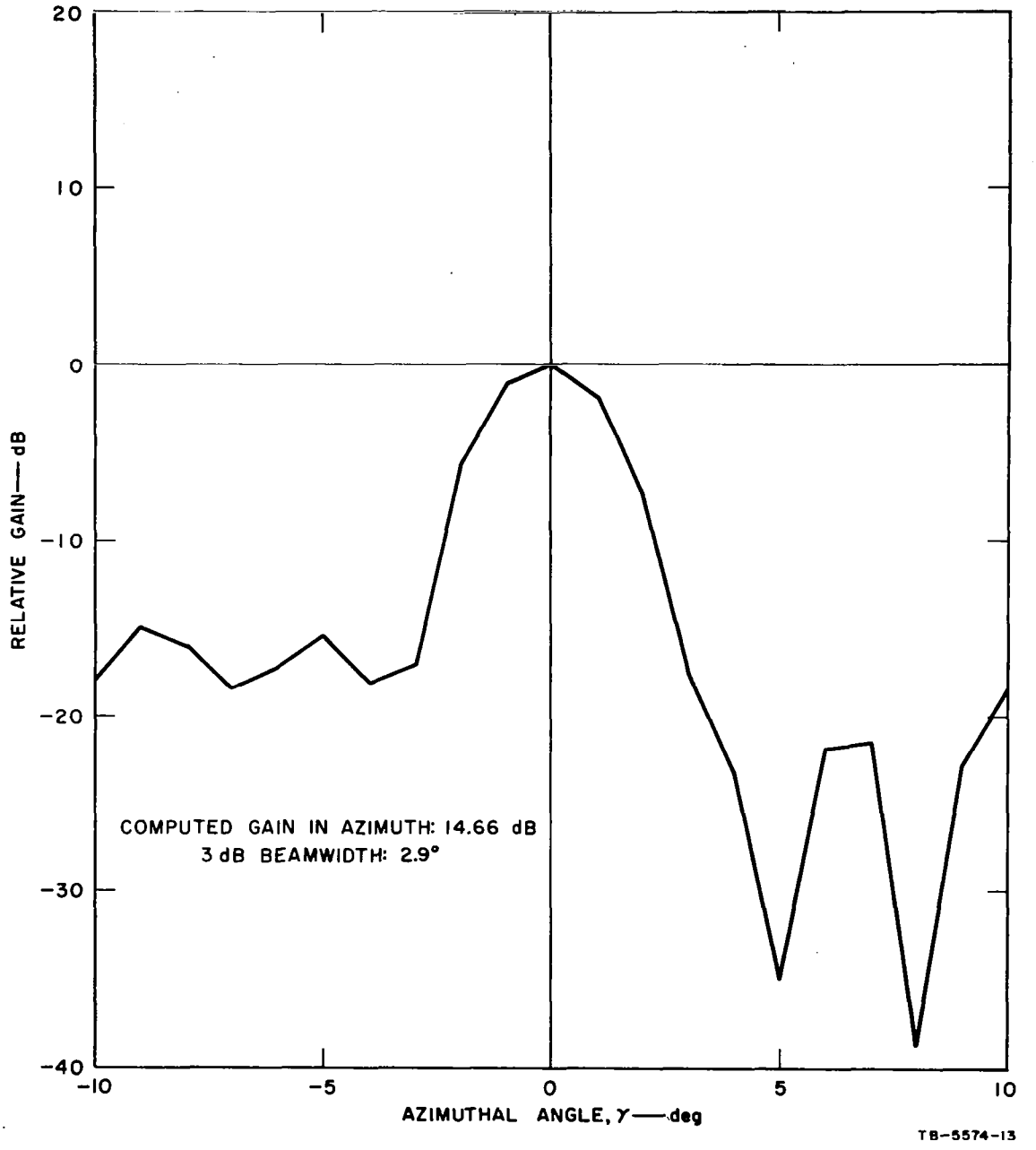

FIG. 50 BASIC ANTENNA PATTERN USED AS REFERENCE (Mode-1 Operation)

2) Variation in ERP with Change in Frequency

The gain in the retrodirection was computed for an antenna with the same characteristics as the reference antenna except that the operating frequency (which again was the same for receiving as for transmitting) was increased by nearly 0.1 percent in increments of 0.01 percent. The ERP, or gain, was found to decrease by 0.06 dB in an apparently linear manner. Since the gain of any antenna would normally *increase* when the frequency is increased it is assumed that the small decrease observed is part of a superimposed cyclical variation. This small gain variation was found to be part of a much larger cyclical variation. For instance, a variation of more than 0.5 dB was observed for a variation of one percent frequency change. Insufficient data points were obtained to establish any definite characteristics but it appears likely that with appropriately chosen parameters the gain could be kept constant over a frequency band of about one percent.

3) Variation in ERP as Retransmitted Frequency is Changed

It is almost certain that the receive and transmit frequencies will be different for any retrodirective system; and this frequency separation is likely to be at least one percent.

If one antenna is used for receiving the pilot beam and each elemental receiver of this antenna is coupled to the corresponding transmitter of a separate transmitting antenna, which has all dimensions exactly scaled in the ratio of the operating wavelengths, then this frequency difference is not very important. If, on the other hand, the same antenna is used, together with simple phase-conjugating networks, then the frequency separation will definitely cause "defocusing," which will reduce the ERP in the retrodirection.[77] If more complex conjugating circuits are employed, involving signal frequency multiplying and dividing, then this defocusing can be removed.[76] Such a scheme is discussed in Sec. V-B-4.

To determine the effect of this defocusing, antenna gains were computed as a function of retransmitted frequency. The gain in the retrodirection was found to fall by nearly 6 dB for a retransmitted frequency increase of 5 percent. Three patterns, one of which is the reference pattern shown in Fig. 50, are shown in Fig. 51. The gain in

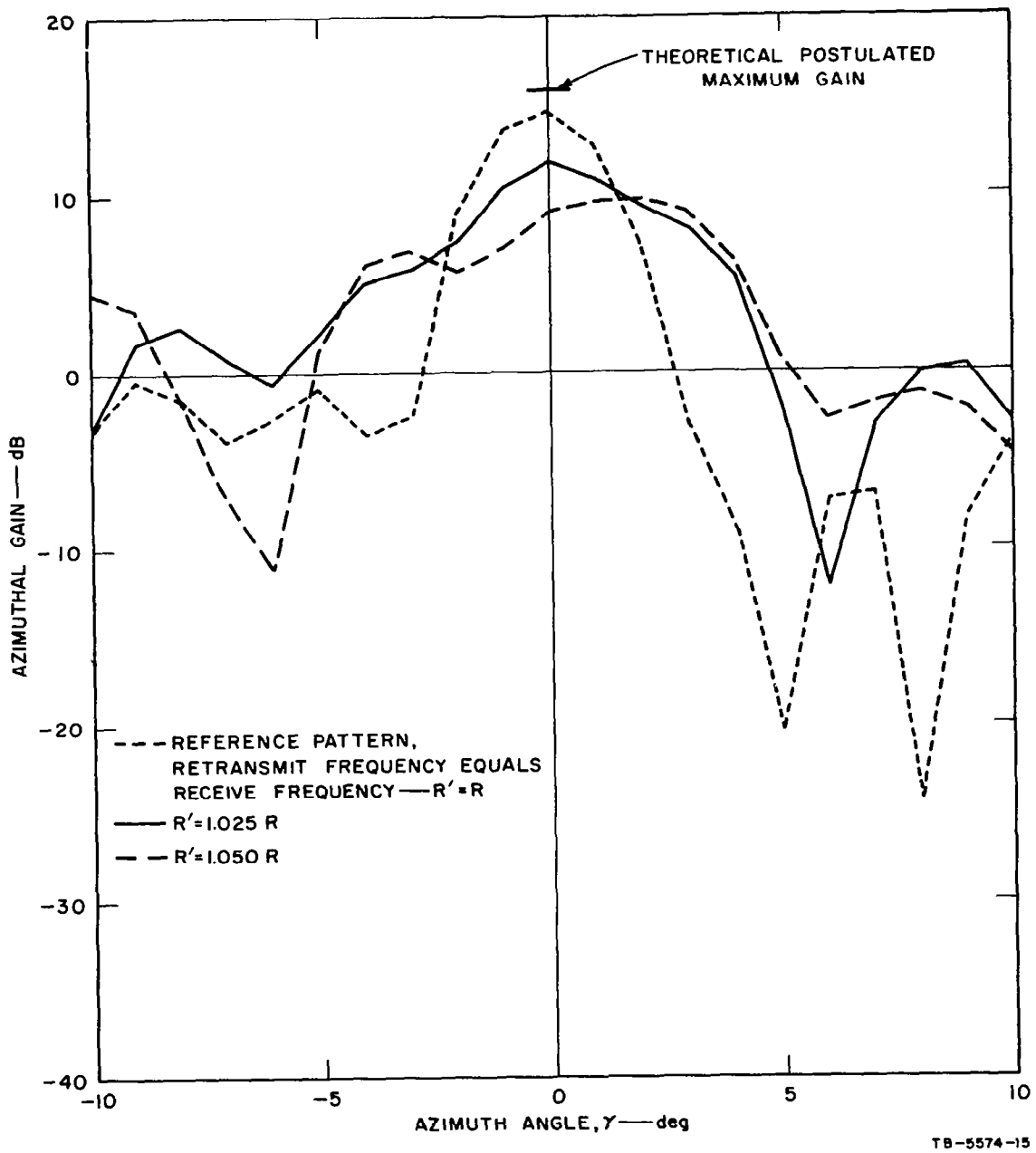

FIG. 51 BEAM SHAPES AS A FUNCTION OF THE RETRANSMITTED FREQUENCY: RECEPTION AND TRANSMISSION USING THE SAME ANTENNA

each case is with respect to an omni-azimuthal element of equal elevation beamwidth. Figure 52 shows the azimuthal gain in the retrodirection with respect to the theoretical maximum value of 16 dB. The fact that the retrodirection was taken as 2 degrees from an axis of symmetry of the

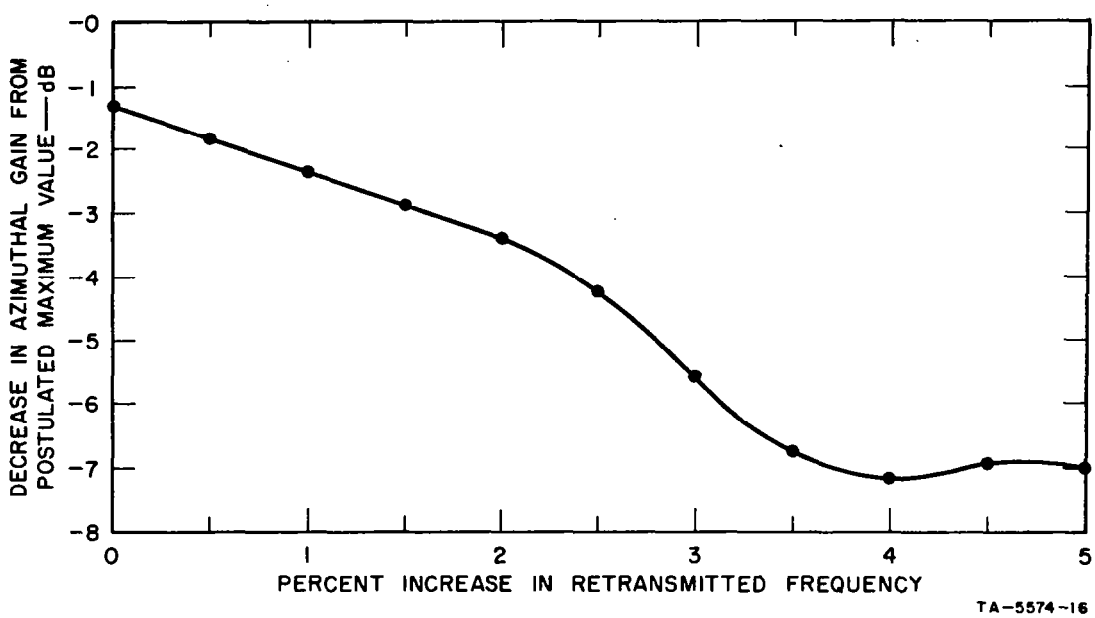

FIG. 52 DECREASE IN GAIN WITH INCREASE OF R'

antenna no doubt accounts for the fact that the maximum ERP is not always in the retrodirection (see Fig. 51 and also Figs. 36-40). However, the non-monotonic shape of the curve in Fig. 52 cannot readily be attributed to the fact that ψ = 2 degrees. It can be seen that from data obtained for the Type-1 antenna (*e.g.*, Figs. 42 and 43) a similar non-monotonic characteristic exists when ψ = 0 degrees if frequency difference values out to 8 percent, or more, are considered.

4) Variation in the Number of Line-Source Radiators, N

Figure 53 shows a set of patterns for three similar antennas. The number of line-source radiators, N, is varied from 40 to 80. The elemental radiation pattern is also automatically modified, as can be seen from the definition of $E(\beta)$ and $T(\alpha)$. The reference pattern of Fig. 50 (N = 80) is again reproduced.

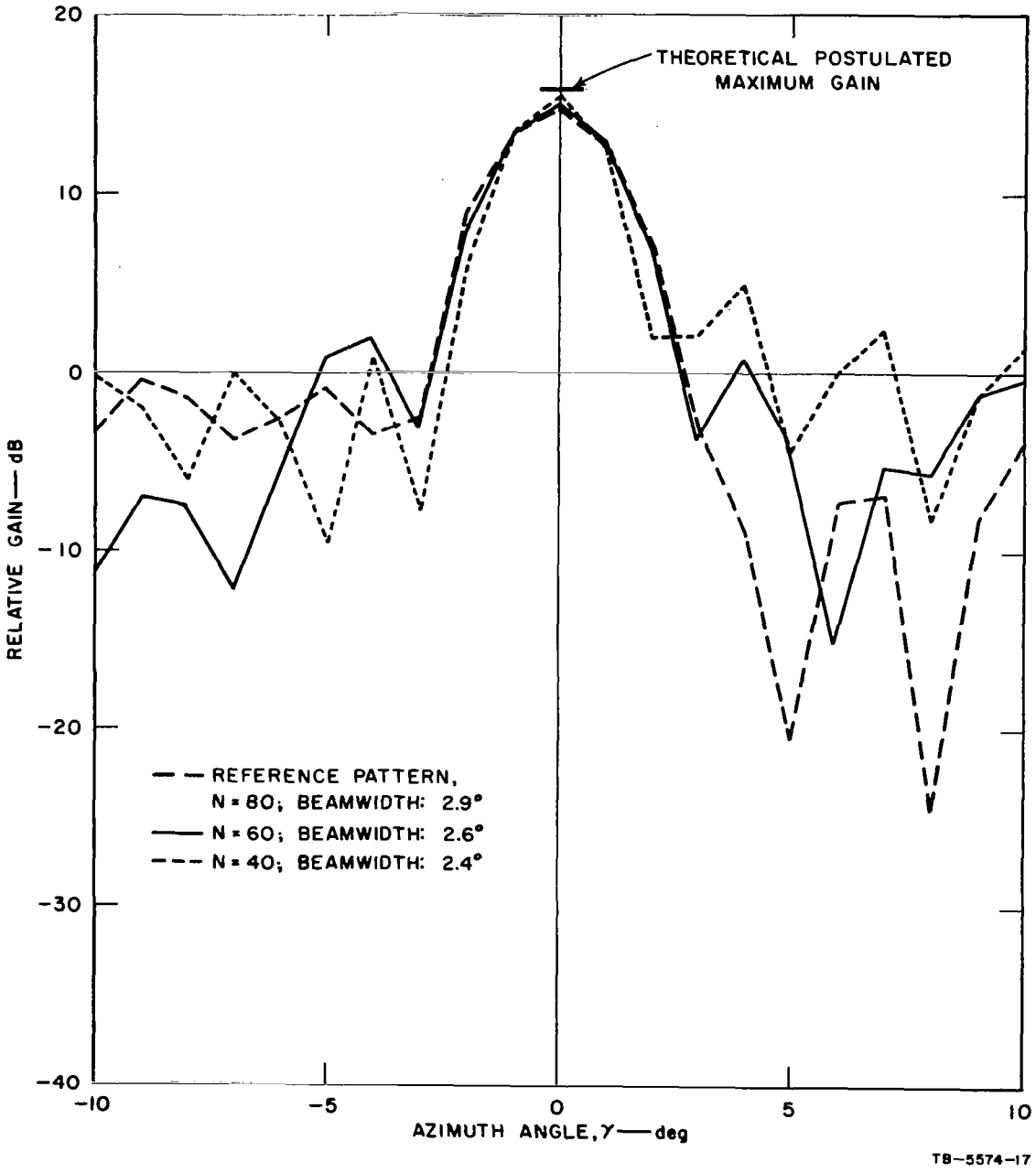

FIG. 53 EFFECT OF CHANGING VALUE OF N ON THE AZIMUTHAL GAIN

It can be seen from Fig. 53 that the gain actually increases as the number of line-source radiators is reduced (although the number of elemental transmitters, M, has been kept constant at 40). There is at present no explanation for the changes in gain and beamwidth.

The inference is that there is no point in increasing the number of line-source radiators and hence the complexity of the antenna, in order to improve antenna gain. It is quite likely, however, that fewer radiators will lead to large gain variation with spin, but no direct measurements have yet been made to confirm this.

5) Variation in the Elemental Radiation Patterns

In all the results presented above, the number of elemental radiators, M, has been kept constant at 40. The radiation pattern of each of these elements denoted by

$$G(\alpha) = 10^{-24(WR\alpha/cM)^2}$$

has also been kept constant (except for minor variations in R as the frequency was varied). The constant $1/c$ is the proportion of available arc at the bottom of the cylindrical lens that is used for each elemental radiator. In the above results c has had the value 2, indicating that twice as many similar elemental radiators could have been fitted into the space available. For such an arrangement— *i.e.*, $M = 80$— the mutual coupling between adjacent radiators might be considerably higher, and previous results[1] have indicated that the antenna gain *per transmitter* would not increase and may very well decrease. The larger number of transmitters would, however, increase the ERP for the same total power input at the expense of more receiver/amplifier/transmitters.

The effect of this parameter c was investigated by assigning it different values and computing the gain in the retrodirection. The following results were obtained:

for c =	1.0	1.5	2.0
gain =	14.58	14.88	14.66 dB

Since the accuracy of the computed gain is only about 0.5 dB, the minor differences between these values of gain are considered insignificant. Thus it would appear that for an antenna of given diameter and given

number of transmitting elements the efficiency with which the available aperture within the lens is used is not very significant.

6) Characteristics of a Smaller Antenna

Continuing the general investigation of the various antenna parameters, the linear dimensions as well as the value of M and N were halved. Computed patterns for the cases of N = 20 and 40 are shown in Fig. 54. It can be seen that the antenna with the smaller number of line-source radiators gives a gain ¾ dB higher than the other one. This is consistent with the results shown in Fig. 53. The beam-width for the higher-gain antenna is also narrower but a very high side-lobe level is apparent. It must be emphasized, however, that unless several parameters of each antenna are investigated it is not possible to obtain any realistic conclusions. For instance, the computed gain of an antenna of this type is very much dependent on its orientation, as is shown in the next section. As has been indicated, the cost of computing each point is high for this configuration.

g. Variation in Max ERP With Antenna Rotation

Although no quantitative attempt has been made to investigate the spectral content of a Type-2 antenna when spinning, some data was obtained on the variation of retrodirective gain with antenna rotation. This variation represents the amplitude component of spectral splitting. As in the case of the Type-1 antenna there will be no phase modulation component when $f_t = f_r$. Figure 55 shows the computed value of gain in the retrodirection as different antennas are rotated through 360/M degrees, which represents one cyclical period for this configuration, provided N is divisible by M and one axis of symmetry of the N elements is coincidental with the azimuthal reference angle as defined in Fig. 49. In this figure the reference angle is shown passing exactly between two phase centers of the N line-source radiators— *i.e.*, through the contiguous edges of a pair of line-source radiators. This condition is referred to as Class-E symmetry. When a phase center lies on the reference angle the condition is labeled Class-C.

It should be noted that the gain scale of Fig. 55 is somewhat expanded when compared with other gain data presented in this report. It should also be noted that the transmitted frequency is assumed to be the same as the pilot frequency for each of the curves.

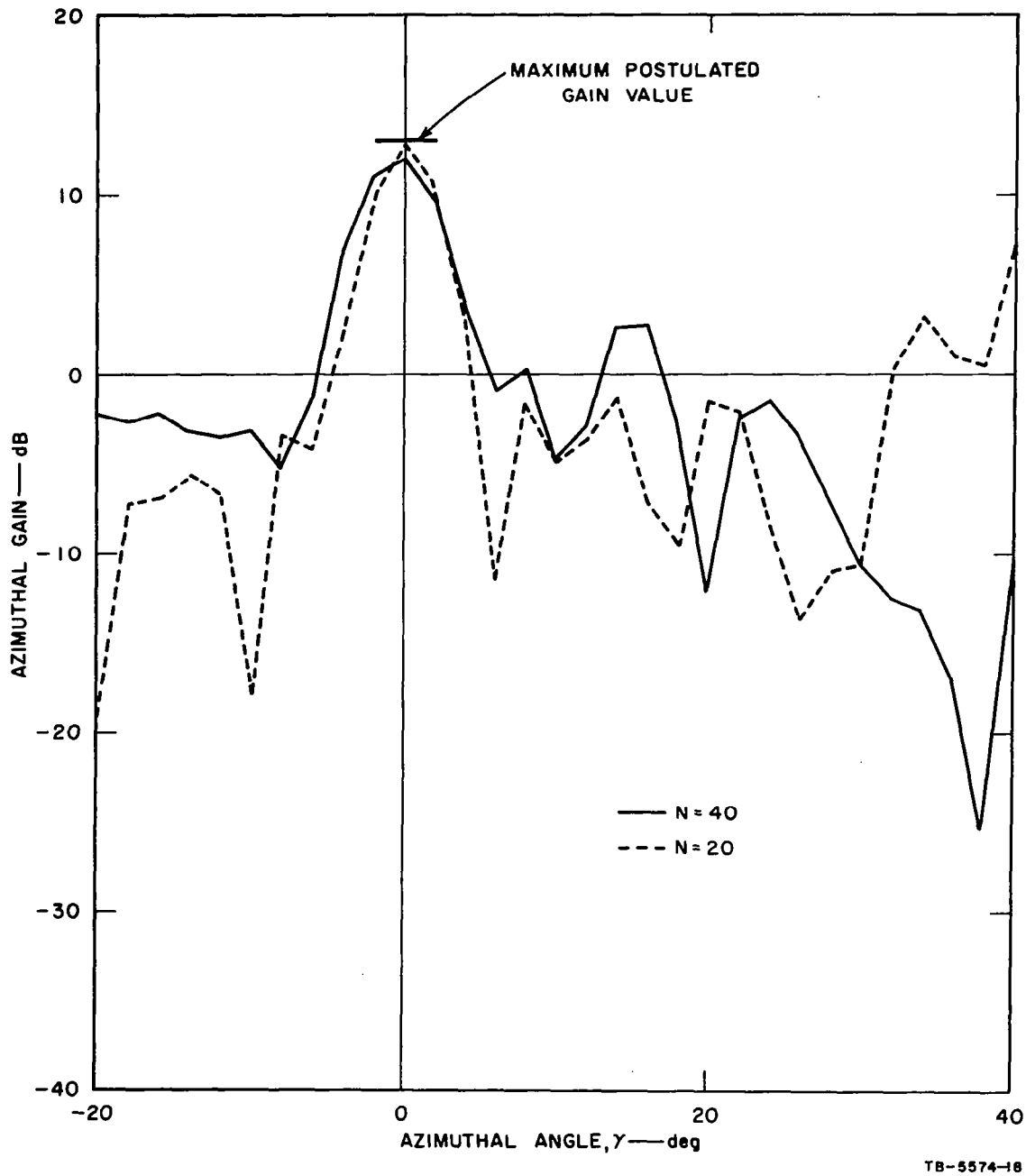

FIG. 54 COMPUTED PATTERN FOR TWO VALUES OF N USING A 10λ-DIAMETER ANTENNA

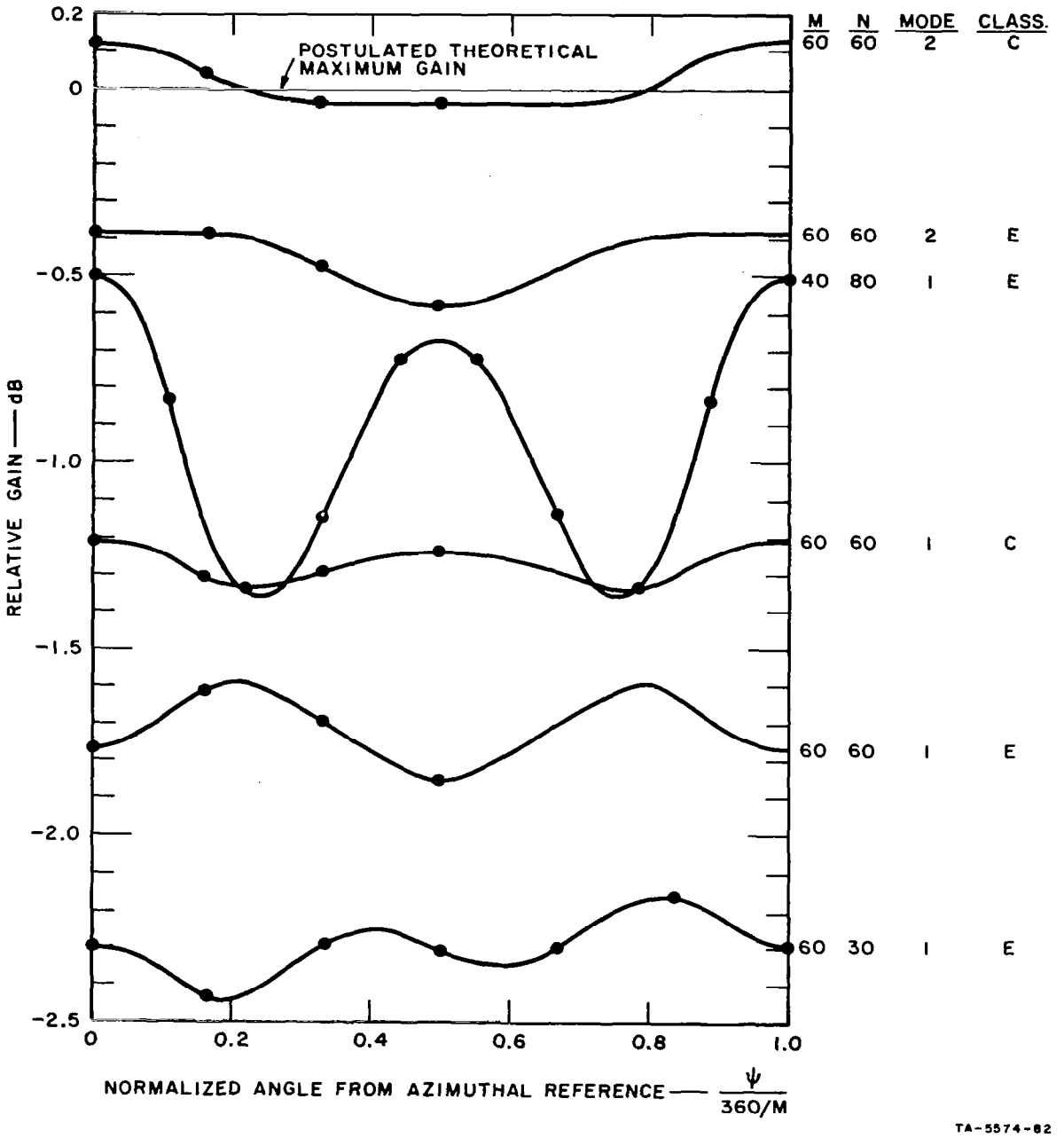

FIG. 55 RETRODIRECTIVE GAIN vs. AZIMUTHAL ANGLE COMPUTED FOR VARIOUS CONFIGURATIONS OF TYPE-2 ANTENNA ($f_t = f_r$)

Other points worth noting concerning Fig. 55 are:

(1) There is a remarkably large variation in average gain relative to the postulated maximum average gain for the particular antenna (17.78 dB when $M = 60$, 16.02 dB when $M = 40$).

(2) It appears as if one of the configurations has an average gain greater than the possible value, but this should not be taken too seriously since the method of computing the values of gain is probably only accurate to a few tenths of a dB.

(3) The alignment of the N elements with respect to the M elements has an appreciable effect on the average antenna gain and also appears, to a lesser extent, to affect the amplitude modulation with rotation. (It should be noted that the curves shown are only based on relatively few computed points, as indicated in the figure.)

(4) Operation in Mode 2 (linear amplifiers) gives appreciably higher gain (more than 1 dB) than for Mode 1. This amount is appreciably more than was shown for the Type-1 antenna in Table VI or in the examples used by Villeneuve.[70]

(5) Unlike the results obtained for the Type-1 antenna it would appear that for most cases the amplitude modulation component of the spectral splitting is likely to cause the energy in the sidebands of the $2M$th harmonic of the spin frequency to be almost as large as for the Mth harmonic. In the case where $M = 40$, and $N = 80$, most of the sideband energy will be in the $2M$th— *i.e.*, the Nth— harmonic.

(6) The characteristics of the lowest curve are very difficult to explain. It is the only curve that is not symmetrical, which is easy to explain since it represents only one-half of a cycle, but the apparent undulations are not explicable. Its low value of gain is also not in keeping with the results shown in Fig. 54, where reducing the value of N actually *increased* the gain.

h. Conclusions Relating to Type-2 Antenna

No general conclusions can be drawn because the various data obtained do not follow definite patterns, with the possible exception of the higher gain for Mode-2 operation. Even this characteristic cannot be accepted with complete generality because it will be noted from Table VI that for $L = 2$ the gain in a Type-1 antenna was actually higher than for Mode-2 at the single value of ψ for which computations were made. Much more analysis will therefore be needed to establish general characteristics for this antenna, but before this is done a study of spectral splitting, including methods of keeping it low, should be undertaken. The assumption that mutual coupling is negligible between elements at the same end of the cylindrical geodesic lens can only be justified if some attempt is made to design well matched transition into the waveguides at each end of the lens. This in turn will complicate the region at one end of the geodesic lens, at least, and will require modification of the sample ray geometry shown in Fig. 49.

5. Cylindrical Retrodirective Array of Discrete Unidirectional Line Sources with Logical Element Switching

a. General

Another configuration of cylindrical antenna, which is particularly significant because mutual coupling between its elemental radiators can be made very small in practice, is one in which a number of discrete unidirectional line-source radiators are located around the exterior surface of the spacecraft. Figure 56 provides an end view of such a cylindrical array, showing particular elemental antenna patterns that are directed radially outward.

For maximum overall gain of such an array, one should consider the use of logical circuitry (or other means) to turn off power to those elements that are not contributing substantially to radiation in the desired direction. Because all elements on the back side of the cylinder are invisible and cannot contribute any field in the desired direction, they could be turned off. Furthermore, the directivity patterns of the elemental radiators would most likely provide significantly less gain in the desired direction as the angle from the radial approaches ±90 degrees, so maximum gain would occur if somewhat less than 180 degrees of the array were energized.

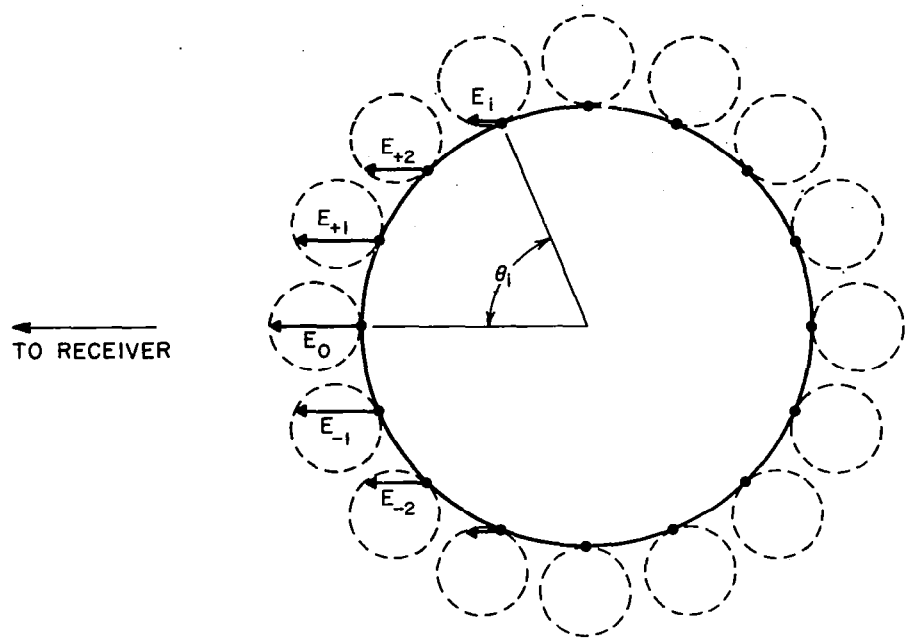

FOR A UNIDIRECTIONAL COS^2 POWER PATTERN:

$$E_i = \begin{cases} 2 \cos \theta_i, 0 \le |\theta_i| \le \pi/2 \\ 0, \pi/2 \le |\theta_i| \le \pi \end{cases}$$

TA-5574-30

FIG. 56 CYLINDRICAL ARRAY OF DISCRETE UNIDIRECTIONAL RADIATORS

The primary objective of this analysis is to determine the optimum included angle of energization for a cylindrical array of such elements. For simplicity, the particular elemental azimuthal pattern used for the computation is the simple cosine-squared function.

b. Assumptions

The following assumptions will be used for the analysis:

Array Configuration - A total of N^* elements are equispaced on the circumference of the cylinder. It is assumed that there is no interaction (mutual coupling) between the elements. Within the included angle of energization, each active element radiates unit power (which implies saturated amplifiers in the retrodirective circuitry) with the pattern described below.

* The symbols used for the discussion of a particular antenna type will in general be applicable only to that type.

Elemental Antennas - Each radiator is assumed to have a unidirectional cosine voltage pattern (*i.e.*, unidirectional cosine-squared power pattern) of the form

$$E_i = \begin{cases} 2 \cos \theta_i, & \text{for} \quad 0 \leq |\theta_i| \leq \pi/2 \\ 0, & \text{for} \quad \pi/2 < |\theta_i| \leq \pi \end{cases} \tag{32}$$

where θ_i is the angle between the radial of the ith element and the radial to the distant receiver. It is to be noted that

$$\frac{1}{2\pi} \int_{-\pi}^{+\pi} (E_i)^2 d\theta_i = 1$$

so all gains will be relative to omniazimuthal. All elements are similarly polarized and it is assumed that adjacent elements have negligible mutual coupling, so that the elemental pattern is constant and not a function of look angle.

Retrodirectivity - The array is phased by retrodirective techniques so that all the individual contributions are precisely in phase upon arrival at the distant receiving antenna; thus, the total field in the desired direction may be obtained by coherently summing the contributions of each active element.

c. Solution

The parameters of interest are (1) RF power into the array, (2) effective radiated power (ERP) in the direction of the receiver, and consequently (3) the power gain, expressed as the ratio of (2) to (1), as a function of the included angle of energization, α.

1) Coordinate System

Let one element be located at $\theta = 0$, and call this the 0th element. Then, for equispaced elements,

$$\theta_i = \frac{2\pi i}{N}, \quad \text{where} \quad i = 0, \pm 1, \pm 2, \ldots \tag{33}$$

and N is the total number of elements on the cylinder and is assumed very large. Thus the voltage contribution of the ith element can be expressed as

$$E_i = \begin{cases} 2\cos\left(\frac{2\pi i}{N}\right), & \text{for} \quad 0 \le |i| \le \frac{N}{4} \\ 0, & \text{elsewhere} \end{cases} . \tag{34}$$

Now, consider an integer I describing the active elements, within an included angle α, as follows:

$$\theta_{max} = \frac{\alpha}{2} = \frac{2\pi I}{N} . \tag{35}$$

From this it can be seen that

$$N_a = 2I + 1 = \text{No. of active elements.} \tag{36}$$

2) Effective Radiated Power

The effective radiated power is proportional to the square of the sum of the voltage contributions of all active elements; thus,

$$\text{ERP} = E_T^2 = \left[\sum_{i=-I}^{+I} E_i\right]^2 \quad \text{in appropriate units.} \tag{37}$$

For $|\theta|_{max} \le \pi/2$, $E_i = 2\cos(2\pi i/N)$, so

$$\text{ERP} = \left[2\sum_{i=-I}^{+I}\cos\left(\frac{2\pi i}{N}\right)\right]^2 \tag{38}$$

Using the fact that

$$\sum_{i=-m}^{+m}\cos ix = 1 + 2\cos x + 2\cos 2x + \ldots + 2\cos mx$$

$$= \frac{\sin(m + 1/2)x}{\sin 1/2x} \tag{39}$$

we have for Eq. (38)

$$\text{ERP} = \frac{4\sin^2\left(\frac{2\pi I}{N} + \frac{\pi}{N}\right)}{\sin^2\left(\frac{\pi}{N}\right)} \tag{40}$$

But,

$$\frac{2\pi I}{N} = \theta_{max} = \frac{\alpha}{2}$$

so

$$ERP(\alpha) = 4 \cdot \frac{\sin^2\left(\frac{\alpha}{2} + \frac{\pi}{N}\right)}{\sin^2\left(\frac{\pi}{N}\right)}, \quad \text{for } \alpha \leq \pi \quad . \tag{41}$$

If, however, $N >> \pi$ and $\alpha/2 >> \pi/N$, we can use the approximations

$$\sin^2\left(\frac{\alpha}{2} + \frac{\pi}{N}\right) \approx \sin^2\left(\frac{\alpha}{2}\right)$$

and

$$\sin^2(\pi/N) \approx \pi^2/N^2 \quad .$$

Then, Eq. (41) becomes

$$ERP(\alpha) \approx \frac{4}{\pi^2} \cdot N^2 \cdot \sin^2\left(\frac{\alpha}{2}\right) \quad . \tag{42}$$

3) . RF Power Input

With unit power in each active element,

$$P_{in} = N_a = 2I + 1 = \left(\frac{\alpha}{2\pi}\right) N + 1 \quad . \tag{43}$$

The above is an exact mathematical expression, but for $N >> \pi$,

$$P_{in}(\alpha) \approx \left(\frac{\alpha}{2\pi}\right) N \quad . \tag{44}$$

4). Power Gain

Using the exact expressions (41) and (43) for ERP and P_{in}, we have

$$G = \frac{ERP}{P_{in}} = \frac{4 \sin^2 (\alpha/2 + \pi/N)/\sin^2 (\pi/N)}{(\alpha/2\pi)N + 1} \quad , \quad \text{for } \alpha \leq \pi \quad . \quad (45)$$

This again is an exact expression; using our simplifying assumptions it reduces to

$$G(\alpha) \approx \frac{4N}{\pi^2} \cdot \frac{\sin^2 (\alpha/2)}{(\alpha/2\pi)} \quad , \quad \text{for} \quad 0 \leq \alpha \leq \pi \quad (46)$$

Figure 57 displays ERP, P_{in}, and G as a function of the included angle α.

5) Angle of Energization for Maximum Gain

The simplified expression (46) for power gain is a transcendental function of α. A numerical solution was obtained for the maximum, at

$$\alpha = 133.57^\circ = 2.3312 \text{ radians} \quad . \quad (47)$$

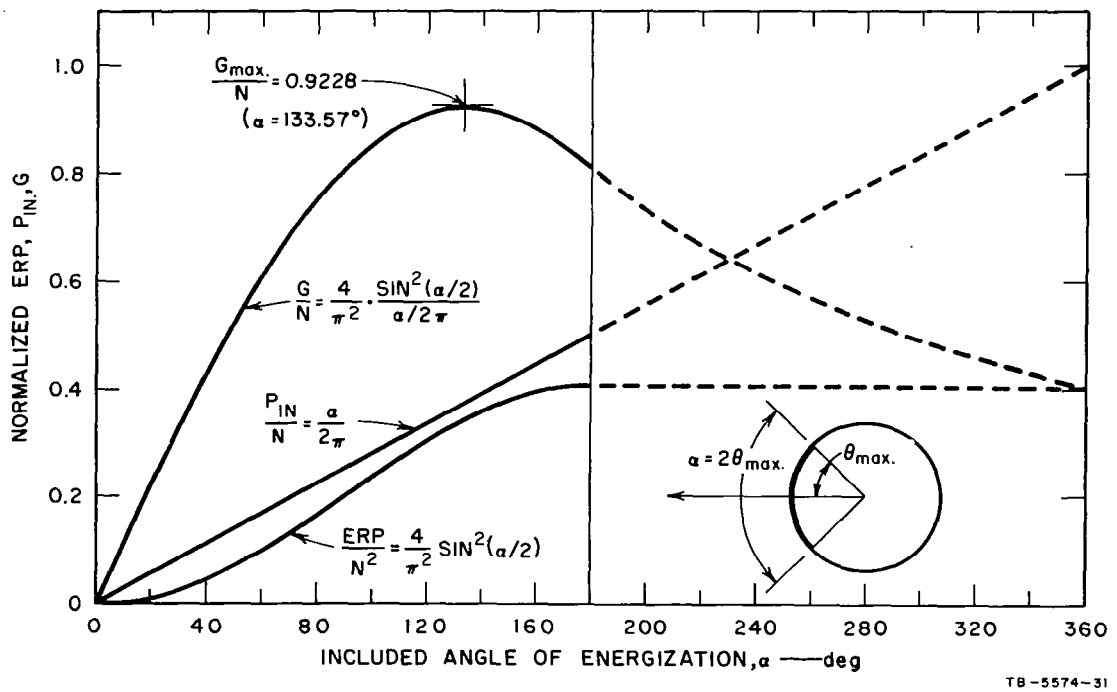

FIG. 57 NORMALIZED ERP, P_{in}, AND G AS FUNCTIONS OF α

At this optimum value of α,

from Eq. (42), ERP = $0.3434\ N^2$

from Eq. (44), P_{in} = $0.371\ N$

from Eq. (46), G = $0.9228\ N$

6) Comparison of Different Angles of Energization

Table VIII below illustrates the gain (above omniazimuthal) of an "optimum" cylindrical array (α = 133.57°), a hemi-cylindrical array, and a full cylindrical array, where the active elements have a unidirectional cosine-squared power pattern.

From Table VIII it may be seen that, for a given number of elements on a cylinder, the gain of the hemi-cylindrical array is two times (3 dB) greater than the full cylindrical array, and that the optimum angle of energization (α = 133.57°) yields approximately 0.56 dB more gain than the hemi-cylindrical array, and an antenna whose gain is only 0.35 dB less than the postulated maximum possible value, based on the total number of elements, not only the active ones. However, the total number of elements, N, or the maximum output power of each, would have to be larger than for a comparable transmitting antenna of Types 1, 2, or 3, in order to realize the same ERP.

Table VIII

COMPARISON OF ARRAY GAINS

ANTENNA TYPE	GAIN (ABOVE OMNIAZIMUTHAL)	
	G	dB
Optimum Cylinder Array (α = 133.57°)	$0.9228\ N$	10 log N - 0.35
Hemi-Cylinder Array (α = 180°)	$0.8104\ N$	10 log N - 0.91
Full-Cylinder Array (α = 360°)	$0.4052\ N$	10 log N - 3.92

IV RECEIVER CONSIDERATIONS

A. Introduction

Although most of the work on this program has been directed toward retrodirective operation of circular antennas, and all signals have been treated as unmodulated by telemetry information, the consideration of spectral splitting related to such an antenna when rotating (*i.e.*, when the vehicle upon which it is mounted is spin stabilized) stimulated consideration of at least one receiving technique for use on the vehicle. How a signal received from a spinning transmitting antenna could be handled is also discussed briefly. As can be seen from Fig. 21 or Fig. 47 the band of frequencies associated with a single element in a spinning circular array is very wide and poses a serious obstacle to the use of adaptive antennas of this type.

B. Adaptive Receiver Technique

The following representative technique, which can be considered as solving the spectral splitting problem at its source, is proposed to be used specifically with an ideal Type-3 antenna (*i.e.*, one in which there is no mutual coupling between elements and each element has an omni-azimuthal radiation pattern, even in the presence of the other elements of the array).

1. Alternatives

Consider a spacecraft spinning about an axis perpendicular to the direction of signal arrival. An antenna element on the circumference of the spacecraft will receive the signal with spin-induced angle modulation in addition to the modulation imposed at the transmitter and that due to the change in the length of the transmitter-to-satellite propagation path (gross Doppler).

In order to experience the optimum gain due to the array of antenna elements the signals received by the individual elements must be processed so that they will add coherently. There are at least three possibilities:

(a) The individual signals can first be detected and then added. This technique is unsatisfactory unless the individual signal-to-noise ratios are well above the detector threshold.

(b) The signals can be individually brought into phase with an arbitrary reference oscillator by phase-locked-loop techniques and then added at IF. The individual signal-to-noise ratios must be above the threshold of the phase-locked loops. However, a common phase-locked loop can be made responsive to the common gross Doppler component of the signals to lessen the burden on the individual loops. This technique has been documented and experimentally verified[4,78] when the remaining individual variations are essentially uncorrelated due to tropospheric irregularities over the relatively large area of the array.

(c) The effects of spectral splitting can be removed by injecting signals that negate its effects. In this case, which is considered below, the remaining individual variations are primarily due to the vehicle spin and are therefore highly correlated. We will explore the possibility of correcting for spin effects with a single common element. Since this is a programmed technique it is not inherently adaptive, and adaptive circuitry must still be added to realize the maximum gain of the receiving antenna.

2. Analysis

A representative partial block diagram is shown in Fig. 58. Let the signal received by the ith element have the phase

$$\theta_i = \theta_o + 2\pi f t + 2\pi f_d t + R \sin(\omega_s t + i\beta) + \theta(t) \qquad (48)$$

where

θ_o is a constant phase (common to all elements)
f is the transmitted frequency
f_d is the gross Doppler frequency
R is the element distance from the spin axis in wavelengths
$\omega_s = 2\pi f_s$ is the spin rate in radians/sec
β is $2\pi/N$ radians
N is the number of equally spaced elements
$\theta(t)$ is the transmitted information modulation.

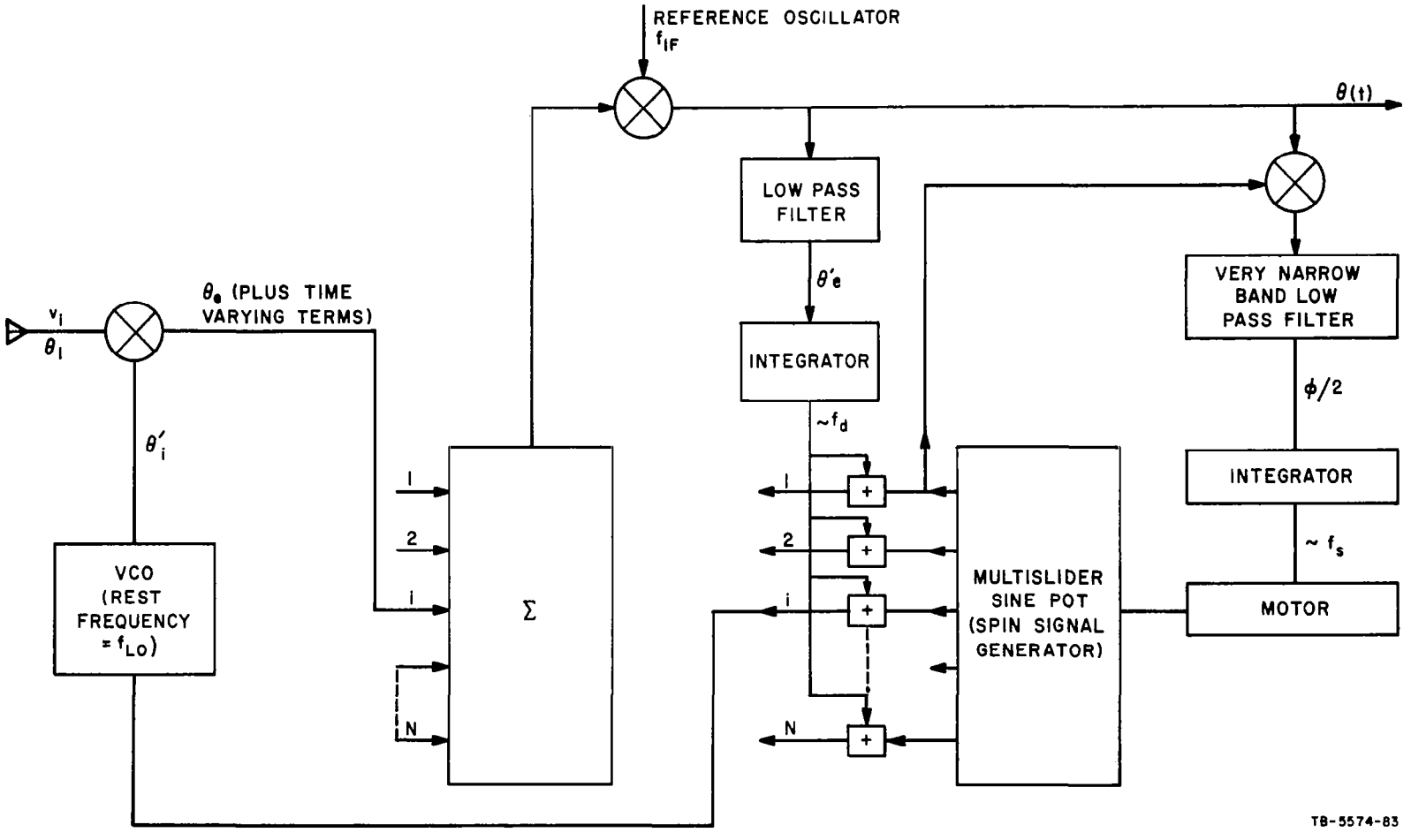

FIG. 58 REPRESENTATIVE ADAPTIVE RECEIVER CIRCUIT FOR TYPE-3 ANTENNA

Consider an ith voltage-controlled oscillator (VCO), beating with the ith signal, whose phase is

$$\theta'_i = \theta'_o + 2\pi f_{LO}^{t} + 2\pi f_d t + R \sin(\omega_s t + i\beta + \varphi) \tag{49}$$

where

$\theta'_i = 90^\circ + \theta_o + \theta_e$

θ_e is an undesired error angle

f_{LO} is the reference frequency (the rest frequency of each of the VCO's)

φ is the error angle of the spin signal generator which produces coherent sinusoidal signals with an average frequency of $\omega_s/2\pi$.

Let the spin signal generator be represented by a motor-driven sine potentiometer with N equally spaced sliders. Errors in both phasing and speed are contained in φ.

The output of the first mixer is given by $\theta'_i - \theta_i$:

$$\theta_e + 2\pi f_{IF} t - \theta(t) + 2R \sin\frac{\varphi}{2} \cos\left(\omega_s t + i\beta + \frac{\varphi}{2}\right) \tag{50}$$

where f_{IF} is the intermediate frequency.

These mixer outputs are then summed and mixed with a second reference frequency f_{IF} to give a phase

$$\theta(t) - \theta_e - 2R \sin\frac{\varphi}{2} \sum \cos\left(\omega_s t + i\beta + \frac{\varphi}{2}\right) \tag{51}$$

where the summation is over all active elements

$\theta'_e = \theta(t) - \theta_e$ is recovered by a low-pass filter with a very long time constant and integrated to produce a voltage proportional to the gross Doppler.

$\theta(t)$ is recovered by a high-pass filter which, of course, implies that the modulation is on a sub-carrier.

If the summation is over all elements and all elements have equal gains in the signal direction, then

$$\sum_{i=1}^{N} \cos\left(\omega_s t + i\,\frac{2\pi}{N} + \frac{\varphi}{2}\right) = 0 \quad .$$

In the likely event that not all elements are operational or not all gains are equal, the sum will yield a voltage of frequency $\omega_s/2\pi$ which can be synchronously detected and low-pass filtered to give a voltage proportional to sin $\varphi/2$. This voltage can then be integrated with, again, a very long time constant to drive the spin signal generator.

This part of the circuit can also provide information relating the angular orientation of the vehicle (specifically the position of the 1st elemental radiator of the antenna, in Fig. 58) to the direction of the transmitting station.

The individual adders can be eliminated as indicated in Fig. 59.

The system, of course, is connected to drive θ_e' and φ to zero.

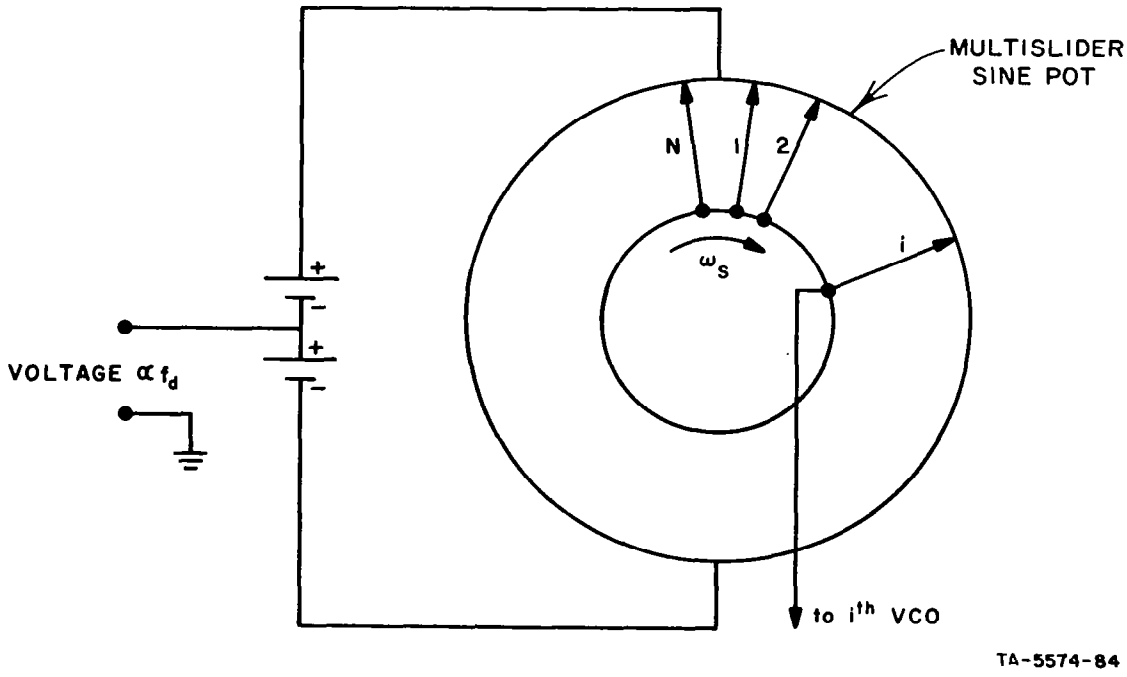

FIG. 59 POTENTIOMETER ARRANGEMENT TO ELIMINATE INDIVIDUAL ADDERS OF FIG. 58

3. Frequency Acquisition

Although the spin rate and the gross Doppler are expected to be very slowly changing, acquisition of the gross Doppler is a potential problem when the signal to the spacecraft has been interrupted. To speed this process, the low-pass filter associated with θ_e' can be broadened. The spin signal will then also pass this filter but will still be detected and corrected by its own circuit.

4. Additional Advantages and Comments Relating to the Technique

The spin rate and instantaneous position is easily available as a telemetry item, should it be desired.

Possibly the angle between the direction of arrival of the signal and, say, the line to the sun or a star could also be derived. If the retrodirective array is used to receive signals from both the earth and the capsule, then the two potentiometers could possibly be driven by a common motor and their relative phasing adjusted with a differential gear. The setting of the differential would measure the angle between the two directions of arrival.

Since gross Doppler, spin rate, and relative angle are explicitly available, suitable transmitter signals can be derived at any desired frequency. Further, the number of antenna elements used for reception need not equal the number used for transmission. In this case the signal transmitted from the vehicle can be made free of spectral splitting.

The spacecraft spin rate is expected to be of the order 6 rpm, making $\omega_s/2\pi$ about 0.1 c/s. This rate can be expected to vary only very, very slowly except possibly at the time of the launch of the capsule when a step change in rate is likely.

If the antenna elements are so mounted that not all can be active at a particular time—for instance, if an antenna similar to Type-4 is used—noise must nevertheless be accepted from all elements. There is no obvious way to sense whether a particular element is active or not. If arrangements were made to disconnect inactive elements, it is important to note that some minimum fraction of the total number would always have to be connected during periods when the incoming signal was interrupted to assure acquisition of the signal when it reappeared.

C. General Considerations

The technique just described is designed to solve the spectral splitting problem at its source with additional on-board equipment. In order to keep the amount of on-board equipment to a minimum, it is also possible to attack the problem at the other end of the link. In general this will require more complex equipment, so is most applicable when this other end is the Earth terminal.

No attempt has been made to devise specific circuitry, but some general remarks follow. The general technique has greater potential than the above on-board technique, which requires that certain assumptions (*e.g.*, that there be no mutual coupling) obtain for its correct operation.

Types of modulation are mentioned, but consideration of suitable modulation methods did not form part of the study.

While a rotating antenna structure will generally give rise to spectral splitting, the retransmitted carrier is definitely related to the characteristics of the antenna and the spin rate and, if the pilot signal is unmodulated, will have a symmetrical line spectrum centered on the carrier with nearly all the power in the carrier. Apart from the carrier only the *N*th sideband (of the spin frequency) has been shown to have appreciable power content (see Sec. III-C-3-j).

While such a signal received at the ground station is moderately complex, it can be synthesized at the final receiver to allow synchronous detection. The synthesis could be done on a computer and would, of course, use the design characteristics of the spacecraft, and consequently have only to track the spin rate of the satellite. For the Type-1 antenna at least, the sidebands other than the *N*th could be ignored, probably resulting in some small amount of distortion. However, except when several elemental radiators were inactive or otherwise faulty such distortion should be minimal.

On the other hand, non-synchronous energy detection is easily implemented if the modulation is frequency-shift-keyed (FSK) and the separation of the two frequencies is made somewhat larger than the spectrum spreading due to the combination of communication bit rate and rotation of the antenna.

Put another way, the spinning antenna can be considered as a signal scrambler. If this scrambling interferes too much with the information

content of the signal, some device is needed to "unscramble" the signal before it can be used. Theoretically, any such signal can be unscrambled if an exact model of the "scrambling device" is available at the receiving point to help in processing the incoming signal. In the case of a modulated retrodirected signal from a spinning vehicle, an analog form of such an "exact model" could be an actual identical antenna that is kept spinning at the identical rate as the space vehicle. The "exact model" could also be in the form of a digital computer. Both devices would have to be periodically normalized or updated by transmitting a known special signal (such as CW) from the vehicle.

Two advantages of such a system are: (1) the condition of each of the elemental radiators can (theoretically, but not explicitly) be determined at any time, and (2) if some asymmetry is purposely introduced into the vehicle, such as leaving out or switching off one of the transmitting elements, then the exact orientation of the vehicle can also be determined at any time. This could be very useful, as already discussed, for determining such "navigational information" as the angle subtended at a bus between the directions of the earth station and the capsule. This assumes that there is, in addition, some direction-finding equipment on board the bus, perhaps of the same basic type, to determine the relative direction of the capsule.

The above considerations apply to a transmitting space vehicle and a receiver at the Earth station. However, the same basic technique could also be used to assist the operation of a spinning vehicle receiving a signal from Earth, if an adaptive receiving antenna was considered necessary. The transmitted ground signal could be "pre-scrambled," to be unscrambled by the rotation of the vehicle antenna. Because of the long return-path time delays associated with interplanetary travel, closing the loop of such a system could present difficulties, depending on the rate of change of conditions on the vehicle.

V. SYSTEMS AND CIRCUITRY CONSIDERATIONS

A. Introduction

This section is concerned with several aspects, apart from the adaptive antennas themselves, of communicating information on an interplanetary mission similar to the one mentioned in the introduction to this report. Apart from the problem of transmitting data that is gathered by sensors on the bus or capsule, and retrieving it at the final receiving station, it is of prime importance that the position of the bus and/or capsule be monitored as well as possible during the mission. It is also important that techniques should be available for re-establishing communication links as soon as possible after they are broken, as is sure to happen.

Some of these many problems are considered below. The list is by no means comprehensive, nor are the individual subjects exhaustively covered.

B. Considerations Relating to Various Links

The basic links that are likely to be used in order to fulfil the mission outlined in the introduction (Sec. I) are considered in this section. System considerations relating to some of them, including amplifier and tracking requirements, are discussed in some detail but primary attention has been paid to the link from the bus back to Earth.

1. Basic Links

Five separate links that are considered desirable, if not essential, are discussed briefly below.

a. Earth-to-Bus

The effective radiated power at the earth terminal is essentially unlimited and the communication bandwidth to carry commands and tracking modulation to the bus is small. Thus an adaptive receiver structure to provide array gain is not considered necessary on the bus. The Earth transmitter frequency can be varied to reduce the gross Doppler shift with which the spacecraft must contend. Since the bus-to-earth link is assumed

to require a retrodirective array on the spacecraft, the earth-to-bus signal, which would act as the pilot, should not have modulation near the carrier frequency; the modulation should be on subcarriers.

b. Bus-to-Earth

The power available is relatively small and the total amount of data may be large particularly during entry of the capsule into a planetary environment. The use of data storage on the bus and a relatively slow data rate over an extended time period seem indicated for the present. High transmitter-array gain is required and the effects of vehicle spin on the transmission link must be compensated. The link must carry experimental data and telemetry, including data and telemetry relayed from the capsule, and return tracking modulation. (The NASA goal of 10^6 bits/sec[79], on which live TV could also be carried, is beyond the consideration of this report.) The transmitted carrier should be coherent with the received carrier (pilot signal) and the gross Doppler should be preserved for navigational purposes.

c. Bus-to-Capsule

This is a low-information-rate link carrying commands and possibly tracking modulation. Again the spectrum near the carrier should be clean to facilitate retrodirective transmission from the capsule. Probably the division of power between this and the bus-to-earth link can be varied with the phase of the mission; this time-sharing of available power would be facilitated by a data-storage capability on the bus.

For instance, when this link is to be established, or re-established the bus would probably transmit at maximum power in an omnidirectional mode. When the capsule acquires this signal on its retrodirective array and returns a CW signal to the bus, the bus would switch its mode from omnidirectional to retrodirective transmission to the capsule. Normal bus-to-earth operation could also then be resumed.

d. Capsule-to-Bus

This link, particularly for a hard-landing capsule, should have a high information rate. Using batteries it could also radiate relatively high power for a short time but the ERP should be increased by antenna gain on the capsule and possibly also for the receiving antenna on the bus.

Again modulation should be on a subcarrier to provide a clean tone for retrodirective operation. The link would carry environmental data as well as provide methods for obtaining accurate range, Doppler, Doppler-rate, etc.

If the capsule is battery-powered only, it might be designed to transmit information only on command from the bus, although its retrodirective array would probably have to transmit a low-power pilot signal to keep the bus retrodirective antenna correctly aligned.

e. Earth-to-Capsule

If a suitable simple antenna could be mounted on the capsule it would be desirable, provided the capsule was not occulted by the planet, to transmit high-power pulses from Earth to be received at both the capsule and the bus. The capsule could then transmit the time of arrival of the pulse to the bus and thereby establish the length of the Earth-bus-capsule triangle much more accurately than by angular or any other measurements made solely from the bus.

2. Estimated Amplifications, and Noise Bandwidths for Retrodirective Elements on a Planetary Bus

a. General

If a bus to Mars, say, is to employ a retrodirective array for transmission back to Earth, then the active circuitry of the bus must provide a very high power gain in order to satisfy mission requirements. A primary purpose of the following calculations is to determine (approximately):

(1) The required power amplification for each active retrodirective element

(2) The maximum allowable noise bandwidth for each element.

b. MARS MISSION PARAMETERS

For estimating purposes, we will take the following parameters from the Mariner IV flight:

d = 135×10^6 statute miles (at Mars encounter)

F_r = 2.1 GHz (spacecraft receive frequency)

F_t = 2.3 GHz (spacecraft transmit frequency)

T_e = 10^4 W (Earth transmitter carrier power) (70 dBm)

We shall also assume that the new 210-foot diameter Goldstone antenna is used, which, if an illumination efficiency of 54 percent is assumed, provides the following gains:

G_t = + 60.3 dB (2.1 GHz)

G_r = + 61.1 dB (2.3 GHz)

And, we shall assume that the active bus transmitters (*i.e.*, retrodirective elements) will develop a total of 20 W of RF at 2.3 GHz.

A look ahead to Table IX and Figs. 60-62 will also show the use of the following assumed parameters:

L_1	= Earth transmission circuit loss	=	1.0 dB
L_2	Bus receiving circuit loss	=	1.0 dB
L_3	= Bus transmitting circuit loss	=	1.0 dB
L_4	= Earth receiving circuit loss	=	1.0 dB
T_h	= Noise temperature of bus receivers	=	1450°K
C/N	= Required carrier-to-noise ratio in each retrodirective circuit of bus	=	+10.0 dB

c. Retrodirective Cylindrical Array Antenna

All previous antenna configurations have been based on the assumption that spin stabilization will obviate the need for pointing the beam of a retrodirective antenna in the elevation plane. It has been generally assumed that the beam would always point somewhere in the plane perpendicular to the spin axis. In the following analysis the more general case of an antenna capable of pointing in nearly any direction (except near the zeniths) is assumed. In addition, the retrodirective cylindrical array on the bus is assumed to have a 10λ radius and 10λ axial dimension. Each element is an axial $\lambda/2$ dipole, spaced $\lambda/4$ above the conducting surface of the cylinder. Elements are spaced

$\lambda/2$ along the axial dimension (yielding 20 elements/row) and are spaced $\lambda/2$ along the circumference (yielding $40\pi \approx 125$ elements/ring), for a total of 2500 elements on the cylinder.

It is further assumed that logic circuitry is employed to turn off those elements that are not substantially contributing to radiation in the desired direction; only those rows within an included angle of 144 degrees (50 rows) are assumed active and all available power is equally distributed among them (see Sec. III-C-5 above), to give near optimum ERP; so there are $50 \times 20 = 1000$ active elements in the array.

For the $\lambda/2$ elemental dipoles described, the gain is approximately +4.4 dB (above isotropic) for the elements directly in line with the direction of the incoming wave ($\theta = 0$ degrees), and is approximately -2.0 dB for the extreme active elements ($\theta = \pm 72$ degrees). The average gain of all active elemental dipoles can be shown to be approximately +3.3 dB. The effect of mutual coupling between dipoles is neglected.)

d. Calculations

With the essential parameters now defined, we proceed with the calculations. For the given array, we shall consider three different bases (configurations) of elemental dipoles and receivers:

(1) One receiver per dipole (Fig. 60)
(2500 receivers required)

(2) One receiver per axial row of dipoles (Fig. 61)
(125 receivers required)

(3) One receiver per array (Fig. 62)
(1 receiver required)

The second configuration (one receiver per row) is probably the only one of practical interest, although inclusion of the other two provides useful references for comparison.

Table IX gives the results of the calculations, and Figs. 60 through 62 display the levels, gains, and attenuations in block diagram form.

Required Amplification—Reference to Table IX shows that each active retrodirective unit must be capable of the order of 150 dB power amplification of the received pilot, in order to produce the required output level. Note that the required amplification per retrodirective unit is the same for all three illustrated configurations. The point is, that

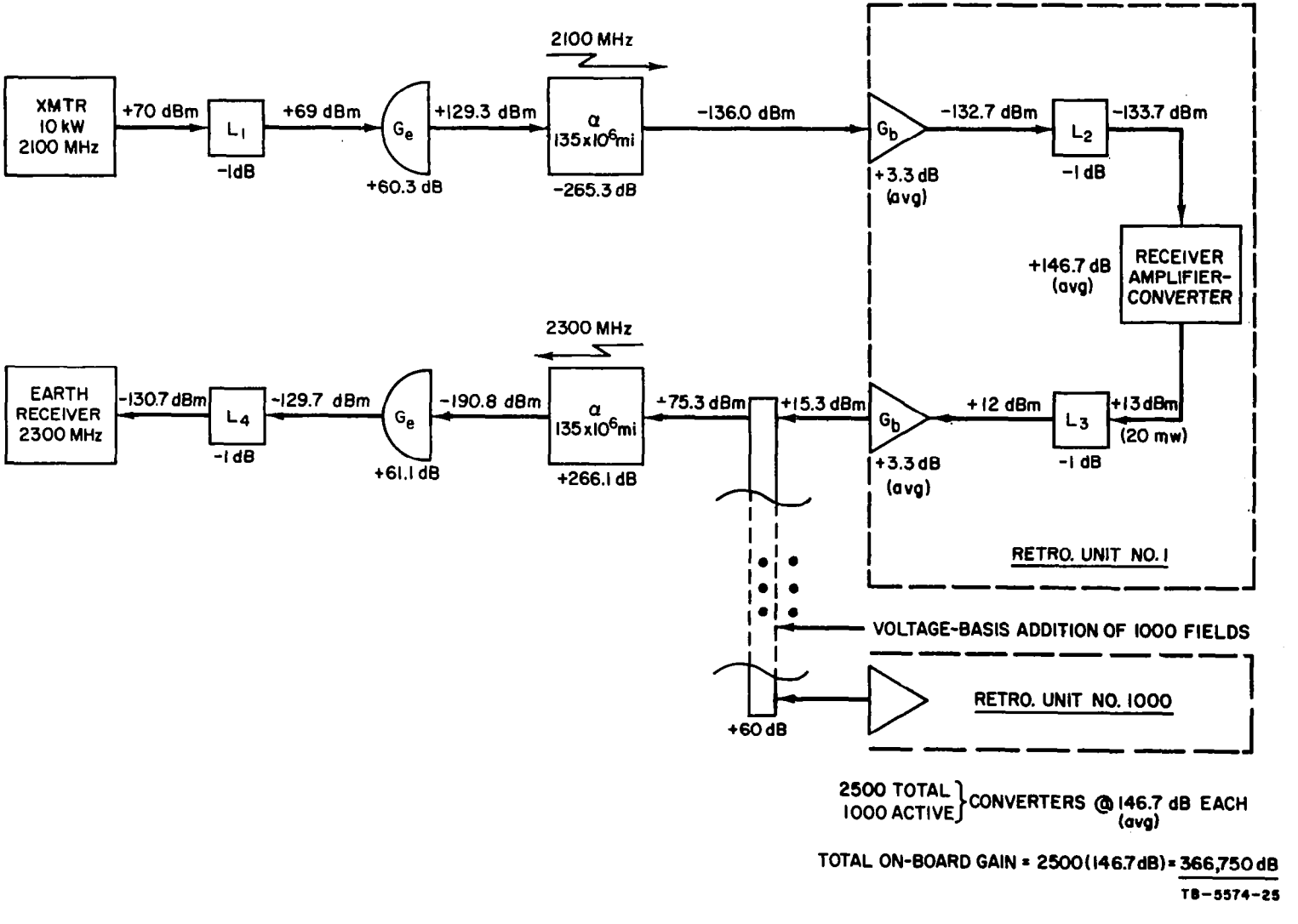

FIG. 60 EARTH-BUS LINK WITH 1000 ACTIVE CONVERTERS (One per active element)

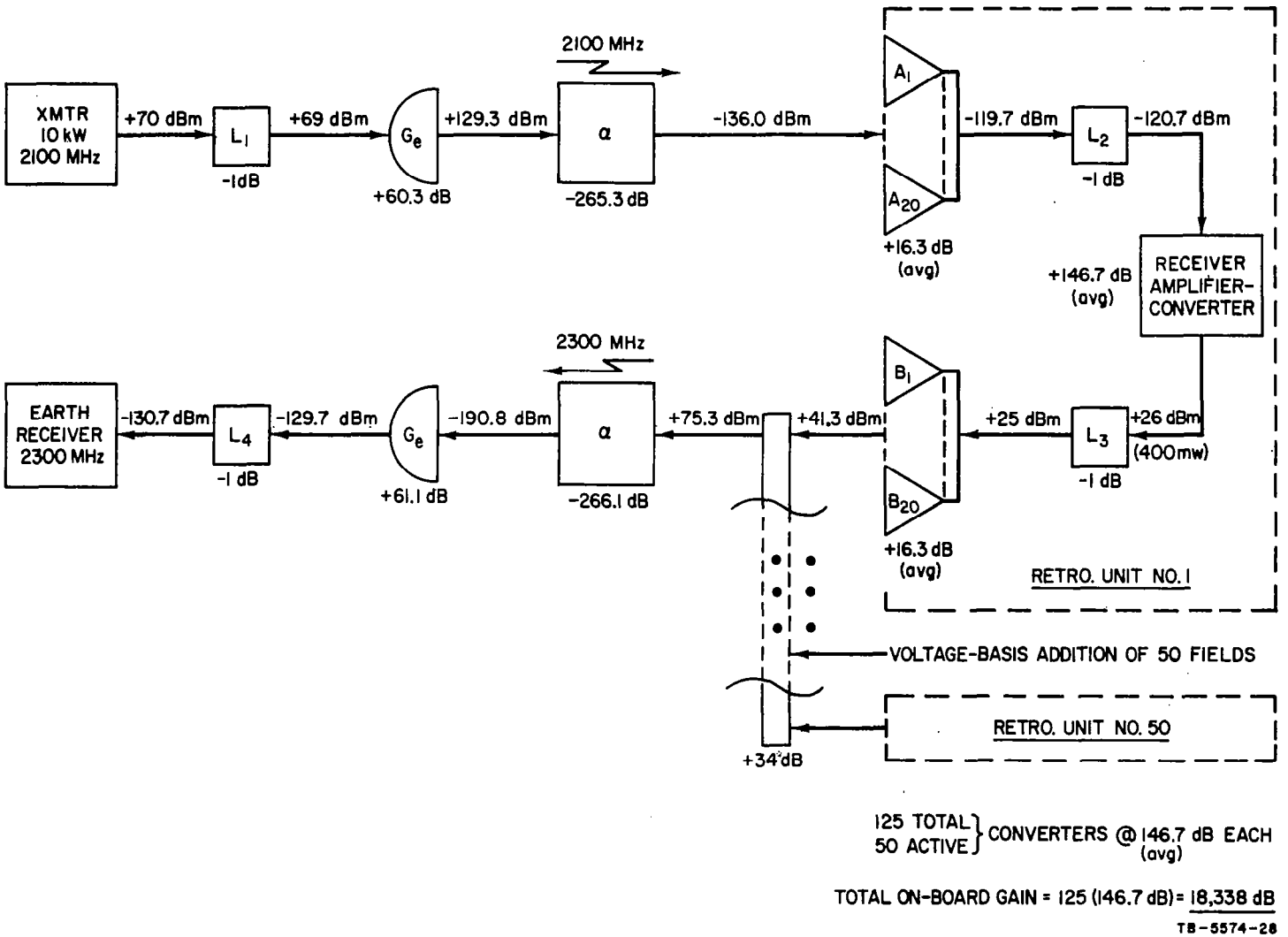

FIG. 61 EARTH-BUS LINK WITH 50 ACTIVE CONVERTERS (One per active row)

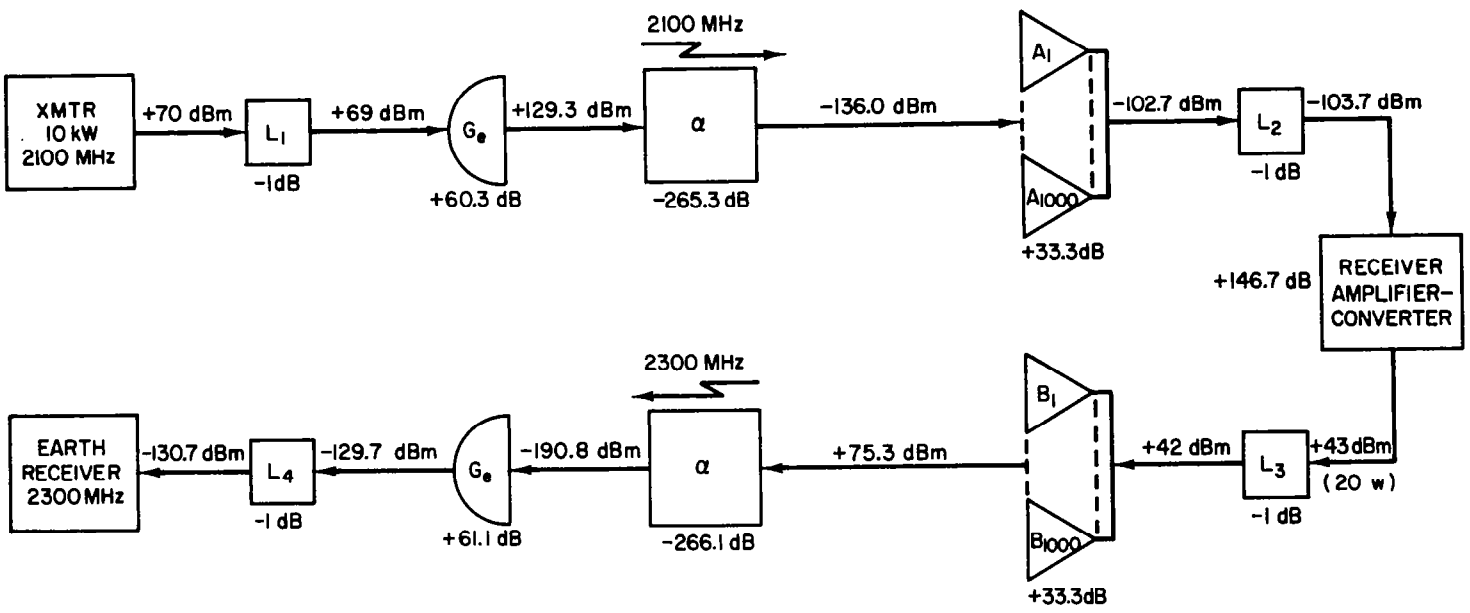

FIG. 62 EARTH-BUS LINK WITH ONE ACTIVE CONVERTER

Table IX

EARTH-BUS LINK WITH VARIOUS RECEIVER BASES

PARAMETER		RECEIVER BASIS		
		ONE/ELEMENT	ONE/ROW	ONE/ARRAY
T_e = Earth transmitter carrier power (10 kW)		+70.0 dBm	→	→
L_1 = Transmission circuit loss		-1.0 dB	→	→
G_e = Earth antenna gain (210 ft dia 54 percent eff)		+60.3 dB	→	→
α = Free-space attenuation (135 x 10^6 miles		-265.3 dB	→	→
G_b = Bus antenna gain per receiver ($\lambda/2$ axial dipoles, spaced $\lambda/4$ above cyl. surface)	Max: $\theta = 0°$	+4.4 dB	+17.4 dB	
	Avg:	+3.3 dB	+16.3 dB	+33.3 dB
	Min: $\theta = 72°$	-2.0 dB	+11.0 dB	
L_2 = Receiving circuit loss		-1.0 dB	→	→
C = Received carrier power	Max:	-132.6 dB	-119.6 dBm	
	Avg:	-133.7 dBm	-120.7 dBm	-103.7 dBm
	Min:	-139.0 dBm	-126.0 dBm	
W = Max. allowable noise bandwidth (T_n = 1450°K, C/N = +10 dB)	Max:	275 Hz	5500 Hz	
	Avg:	214 Hz	4280 Hz	214 kHz
	Min:	63 Hz	1260 Hz	
P_o = Required receiver-amplifier output level (for 20 W total)		+13 dBm (20 mW)	+26 dBm (400 mW)	+43 dBm (20 W)
G_a = Required receiver amplification	Min:	145.6 dB	→	
	Avg:	146.7 dB	→	→
	Max:	152.0 dB	→	
N = No. of receivers required		2500	125	1
G_T = Total on-board gain required = $N \cdot G_a$ (Avg.)		366,750 dB	18,338 dB	146.7 dB

for assumptions of (1) fixed total antenna aperture size, and (2) fixed total RF power in and out of the total aperture, then the required gain per subaperture is independent of the number of subapertures into which the total aperture is subdivided.

Noise Bandwidth—The maximum allowable noise bandwidth of each retrodirective unit does depend upon the subaperture size (how many elemental antennas per receiver), and upon the minimum tolerable S/N in the retrodirective units. If we arbitrarily say that the average S/N shall be +10 dB, then reference to Table IX shows that the second scheme (one receiver per row) has a maximum allowable noise bandwidth of approximately 4280 Hz.

e. Conclusions

It has been shown that each active retrodirective unit on a Mars bus must be capable of approximately 150 dB power amplification of the received pilot, and that for one receiver per row the maximum allowable noise bandwidth is approximately 4 kHz.

The circuitry for retrodirective units of this performance will be quite complex, compared to the retrodirective circuitry that has appeared in the literature for earth satellite application, where gains of less than 40 dB are specified and much wider bandwidths are employed.

With this high-gain requirement, one important problem will be transmitter-receiver isolation.

A critical parameter in any retrodirective array is the phase stability and uniformity of the circuitry. It may be expected that, for conversion from 2.1 to 2.3 GHz with 150 dB power gain and 4 kHz noise bandwidth, phase stability and uniformity on the order of ±10 degrees will be a significant problem.

3. Range and Range-Rate Tracking

a. Philosophy

Both range and range-rate tracking involve phase (or frequency) comparison of a transmitted signal with the same signal reflected or transponded by the spacecraft being tracked. If the spacecraft transponder is other than an RF amplifier, a local oscillator is required in

the spacecraft. Such an oscillator may be phase-locked to the received signal and hence has a frequency derived from and coherent with the received frequency. Relatively complex circuitry is required and signal acquisition may be a problem. Alternatively, the local oscillator may be free-running and the signal returned by the spacecraft must be designed so that the oscillator-frequency as well as range and range-rate information can be extracted by the tracking station.

The Goddard Space Flight Center system[80] is based on the second concept. The returned signal consists of a carrier and a modulated subcarrier; both the carrier frequency and the subcarrier frequency relative to that of the carrier are linear functions of the local oscillator frequency and of the Doppler offset.

b. Range-Rate Tracking

For nonrelativistic radial velocities, the shift in frequency is directly proportional to the radial velocity. In the two-way systems considered here it is assumed that the velocity can be considered constant over the round-trip propagation time. Otherwise, more complex systems are needed or the measured Doppler can be considered as an average over the propagation time. Typically, the measurement is considered to be the vehicle radial velocity at the instant one-way propagation time in the past.

Range-rate systems require that the frequencies transmitted and those received be measured. The velocity is then easily calculated.

c. Range Tracking

If a range-rate system can be kept in continuous operation starting from a known range, range can obviously be obtained from a simple integration of velocity. More typically, continuous operation is not obtained due to equipment malfunction and earth rotation and so cannot be relied upon. Then range must be determined separately.

Periodic ranging signals are frequently used. They should have three distinct properties:

(1) Minimum range uncertainty.

(2) No range ambiguity.

(3) Indication of needed correction.

The range uncertainty depends upon the width of the autocorrelation function peaks, which should be small. When tones are used, a high frequency is required; with pulses, narrow widths are needed.

The range ambiguity depends upon the spacing of the periodic peaks of the autocorrelation function. Thus the period should exceed the round-trip propagation time for the maximum range of interest. With tones, a low frequency is required; with pseudorandom pulse sequences, a long period is required. Frequently, the ambiguity problem becomes much less severe because the approximate range is already known.

When, as is typically done, a copy of the transmitted signal is delayed and cross-correlated with the returned signal, the correlator output should indicate the change in delay required to achieve coincidence of the two signals. Tones have this property; pulse sequences do not. However, a pulse sequence derived from several shorter sequences can be used to simplify this search problem.

d. Goddard System

The Goddard system uses a free-running transponder oscillator. The up-signal is modulated with tones and/or pseudorandom codes. The signal received by the spacecraft is doubly converted to produce a subcarrier, which modulates a down-carrier derived from the same oscillator. Cascade phase-locked loops in the earth receiver extract Doppler and, incidentally, the transponder oscillator frequency. The transponder can receive up to three modulated signals simultaneously and convert the modulation to separate subcarriers.

e. Extension of Goddard System

For a configuration consisting of an earth station, a spacecraft bus, and a capsule, the returned signal must be designed so that the following can be extracted:

(1) Bus local oscillator frequency

(2) Capsule local oscillator frequency

(3) Earth bus Doppler

(4) Bus capsule Doppler.

A feasible configuration using one unmodulated and two modulated subcarriers is presented in Appendix E. Such configurations have not been considered in relation to a retrodirective array or any other type of adaptive antenna but no severe difficulties are anticipated in selecting the appropriate circuitry and different frequencies, where necessary, to ensure that the range rate can still be determined with sufficient accuracy.

f. Conclusions

Except for the fact that many amplifier/transmitters are required on a retrodirective array, only minor modifications of the basic Goddard transponder are required to derive Doppler for the earth/bus and the bus/capsule links. The resulting signals, when suitable ranging modulation is used, also can be processed to yield earth/bus and earth/bus/capsule range information.

No phase-locked circuits are required on either the bus or the capsule and only readily achievable oscillator stabilities are required in the vehicles.

4. A Duplex Retrodirective Scheme for a Mars Bus

a. Requirements for a Retrodirective Scheme

It has been shown in Sec. V-B-2 above that each retrodirective transmitting unit on a Mars bus will require on the order of 150 dB of power amplification of the received pilot, and that the allowable noise bandwidth in each retrodirective unit is quite narrow (approximately 4000 Hz for the Type-4 antenna assumed).

In addition, there are several other design constraints on a retrodirective scheme, for example:

(1) The scheme should permit precise determination of bus range rate (Doppler shift) at the earth station.

(2) Duplex operation will be required, which means, since both signals are CW, that there must be a frequency offset between receive (pilot) and transmit frequencies, and a relatively large separation (several percent) will ease filter requirements.

(3) Phase taper of the transmitted wave over the cylinder due to frequency offset should be negligible ($< \pi/8$) to realize maximum gain. This implies some form of compensation, if a substantial frequency offset is employed.

b. Basic Operation of the Scheme

The basic operation of the scheme presented here is that, by coherent division and multiplication, the retrodirective array transmits a frequency that is 9/8 of the received (pilot) frequency.* The scheme can use the carrier of the earth-bus command link as the retrodirective pilot; a separate pilot frequency is not required.

1) Master Receiver

First, an omniazimuthal receiving antenna located on the spin axis (see Fig. 63) provides one master phase-lock receiver with the basic Earth carrier (pilot) frequency, shifted by one-way Doppler, but free from any spectral splitting caused by spin.

This master receiver should be continuously phase-locked to the received carrier, except during transfer from one earth station to the next, as the on-axis antenna is always visible to the earth. Also this master receiver is used as the command receiver. This scheme requires that the signal-to-noise ratio at this low-gain omniazimuthal antenna be greater than unity.

2) Retrodirective Units

Each retrodirective unit contains a phase-lock loop, and the general functions of each retro unit (see Fig. 64) are:

(1) *Frequency Offset*—the pilot frequency is multiplied by 9/8 before amplification and retransmission.

(2) *Retrodirectivity*—each retro unit multiplies the spatial phase (relative to the plane of the incoming pilot wave) by 9/8, and conjugates, so the composite outgoing wave (at 9/8 F_r) is also planar and is radiated

* Any other convenient ratio of integers could be used.

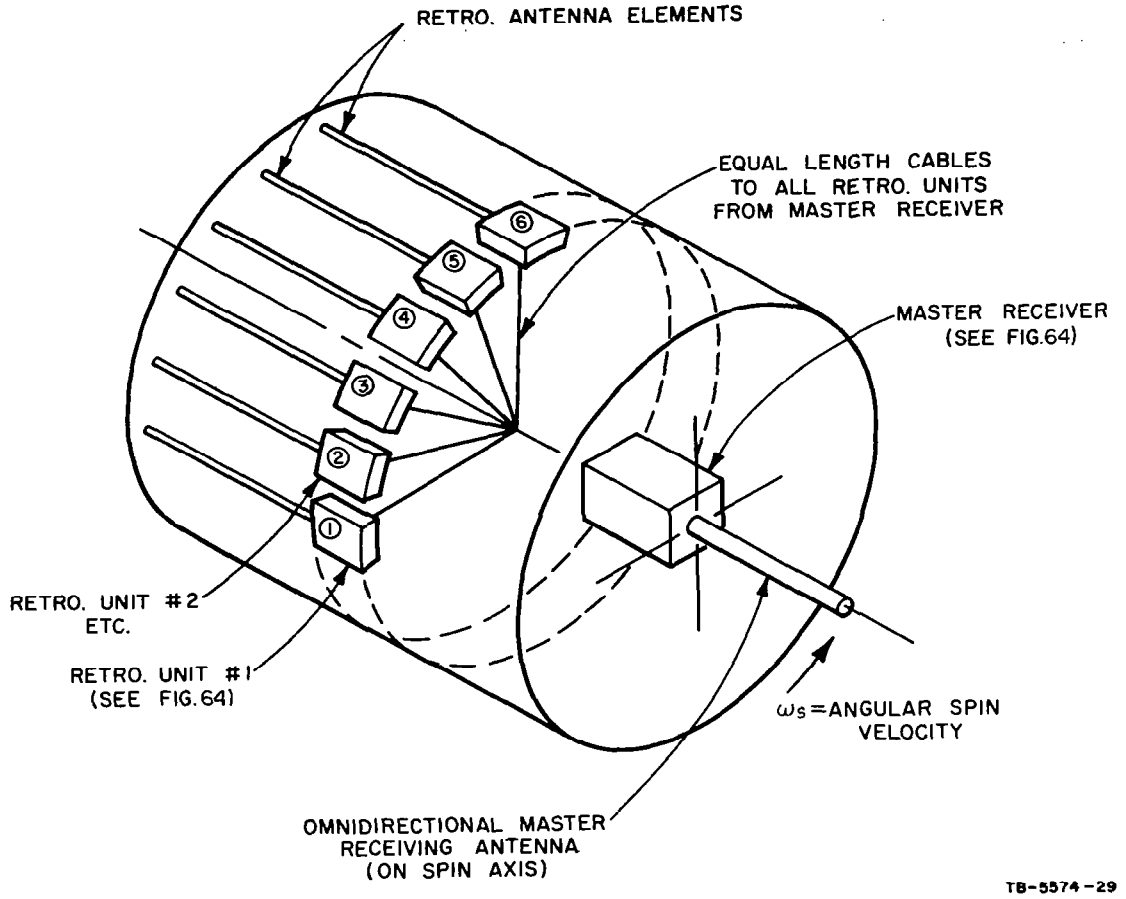

FIG. 63 PHYSICAL LAYOUT OF RETRODIRECTIVE ARRAY ON CYLINDRICAL LENS

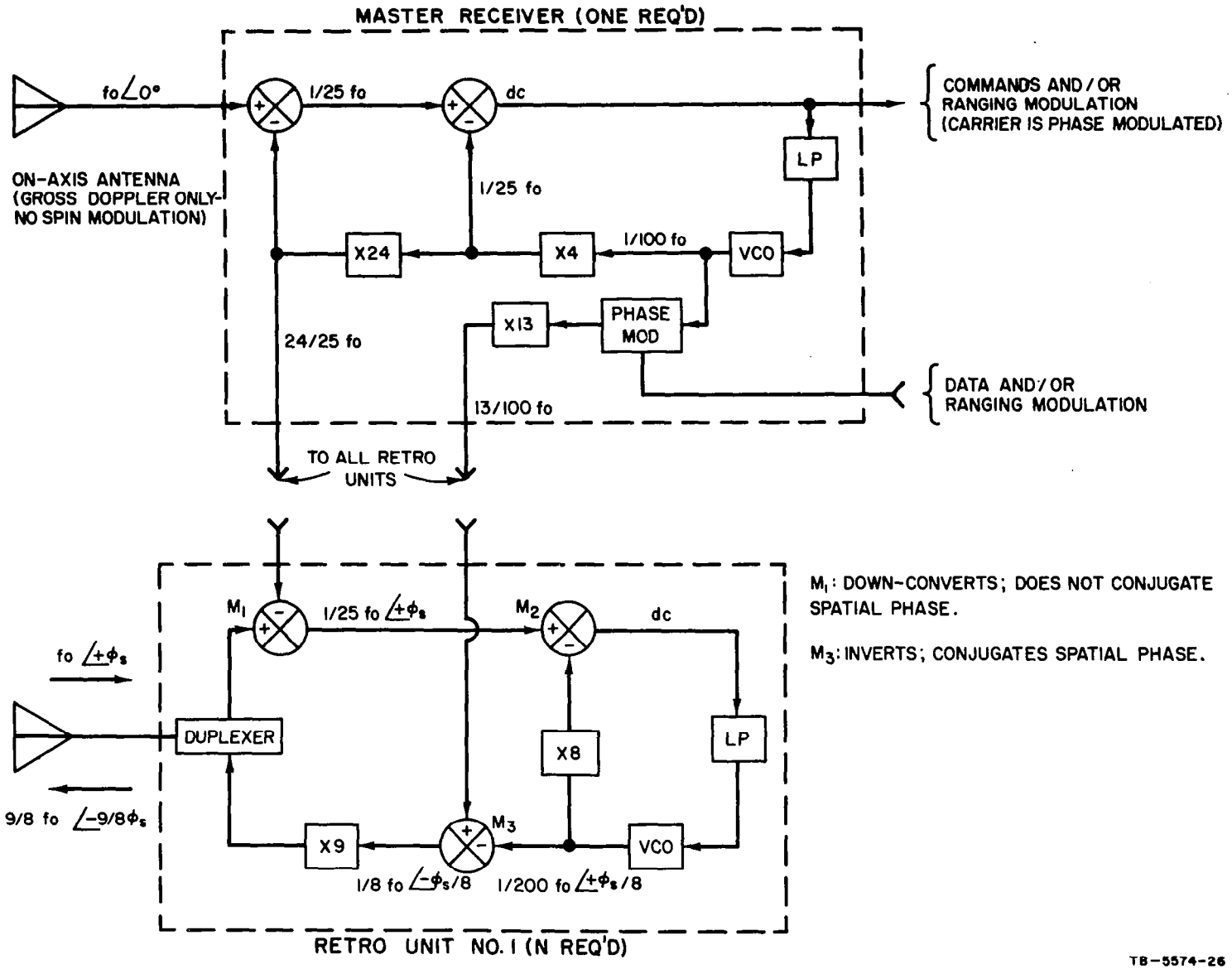

FIG. 64 CONVERSION SCHEME FOR A DUPLEX RETRODIRECTIVE SYSTEM

back in the direction from which the pilot signal (F_r) was received. Multiplication of the *spatial phase* by the same factor as the *frequency* (*e.g.*, 9/8) eliminates all phase taper.

(3) *Data Modulation*—the retransmission from each retro unit is phase modulated with spacecraft data and/or ranging modulation received from the Earth.

3) Features of the Scheme

The following features of this retrodirective scheme may be compared with a simple "conventional" heterodyne approach:

(1) First mixer does not conjugate spatial phase as in the image frequency converter, for instance, because the injection frequency is *below* the receive frequency.

(2) Receive leg employs an IF of 1/25 F_r*, permitting amplification at a relatively low frequency.

(3) Phase-lock loop employed in retro units to extract pilot, permits

(a) Very narrow noise bandwidth, and

(b) Potential for extracting phase-lock information for logical applications (*e.g.*, to control transmit leg, to determine attitude, and to sense malfunctions).

(4) Multipliers rather than RF amplifiers can be used in transmit legs.

c. Gross Doppler Shift

Considering only Doppler shifts due to gross velocity of the bus, and assuming that the velocity does not change in one round-trip time, the bus receives a frequency that is precisely (relativistic)

$$F_r = \sqrt{\frac{1 - V/c}{1 + V/c}}\, f_{eB}$$

* Any other convenient ratio of integers could be used.

where

f_{eB} = Earth transmit frequency

Gross velocity of bus c.g.

Our retrodirective scheme retransmits a signal of frequency

$$F_t = (9/8)F_r$$

and applying the (relativistic) down-link Doppler, the earth receiver sees a frequency

$$F_e = \sqrt{\frac{1 - V/c}{1 + V/c}}\, F_t$$

which yields

$$F_e = \sqrt{\frac{1 - V/c}{1 + V/c}}\, \frac{9}{8}\, F_0 \quad .$$

This is *precisely* equal to the two-way (radar) Doppler shift of a signal whose frequency is $(9/8)F_0$.

d. Conclusions

A method has been presented, by means of coherent division and multiplication, to obtain a relatively wide spacing between the receive (pilot) and transmit frequencies of a retrodirective cylindrical array. This method would be applicable to a scheme where duplexers were used on elemental antennas, or where separate transmit and receive antennas were used but associated antennas are on the same axial line of the surface of the cylinder.

Phase-lock loops are employed for the division function. If the low-pass filter in the loop passes only the modulation frequency, which is the same as the spin (1 Hz or less), any modulation of higher frequency will not pass through the retrodirective unit. Thus the carrier of the Earth-to-bus command link could also be used as the pilot for the retrodirective array, without having the command modulation appearing on the down-link signal, as long as the spectrum of the command modulation has no components in the passband (dc to 1 c/s) of the phase-lock loops.

Frequency multiplication is employed in the output of the retrodirective unit, so transistor and/or varactor multipliers would be a convenient way of producing power at approximately 2 GHz with good dc-to-RF conversion efficiency.

By using a signal derived from an antenna on the spin axis for the local oscillator, the scheme permits precise determination of bus range rate (Doppler shift) at the earth station. (It would perhaps be feasible to derive this signal by means of a summation of the signals from all retrodirective units, but the antenna on the spin axis is in any event conceptually useful.)

C. Signal Acquisition

1. General

In any mission similar to the one described in the introduction to this report, and in Sec. V-B, it must be assumed that communications will at some stage be disrupted and must then be re-established. In the case of the Earth-to-bus and bus-to-Earth links this should not present any great problem since the direction of the bus in space will in general be known to within at least one beamwidth of the ground station. Consequently, if a pilot beam is transmitted in this direction by the ground-station transmitter to a retrodirective antenna on the bus, then the instant this signal is received at the bus a retrodirection will be established and the bus will transmit with its full antenna gain in this direction. There could be a delay of the order of one second if very narrowband filters are used in association with phase-locked loops in the bus circuitry. There might also be a longer delay as the frequency of the ground transmitter is swept across a small band, but such delays should be small compared with the delay of several minutes for the return path from the ground station to a bus and back. This delay is important because it represents time wasted before it can be established that the link has been reinstated satisfactorily.

The link between bus and capsule is not so easy to re-establish, however, since the problem must be solved remotely. Because the beamwidth of the antenna transmitting from the bus to the capsule is always likely to be relatively broad, probably no less than one degree for any spinning antenna configuration, it may be possible to control the pointing direction of this antenna remotely from the ground station and to direct

the beam in the probable direction of the capsule. However, if the bus is spinning continuously as has been assumed throughout this program, the circuitry to provide this pointing in a specific direction could be quite complex and of little use for any other purpose than establishing contact with the capsule. Once a link has been established it is assumed that antenna pointing will be maintained, for the bus-to-capsule link, by a retrodirective technique. Consequently, it would be desirable if the same general circuitry could be used for acquisition as well as for actual communication.

2. Acquisition Techniques

One method by which the link between bus and capsule can be established, provided at least one of them employs a retrodirective array, is for the other vehicle to transmit energy in all the directions in which the first vehicle might exist. For the present let us assume that both vehicles have the same cylindrical configuration with their axes parallel and that the bus antenna is organized to establish the link when necessary. The operation would then be as follows: Once logic circuitry has determined that no link esists, the bus antenna would automatically radiate the pilot beam in all azimuthal directions. The total power in this omni-azimuthal pilot signal could possibly be increased during this operation by using power that would normally be employed for some other operation such as transmitting to the ground station. When this pilot signal reaches the capsule antenna it will automatically phase the capsule array elements to direct previously random radiation in the retrodirection. When the capsule energy reaches the bus, it in turn will automatically direct its antenna, which might be used for both transmitting and receiving information, in the direction of the capsule. The link will then have been re-established. One of the requirements for the bus antenna would thus be that it should be capable of radiating an omni-azimuthal beam.

Some discussion of how this might best be done follows, commencing with consideration of the Type-3 antenna configuration because it is the simplest in concept.

a. Type-3 Antenna

The proper way to form an omniazimuthal pattern with a Type-3 array is to feed all elements with equal current magnitude and with a progressive phase difference between adjacent elements such that there

is an integer number of 2π radians phase change in going around the array. This technique was applied by Tillman, *et al.*,[65] see also references given in that paper. Out of the azimuth plane, the array factor provides directivity in addition to that provided by the elements in the array.

A second, but not recommended, way to approximate an omniazimuth pattern would be to feed all the elements with the same phase. The array factor for an infinite number of elements would then have a pattern given by[58]

$$E = J_0(2\pi R \sin \theta) \tag{52}$$

where θ is the angle measured from the array spin axis (perpendicular to the plane of the array). The peak of the array factor is along the array spin axis, but the array diameter in wavelengths could be chosen so that one of the sidelobes was in the azimuth plane. The element pattern of the individual array elements could then be chosen, in principle, to suppress the main beam and other sidelobes of the array factor. There are three problems with this approach. First of all, the positions of the sidelobes of the array factor change with frequency, so that a small change in operating frequency would scan the desired "sidelobe" of Eq. (52) out of the azimuth plane. As an example, with an array about 20 wavelengths in diameter, a frequency change of only ±2.5 percent would place a null rather than a peak of the array pattern in the azimuth plane. Secondly, the element pattern would have to have a very low response off of its peak in order to be effective in suppressing the main beam and other sidelobes of the array factor. Thirdly, for a finite number of elements, correction terms have to be added to Eq. (52), which will produce ripple in the azimuth pattern of the array.[58] For a given number of array elements, the ripple would be greater if the elements are driven in phase rather than with the proper phase progression. This statement is based on examination of Eq. (18) of Ref. 65.

b. Type-1 Antenna

In order to produce an omni-azimuthal pattern in this configuration it is only necessary to drive each of the elemental transmitters in phase. This will set up a plane wavefront within the cylindrical geodesic lens—that is to say, only the fundamental TEM mode will exist in the lens section which is after all just an oversized coaxial line. Fed

in this manner the biconical horn radiation would be indistinguishable from that of an ordinary biconical horn fed from a small-diameter coaxial line.

There appears to be no advantage in generating a spiral-phase-front omnidirectional pattern, although it is just conceivable that a higher (or lower) gain in the axial plane might be achieved by doing so in some practical biconical horn configurations. It is also possible however, that driving the elemental transmitters in the same manner as suggested for the Type-3 antenna (which would not produce the same phase-front shape) could produce undesirable results due to the several ray paths that can be associated with each element. Although it would be relatively simple to compute the radiation pattern using progressively advancing phase difference between elements, no such investigation was carried out in this program.

c. Type-2 Antenna

This antenna configuration is a combination of Types 1 and 2, in that it uses a cylindrical geodesic lens and discrete- (but not omni-azimuthal) line-source radiators. However, if the elemental transmitters were all driven in phase the result would be that each of the discrete radiators would also be driven in phase and thus, by the same argument used for the Type-1 antenna, each of the line-source radiators would be driven in phase. The resultant radiation into space would not be identical to that for the Type-3 antenna with its omni-azimuthal elemental radiation because the Type-2 antenna line-source radiators have appreciable azimuthal gain in the outward radial direction. However, it might be expected that the results would be similar. That is to say, the peak of the array factor would still be along the axis and the particular gain in the azimuth plane would be a function of the side-lobe structure of this array pattern, which in turn would be a function of the frequency. Computations did indicate that the azimuthal gain varied with frequency, but since no pattern was established and the cost of each computation is high, and because no simple mathematical expression has been obtained for the sidelobe structure, no quantitative conclusions can be drawn.

Similarly, the arguments used by Tillman *et al.*[65] to justify the use of progressive phase shift between elemental radiators for a Type-3 configuration do not necessarily apply to the case of the Type-2 (or Type-4) antenna configurations where the elements do not have omni-azimuthal characteristics.

In addition, phase in the Type-2 antenna can only readily be controlled at the transmitting elements, not at the line sources (*i.e.*, the space radiators), and it would be almost impossible to adjust these phases to produce a progressive phase shift along the line-source radiators because of the multiplicity of energy coupling paths within the geodesic lens between each transmitter and each line-source radiator.

Because the computer program could readily be modified to make them, several computations of gain were made for the case of progressive phase shift between the transmitting elements but the results were again inconclusive. Large variations in gain relative to a single omni-azimuthal element (more than 6 dB) were noted, for various conditions of number of elements, azimuthal angle, *etc.*, but insufficient data was obtained to establish any pattern.

d. Type-4 Antenna

Although no specific investigation was made on methods of producing omni-azimuthal patterns from an antenna of this type it should be noted that the line-source radiators of this antenna type are similar to those of the Type-2 antenna. It should also be noted that all elemental transmitters would have to be activated simultaneously. When it is remembered that the power amplifiers usually have a duty cycle of only about one-third, the total radiated power could be increased by a factor of three, for at least a short period. Provided the additional dc power can be made available during such a period, either from batteries or by diverting its use by other equipment until communications are re-established, this configuration does offer a possible advantage over the other types during any acquisition phase. This advantage can be obtained by exploiting what must otherwise be considered the disadvantage of much higher transmitter capacity needed for normal operation.

VI CONCLUSIONS

Various aspects of four different antenna configurations have been examined during the program. Each configuration appears to be feasible for use on at least one of the two vehicles (the bus and the probe) of the mission model outlined in the introduction (Sec. I). Because so many aspects of the mission were investigated, the conclusions relating to many of them have been included at the end of the section in which they were discussed. In addition, within the limitations of present-day knowledge, and without specific reference to any of the particular antenna configurations, a comprehensive study has been made of the environmental effects to be anticipated by each of the two vehicles of the Earth-bus-capsule system model. Attention has been paid to antennas in general and retrodirective arrays in particular in the various environments to be expected, particularly near Mars.

It is concluded that retrodirective signal characteristics (amplitude, phase, and frequency) for the Earth-bus link are readily calculated within reasonable limits and are not constrained by environment. Multipacting breakdown in antennas on a planetary bus can cause mechanical damage to the antenna, and as a result the antenna function could be degraded or destroyed.

On the other hand, signal characteristics for adaptive antennas, or even for conventional antennas, on an entry capsule are not easily predicted, owing to uncertainties in the atmospheric structure and composition and in the plasma that would surround the capsule. Particular problems of entry pertaining to the retrodirective antenna that require experimental investigation are antenna plasma coupling and the effects of the spatial and frequency correlation, magnitude, and frequency spectrum of the refractive fluctuations in the entry wake and rocket exhaust. Antennas operating at millimeter wavelengths are an attractive means of reducing or eliminating plasma effects during entry.

Voltage breakdown of antennas on entry capsules may occur even at the surface of planets with thin atmospheres such as Mars. Antenna voltage breakdown, in addition to plasma signal attenuation and antenna near-field effects, will determine the maximum signal margin of a planetary capsule-bus communication link.

The retrodirective antenna system may be superior to systems using other antenna types, in radiating more signal power per unit weight. A system weight saving using a retrodirective antenna on an entry capsule could increase the entry time available for communication.

Limitations on a retrodirective antenna system in measuring Doppler and phase effects in a planetary atmosphere are no more severe for bus-to-Earth occulation-type measurements than for the Mariner IV reflector antenna, for instance. Measuring planetary refractive characteristics using a capsule-bus signal is limited principally by entry plasma effects that are difficult to predict. Other limitations include the accuracy to which spatial and time-varying coordinates can be determined, the choice of radio frequency, and the relative motion of capsule and bus.

Only one of the four antenna types was examined in sufficient detail to demonstrate that it would be suitable for certain applications. This was the Cylindrical-Geodesic-Lens Biconical-Horn, or Type-1 antenna, for which all of the assumptions made are readily realizable in practice. The configuration analyzed does not lend itself too readily to obtaining high directivity in the axial plane, as does each of the other three, but this is not an insurmountable problem. A torroidal lens or reflector could be used to obtain arbitrarily high gain and the new ray geometry could readily be computed.

Obtaining high axial gain is very worthwhile if, and only if, the antenna spin axis can be maintained at the same angle to the line of transmission (probably but not necessarily 90 degrees) throughout the flight of the vehicle. Generally there will be no point in arraying adaptive antenna elements in the axial as well as the azimuthal plane unless there is less of a restriction on the length than on the overall diameter of the antenna. (In antenna Types 2, 3, and 4, where discrete line-source radiators are used as the subapertures, it is assumed that each discrete element is itself an array that is permanently rather than adaptively phased. Each whole axial array is therefore treated simply as a single element.) This aspect is discussed more fully from another point of view in the Systems

and Circuitry section, dealing with the amplification needed for each elemental amplifier of a general two-dimensional array having a configuration similar to the Type-4 antenna.

The effective radiated power (ERP) of a retrodirective antenna is generally proportional to the overall axial gain, the number of transmitting elements in (each) azimuthal array, and the total power radiated. Or, put another way, it is proportional to the axial gain of one of the azimuthal arrays, to the total number of elemental transmitters, and to their total output power. Thus, in order to maximize ERP with a given number of elemental transmitters and total power, it is advantageous to have as high an axial gain—or directivity—as possible for each element, limited only by the accuracy to which the vehicle spin axis can be stabilized.

The mutual coupling between adjacent elements of the Type-1 antenna can never be completely eliminated, except perhaps at spot frequencies; however, since the elemental radiators are in each other's *H*-plane, the coupling is inherently low. Although the neighboring elements will introduce sidelobes into the elementary radiation pattern, this effect of mutual coupling can be taken into account by using a polynomial for the gain function of each elemental radiator, $G(\alpha)$, rather than the single power term used throughout this study. Thus an appropriate next step would be to make an experimental determination of the function $G(\alpha)$ for a single element in the presence of its neighbors and then to devise a suitable polynomial to describe the function more fully, before making additional computations. It would be very desirable to eliminate the effects of mutual coupling on the input impedance to the elemental radiators in order to simplify matching these elements to the electronic circuits. However, consideration of specific circuit elements has not been a part of this study.

The mutual-coupling problem can be dealt with just as easily for the Type-4 antenna, where each elemental radiator has relatively high gain, and with somewhat more difficulty, because of intra-lens coupling, for the Type-2 antenna. However, for the Type-3 antenna, mutual coupling remains an inherently serious problem. That is not to say that the configuration cannot be used to electrically de-spin a physically spinning communication antenna. It is in fact the only one of the four configurations that is known by the authors to have been exploited, for instance

on the spin-stabilized Application Technology Satellite[67] due to be launched into synchronous orbit in late 1966. However, the de-spinning antenna used on this vehicle cannot readily be analyzed with any accuracy because of mutual coupling effects. The experimentally determined spin modulation was found to be more than 1 dB while the theoretical value was less than one percent of this.[67]

Spin (amplitude) modulation, together with the phase modulation component of the *spectral splitting* has formed an important part of the present study although it has not been exhaustively examined. Provided all the electronic and radiator elements of the array work "perfectly," it has been indicated that this spectral splitting problem can generally be taken care of in the two antenna types that were analyzed. However, no attempt was made to examine exactly what would happen if one or more of the elements acted less than perfectly, except to propose a general solution to the spectral-splitting problem, especially for use with coherent receiving techniques. A more detailed analysis of the phenomenon is given in Ref. 3.

Unfortunately the particular Type-1 antenna configuration chosen for detailed examination is probably not the most suitable since the elements are spaced more than one wavelength apart around the circumference of the cylindrical lens. There are indications that if this spacing had some value less than a wavelength, both the sidelobes and spectral content of a spinning retrodirective antenna would be considerably lower. There are also strong indications that the spectral splitting can be made negligible (all sidebands less than about 35 dB) by careful choice of antenna and system parameters even if the inter-element spacing is not made less than one wavelength. This implies operation over a narrow band but in the present study the bandwidth has been assumed to be narrow. With the exception of the Type-4 antenna each of the types considered is more applicable to narrowband than to broadband implementation, but for some system models, operation over a broad band would apparently not be appreciably inferior. Further study of a more comprehensive range of parameters and system models is needed, however, before any such general conclusions can be drawn.

In studying the Type-1 and -2 antennas only a cylindrical configuration for the lens was considered, but other configurations could well prove more suitable for some applications. For instance, if it were desirable to stack several Type-1 antennas axially, to obtain beam control

in the axial plane, a conical lens would be better mechanically. Electronically, the performance is expected to be comparable to the configurations examined but new and more general analysis techniques would have to be developed to take account of the different ray geometry.

Determination of antenna gain, or, more correctly, effective radiated power (ERP), was made by several methods in the case of the Type-1 antenna, and each gave approximately the same result for the corresponding configuration. This result could, therefore, be discussed with some confidence in its accuracy. Such was not the case for the other antenna types, however, since there were some apparent discrepancies between the gain values computed by different methods. This was due in part to the fact that the behavior of the pattern in the axial plane was assumed to be unrelated to the particular azimuthal plane element configurations used. Consequently, some of the results, particularly those used to examine the gain in the retrodirection of various configurations and modes of operation of the Type-2 antenna, can only be used as preliminary data. It is significant that none of the computed values of retrodirective gain, averaged over all azimuthal angles, is greater than the postulated maximum value for any array (which is equal to the number of array elements), although in some cases this maximum value is reached. This fact does give some confidence in the method used for computation of at least the high values of gain, but more assurance is needed that all the values of gain computed for the several configurations are reliable. For instance, one of the Type-2 antenna configurations indicated an average gain 2.3 dB less than the maximum postulated value. There is presently no reasonable explanation for such a result, and further investigation of the radiation characteristics by computation and integration of the radiation pattern, or some other method, would be necessary to substantiate or modify this data.

The Type-2 antenna represents only one method of increasing the axial gain of the basic geodesic-lens phased-array antenna. It is particularly applicable for very-narrowband operation—for instance, 1 to 4 MHz for an antenna having a diameter and a length of one meter, irrespective of the nominal operating frequency. If some other axial beam-narrowing technique is used, such as a toroidal lens or reflector, the bandwidth is likely to be several times as large but the structure will be more cumbersome.

The Type-3 antenna is one apparently simple method by which arbitrarily high gain can be obtained in the axial direction, and consequently it was analyzed in some detail except that, as has been stressed, mutual coupling has been neglected.

Calculations have been carried out for a circular array of omni-azimuthal elements, such as the Type-3 antenna, which might be mounted at one end of a cylindrical space probe. The data presented in the main test are the pattern shape and directivity gain at the peak of the main beam for 30, 60, and 90 elements equally spaced around a 20-wavelength-diameter circle, the same diameter used for most of the other antenna models. Also presented is the variation in directivity with changing array orientation with respect to the retrodirective direction, and the dependence of array directivity on the number of elements in a 20-wavelength-diameter array. Although existing formulas were used in the calculations, the work extended the numerical results to the case of large array diameters and large numbers of elements, which case is of more interest in the application of retrodirective arrays to space probes. The shape of the radiation pattern was discussed in some detail as aid in understanding why the directivity at the peak of the main beam is a function of the orientation of the array elements with respect to the main-beam direction.

The directivity variation with array orientation, which is an important component of any spectral splitting, has been calculated for 40, 41, 50, 51, 60, 61, and 70 elements in 20-wavelength-diameter arrays. The peak-to-peak variation of directivity ranges from 0.01 dB for 61 elements, to 1.1 dB for 50 elements. The specific examples, plus the discussion given in the body of the report, indicate a general preference for an odd number of elements. There are, however, combinations of array diameter and element spacing for which even numbers of elements give directivity variation as low as or lower than do odd number of elements. The directivity variation is a cyclical function of the number of elements, and probably also of the array diameter, for element spacings greater than 0.5 wavelength. For element spacing less than about 0.5 wavelength there is no variation in directivity with changes in array orientation, and also a maximum value of gain is reached that is independent of the addition of more elements. Since these calculations neglect the effects on the array pattern of mutual coupling between array elements, as well as blocking some elements by other elements, the theoretical performance

of this somewhat idealized array technique can be used only as a standard against which practical arrays can be compared.

Several alternative *"modes" of operation* were used in examining the various antenna models when used as retrodirective arrays. These related to the type of amplifier associated with each array element. When linear amplifiers (Modes 2 and 3) were used so that the power radiated from an element was weighted in proportion to the gain of that element in the retrodirection, a higher gain was generally achieved than when all elements were driven with equal power. The difference in gain, usually less than 1 dB, that can be achieved by this element-weighting technique, must be weighed against the complexity of implementing the necessary circuitry. In practice, the increase in ERP will not be as great as the theoretical increase in antenna gain, for a given number of elements, because of the difficulty of distributing the available power in anything but a uniform manner. In addition, the total potential radiating power must always be larger than for Mode 1 (assuming the same total power) because the duty cycle is less than one.

Rather than reducing the contribution from some elements in a continuously variable manner, a digital approach can also be used, whereby each element either radiates with full power or not at all. This approach led to some consideration being given to a fourth type of configuration. The main problem in this case is devising a satisfactory mechanism for deciding which elements shall be switched off. No such mechanism was sought during the study. Provided there are no multipath effects it should, however, be easy to obtain such a mechanism.

The Type-4 antenna was analyzed only for a "large," rather than a specific, number of elemental radiators, and the results indicate a value of gain very nearly equal to the theoretical maximum. It should be noted that this large value of ERP, within a fraction of a decibel of the postulated maximum value for any given total number of transmitting elements, is obtained even though only a fraction of these elements are used at any one time. It is, of course, necessary that each of the transmitters be capable of delivering higher output power than would be necessary to obtain the same total ERP with all the transmitting elements active simultaneously. This higher value of "installed transmitter capacity," plus the switching circuitry, may be the price that has to be paid for a retrodirective antenna system that does not suffer at all from the spectral splitting effects of vehicle spin. Spectral splitting is low because the antenna can be made

with relatively low mutual coupling between the receiver/transmitter/radiator elements, leading in turn to a communication system in which the effects of spectral splitting of the retransmitted signal caused by spinning of the vehicle can, theoretically, be eliminated by some phase-conjugating techniques operating over a narrow band of frequencies.

No attempt was specifically made to investigate the effects of vehicle spin on modulation of the ERP from the Type-4 antenna, but consideration of a specific finite number of radiators, rather than a "large" number, is likely to indicate modulation of ERP (amplitude modulation) with vehicle spin for specific configurations. The situation will be further complicated by the power-switching operation, which could also produce modulation.

Basic circuitry has been proposed for conjugating the phase in such a manner that a retrodirective antenna transmitting at a rational fraction of the pilot frequency will be exactly phased. The technique has been examined only for a conventional type of array of radiating elements in which only one ray—or geodesic—can exist between each element and the distant point at which the net contribution of the elements is being observed. It is therefore directly applicable to the Type-4 antenna, in which case it can also eliminate the phase-modulation component of spectral splitting, as just discussed. However, where there are two or more alternative ray paths associated with each element, as in the Type-1 or Type-2 antenna, or where mutual coupling is an important consideration, such as in the Type-3 antenna, the technique is not necessarily directly applicable.

The technique will need further study and possible modification before it can be considered suitable for these other types. Another possible problem with the technique, when applied to communication over very great distances, is that it employed separate, albeit phase-locked, oscillators for each element. As discussed in the Introduction, if these oscillators are not all operating at *exactly* the same frequency there can be a significant reduction in received signal intensity. This potential problem should be considered in relation to the particular hardware planned for *any* phased array antenna as one end of a very long communication link. This has not been done to any extent during this program.

Another important system problem that was considered is that of retrieving accurate information on range and its time derivatives (Doppler shift, etc.). A technique has been presented whereby such data, relating to both the bus and the capsule can be retrieved without the need for an accurate frequency source (local oscillator) on-board either vehicle.

APPENDIX A

SPECTRAL SPLITTING FOR A SINGLE ELEMENT IN A CIRCULAR ARRAY OF OMNIDIRECTIONAL ELEMENTS (TYPE-3 ANTENNA)

APPENDIX A

SPECTRAL SPLITTING FOR A SINGLE ELEMENT IN A CIRCULAR ARRAY OF OMNIDIRECTIONAL ELEMENTS (TYPE-3 ANTENNA)

Consider a ring of antenna elements on the circumference of a cylinder (see Fig. A-1) spinning at a rate of $\omega_s = 2\pi f_s$ rad/sec. Let a signal be received in the plane containing the ring of elements and hence perpendicular to the spin axis of the satellite. The geometry is shown in Fig. A-1. Mutual coupling is assumed to be negligible so that the radiation pattern of each elemental antenna can be assumed to be omnidirectional (an assumption that is far from true in practice).

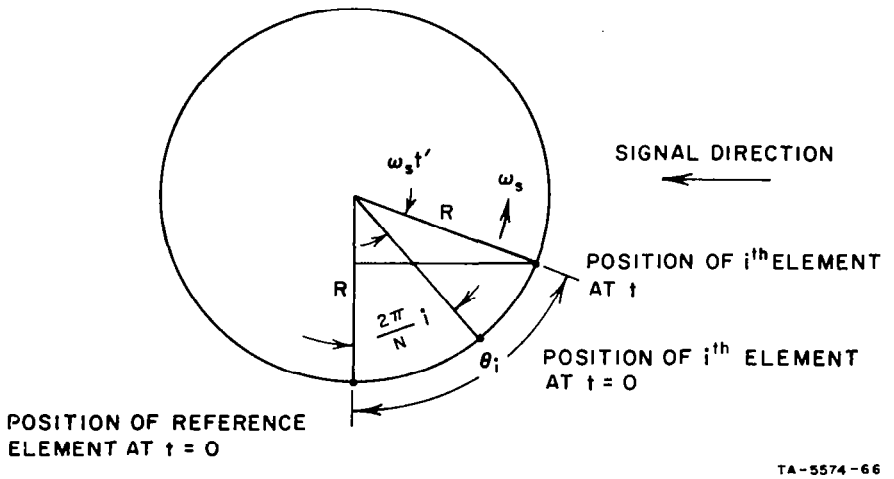

FIG. A-1 GEOMETRY OF PHASE CENTERS OF ELEMENTAL OMNIDIRECTIONAL RADIATORS

We take the phase at the center of the cylinder as reference and hence write the voltage at that point as

$$v = \cos \omega_0 t$$

where

$$\omega_0 = 2\pi f_0$$

and f_0 is the received frequency which may include a Doppler shift. Such a shift, since it applies equally to all antenna elements, will be called gross Doppler.

Let θ_i be the angle of the ith element with respect to the reference condition. Then,

$$\theta_i = 2\pi \frac{i}{N} + \omega_s t$$

where N is the total number of equally spaced elements. The horizontal displacement from reference is given by

$$\text{disp} = R \sin \theta_i$$

where R is the radius of the circle on which the phase centers of the elemental omnidirectional antennas lie. If we measure this radius in wavelengths and convert to phase in radians, then the signal received by the ith element is

$$\begin{aligned} v_i &= \cos \left[\omega_0 t + 2\pi R \sin \left(\frac{2\pi i}{N} + \omega_s t \right) \right] \\ &= \cos \omega_0 t \cos \left[2\pi R \sin \left(\frac{2\pi i}{N} + \omega_s t \right) \right] \\ &\quad - \sin \omega_0 t \sin \left[2\pi R \sin \left(\frac{2\pi i}{N} + \omega_s t \right) \right] . \end{aligned} \tag{A-1}$$

But from Bessel function theory we have

$$\cos (A \sin \theta) = J_0(A) + 2 \sum_{n=1}^{\infty} J_{2n}(A) \cos 2n\theta \tag{A-2a}$$

$$\sin (A \sin \theta) = 2 \sum_{n=0}^{\infty} J_{2n+1}(A) \sin (2n + 1)\theta . \tag{A-2b}$$

Hence, from Eqs. (A-1) and (A-2),

$$\begin{aligned} v_i &= \cos \omega_0 t \left[J_0(2\pi R) + 2 \sum_{n=1}^{\infty} J_{2n}(2\pi R) \cos 2n \frac{2\pi i}{N} + \omega_s t \right] \\ &\quad - \sin \omega_0 t \left[2 \sum_{n=0}^{\infty} J_{2n+1}(2\pi R) \sin (2n + 1) \frac{2\pi i}{N} + \omega_s t \right] . \end{aligned} \tag{A-3}$$

But note that

$$\cos\alpha\cos\beta = \frac{1}{2}[\cos(\alpha+\beta)+\cos(\alpha-\beta)] \qquad \text{(A-4a)}$$

and

$$\sin\alpha\sin\beta = \frac{1}{2}[\cos(\alpha-\beta)-\cos(\alpha+\beta)] \qquad \text{(A-4b)}$$

and using Eq. (A-4) in (A-3),

$$\begin{aligned} v_i = {} & J_0(2\pi R)\cos\omega_0 t \\ & + \sum_{n=1}^{\infty} J_{2n}(2\pi R)\left\{\cos\left[(\omega_0 + 2n\omega_s)t + \frac{4\pi n i}{N}\right]\right. \\ & \left. + \cos\left[(\omega_0 - 2n\omega_s)t - \frac{4\pi n i}{N}\right]\right\} \\ & + \sum_{n=0}^{\infty} J_{2n+1}(2\pi R)\left(\cos\left\{[\omega_0 + (2n+1)\omega_s]t + \frac{2\pi(2n+1)i}{N}\right\}\right. \\ & \left. - \cos\left\{[\omega_0 - (2n+1)\omega_s]t - \frac{2\pi(2n+1)i}{N}\right\}\right) . \end{aligned} \qquad \text{(A-5)}$$

Thus, for the case of ω_0 constant, the voltage at the frequency $(1/2\pi)[\omega_0 + k\omega_s]$ has a magnitude $J_k(2\pi R)$ and a phase $k(2\pi i/N)$.

Note that the phase for $k' = k + \beta N$ for all integers β is the same as for k.

Since it is desirable to maximize the carrier voltage, the antenna radius should be chosen to maximize $J_0(2\pi R)$. If R is near 10 wavelengths, then

$$J_0(2\pi R) \sim \sqrt{\frac{2}{\pi(2\pi R)}}\cos\left(2\pi R - \frac{\pi}{4}\right) \qquad \text{(A-6)}$$

which has a peak when

$$2\pi R - \frac{\pi}{4} = k(2\pi) \qquad \text{(A-7a)}$$

or

$$2\pi\left(R - \frac{1}{8}\right) = k2\pi \qquad \text{(A-7b)}$$

or

$$R = k + \frac{1}{8} \quad . \tag{A-7c}$$

For example, we could take

$$R = 10.125 \quad .$$

When $X > n^2$,

$$J_n(X) \sim \sqrt{\frac{2}{\pi(X)}} \cos\left(X - \frac{n\pi}{2} - \frac{\pi}{4}\right) \quad .$$

The choice of $X = 2\pi[k + (1/8)]$ will make $[X - (n\pi/2) - (\pi/4)]$ mod $2\pi = (\pi/2)n$ and hence the lower odd sidebands will vanish.

The spectrum resulting from this particular model is given in Table A-1.

Table A-1*

SPECTRAL CONTENT *vs.* SIDEBAND NUMBER

n	$J_n(63.61)$	$\lvert J_n(63.61)\rvert^2$	RELATIVE dB
0	.10003	.010006	0.0
1	-.00013	.000000	- ∞
2	-.10003	.010006	0.0
3	-.00615	.000038	-24.2
4	.09945	.009890	0.0
5	.01866	.000348	-14.6
6	-.09652	.009316	- 0.3
7	-.03687	.001359	- 8.7
8	.08840	.007815	- 1.1
9	.05911	.003494	- 4.6
10	-.07168	.005138	- 2.9
11	-.08146	.006636	- 1.8
12	.04344	.001887	- 7.3
13	.09804	.009612	- 0.2
14	-.00337	.000011	-29.8
15	-.09952	.009904	0.0
16	-.04356	.001897	- 7.2
17	.07760	.006022	- 2.2
18	.08504	.007232	- 1.4
19	-.02947	.000868	-10.6
20	-.10265	.010537	0.2
21	-.03507	.001230	- 9.1
22	.07949	.006319	- 2.0
23	.09006	.008111	- 0.9
24	-.01436	.000206	-17.0
25	-.10090	.010181	0.1

Table A-1* (Concluded)

n	$J_n(63.61)$	$\lvert J_n(63.61)\rvert^2$	RELATIVE dB
26	-.06495	.004219	- 3.7
27	.04780	.002285	- 6.5
28	.10553	.011137	0.5
29	.04510	.002034	- 7.0
30	-.06440	.004147	- 3.8
31	-.10585	.011204	0.5
32	-.03877	.001503	- 8.2
33	.06685	.004469	- 3.5
34	.10813	.011692	0.7
35	.04874	.002376	- 6.3
36	-.05449	.002969	- 5.3
37	-.11042	.012193	0.9
38	-.07396	.005470	- 2.6
39	.02204	.000486	-13.1
40	.10100	.010201	0.1
41	.10498	.011021	0.4
42	.03432	.001178	- 9.3
43	-.05964	.003557	- 4.5
44	-.11497	.013218	1.2
45	-.09940	.009880	- 0.5
46	-.02567	.000659	-11.8
47	.06227	.003878	- 4.1
48	.11769	.013851	1.4
49	.11535	.013306	1.2
50	.06002	.003602	- 4.4
51	-.02099	.000441	-13.5
52	-.09368	.008776	- 0.6
53	-.13218	.017472	2.4
54	-.12658	.016022	2.0
55	-.08273	.006844	- 1.6
56	-.01649	.000272	-15.7
57	.05369	.002883	- 5.4
58	.11273	.012708	1.0
59	.15187	.023064	3.6
60	.16901	.028564	4.6
61	.16695	.027872	4.5
62	.15120	.022861	3.6
63	.12780	.016333	2.1
64	.10194	.010391	0.2
65	.07733	.005980	- 2.2
66	.05610	.003147	- 5.0
67	.03909	.001528	- 8.2
68	.02625	.000689	-11.6
69	.01703	.000290	-15.4
70	.01070	.000114	-19.5
71	.00652	.000043	-23.7
72	.00385	.000015	-28.2
73	.00220	.000005	-33.1
74	.00120	.000001	-40.0
75	.00059	.000000	- ∞

* *Tables of the Bessel Functions of the First Kind*, ANNALS III of the Computation Laboratory of Harvard University (Oxford University Press, 1947).

APPENDIX B

DERIVATION OF SPECTRUM IN THE CYLINDRICAL-GEODESIC-LENS BICONICAL-HORN ADAPTIVE (TYPE-1) ANTENNA DUE TO VEHICLE ROTATION

APPENDIX B

DERIVATION OF SPECTRUM IN THE CYLINDRICAL-GEODESIC-LENS BICONICAL-HORN ADAPTIVE (TYPE-1) ANTENNA DUE TO VEHICLE ROTATION

This antenna has been described in the First Quarterly Report, and its general configuration is shown in Fig. 3 in the main text. For the present purpose we note that each elemental radiator, at the instant when its angular position relative to the direction of the received signal is

$$\gamma, \quad -\pi \leq \gamma \leq \pi \tag{B-1}$$

receives signals from an infinite number of directions, α_i, where α_i is measured relative to the direction of maximum gain and

$$-\frac{\pi}{2} < \alpha_i < \frac{\pi}{2} \tag{B-2}$$

(see Fig. 4).

Due to the nature of the lens and the geometry we find

$$\alpha_i + L \tan \alpha_i = 2\pi i + \gamma \tag{B-3}$$

where $i = 0, \pm 1, \pm 2, \pm 3, \pm \ldots$, and L is the ratio of the height of the lens to its radius.

It can be shown[1] that each signal can be written as

$$F_i(\gamma) = \frac{G(\alpha_i)}{\left(1 + \dfrac{L}{\cos^2 \alpha_i}\right)^{1/2}} \exp j \left[\omega_0 t + 2\pi R \left(\frac{L}{\cos \alpha_i} - \cos \alpha_i\right)\right] \tag{B-4}$$

where $G(\alpha)$ is the voltage gain function of the elemental radiator within the "parallel plate" lens region. A typical gain function can be described by:

$$G(\alpha) = 10^{-2.4(\pi R\alpha/N)^2} \tag{B-5}$$

where R is the radius in wavelengths, N is the number of elemental radiators, and the phase is measured with respect to a fixed but arbitrary point.

The $[1 + (L/\cos^2 \alpha)]^{-1/2}$ term is due to space taper in the lens. ω_0 is, of course, the RF angular frequency including gross Doppler.

If the antenna is rotating (spin-stabilized), then the angle γ is a periodic sawtooth function of time; hence both the amplitude and relative phase of $F_i(\gamma)$ are also periodic and have a fundamental frequency proportional to the spin rate.

Let ω_s be the angular velocity of the antenna in radians per second. Then γ is periodic and can be written

$$\gamma = \omega_s t \text{ for } |t| \leq \frac{\pi}{\omega_s} \quad . \tag{B-6}$$

Thus the signals, from Eqs. (B-4) and (B-6), can be written as

$$F_i(t) = \frac{G(\alpha_i)}{H(\alpha_i)} \exp j[\omega_0 t + \varphi(\alpha_i)] \tag{B-7}$$

where

$$H(\alpha_i) = \left[1 + \frac{L}{\cos^2 \alpha_i}\right]^{1/2} \tag{B-8}$$

and

$$\varphi(\alpha_i) = 2\pi R \left[\frac{L}{\cos \alpha_i} - \cos \alpha_i\right] \quad . \tag{B-9}$$

Of course, since

$$\alpha_i + L \tan \alpha_i = 2\pi i + \omega_s t \quad , \tag{B-10}$$

α_i is a function of t and is also periodic. Since $F_i(t)$ is periodic, we can write it in terms of a carrier and sidebands as

$$F_i(t) = \sum_{k=-\infty}^{\infty} C_{ik} e^{j(\omega_0 t + k\omega_s t + \varphi_{ik})} \quad . \tag{B-11}$$

Now, equate Eqs. (B-7) and (B-11) and cancel $e^{j\omega_0 t}$, getting:

$$\sum_{k=-\infty}^{\infty}\left(C_{ik}e^{j\varphi_{ik}}\right)\cdot e^{jk\omega_s t} = \frac{G(\alpha_i)}{H(\alpha_i)}\, e^{j\varphi(\alpha_i)} \quad . \tag{B-12}$$

Multiply both sides by $e^{-jk\omega_s t}$ and integrate over a period:

$$C_{ik}e^{j\varphi_{ik}} = \frac{1}{T}\int_{-T/2}^{T/2}\frac{G(\alpha_i)}{H(\alpha_i)}\, e^{j[\varphi(\alpha_i)-k\omega_s t]}\, dt \quad . \tag{B-13}$$

Now, transform the integration from t to α according to Eq. (B-10) and note that

$$\omega_s = 2\pi f_s = \frac{2\pi}{T} \quad . \tag{B-14}$$

Now,

$$d\alpha_i\left(1 + \frac{L}{\cos^2\alpha_i}\right) = \omega_s dt \tag{B-15}$$

and when $t = -(T/2)$,

$$\alpha_i + L\tan\alpha_i = 2\pi i - \pi = (2i-1)\pi \quad . \tag{B-16}$$

Let the solution of Eq. (B-16) be B_i. Similarly, when $t = +(T/2)$,

$$\alpha_i + L\tan\alpha_i = 2\pi i + \pi = (2i+1)\pi \tag{B-17}$$

and let the solution be C_i. Thus we are numbering the rays as $i = 0$, ±1, ±2, ±3 etc., and we have

$$B_i + L\tan B_i = (2i-1)\pi \tag{B-18a}$$

$$C_i + L\tan C_i = (2+1)\pi \quad . \tag{B-18b}$$

Using these results in Eq. (B-13), we obtain

$$C_{ik}e^{j\varphi_{ik}} = \frac{1}{2\pi}\int_{B_i}^{C_i} G(\alpha_i)H(\alpha_i)e^{j(\varphi\alpha_i)-k(\alpha_i+L\tan\alpha_i+2\pi i)}d\alpha_i \quad . \tag{B-19}$$

Since $e^{-j(k2\pi i)} = 1$, it can be omitted.

Now consider the summed effect over all rays:

$$C_k e^{j\varphi_k} = \sum_{i=-\infty}^{+\infty} C_{ik} e^{j\varphi_{ik}}$$

$$= \frac{1}{2\pi} \sum_{i=-\infty}^{\infty} \int_{B_i}^{C_i} G(\alpha) H(\alpha) e^{j[\varphi(\alpha) - K(\alpha + L \tan\alpha)]} d\alpha \quad . \qquad \text{(B-20)}$$

These are non-overlapping adjacent ranges of integration. From the monotonic functions of Eq. (B-18):

$$\begin{aligned} C_0 &\sim \pi, & B_1 &\sim \pi \\ C_1 &\sim 3\pi, & B_2 &\sim 3\pi \\ B_0 &\sim -\pi, & C_{-1} &\sim -\pi \\ B_{-1} &\sim -3\pi, & C_{-2} &\sim -3\pi \quad . \end{aligned}$$

Further,

$$\lim_{i\to\infty} B_i = \lim_{i\to\infty} C_i = \pi/2$$

and

$$\lim_{i\to-\infty} B_i = \lim_{i\to-\infty} C_i = -\pi/2 \quad .$$

Thus, Eq. (B-20) becomes

$$C_k e^{j\varphi_k} = \frac{1}{2\pi} \int_{-\pi/2}^{\pi/2} G(\alpha) H(\alpha) e^{j[\varphi(\alpha) - k(\alpha + L \tan\alpha)]} d\alpha \quad . \qquad \text{(B-21)}$$

Now use Euler's equation, $e^{j\varphi} = \cos\varphi + j \sin\varphi$, to write

$$C_k \cos\varphi_k = \frac{1}{2\pi} \int_{-\pi/2}^{\pi/2} G(\alpha) H(\alpha) [\cos\varphi(\alpha) \cos k\delta - \sin\varphi(\alpha) \sin k\delta] d\alpha \qquad \text{(B-22)}$$

where

$$\delta = \alpha + L \tan\alpha \quad . \qquad \text{(B-23)}$$

From Eqs. (B-5), (B-8), and (B-9) we note that $G(\alpha)$, $H(\alpha)$, and $\varphi(\alpha)$ are all even functions of α. Cos $k\delta$ is also even in α, but sin $k\delta$ is odd.

Since the integral of an even function over a range symmetrical about the origin is twice the integral over the half-range and the integral of an odd function is zero, we have

$$C_k \cos \varphi_k = \frac{1}{\pi} \int_0^{\pi/2} G(\alpha)H(\alpha) \cos \varphi(\alpha) \cos k(\alpha + L \tan \alpha) d\alpha \quad . \quad \text{(B-24)}$$

Similarly,

$$C_k \sin \varphi_k = \frac{1}{2\pi} \int_{-\pi/2}^{\pi/2} G(\alpha)H(\alpha) \sin \varphi(\alpha) \cos k\delta - \cos \varphi(\alpha) \sin k\delta] d\alpha$$

$$= \frac{1}{\pi} \int_0^{\pi/2} G(\alpha)H(\alpha) \sin \varphi(\alpha) \cos k(\alpha + L \tan \alpha) d\alpha \quad . \quad \text{(B-25)}$$

Note further that Eqs. (B-24) and (B-25) are even functions of k so that

$$C_{-k} \cos \varphi_{-k} = C_k \cos \varphi_k \quad \text{(B-26a)}$$

and

$$C_{-k} \sin \varphi_{-k} = C_k \sin \varphi_k \quad . \quad \text{(B-26b)}$$

Thus the spectrum is symmetrical about the carrier.

Equations (B-24) and (B-25), by a change in the upper limit of integration, can also be used to find the spectrum of Ray 0 and the spectrum for Rays -1, 0, and 1. By changing both limits of integration, the spectrum for Rays -1 and 1 can also be found.

An Algol program for the Burroughs 5500 has been prepared and run to obtain spectrum data, using $R = 10$, $L = 3$, $N = 60$, for the following ray groupings:

Ray 0

Rays -1 and +1

Rays -1, 0, and +1 .

The following was computed for each sideband:

Inphase component	$C_k \cos \varphi_k$
Quadrature components	$C_k \sin \varphi_k$

Amplitude	C_k
Phase angle	φ_k
Power relative to carrier	P_{dB}
Cumulative power	$\sum_{i=0}^{k} P_k$

APPENDIX C

DERIVATION OF POWER IN THE TYPE-1 ANTENNA

APPENDIX C

DERIVATION OF POWER IN THE TYPE-1 ANTENNA

Since a lossless system has been assumed, it is of interest to calculate the power emitted from an elemental radiator in each ray.

The voltage gain function of each elemental radiator as measured in the "parallel plate" region of the lens is assumed given by:

$$G(\alpha) = 10^{[-2.4(\pi R\alpha/N)^2]} \quad . \tag{C-1}$$

Hence the power gain is

$$G^2(\alpha) = 10^{[-4.8(\pi R\alpha/N)^2]} \tag{C-2a}$$

$$= e^{-(K^2\alpha^2/2)} \quad . \tag{C-2b}$$

Hence

$$ln\ G^2(\alpha) = -\frac{K^2\alpha^2}{2} = -48\left(\frac{\pi R\alpha}{N}\right)^2 ln\ 10$$

or

$$K = \pi \frac{R}{N} (4.701). \tag{C-3}$$

Then the power can be written

$$P_0 = \int_0^{\alpha_0} G^2(\alpha)d\alpha \quad \text{for Ray 0} \tag{C-4a}$$

$$= 2\int_0^{\pi/2} G^2(\alpha)d\alpha \quad \text{for all rays} \tag{C-4b}$$

$$= 2\int_{\alpha_0}^{\alpha_1} G^2(\alpha)d\alpha \quad \text{for Rays -1 and +1} \tag{C-4c}$$

$$= 2\int_0^{\alpha_1} G^2(\alpha)d\alpha \quad \text{for Rays -1, 0, and +1} \tag{C-4d}$$

where $\alpha_0 = 0.687$ radians, and satisfies

$$\alpha_0 + L \tan \alpha_0 = \pi \text{ for } L = 3 \tag{C-5}$$

and $\alpha_1 = 1.226$ radians, and satisfies

$$\alpha_1 + L \tan \alpha_1 = 3\pi \text{ for } L = 3 \tag{C-6}$$

But in all cases

$$P = 2 \int_0^{\hat{\alpha}} G^2(\alpha) d\alpha$$

$$= 2 \int_0^{\hat{\alpha}} e^{-(K^2 \alpha^2/2)} d\alpha \tag{C-7}$$

and setting $x = K\alpha$, $dx = Kd\alpha$,

$$P = \frac{2}{K} \times \frac{\sqrt{2\pi}}{\sqrt{2\pi}} \int_0^{K\hat{\alpha}} e^{-(x^2/2)} dx$$

$$= \frac{2\sqrt{2\pi}}{K} \left(\frac{1}{\sqrt{2\pi}} \int_0^{K\hat{\alpha}} e^{-(x^2/2)} dx \right) \tag{C-8}$$

where the expression in parentheses can be found in the tables of the normal probability density.

When Eq. (C-8) is evaluated for $R = 10$ and $N = 60$ and compared with the cumulative power from the computer runs, we find:

Rays	Eq. (C-8)	Computer (200 sidebands)
All	1.020	--
0	0.926	0.918
-1,1	0.089	0.098
-1,0,1	1.014	1.008

These results show sufficient agreement to verify the computer algorithm used.

The relative power in Rays -1, 0, and +1 as compared with the total power from an elemental radiator (1.014/1.020) certainly indicates that the higher-ordered rays should have a negligible effect on the overall spectrum of the signals.

APPENDIX D

RETRANSMITTED SIGNAL FROM A CYLINDRICAL-GEODESIC-LENS BICONICAL-HORN ADAPTIVE (TYPE-1) ANTENNA

APPENDIX D

RETRANSMITTED SIGNAL FROM A CYLINDRICAL-GEODESIC-LENS BICONICAL-HORN ADAPTIVE (TYPE-1) ANTENNA

1. Introduction

As discussed earlier in this report, almost all the power is contained in Rays -1, 0, 1 and therefore the present discussion will be restricted to these rays. It is assumed that each elemental antenna of the array is connected to a simple conjugating circuit.

Power is received at each elemental radiator along each of the three ray paths. The corresponding voltages are added and mixed with a pure sinewave at twice pilot frequency. The difference signal from the mixer is then retransmitted along each of the three ray paths.

To begin with, let us assume the following:

(1) The local oscillator is at exactly twice the incoming pilot frequency.

(2) All operations are linear.

(3) Phase delays are negligible compared to spin period.

Each signal in passing from the plane external wave to the elemental radiator in either direction has its amplitude reduced by $G(\alpha)/H(\alpha)$ and undergoes a phase delay of $2\pi R[(L/\cos\ \alpha) - \cos\alpha]$ where

$$G(\alpha) = e^{-(K^2\alpha^2/2)} \tag{D-1}$$

$$H(\alpha) = \left(1 + \frac{L}{\cos^2\ \alpha}\right)^{1/2} \tag{D-2}$$

R = Radius in wavelengths

L = Length in radii

and

$$\alpha_{-1} + L \tan \alpha_{-1} = -2\pi + \gamma \qquad \text{(D-3a)}$$

$$\alpha_0 + L \tan \alpha_0 = \gamma \qquad \text{(D-3b)}$$

$$\alpha_1 + L \tan \alpha_1 = 2\pi + \gamma \qquad \text{(D-3c)}$$

where γ is the angle of arrival with respect to the position of the elemental radiator.

For convenience, let

$$\varphi_i = 2\pi R\left(\frac{L}{\cos \alpha_i} - \cos \alpha_i\right) \qquad \text{(D-4)}$$

$$A_i = \frac{G(\alpha_i)}{H(\alpha_i)} \quad . \qquad \text{(D-5)}$$

Note that the effect of the mixer is to change the sign of the phase.

2. Derivation

The voltage reaching the elemental radiator (assuming unit voltage in the arriving wave) is

$$A_{-1}\angle\varphi_{-1} + A_0\angle\varphi_0 + A_1\angle\varphi_1 \qquad \text{(D-6)}$$

After mixing, we have

$$A_{-1}\angle-\varphi_{-1} + A_0\angle-\varphi_0 + A_1\angle-\varphi_1 \quad . \qquad \text{(D-7)}$$

Then the total retransmitted signal in the direction γ consists of nine terms:

$$V = A_{-1}^2\angle 0 + A_{-1}A_0\angle(\varphi_0 - \varphi_{-1}) + A_{-1}A\angle(\varphi_1 - \varphi_{-1})$$
$$+ A_0A_{-1}\angle(\varphi_{-1} - \varphi_0) + A_0^2\angle 0 + A_0A_1\angle(\varphi_1 - \varphi_0)$$
$$+ A_1A_{-1}\angle(\varphi_{-1} - \varphi_1) + A_1A_0\angle(\varphi_0 - \varphi_1) + A_1^2\angle 0 \quad . \qquad \text{(D-8)}$$

Rearranging Eq. (D-8) and combining terms having equal positive and negative angles gives:

$$V = (A_{-1}^2 + A_0^2 + A_1^2)\angle 0 + 2A_{-1}A_0 \cos(\varphi_0 - \varphi_{-1})\angle 0$$
$$+ 2A_{-1}A_1 \cos(\varphi_1 - \varphi_{-1})\angle 0 + 2A_0A_1 \cos(\varphi_1 - \varphi_0)\angle 0 \quad . \quad \text{(D-9)}$$

Equation (D-9) indicates that all components of the retransmitted signal are in phase, but the amplitude of the signal varies with γ and hence with time.

3. Effect of Different Receiving and Transmitting Frequencies

If Assumption 1 is dropped, then R, which is measured in wavelengths, will be different for reception and transmission. L is unchanged.

R enters in the K of Eq. (D-1) and in the phase term. Let R, $G(\alpha)$, A, and φ refer to the received frequency, f_R, and $\hat{R}$, $\hat{G}(\alpha)$, $\hat{A}$, and $\hat{\varphi}$ refer to the transmitted frequency f_T.

Then,

$$\hat{R} = \frac{f_T}{f_R} R = CR \qquad \text{(D-10a)}$$

$$\hat{K} = CK \qquad \text{(D-10b)}$$

$$\hat{\varphi} = C\varphi \quad . \qquad \text{(D-10c)}$$

Note that Eq. (D-3) does not involve R and therefore the $\gamma - \alpha$ relationships are the same for both transmission and reception. Equation (D-7) is still valid, but the equivalent of Eq. (D-8) is

$$\hat{V} = \hat{A}_{-1}\hat{A}_{-1}\angle(\hat{\varphi}_{-1} - \varphi_{-1}) + \hat{A}_{-1}\hat{A}_0\angle(\hat{\varphi}_0 - \varphi_{-1})$$
$$+ A_{-1}\hat{A}_1\angle(\hat{\varphi}_1 - \varphi_{-1}) + \hat{A}_0\hat{A}_{-1}\angle(\hat{\varphi}_{-1} - \varphi_0)$$
$$+ \hat{A}_0\hat{A}_0\angle(\hat{\varphi}_0 - \varphi_0) + \hat{A}_0\hat{A}_1\angle(\hat{\varphi}_1 - \varphi_0)$$
$$+ \hat{A}_1\hat{A}_{-1}\angle(\hat{\varphi}_{-1} - \varphi_1) + \hat{A}_1\hat{A}_0\angle(\hat{\varphi}_0 - \varphi_1)$$
$$+ \hat{A}_1\hat{A}_1\angle(\hat{\varphi}_1 - \varphi_1) \quad . \qquad \text{(D-11)}$$

Unlike the previous case, Eq. (D-11) indicates that both amplitude and angle modulation will be present.

APPENDIX E

EXTENSION OF GODDARD SYSTEM TO EARTH-BUS-CAPSULE BUS EARTH

APPENDIX E

EXTENSION OF GODDARD SYSTEM TO EARTH – BUS–CAPSULE BUS EARTH

This system is shown in Fig. E-1 and the corresponding spectra in Fig. E-2. We define the frequencies of the following signals as:

	Signal	Nominal Value (MHz)
f_{eB}	Carrier (w/mod) from earth to bus	2399
D_u	Doppler shift earth/bus path	
f_0	Bus local oscillator	30
f_{BC}	Carrier (w/mod) from bus to capsule	2491
D_C	Doppler shift bus/capsule path	
f_C	Capsule local oscillator	89
f_{CB1}	Carrier (w/mod) capsule to bus	2402
f_{CB2}	Carrier capsule to bus	2403
f_{Be}	Carrier bus to earth	1800
f_1	First subcarrier (w/mod)-bus to earth	1
f_2	Second subcarrier (w/mod)-bus to earth	2
f_3	Third subcarrier-bus to earth	3
D_0	$D_u/80$	

The signals received at the earth station have frequencies:

(1) $60\ f_0 + 3/4\ D_u$

(2) $60\ f_0 + 3/4\ D_u + 80\ f_0 - f_{eB} - D_u$

(3) $60\ f_0 + 3/4\ D_u + 83\ f_0 - f_{eB} - D_u + 2\ D_C - f_C$

$60\ f_0 + 3/4\ D_u + D_C - 80\ f_0 + 27\ f_C$

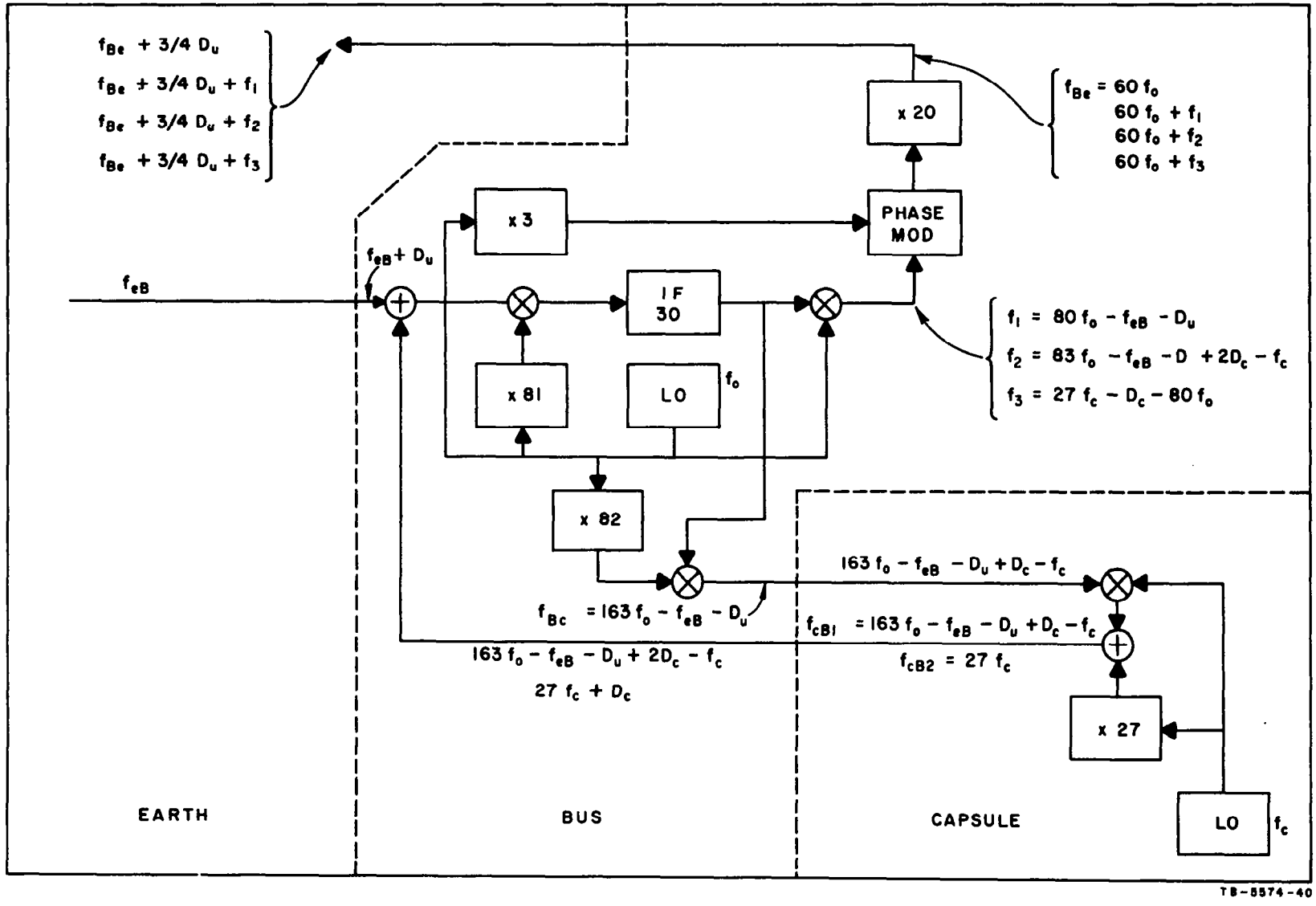

FIG. E-1 TWO-TRANSPONDER SYSTEM

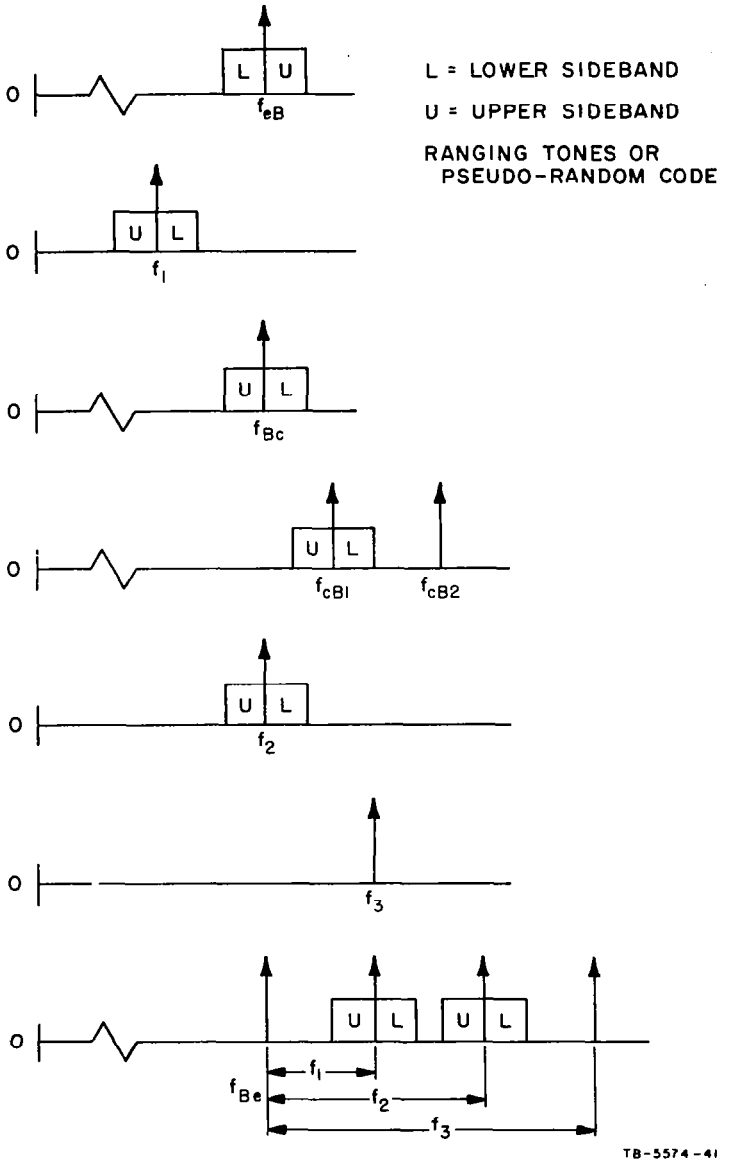

FIG. E-2 SPECTRA OF SIGNALS IN TWO-TRANSPONDER SYSTEM

Since f_{eB} is known at the receiver, signals (1) and (2) can be processed in a double phase-locked receiver to evaluate f_0 and D_u (see Fig. E-3). Then the remaining subcarriers C and d can be further processed to evaluate f_C and D_C (see Fig. E-4).

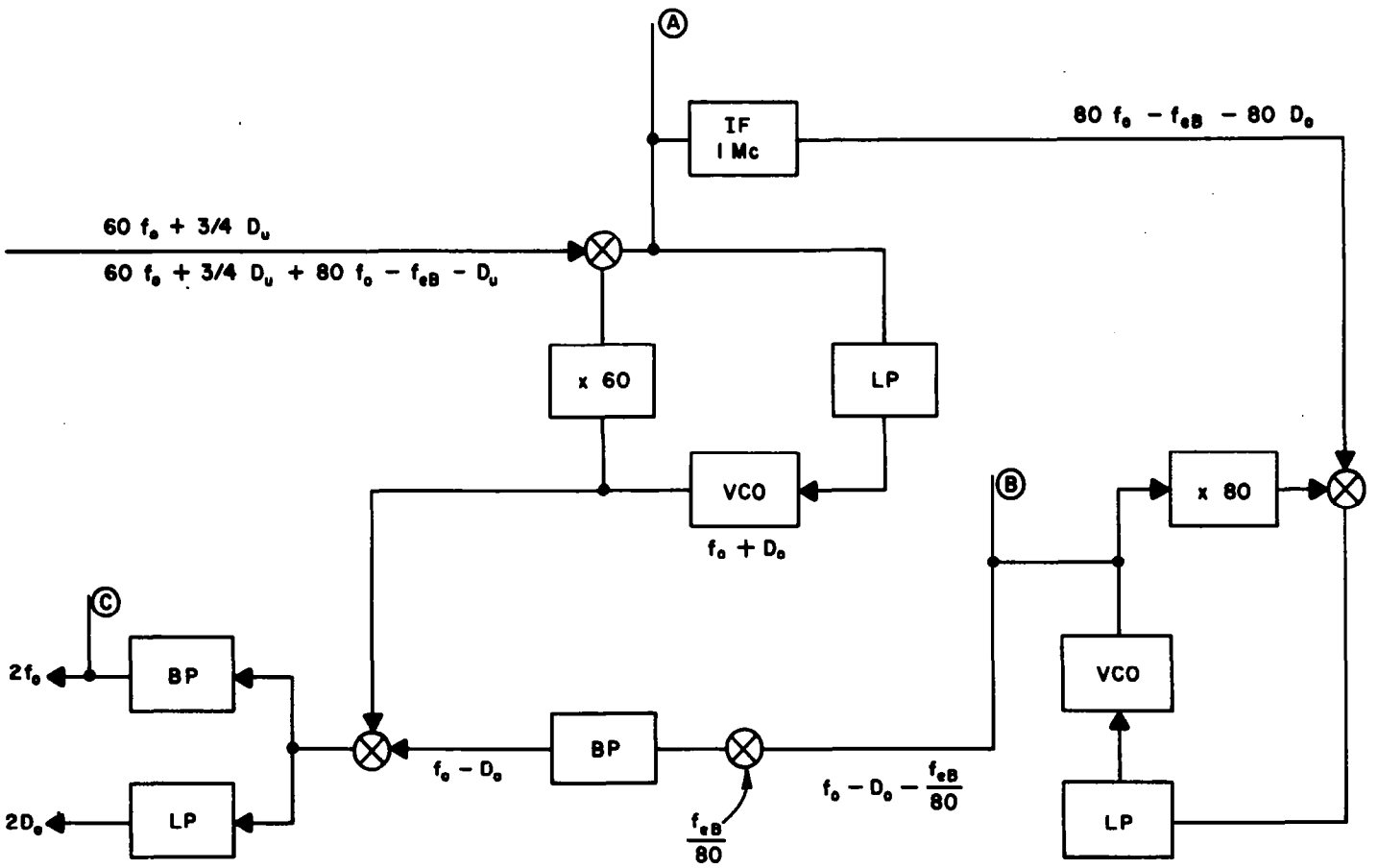

FIG. E-3 EVALUATION OF f_0 AND D_0

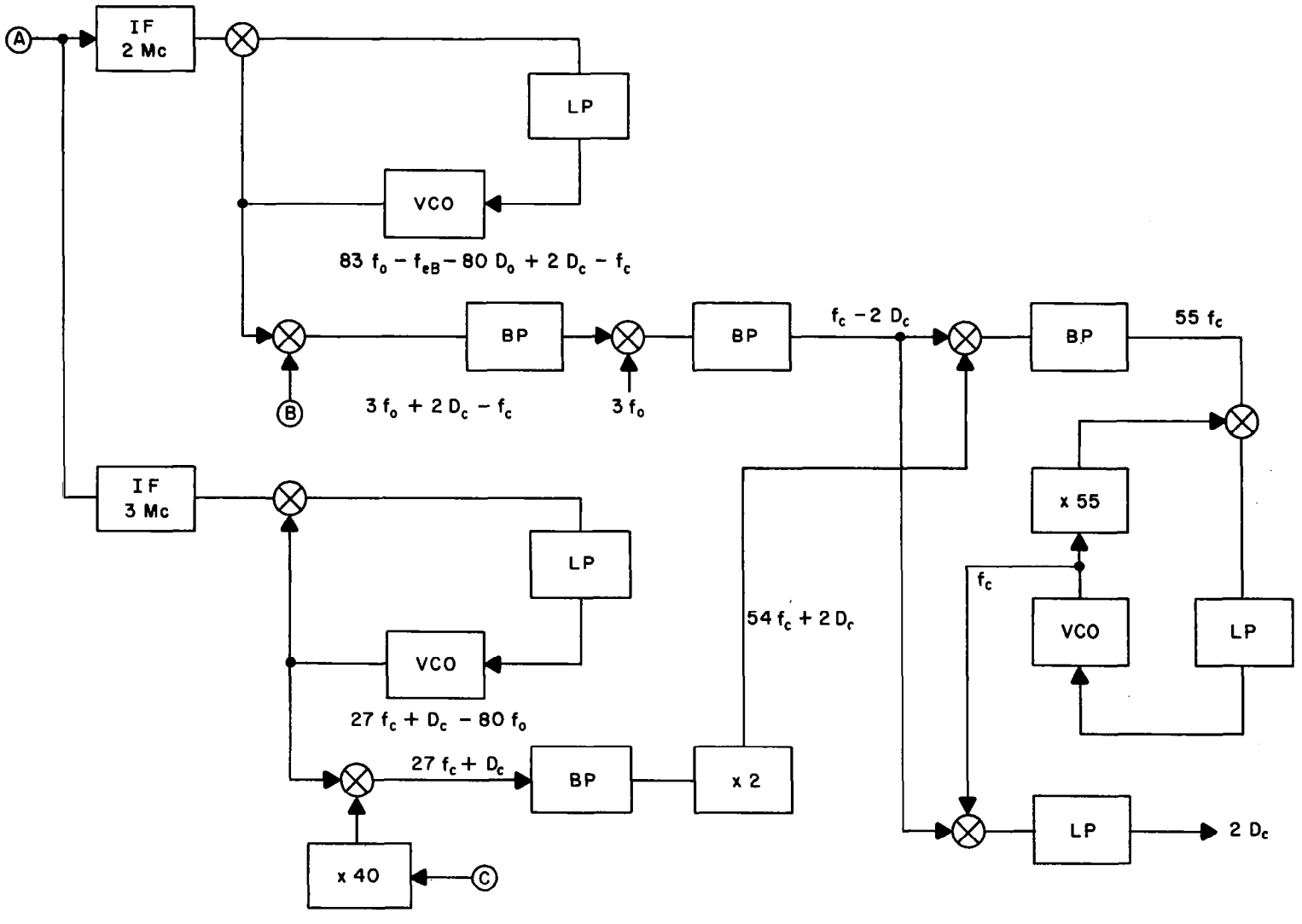

FIG. E-4 EVALUATION OF f_C AND D_C

REFERENCES

1. C. A. Hacking and J. A. Martin, "Study and Application of Retrodirective and Self-Adaptive Electromagnetic Wave Controls to a Mars Probe," First Quarterly Report, Contract NAS 2-2933, SRI Project 5574, Stanford Research Institute, Menlo Park, California (November 1965).

2. C. A. Hacking *et al.*, "Study and Applications of Retrodirective and Self-Adaptive Electromagnetic Wave Controls to a Mars Probe," Second Quarterly Report, SRI Project 5574, Contract NAS 2-2933, Stanford Research Institute, Menlo Park, California (February 1966).

3. C. A. Hacking and C. H. Dawson, "Study and Application of Retrodirective and Self-Adaptive Electromagnetic Wave Controls to a Mars Probe," Third Quarterly Report, Contract NAS 2-2933, SRI Project 5574, Stanford Research Institute, Menlo Park, California (October 1966).

4. R. B. Battelle, Ed., "Feasibility Analysis of a Deep-Space Receiving Terminal Array of Large Equivalent Aperture," Final Report, Contract NAS 1-3075, Stanford Research Institute, Menlo Park, California (May 1964).

5. "Investigation and Study of a Multi-Aperture Antenna System," Final Report, Contract NAS-5-3472, Electronic Communications, Inc., Timonium, Maryland (April 1964).

6. P. G. Smith, *et al.*, "Analytical Study to Define an Experimental Program for the Evaluation and Optimization of Multi-Element Large Aperture Arrays," Final Report, Contract NAS-1-3780, Research Triangle Institute, Durham, North Carolina (October 1964).

7. B. B. Lusignon, "Detection of Solar Particle Streams by High Frequency Radio Waves," *J. Geophys. Research*, Vol. 68, No. 20, pp. 5617-5632 (October 15, 1963).

8. M. Easterling and R. Goldstein, "The Effect of the Interplanetary Medium on *S*-band Tele-Communications," Tech. Report No. 32-825, Jet Propulsion Laboratory, Pasadena, California.

9. R. L. Koehler, "Interplanetary Electron-Density Measurements With the Pioneer VI Spacecraft," Abstract, Stanford Electronics Laboratory, Stanford, California, Quoted in *Electronics Research Review*, 15 (16 August).

10. A. J. Kliore, D. L. Cain, G. S. Levy, V. R. Eshleman, G. Fjeldbo, and F. D. Drake, "Occultation Experiment: Results of the First Direct Measurement of Mar's Atmosphere and Ionosphere," *Science, 149*, 1965, pp. 1243-1248.

11. G. Fjeldbo, W. Fjeldbo, and V. R. Eshleman, "Models for the Atmosphere of Mars Based on the Mariner IV Occultation Experiment," Scientific Report No. 15 under NASA Grant NsG-377, Scientific Report No. 2 under NASA Grant NGR-05-020-065, RSL, Stanford Electronics Laboratory, Stanford, California (January 1966).

12. E. F. Vance and J. E. Nanevicz, "RF Breakdown in a Space Environment," *Abstracts of the Fourteenth Annual Symposium U.S. Air Force Antenna Research and Development Program*, Sponsored by Air Force Avionics Laboratory, Wright-Patterson Air Force Base, Ohio, Robert Allerton Park, Monticello, Illinois, 6,7,8 October 1964.

13. Edward F. Vance, "One-Sided Multipactor Discharge Modes," *J. Appl. Phys.*, Vol. 34, No. 11, pp. 3237-3242 (November 1963).

14. L. D. Kaplan, G. Munch, and H. Spinrad, "An Analysis of the Spectrum of Mars," *Astrophys. J.*, Vol. 139, No. 1 (January 1964).

15. G. V. Spiegel, "Effects of Mars Atmospheric Uncertainties on Entry Vehicle Design," *Aerospace Eng.*, Vol. 21, pp. 62-63 and 103-107 (December 1962).

16. G. deVaucoulers, *Physics of the Planet Mars* (Faber & Faber, Ltd., London, 1953).

17. G. F. Schilling, "Limiting Model Atmospheres for Mars," R-402 JPL, the RAND Corporation, Santa Monica, California (August 1962).

18. G. M. Levin, *et al.*, "NASA Engineering Models of the Mars Atmosphere for Entry Vehicle Design," NASA TND-2525 (1964).

19. G. M. Levin, "A Proposed Solution to Entry Vehicle Design Penalties Caused by Lack of Knowledge of the Mars Atmosphere," *AIAA* Paper 65-493 (1965).

20. L. Roberts, "Entry Into Planetary Atmospheres," *Astronautics and Aeronautics*, Vol. 2, No. 10, pp. 30-40 (October 1964).

21. R. A. Hanel, "Exploration of the Atmosphere of Venus by a Simple Capsule, NASA TN D-1909 (July 1964).

22. A. Seiff and D. E. Reese, Jr., "Use of Entry Vehicle Responses to Define the Properties of the Mars Atmosphere," Preprint 65-24, American Astronautical Society Symposium on Unmanned Exploration of the Solar System, Denver, Colorado, February 8-10, 1965.

23. V. L. Peterson, "A Technique for Determining Planetary Atmosphere Structure from Measured Accelerations of an Entry Vehicle," NASA TN D-2669 (1965).

24. "The Reentry Plasma Sheath," *Space Astronautics*, pp. 63-67 (May 1964).

25. E. D. Shane, "Equilibrium Electron Density on Mars," *AIAA J.*, Vol. 2, No. 8, pp. 1497-1499 (August 1964).

26. A. Ambrosio, "A General Atmospheric Entry Function and Its Characteristics," *ARS Journal*, Vol. 32, No. 6, pp. 906-910 (June 1962).

27. J. Spiegel, "Effects of Mars Atmospheric Uncertainties on Entry Vehicle Design," *Aerospace Engineering*, Vol. 21, No. 12, pp. 62-63, 103-107 (December 1962).

28. W. H. Krase, "Mars Environmental Measurements in Support of Future Manned Landing Expeditions," Memorandum RM-4437-NASA, RAND Corporation, Santa Monica, California (April 1965).

29. H. Rothman, *et al.*, "Transmission Through an Ionized Medium in the Presence of a Strong Magnetic Field," Second Symposium on the Plasma Sheath, Boston, Massachusetts (April 1962).

30. A. G. Hammitt, *et al.*, "Wake Cooling by Fluid Injection (U)," *Proc. of AMRAC*, Monterey, California (April 1963), SECRET.

31. D. F. Spencer, "An Evaluation of the Communication Blackout Problem for a Blunt Mars-Entry Capsule and a Potential Method for the Elimination of Blackout," Technical Report No. 32-594, Jet Propulsion Lab. (April 15, 1964).

32. A. J. Kelly, "An Experimental Feasibility Study of Injectant Materials to Aleinate Mars Entry Communications Blackout," Paper presented at the Third Symposium on the Plasma Sheath, Boston, Massachusetts, September 21-23, 1965.

33. W. F. Cuddihy, and J. K. Hughes, "Simulated Re-Entry Tests of a Method for Reducing Radio Blackout by Material Addition to the Ionized Flow-Field," NASA TM X-988 (1964).

34. P. W. Huber and T. E. Sims, "The Entry-Communications Problem," *Astronautics and Aeronautics*, Vol. 2, No. 10, pp. 30-40, (October 1964).

35. *Proceedings of NASA Conference on Communicating Through Plasmas of Atmospheric Entry and Rocket Exhaust*, January 14-15, 1964, Langley Research Center, Langley Station, Hampton, Virginia SP-52, CONFIDENTIAL.

36. "Project RAMC (Radio Attenuation Measurements—Series 'C') Revision B" Project Development Plan, NASA Langley Research Center (June 1965).

37. W. Taylor and D. Weissman, "The Effects of a Plasma in the Near-Zone Field of an Antenna," Final Report, SRI Project 4555, Contract NAS 1-3099, Stanford Research Institute, Menlo Park, California (June 1964).

38. W. C. Taylor, "Study of the Effects of a Plasma in the Near-Zone Field of an Antenna," Final Report, SRI Project 5514, Contract NAS 1-4973, Stanford Research Institute, Menlo Park, California (May 1966).

39. C. H. Dawson, Ed., "The Design of an Experiment to Determine the Limitations Imposed on a Multiple-Aperture Antenna System by Propagation Phenomena," Final Report, SRI Project 5067, Contract NAS 5-3974, Stanford Research Institute, Menlo Park, California (June 1965).

40. R. B. Muchmore and A. R. Wheelon, "Frequency Correlation of Line of Sight Signal Scintillations," *Trans. IEEE AP-11*, 1, pp. 48-51 (January 1963).

41. W. E. Scharfman and T. Morita, "Voltage Breakdown of Antennas at High Altitudes," Tech. Report 69, SRI Project 2494, Contract AF 19(604)-3458, Stanford Research Institute, Menlo Park, California (April 1960).

42. J. B. Chown, "Study of Plasma-Induced Voltage Breakdown at Low Pressure," Final Report, SRI Project 3369, Contract AF 33(600)-41517, Stanford Research Institute, Menlo Park, California (July 1961).

43. W. E. Scharfman, W. C. Taylor, and T. Morita, "Research Study of Microwave Breakdown of Air at High Altitudes," Final Report, SRI Project 3345, Contract AF 19(604)-7367 Stanford Research Institute, Menlo Park, California (August 1962).

44. J. B. Chown, "Effects of Re-Entry Environment on ECM Antenna System Performance," Final Report, SRI Project 4583, Sperry Gyroscope Co. PO 259160, Stanford Research Institute, Menlo Park, California (August 1964).

45. J. B. Chown, W. E. Scharfman, and T. Morita, "Effect of Ambient Plasma on Antenna Breakdown," *6th Symposium on Ballistic Missile and Aerospace Technology*, pp. 51-68 (Academic Press, New York, New York, 1961).

46. J. B. Chown, *et al.*, "Effects on Re-Entry and Space Environments on Antenna Performance," Paper presented at the Third Symposium on the Plasma Sheath, Boston, Massachusetts, September 21-23, 1965.

47. J. A. Martin and J. B. Chown, "Study of the Breakdown Characteristics of Antennas in the Atmospheres of Mars and Venus," Final Report, Contract 950380 under NASA Contract NAS 7-100, SRI Project 4208, Stanford Research Institute, Menlo Park, California (February 1963).

48. V. A. Hughes, "Roughness of the Moon as a Radar Reflector," *Nature*, Vol. **186**, No. 4728, pp. 873-874 (1960).

49. R. L. Leadabrand, R. B. Dyce, A. Frediksen, R. I. Presnell, and J. C. Schlobohm, "Radio Frequency Scattering from the Surface of the Moon," *Proc. IRE*, Vol. **48**, pp. 932-933 (May 1960).

50. R. B. Dyce and R. A. Hill, "Lunar Echoes Received on Spaced Receivers at 106.1 Mc," *Proc. IRE*, Vol. 48, pp. 934-935 (May 1960).

51. M. I. Skolnik, *Introduction to Radar Systems*, Chapter 14, (McGraw-Hill Book Company, Inc., New York, New York, 1962).

52. J. V. Evans and G. H. Pettengill, "The Scattering Behavior of the Moon at Wavelengths of 3.6, 68, and 784 Centimeters," *J. Geophys. Research*, Vol. 68, No. 2, pp. 423-453 (January 15, 1963).

53. P. Beckman and A. Spizzichino, *The Scattering of Electromagnetic Waves from Rough Surfaces*, pp. 334-340 (The MacMillan Company, New York, New York, 1963).

54. N. I. Skolnik, "An Analysis of Bistatic Radar," *IRE Trans. Aerospace and Navigational Electronics*, Vol. ANE-8, No. 1, pp. 19-27 (March 1961).

55. G. Fjeldbo and V. R. Eshleman, "The Bistatic Radar-Occultation Method for the Study of Planetary Atmospheres," Scientific Report No. 5, Research Grant No. NsG-377, Radioscience Laboratory, Stanford University, California (February 1965).

56. A. J. Kliore, D. L. Cain, G. S. Levy, V. R. Eshleman, F. D. Duke, and G. Fjeldbo, "The Mariner 4 Occultation Experiment," *Astronautics and Aeronautics*, pp. 72-80 (July 1965).

57. R. C. Hansen (guest Editor) "Special Issue on Active and Adaptive Antennas," *IEEE Trans.*, *AP*-12, 2, pp. 140-233 (March 1964).

58. H. L. Knudsen, "The Necessary Number of Elements in a Direction Ring Aerial," *J. Appl. Phys.* **22**, No. 11, pp. 1299-1306 (November 1951).

59. H. Stenzel, *Elek. Nachr.-Tech.* 6, pp. 165-181 (May 1929).

60. C. E. Hickman, H. P. Neff, and J. D. Tillman, "The Theory of Single-Ring Circular Antenna Arrays," Scientific Report 4, AFCRL 543, Contract AF 19(604)-4967, University of Tennessee College of Engineering, Knoxville, Tennessee (1 July 1961), AD 262 662.

61. W. T. Patton and J. D. Tillman, "An Analysis of the Terminal Properties of a Circular Antenna Array with a Synthesis Technique for Obtaining a Prescribed Radiation Pattern," Scientific Report 2, AFCRC-TN-58-148, Contract AF 19(604)-1557, University of Tennessee College of Engineering, Knoxville, Tennessee (1 June 1958). AD 152 379.

62. H. A. Rosen, "Directive Array for a Spinning Vehicle," *Proc. 1962 National Telemetering Conference*, 1, Sec. 1-4 (23-25 May 1962).

63. H. Page, "Radiation Resistance of Ring Aerials," *Wireless Engineer*, 25, pp. 102-109 (April 1948).

64. H. Page, "Ring Aerial Systems," *Wireless Engineer*, **25**, pp. 308-315 (October 1948).

65. J. D. Tillman, W. T. Patton, C. E. Blakely, and V. F. Schultz, "The Use of a Ring Array as a Skip Range Antenna," *Proc. IRE*, **43**, No. 11, pp. 1655-1660 (November 1955).

66. D. E. N. Davies, "Some Properties of Van Atta Arrays and the Use of 2-Way Amplification in the Delay Paths," *Proc. IEE*, Vol. 110, No. 3, pp. 507-512 (March 1963).

67. Hughes Aircraft Co., Space Systems Division, "Design Release Report, Phased Array Transmitting Antenna and PACE, Applications Technology Satellite," Hughes Report SSD60196R, NASA Contract NAS 5-3823 (October 1966).

68. S. Andre and D. Leonard, "Gain Limitations of Electronically Despun Antennas for Communication Satellites," Paper No. 66-325, read at AIAA Communication Satellite Systems Conference, Washington, D.C., 4 May 1966.

69. J. T. Bolljahn, "Effects of Satellite Spin on Ground-Received Signal," Tech. Report 6, Contract DA 04-200-ORD-273, Stanford Research Institute, Menlo Park, California (August 1957). Also *Trans. IRE, PGAP-6*, 3, pp. 260-267 (July 1958).

70. A. T. Villeneuve, "Optimization of Gain of Arbitrary Array Antennas," Scientific Report No. 5, Contract AF 19(628)-4349, Hughes Aircraft Co., Culver City, California, Report No. P65-153, HAC Ref. No. A5034 (December 1965).

71. E. Jahnke and F. Emde, *Tables of Functions with Formulae and Curves*, Fourth Ed., Chapter 8 (Dover Publications, Inc., New York, New York, 1945).

72. G. N. Watson, *A Treatise on the Theory of Bessel Functions*, Second Ed., Chapter 8 (Macmillan Company, New York, New York, 1948).

73. W. W. Hansen and J. R. Woodyard, "A New Principle in Directional Antenna Design," *Proc. IRE*, **26**, No. 3, pp. 333-345 (March 1938).

74. C. A. Hacking, "Final Report on TLA-3 Antenna System," Contract AF 30(602)-2259, AD-334-435, (15 August 1962), CONFIDENTIAL.

75. C. A. Hacking, "Microscan Antenna System (U)," *Proceedings of the Eleventh USAF Antenna Symposium*, University of Illinois (Part 2)(October 1961), SECRET.

76. C. C. Cutler, R. Kompfner, and L. C. Tillotson, "A Self Steering Array Repeater," *Bell System Tech. J.* **43**, No. 5, pp. 2013-2032 (September 1963).

77. E. M. Butz-Philipp, "Spherical Retrodirective Array." *IEEE Trans. AP*-12, No. 2, pp. 187-194 (March 1964).

78. J. H. Schrader, "A Phase-Lock Receiver for the Arraying of Independently Directed Antennas," *IEEE Trans.*, Vol. AP-12, No. 2, pp. 155-161 (March 1964).

79. L. C. Van Atta, "Interplanetary Communication," *International Science and Technology*, pp. 50-61 (November 1966).

80. G. C. Kronmiller, Jr. and E. J. Baghdady, "The Goddard Range and Range-Rate Tracking System: Concept, Design, and Performance," Report X-531-65-403 Goddard Space Flight Center, Greenbelt, Maryland (October 1965).